Technische Universität München

Department für Chemie
Professur für Strukturelle Membranbiochemie

NMR structural studies of full-length Bcl-xL in nanodiscs

Kolio Pavlinov Raltchev

Vollständiger Abdruck der von der Fakultät für Chemie der Technischen Universität München zur Erlangung des akademischen Grades eines

Doktors der Naturwissenschaften (Dr. rer. nat.)

genehmigten Dissertation.

Vorsitzende/-r: Priv.-Doz. Dr. Gerd Gemmecker

Prüfende/-r der Dissertation:

1. Prof. Dr. Franz Hagn

2. Prof. Dr. Bernd Reif

Die Dissertation wurde am 26.11.2019 bei der Technischen Universität München eingereicht und durch die Fakultät für Chemie am 16.01.2020 angenommen.

Declaration

I hereby declare that parts of this thesis are already submitted to scientific international journals or are already published:

- Raltchev, K., Pipercevic, J. & Hagn, F. Production and Structural Analysis of Membrane-Anchored Proteins in Phospholipid Nanodiscs. *Chemistry* **24**, 5493-5499 (2018).

- Häusler, E., Fredriksson, K., Goba, I., Peters, C., Raltchev, K., Steiner, A., Hagn, F. Quantifying the insertion of membrane proteins into lipid bilayer nanodiscs using a fusion protein strategy. *Biochim Biophys Acta Biomembr* **1862**, 183190 (2020).

Other contributions:

- Rodriguez Camargo D.C., Korshavn K.J., Jussupow A., Raltchev K., Goricanec D., Fleisch M., Sarkar R., Xue K., Aichler M., Mettenleiter G., Walch K.W., Camilloni C., Hagn F., Reif B., Ramamoorthy A. Stabilization and structural analysis of a membrane-associated hIAPP aggregation intermediate. *Elife* **6**, doi:10.7554/eLife.31226 (2017)

Abbreviations

ATP	adenosine-5’-triphosphate
Apo A1	Apolipoprotein A-1
Bak	Bcl-2 antagonist killer 1
Bax	Bcl-2-associated x protein
Bcl-xL	B-cell lymphoma-extra large
BH	Bcl-2 homology
CD	circular dichroism
CL	1',3'-bis[1,2-dimyristoyl-sn-glycero-3-phospho]-glycerol
cmc	critical micellar concentration
CSA	chemical shift anisotropy
DD	dipolar couplings
DIBMA	diisobutylene/maleic acid
DLS	dynamic light scattering
DMPC	1,2-dimyristoyl-sn-glycero-3-phosphocholine
DMPG	1,2-dimyristoyl-sn-glycero-3-phospho-(1'-rac-glycerol)
DPC	dodecyl phosphocholine
DSC	differential scanning calorimetry
E. coli	*Escherichia coli*
EDTA	ethylenediaminetetraacetic acid
EPR	electron paramagnetic resonance
GPCR	G protein-coupled receptor
GPI	glycosylphosphatidylinositol
HDL	high-density lipoprotein
HFS	hemifluorinated surfactants
HSQC	Heteronuclear single quantum coherence spectroscopy
IMM	inner mitochondrial membrane
IMP	integral membrane proteins
INEPT	insensitive nuclei enhanced by polarisation transfer
IPTG	isopropyl β-D-1-thiogalactopyranoside
ITC	isothermal titration calorimetry
LCP	lipidic cubic phases
LUV	large unilamellar vesicles
MNG	maltose–neopentyl glycol
MOM	mitochondrial outer membrane
MOMP	mitochondrial outer membrane permeabilisation
MP	membrane protein
MSP	membrane scaffold protein
ND	nanodisc
NMR	nuclear magnetic resonance
NOE	nuclear Overhauser effect
OMM	outer mitochondrial membrane
PCS	pseudo-contact shifts
PRE	paramagnetic relaxation enhancement
PTM	post-translational modifications
PUMA	p53 upregulated modulator of apoptosis
RDC	residual dipolar couplings
Salipro	saposin A lipoprotein discs
SAXS	small angle X-ray scattering
SDS	sodium dodecyl sulfate
SMA	styrene maleic acid
SMALP	styrene maleic anhydride copolymer-lipid nanoparticles
Solu	soluble domain
SUV	small unilamellar vesicles
TA	tail-anchored
TEM	transition electron microscopy
TM	transmembrane
TMH	transmembrane helix
TROSY	Transverse relaxation-optimised spectroscopy

Summary

Membrane proteins (MPs) represent a crucial protein class that is mediating signal and material transduction in cells. These proteins require the presence of a membrane and are therefore challenging to produce and study *in vitro*. Thus, a suitable native membrane mimetic is required for *in vitro* investigations of membrane proteins. In recent years, one of the most used and well-studied platforms for studying membrane protein structure and function in a near native environment are phospholipid nanodiscs. Nanodiscs are a membrane mimetic system that is a small, well defined discoidal bilayer, confined by two copies of high-density lipoprotein. By this, membrane proteins can be in aqueous solutions without the use of detergents. The versatility of this system allows a tuneable and ideal surrounding for the membrane protein of interest and to further study it with different biophysical and structural biological methods.

The focus in this study is the development of new methods for the production of the full-length tail-anchored membrane proteins, specifically the B-cell lymphoma-extra large (Bcl-xL), a member of the Bcl-2 family, as well as their structural investigation in phospholipid nanodiscs. Bcl-xL and other tail-anchored Bcl-2 proteins have mostly been studied as truncated soluble proteins, as the presence of a transmembrane helix (TMH) lowers their solubility and leads to aggregated or misfolded protein in *E. coli*. The developed methods are applied to studying the membrane-bound and inserted Bcl-xL and to probe its membrane location and possible membrane insertion processes in a native-like environment.

In the first part of the thesis, a Sortase A mediated approach for the production of full-length Bcl-xL is developed, where Bcl-xL is produced in two separate parts, the soluble domain with a Sortase A recognition motif (LPETG) and the TMH as a GB1-fusion. Following nanodisc insertion of the TMH and removal of the GB1-tag, Sortase A enzyme is used to ligate both parts and produce the full-length protein in a nanodisc. The applicability of this method is confirmed by subsequent structural studies that led to the first 3D-structure of a functional full-length Bcl-xL in nanodiscs by nuclear magnetic resonance (NMR) spectroscopy. Additionally, using the TMH-GB1 construct, it was possible to establish a new method for the analysis of the oligomeric state of membrane proteins in lipid bilayer nanodiscs. Determining the amount of cut-off GB1 from the TMH in nanodiscs allowed to calculate the initial amount of helix inside the disc.

In the second part of the thesis the role of the membrane and the effect of its composition on the Bcl-xL structure and localisation was studied. Moreover, the interaction with the binding partner PUMA and its mechanism was studied dependent on the membrane composition.

In the final part, a new method for the production of tail-anchored proteins in *E. coli* is investigated, employing co-expression of the chaperone Asna1/TRC40 or Get3 together with Bcl-xL. This allowed the production of the insoluble and aggregation-prone full-length Bcl-xL as a soluble chaperon-protein complex. Removal of Asna1/TRC40 or Get3 by mild detergents enabled transfer of full-length Bcl-xL into various membrane mimetics, without the need of inclusion-body solubilisation and refolding. The developed method was further shown to facilitate the high-yield production of toxic or hardly accessible TM helices.

Zusammenfassung

Membranproteine (MP) bilden eine entscheidende Proteinklasse, welche die Signalweiterleitung und den Transport von Molekülen in der Zelle vornehmen. Da diese Proteine für ihre Stabilität und Funktion eine Membran benötigen, stellt deren Herstellung und Untersuchung *in vitro* eine Herausforderung dar. Dazu wird ein natives Modellmembransystem benötigt, welches kompatibel ist mit *in vitro* und strukturellen Studien. In den letzten Jahren ist eine der am häufigsten verwendeten und am besten untersuchten Plattformen, um die Struktur und Funktion von Membranporteinen in einer nahezu nativen Umgebung zu untersuchen, die Phospholipid Nanodiscs. Nanodiscs sind ein Membranmimetikum, welches aus einer definierten Lipiddoppelschicht besteht, die von je zwei Kopien von Apolipoprotein-A1 umschlossen ist. Durch diese können Membranproteine ohne die Zugabe von Detergenzien in Lösung gehalten werden. Die Vielseitigkeit dieser Methode erlaubt die Verwendung einer definierten und idealen Umgebung für ein Membranprotein und dessen Untersuchung mit verschiedenen biophysikalischen und strukturbiologischen Methoden.

Der Fokus dieser Arbeit ist die Entwicklung neuer Methoden zur Produktion von endständig-verankerter (*tail-anchored*) Membranproteinen, insbesondere von Bcl-xL (B-cell lymphoma extra large), welches ein Mitglied der Bcl-2 Proteinfamilie ist, sowie deren strukturelle Untersuchung in Phospholipid Nanodiscs. Bcl-xL und andere *tail-anchored* Bcl-2 Membranproteine wurden meist als gekürzte lösliche Domänen untersucht, da die Transmembranhelix (TMH) deren Löslichkeit herabsetzt und zur Aggregation oder Fehlfaltung in *E. coli* führt. Die entwickelten Methoden werden angewendet, um die membrangebundene und verankerte Form von Bcl-xL zu untersuchen und um deren Membranlokalisation beziehungsweise mögliche Membraninsertionsprozesse in einer möglichst nativen Umgebung zu erforschen.

Im ersten Teil der Arbeit wird eine durch Sortase A vermittelte Kopplung für die Herstellung von volllängen Bcl-xL etabliert, wobei Bcl-xL in zwei gesonderten Teilen produziert wird, der löslichen Domäne mit einem Sortase A Motiv (LPETG) und der TMH als GB1-Fusionskonstrukt. Nach der Nanodisc Insertion der TMH und dem Entfernen des GB1-Fusionstags wird Sortase A verwendet, um beide Proteinteile zu ligieren und so das Volllängenprotein in einer Nanodisc herzustellen. Die Anwendbarkeit dieser Methode wird durch weiterführende NMR-basierte (Kernspinresonanz) strukturelle Untersuchungen gezeigt. So konnte die erste 3-D Struktur eines funktionalen volllängen Bcl-xL in Nanodiscs erstellt werden.

Zusätzlich wird durch die Verwendung eines GB1-TMH-Fusionskonstruktes eine neue Methode über die Ermittlung des Oligomerisierungszustandes eines Membranproteins in Nanodiscs entwickelt, was die Bestimmung der Menge von GB1, die von den GB1-TMH-Nanodiscs abgeschnitten wird, ermöglicht.

Im zweiten Teil dieser Arbeit wird der Einfluss der Membran und der Effekt ihrer Zusammensetzung auf die Struktur und Lokalisation von Bcl-xL untersucht. Außerdem wird besonders die Interaktion mit dem Bindungspartner PUMA und der Mechanismus davon an der Membran, in Abhängigkeit der Lipidzusammensetzung, erforscht.

Im letzten Teil wird eine neue Methode für die Herstellung von *tail-anchored* Proteinen in *E. coli* erforscht, bei der eine Co-Expression der Chaperone Asna1/TRC40 oder Get3 zusammen mit volllängen Bcl-xL verwendet wird. Durch diese Methode gelingt es, das unlösliche und aggregationsanfällige Bcl-xL als löslichen Chaperon-Proteinkomplex herzustellen. Die Abtrennung von Asna1/TRC40 oder Get3 durch milde Detergenzien ermöglichte den Transfer von volllängen Bcl-xL in verschiedene Modellmembransysteme, wodurch die Produktion von *inclusion bodies* und deren Rückfaltung vermieden werden kann. Darüber hinaus ermöglichte die entwickelte Methode die effiziente Produktion toxischer und schwer zugänglicher TMHs.

Table of Contents

1 Introduction

1.1 Biological background

1.1.1 Membrane proteins

The continuously growing, complex and diverse world of proteins can be categorised depending on their properties, such as their amino acid sequence or usually their three-dimensional structures and evolutionary function[1-5]. Membrane proteins (MPs) are one of the main protein types, besides disordered, fibrous and globular ones and are located at or in the membranes of all cells and enveloped viruses[6-9]. Most of them are not soluble and require the presence of a membrane to attach or integrate themselves into. The ideal surrounding is comprised by the amphipathic and primarily hydrophobic properties the membrane components, e.g. phospholipids, cholesterol, glycolipids and other bound or integrated proteins[10,11]. The membrane protein content may vary from the lowest amount of approximately 20 % in myelin sheaths, where lipids are used to insulate neurons, to 75 % in the inner mitochondrial membrane (IMM), where they serve in the production of energy[8]. Generally, the plasma membranes of most cells contain 50 % of membrane proteins by mass, which clearly shows their abundance and significance. An estimated 20 to 30 % of all encoded genes, based on structure prediction and genome analysis[12,13], encode membrane proteins and approximately 23 %[14] of the human proteome. Since membranes and therefore membrane proteins not only envelope cells and compartmentalise their inside but also help to build large surfaces, chemical or charge gradients and insulations, they are one of the primary cell components and are involved in almost all cellular processes[6,8,15]. Hence membrane proteins govern mainly all transport of signals, chemicals, nutrients and charges through those membranes and from cell to cell. They also make the transfer of external signals, stimuli and senses such as light[16,17], heat[18] and cold[19], smell[20] or pain[18,21] possible and are always the starting point of each known signalling cascade. Overall this makes them an interesting and ideal drug target. It is therefore not surprising that more than 60 % of the FDA approved drugs target membrane proteins[22]. Continuous research expands the amount of known protein structures and identifies new possible drug targets or pathways that can be altered[22]. Simultaneously, new drug compounds that fit and interact with a known structure are being invented. Furthermore, established drugs and small molecules or functional groups are being screened on newly found membrane proteins with versatile high-throughput methods[22-27].

That way, with the help of structural biology, new drugs are developed, and new targets and interactions shift into the spotlight. This pharmacological and medicinal potential of membrane proteins makes it so attractive and relevant to study them.

1.1.2 Structure of membrane proteins

1.1.2.1 Peripheral membrane proteins

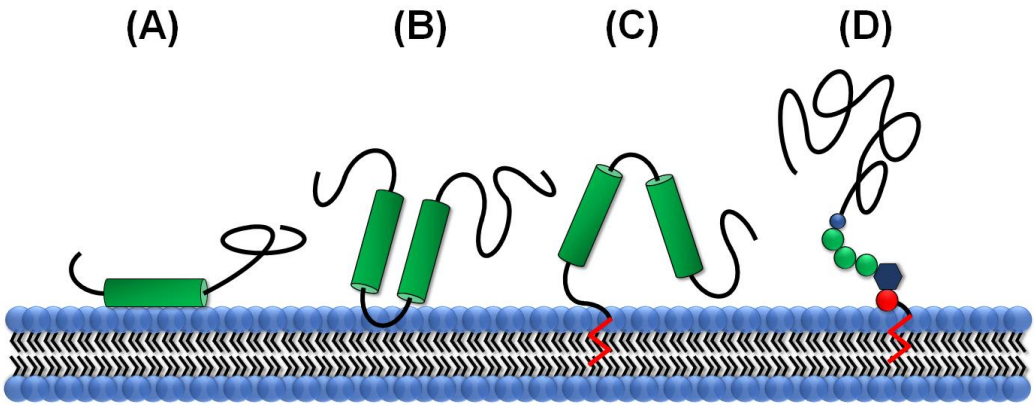

Figure 1: Depiction of types of peripheral membrane proteins; loosely attached through a) amphipathic helix motif in green or with b) hydrophobic patch in an unstructured loop in black; c) lipid anchored with usually one to two lipid-anchors, depicted in red; d) glycosylphosphatidylinositol (GPI) linked, with lipid anchor and attached phosphate, both in red; phosphatidylinositol in dark blue with attached sugar groups (trimannosyl-non-acetylated glucosamine) in green, following a phosphoethanolamine in blue, connected to the protein, which is depicted in black.

So far, many types of membrane proteins have been identified, but they are not always easy to distinguish, as they tend to blend into each other gradually[6,8,15]. It is difficult to say how many unique types exist or have been found so far. For simplification purposes, membrane proteins are sorted into two main categories depending on their kind of membrane interaction and localisation. Firstly, the loosely attached peripheral membrane proteins (see Figure 1), that are held by weak electrostatic or hydrophilic interactions at the membrane surface, either by binding to the membrane directly or to other already integrated proteins[6,8,15,28]. They are related to water-soluble globular proteins and are extracted easily from the membrane by breaking those interactions. This is done, e.g. by altering the pH or with different polar chemicals. Therefore, they are found in the soluble part of a protein purification, where they are stable. This is possible since they have a hydrophilic surface and do not extensively penetrate the membrane and are almost entirely solvent accessible.

A well-studied and pivotal member of the protein-attached peripheral proteins is cytochrome c, which is found at the inner mitochondrial membrane (IMM) where it is weakly bound to the cytochrome c oxidase[29]. It is actively involved in the generation of energy in the form of ATP by participating in the electron transportation and has also been shown to be involved in the induction of cell death (see chapter 1.2.1)[30-32]. Exceptions in the attachment-mode are lipid-modified proteins such as glycosylphosphatidylinositol (GPI) linked proteins in the outer leaflet of membranes, as well as other lipid-bound proteins with at least two lipid-anchors, that are more firmly attached and behave more like integrated proteins (see Figure 1)[15,33]. Without those lipid anchors, the proteins would not be able to attach themselves to the membrane surface properly.

1.1.2.2 Integral membrane proteins

Secondly, there are integral membrane proteins (IMPs), that are the main class dealt with in this thesis (see Figure 2). They are typically divided into different types, depending on how and in which direction they are embedded in the membrane and how many times they span it[34,35].

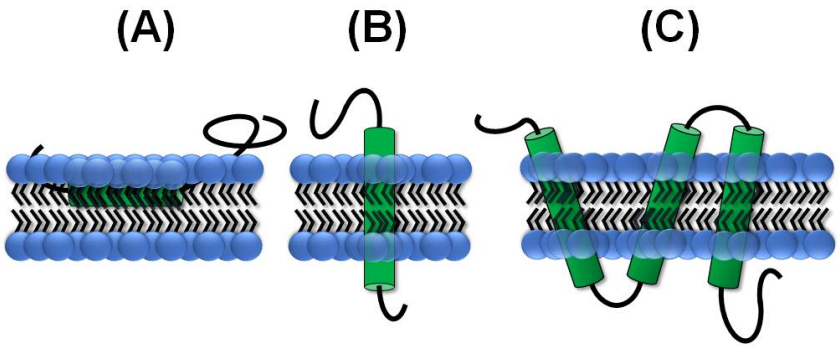

Figure 2: Depiction of different integral membrane proteins; a) monotopic b) single pass or bitopic, where two orientations with N- (type I) or C-terminus outside the cell membrane (type II) are possible; c) multipass or polytopic, considered type III.

Monotopic membrane proteins are embedded without spanning the membrane bilayer through a reentrant domain, entering and exiting at the same site of the lipid monolayer. Even though they are widespread, they only comprise around 0.06 % of nonredundant structures so far[35,36]. Whereas, bitopic integral proteins span the bilayer once with a transmembrane (TM) anchor and may be orientated with their N-terminus (type I) or C-terminus (type II) pointing outside.

They represent the most abundant type of membrane proteins with a plethora of functions, including regulation of cell death[31,37-40], cell adhesion[41,42], and signalling[20,43,44], also transport[45,46], metabolism[47] or immune responses[48,49]. Notable family members are outer mitochondrial proteins of the Bcl-2 family, which are mostly anchored via one single transmembrane helix and which are the focus of this work (See chapter 1.2). Larger and more connected proteins with several TM in a single polypeptide chain that spans the membrane are called polytopic and categorised as type III. In nearly all type III proteins, with determined protein structure, only two different types of protein folds, the α-helices (bound to helical bundles) and the β-barrels[50,51] were found so far. Those two very different folds maximise the proteins hydrogen-bond formation of hydrophilic groups in the backbone, which shields these sidechains from the hydrophobic lipid environment[15,52]. At the same time, both folds allow the hydrophobic groups of the sidechains to engage in hydrophobic interaction with the surrounding membrane and stabilise the membrane proteins. However, α-helical bundles are more hydrophobic and prone to aggregation and are therefore inserted into the inner membranes directly from the translocons, while the more water-soluble β-barrels are secreted to the periplasm, following insertion into the outer membranes[15].

One of the preeminent representatives of the α-helical structural type are the seven-transmembrane receptors (7TMRs) or G protein-coupled receptors (GPCRs) which are a large family of cell surface receptor that detect light[17,53] and bind, e.g. hormones[43], neurotransmitters[44,54] or even molecules responsible for odours[20,55]. They are one of the best-studied membrane proteins since they are so far the most potent drug targets (~34 % of FDA approved drugs)[22,23,55]. GPCRs are also a perfect example of the abovementioned interplay of integral and peripheral membrane proteins, as they bind and activate a peripheral heterotrimeric G-protein unit for further downstream signalling. Two of the subunits, the alpha subunit (Gα) are able to bind reversibly with a lipid anchor (myristoyl, palmitoyl, or both) to the membrane, while the γ-subunit is stably anchored in the membrane via prenylation[56-58].

The β-barrel proteins are usually only found in outer membranes of gram-negative bacteria (except for *Mycobacterium*[59,60]), chloroplasts[61] and mitochondria of eukaryotic organisms[45,62,63], because they have similar properties to prokaryotes and are believed to be assimilated through endosymbiosis[50,51,64-67]. The β-barrel proteins play a crucial role in pore formation and membrane anchoring, translocation of virulence factors or even passive transport of nutrients and ions[45,46,59,60,62,63,68-70]. Except for one protein (VDAC-1), those barrels usually consist of an even number (8-24) of antiparallel β-strands held together via strong hydrogen bonds between the N-H and C=O groups.

Overall, just as helical proteins, β-barrel proteins are also able to form oligomers resulting in even larger pores (porins[71]) that allow passive diffusion, such as the trimeric maltoporin[70] used by Gram-negative bacteria to accelerate the diffusion of maltodextrin through the outer membrane. Such oligomers of several bitopic proteins that interact with each other through their TM domains (α-helical or β-barrel) are called type IV or oligomeric[72].

1.1.3 Challenges of working with integral membrane proteins

Despite significant structural biological advances in the field over the past decades, the process of protein structure determinations is still slowly ongoing. Although they are prevalent and the primary drug targets of interest, integral proteins comprise only 4.6 % of the determined nonredundant structures. So far, as of 04.01.2019, from 147678 solved and submitted protein structures in the PDB database, only 2.7 % are transmembrane proteins, of which 88.8 % are helical, and only 11.2 % are β-sheet proteins. Another fact that highlights how difficult it is to work with membrane proteins and how slowly even modern research is proceeding is that during this work, 24.5 more soluble protein structures were solved than membrane protein ones. The question arises, why even with modern techniques and regardless of extensive worldwide academic and industrial research the amount of growth in the field does not match the effort. In general, membrane proteins are more challenging to express and produce than globular ones and are usually not abundant in their native environment[9,73-75]. They are fixed in a mosaic-type membrane, which in all organisms is a very complex, massive and highly dynamic and heterogeneous environment. Therefore, it is almost impossible to study membranes or membrane proteins *in vivo* with current structural biological methods[76,77]. Consequently, most protein studies and experiments are carried out *in vitro*. Here, also membrane proteins must meet the same requirements for structural biological examinations in terms of, e.g. sample amount, homogeneity, proper folding, function or stability, which is hindered by many challenges. For one, targeting of a folded membrane protein in an expression host is naturally limited to membranes[9,75]. They have a defined space and orientation, but also need to harbour many different host membrane proteins to function. So, obtaining high expression yields without overloading the host is very challenging. Typically, the first obstacle is to find the most suited host system for recombinant (over)expression of the membrane protein of interest[73,78-81]. Applicable are fast-growing and easy to handle bacteria hosts, or simple eukaryotic systems as yeast, to more challenging, expensive and time-consuming insect or human cell lines.

Usually, a more straightforward expression system such as prokaryotic *E. coli*[79-82], or eukaryotic *Pichia pastoris*[83,84] is applicable for a fast and cheap expression of a wide range of medium-sized membrane proteins for homo or heterologous expression. However, their proper folding and further post-translational modifications (PTM) are limited in those hosts. In such cases, where correct disulfide bond formation and complex PTM are necessary, insect[85,86] or mammalian cells[87,88] should be considered[73]. Their drawbacks are high costs, lower expression yields, and complicated and time-consuming workflows. Other alternatives are cell-free expression systems[32,78,89-92], which are convenient for toxic or hardly accessible protein targets with low expression yields, or overexpression of membrane proteins in *E. coli* inclusion bodies[80,93,94]. The latter overcomes the problems of limited space and low yield while sacrificing proper folding and increasing the difficulty of solubilisation.

After finding an expression system, it needs to be optimised, choosing from many different cell lines or strands and testing appropriate conditions. Some proteins, mutants or protein constructs do not express and need to be optimised. This can be achieved, for example, by N- or C-terminal fusion constructs[79,84,95,96]. Such optimised screening protocols and methods exist for protein overexpression in cell membranes or inclusion bodies. However, all these are laborious and empirical iterative steps, making membrane protein research very challenging and time-consuming.

The second challenge is that membrane proteins need to be extracted for *in vitro* studies after their successful expression from their hydrophobic lipid environment in which they are embedded[74,97-99]. However, they are not water-soluble, prone to aggregation and always need to be kept in a hydrophobic environment. This extra step needs to be accomplished without damaging their structure while retaining their activity and function, which makes them difficult to isolate and consequently to purify. A major drawback is that most membrane protein structures and activities depend on other bound proteins, ligands, surrounding lipids, or bound lipid molecules[100-105]. Many of them are not water-soluble or abundant in the host organism and are difficult to substitute, for example, cholesterol[100]. Such interactions with surrounding lipids also influence intermolecular interactions with other proteins or ligands that are hard to reconstruct[102,105-107]. Once a membrane protein is extracted, the membrane is destroyed, and it is not possible to reconstitute it into the same conditions, which may alter structure or function.

1.1.4 Membrane mimetics

In order to overcome the problems of isolating a membrane protein and keeping or reconstituting it in a near-native environment (membrane mimetic), several different techniques have been developed. The method of choice ultimately depends on the envisaged structural biological methods and experiments, which in turn dictate the sample requirements in terms of amount, homogeneity and other prerequisites, including stability and solubility. Usually, experiments are done *in vitro*, so a stable, water-soluble and homogeneous sample is required. The sample should also retain a fairly functional protein with the highest possible amount of native structure[7,11,74,99,108]. However, not all techniques meet those requirements or are applicable to all types of membrane proteins or structure biological methods. Depending on their complexity and the properties of the target, a compromise must be made.

Despite many available and diverse membrane mimetic systems, there are only a few options for extracting and solubilising membrane proteins. Classically, an extraction starts with detergents or other surfactants, potent enough to destroy the integrity of the membrane and solubilise the integrated proteins[74,97,99,108-110]. Detergents have been used for the extraction, purification and characterisation of membrane proteins for more than 40 years[97,110-113]. So far, due to the small sample size, most of the nuclear magnetic resonance spectroscopy (NMR) studies and structure determinations of membrane proteins have been done in detergent solutions. The amphipathic properties of a detergent allow binding to the protein with its hydrophobic tail, while a typically hydrophilic headgroup is pointing outward to the aqueous solution[97,110,112-114]. Above the critical micellar concentration (cmc), the detergent molecule forms ball-shaped multimers with itself called micelles, that are able to enclose hydrophobic lipids or proteins in their hydrophobic core and keep them in solution. Depending on the hydrophobic chain length, headgroup, charge distribution and distance to the chain, detergents are classified as mild or harsh, concerning the conservative influence on the protein structure[97,109,110,112,113]. Detergents with a short chain are considered harsher than one with a long one. Also, ionic ones, such as sodium dodecyl sulfate (SDS), are amongst the harshest[115,116], zwitterionic detergents including CHAPS[115,117] are considered less harsh, while non-ionic detergents such as Triton X-100 are considered mild[74,111,115]. Those different types of detergents exhibit a diverse lipid and protein solubilisation property, so they need to be screened and optimised for each new expression system and protein of interest. Often it is beneficial to solubilise also bound lipids or lipid patches of the native membrane, to retain proper structure and biological function[118,119]. Once the target protein is solubilised and stable in detergent, it is possible to further purify and enrich it via, e.g. affinity- or gel chromatography.

Hereof, different structural biological methods, such as NMR, small-angle X-ray scattering (SAXS), or X-ray crystallography, are feasible to study the protein in a detergent environment[74,99,120]. If the protein is not stable or functional enough in the detergent used for extraction, it can be exchanged to milder ones, to regain its native folding and biological behaviour, or transferred to other more membrane-like systems.

Similar, but less artificial alternatives for a transfer or purification strategy are mixed lipid-detergent micelles[108] that are less harsh and provide a lipid bilayer core. Even more natural are lipid-detergent or lipid-lipid-like mixtures called bicelles[121]. They have been successfully established and used for several structural biological methods, as crystallisation, solution and solid-state NMR[108,121-123]. Their structure consists of long-chained phospholipids mixed with short-chained phospholipids. Due to the short acyl chain, the latter is the detergent-like component, that helps to close the edges of the bilayer and is even able to extract and solubilise IMPs from their native membranes directly. They are moderately stable, more comfortable to handle than some detergent systems, and there are many versatile and tuneable compositions possible. However, their size heterogeneity and the limited possible combinations of compounds limit their use. A bigger and purely lipid-based system are spherical lipid bilayer particles called vesicles that enclose an aqueous phase in their core and resemble a condensed and empty cell[108]. Despite their increased size, in contrast to detergents, they are used for IMP crystallisation, fluorescence-based methods, or solid-state NMR, where larger particles are not detrimental[124,125]. The size distribution and inhomogeneous nature of large unilamellar vesicles (LUV) (larger than 100 nm) limit their application in other structural biological methods. Therefore, smaller unilamellar vesicles (SUV) between 20 to 100 nm are prepared, to gain minor particles with a more tuneable size (See Chapter 3.1.8). However, liposomes are very unstable and have a shelf life in the range of hours to one day, which only makes them applicable to fast biochemical methods and measurements. Another lipid-based method used mainly in the protein crystallisation field is the lipidic cubic phases (LCP) technology[126,127]. It has proven to be very useful and more advantageous than bicelles or vesicle-based crystallisation. The lipidic cubic matrix, consisting of water, lipid and protein, forms connected three-dimensional pores and channels. These allow diffusion and nucleation of different types of IMP.

Recent advances in the field over the past decades resulted in novel synthetic amphipathic substitutes for detergents, that allow a detergent-free extraction or handling of sensitive IMP, and also enable to skip the problem of reconstitution in more natural systems. Peptide-based lipophilic examples have been designed, including lipopeptide detergents, peptitergents or short peptide surfactants, but have not gained broad acceptance so far.

In recent years, a styrene maleic acid (SMA) copolymer-based system has been found to be a useful detergent replacement, which forms styrene maleic anhydride copolymer-lipid nanoparticles (SMALPs) when added to lipids or membranes[98,124,128]. Patches of membranes with incorporated IMPs and partner proteins are extracted and can be studied in solution. The method was even improved using non-UV absorbing diisobutylene/maleic acid (DIBMA)[129] or other copolymers[130,131], which is also less prone to precipitation due to divalent cations than SMALPs are. Still, these two systems suffer from drawbacks of large artificial polymers that comprise most of the structure and often yield large and heterogeneous size distributions[124]. Additionally, the polymer to membrane lipid ratio in those systems is vast, ranging from 1:4 to 1:10, if smaller sizes of 12 to 20 nm are required.

Synthetic amphiphiles of smaller molecular weight have been developed, such as hemifluorinated surfactants (HFS)[132,133] and others based on, e.g. cholic acid[134] or maltose–neopentyl glycol (MNG)[135]. They have been shown to stabilise IMPs and are useful for several biochemical studies, but their scope of applications and their current numbers are limited. So far, there are no versatile and well-engineered synthetic detergent or surfactant replacements available that are suitable for different types of IMPs. Therefore, amphiphiles are not generally accepted and found in recent biochemical studies.

One exception in terms of utilisation and mode of action are amphipols[132,133,136]. These short and water-soluble polymers have numerous hydrophobic side chains that allow a direct, but a non-covalent association with the transmembrane surface of integral membrane proteins, very similar to SMALPs. This way, they are able to wrap around the target and keep it water-soluble and stabilise them in the absence of detergents. Unlike detergents or SMALPs, the non-covalent but strong nature of bonding allows strictly irreversible associations, until displaced by other surfactants or detergents. This artificial system has a few advantages compared with detergents, such as higher stabilisation and solubilisation properties of IMPs, but is highly artificial and lipid-deficient, making it as non-native as detergents themselves. This system is useful in case the IMP is prone to precipitate or is hard to handle in detergent environment.

Another peptide-based tool is the saposin lipid nanoparticle or saposin A lipoprotein discs (Salipro)[137-139]. They are not meant to be a replacement for detergents, but an independent membrane mimetic system. Saposin peptides have soluble and lipid-bound states and are therefore considered membrane-active proteins. This ability allows them to associate to lipids or membrane bilayers and wrap around them, encapsulating a small membrane patch with associated IMPs. Recent studies have found four different saposins (A, B, C, D)[138] with different lipid binding affinities, of which saposin A has proven to be the most versatile.

The formed saposin A lipoprotein discs incorporate and solubilise different classes of lipids, such as cholesterol, phospholipids, sphingolipids in small-sized (27 kDa) and monodisperse particles. However, their lipid-bound state forms discontinuous structures and “belts” around the membrane patches, resulting in heterogeneous particles with distorted globular shapes and gaps between the proteins. Also, they do not hinder oligomerisation of the integrated target protein, leading to several different sample species that may change or oligomerise spontaneously. Due to the low amount of bound lipids, interactions between the saposin A belt and the inner IMP are possible, that could lead to artefacts and structural changes. Overall, compared to SMALPs, they are less prone to precipitation, stable at low pH and can yield small particles, e.g. for NMR structural studies, but not homogeneous ones. Until now, only two labelled proteins have been studied with NMR, OmpX and turkey β_1-adrenergic receptor (β1AR)[137]. In future, the tenacity and utility of this relatively new tool still need to be explored.

1.1.5 The Nanodisc technology and recent advances

Since their discovery[140] in 2002, the phospholipid nanodiscs, see Figure 3, are one of the most used and well-studied new platforms for studying membrane protein structure and function in a near-native environment. The employed nanodisc is a membrane mimetic system that is a small, well-defined discoidal bilayer, based on high-density lipoprotein (HDL) particles[101,141-143], with 10-12 nm in diameter[144]. It is typically composed of two copies of an amphipathic protein that are non-covalently wrapped around a phospholipid bilayer patch which can be premixed in any required composition[140,144-147]. The “belt-protein”, termed “membrane scaffold protein” (MSP)[140,144], is derived from the 243 amino acid long Apolipoprotein A-1 (Apo A1), the main protein component of HDL[148,149]. In nature, HDL particles serve as a lipid and cholesterol uptake and transport system in the body, capable of binding and solubilising up to a hundred of lipid molecules, which made them an interesting system to investigate. Early studies by Jonas *et al*.[101,141-143,150,151] and later by Stephen G. Sligar *et al*.[150,152,153] on formation and characterisation of lipoprotein discs with Apolipoprotein A-1 yielded very heterogeneous assemblies of discoidal particles. In order to obtain monodisperse and homogeneous samples for further experiments, the protein-belt needed to be redesigned, removing all parts not being part of the belt which wraps around the lipid molecules and therefore not contributing in the formation of the discoidal particles[140,144,154].

The genetic engineering resulted in the mainly helical protein MSP1 that consists of a string of 10 amphipathic α-helices without the globular N-terminal domain (residues 1-54)[144,155] of native Apo A-1[140,146].

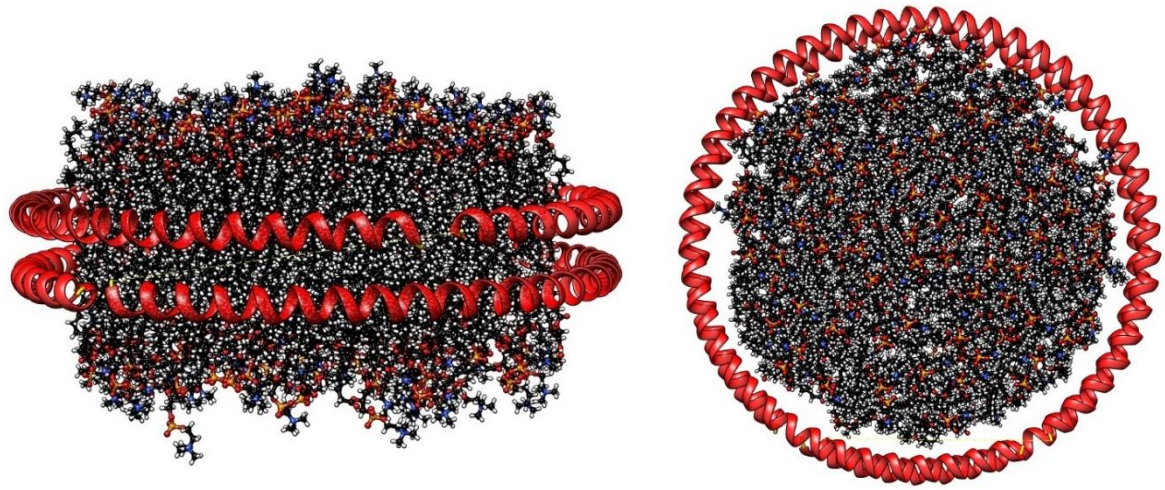

Figure 3: 3-D representation of nanodiscs made by Franz Hagn. Side view (left) and on the right the view onto the nanodisc from the top. The membrane scaffold protein (MSP) belt, consisting of two copies of MSP protein, is depicted in red, the open ends are marked in yellow. The lipid bilayer inside the disc is coloured according to the heteroatoms of each lipid. Phosphate groups and nitrogen-containing headgroups are on the surface of the bilayer, in orange-red or blue, respectively.

Newer findings from Pourmousa *et al.*[156] (2018) from molecular dynamics simulations (MDS), molecular modelling, and cross-linking experiments confirmed the double-belt structure of nascent HDL particles. They could even explain and show the mechanism behind their formation. Recent structural analysis of nanodiscs and the MSP by Bibow *et al.*[157] (2017) with NMR, electron paramagnetic resonance (EPR) and transition electron microscopy (TEM) resulted in the first three-dimensional structure of the MSP double belt. A shortened version, missing the 5th helix (MSPΔH5)[158], was used to study the structure and the rearrangements that take place upon the formation of the discs and compare them to the published X-ray structure[159] of lipid-deficient MSP in solution. It was found, that the double belt in a nanodisc is formed in an antiparallel fashion, by a slightly bent MSP facing the lipids with its hydrophobic residues, while 28 salt bridges are stabilising the protein dimer (PDB: 2N5E). Additionally, a very stable zipper-like formation of cation-π interactions between helix four and six helps to maintain the integrity of the structure and proves to be a vital component. For this formation and lipid binding, a structural rearrangement needs to take place, where the helices of soluble MSP and their buried hydrophobic rotate towards the lipid's bilayer. Overall, the formation of nanodiscs is based on the strong tendency of phospholipids to form bilayers and on the stability gain of MSP amphipathic helices due to interaction with hydrophobic lipid acyl chains and additionally because of the mentioned homo-dimerisation rearrangement.

This yields a discoidal bilayer system that harbours up to 100 lipid molecules, as known from HDL particles, and proves the existence of the MSP homodimer double-belt. Empirically determined stoichiometry of phospholipids allowed creating monodisperse discs of controlled size, that were even able to incorporate integral membrane proteins of interest, which were added to the assembly mixture[86,140,160]. A target IMP may be added to the assembly in detergent solution or any lipid-detergent based system of choice. Depending on the size of the incorporated protein, the employed MSP and the lipids of choice, the lipid to MSP ratio[144,154,158] and the protein to MSP ratio need to be adjusted[86,140,144,160,161]. The following formation of nanodiscs is a self-assembly process that starts once cholate or other detergents, necessary to solubilise the lipids or the target IMP, are removed[140,144]. This process may be completed through detergent removal via, e.g. dialysis[141], detergent precipitation, or the addition of hydrophobic and small polystyrene beads called “biobeads” (BB), which is the most common method of choice[162-164]. The resulting miniature model membranes are with of a user-defined composition, tuneable in shape and size, monodisperse and water-soluble. Like bicelles or liposomes, they resemble a native bilayer, but are more stable, homogeneous and in contrast to those systems, controllable in size. Engulfed target membrane proteins stay in solution and can be further analysed and studied in a native-like environment, like with SMALPs or saposin A discs. However, compared to those model systems, nanodiscs have superior physicochemical properties and can be subjected to several modifications. They are very temperature stable, also for extended periods of days or weeks. This is due to the fact that the MSP-belt starts to melt at 80-85 °C, which is sufficient for common biochemical analysis methods[158,165,166]. Nanodiscs may be used for e.g. week-long NMR experiments at higher temperatures[158,166], long-term fluorescence spectroscopy[167,168], or cryogenic electron microscopy (cryo-EM) measurements[102,169,170]. Another advantage to previously mentioned systems is the wide range of possible buffers that can be employed, for example, with different divalent or monovalent ions, reducing agents, or native pH ranges, which makes them a very versatile system. Compared to liposomes or detergent samples, their shelf life in aqueous buffers is extremely high. Finally, the ability to freeze or freeze-dry them enable long-term storage, safe packaging and shipping of samples and demanding applications, like mass spectrometry of full-length proteins in a lipid environment[171]. The drawback of the nanodisc system is the impossibility of simultaneous detergent use in concentrations beyond their cmc, or high content of organic solvents, making, e.g. addition of ligands or partner proteins solved in high detergent concentrations or organic solvents difficult. Once a target IMP is embedded in a nanodisc, the extraction and reconstitution in another membrane mimetic can be challenging. Recent advances in using nanodiscs in different applications and structural biological methods have been made[163,164,172,173].

One of them is engineering and fine-tuning of MSPs, changing their size and properties to accommodate sample needs or broaden the scope of the nanodisc system[154]. Our group and collaborators contributed to said process[158,165,166,173]. In 2013, Hagn *et. al*[158] established newer, modified versions of MSP by deletion or addition of helices, which made it possible to create even smaller or bigger discs and fine-tune their size, according to the chosen target or method. Depending on the length of the MSP construct, for example, the shorter MSPΔH5 with a deleted helix 5, the size of the nanodisc is decreased, making it accessible for solution NMR and incorporation of small monomeric proteins. Additionally, covalently circularised MSPs (cMSP) were developed to increase the homogeneity of the size-distribution and the overall stability of the system, as especially smaller discs tend to open due to higher strain on the belt[165,166]. Different new methods, from Sortase A ligation (see chapter 1.1.6.2) by Nasr *et al*.[165] (2017), to split-intein based methods by Miehling *et al*.[166] (2018) were recently developed for this purpose. The result are enzymatically ligated[165], or in the latter case *in vivo* self-ligated through self-splicing[166], covalently fixed MSPs, which creates the opportunity for a new class of more stable nanodiscs with a fixed size, with even better physicochemical properties. The Sortase A mediated ligation method also produces larger MSP constructs of several MSP linked together, creating a new class of large to very large nanodiscs. Adding affinity tags, from his-, biotin-, to FLAG-tags, or introducing cysteines to the MSPs for site-specific labelling is another possibility to alter the MSP, and therefore the nanodiscs, and improve their purification, labelling and make even high-throughput screening possible[154,158,163]. For some protein-based applications, however, the contribution of the nanodisc belt can be hindering and therefore further “invisible” MSPs were created. The UV-Vis absorption of MSP was negated with the engineering of “dark” MSP[174], where the two tryptophan residues were exchanged for phenylalanine. By further changing MSP and the phospholipids through isotope labelling, MSP and therefore nanodiscs become invisible in small-angle neutron scattering (SANS) experiments, where only the integrated protein is of interest[175,176]. In recent years, nanodiscs have been successfully used for studying IMPs by, e.g. NMR[158,165,173], SAXS and cryo-EM and have proven to be very useful in this field[163,164,170,172,177]. Their application in NMR and cryo-EM protein structural characterisation has gained popularity and significance, and their constant adaptation and improvement are ongoing.

Recent high-quality NMR-structures of several proteins in or on nanodiscs have been published[178]. However, their application in X-ray crystallography still needs to be tested and advanced, and there is still a need for improvement of the nanodisc system.

1.1.6 Membrane protein methods

1.1.6.1 Asna1/Get3

Tail-anchored (TA) proteins have a single C-terminal TM domain and a cytosolic N-terminal domain[179]. Their transmembrane region is vital for post-translational insertion into the membrane of the endoplasmic reticulum (ER)[179,180]. Since they comprise around 5 % of all membrane proteins[181], govern several biochemical activities and do not access the standard co-translation pathway, their targeting and insertion pathways have been studied extensively in recent years[182,183]. It has been found that in eukaryotes a highly conserved 40 kDa ATPase TRC40/Asna1 recognises and binds selectively to the TM domain of tail-anchored proteins, once they are translated and released into the cytosol[183-185]. This soluble complex then targets to membrane receptors and partner proteins at the ER, where the cargo is released and inserted with its TM into the membrane. The possibility to employ this native system for selective *in vitro* membrane insertion of recombinant Asna1/TA protein complexes and ER-derived membranes has been successfully tested[183].

Studies found that the ATPase mediates membrane insertion of two test proteins (RAMP4 and Sec61beta) without the need for additional cytosolic partners. The mechanism *in vitro* and *in vivo* was shown to depend on ADP or ATP, but also a protease-sensitive receptor in isolated ER membranes. In the RAMP and Sec61beta study, Asna1 has been shown to be useful as a co-expression partner protein, similar to fusion proteins, for the successful expression and purification of insoluble TA proteins. Further insertion test with artificial membranes or membrane mimetics or large-scale expression and purification of hardly accessible TA target proteins have not been reported so far. An analogous system revolving around the ATPase Get3 (Figure 4) has been discovered in yeast[181,186,187]. Through crystallisation and X-ray structural studies, several different structures in ADP-bound or nucleotide-free conformation have been solved in good resolution[181,187]. Both forms show a Zn^{2+}-dependent head-to-head homodimer in an open conformation. Further cross-linking experiments suggest a TA-protein realising and ATP-hydrolysis dependent closed structure. Also, a mechanism that mediates the insertion of the cargo by a DTAPTGH motif was proposed, identifying vital aspects of this complex process and possibly the analogous eukaryotic one.

Recently, several structures of Get3 dimers with cargo were obtained through antibody-mediated crystallisation (one example in Figure 4)[188].

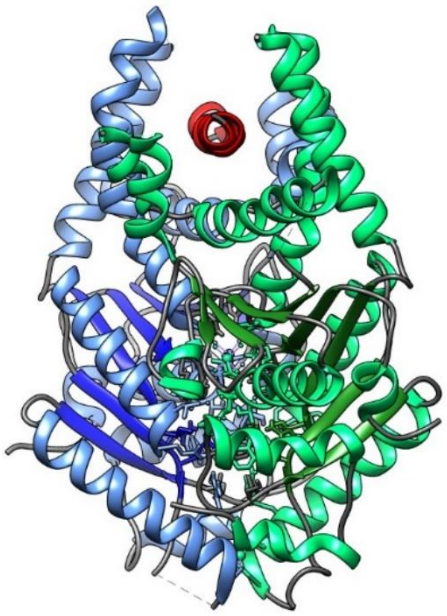

Figure 4: X-ray structure of a dimeric *Saccharomyces cerevisiae* Get3 complex, each monomer in blue and green, with the transmembrane domain of Pep12 in red on the top (PDB 4XTR)[188]. Antibody fragments were removed for clarity and β-structural elements were coloured darker than the helical one. Both helical parts of each monomer (top) hold their cargo like a pincer.

More recent investigations proteins in *Saccharomyces cerevisiae* revealed a more complex system involving two other (Get4 and Get5) partner to form a large complex with two Get4-Get5 heterodimers in solution[189,190], that target the ER and bind to membrane-bound receptors Get1 and Get2[186,191]. Generally, the system is well-behaving and more robust for structural biological studies and *in vitro* tests, than the eukaryotic TRC40/Asna1 analogue. In several years, structural and functional information was obtained, and individual roles of several components of this system have been assigned, which makes it a valuable test system to understand and study the *in vivo* and *in vitro* membrane insertion of tail-anchored proteins[181,182,186,187,189-194].

1.1.6.2 Sortase A mediated ligation

Sortases are a family of selective transpeptidases that anchor specific secreted proteins and assemble pili to Gram-positive bacterial cell surfaces and walls, including a variety of virulence factors of bacterial pathogens[195-197]. Their function thereby is to recognise a highly conserved LPXTG cell-wall sorting signal motif, found in the C-terminus of the target protein, and attach it covalently through a peptide bond to a nucleophilic N-terminal group, typically a glycine[195-198].

Therefore, Sortases are potent targets for new inhibitory and antimicrobial drug developments[199,200]. Their structure and function have been investigated thoroughly to understand the mechanisms of catalysis and specific substrate recognition.

A crystal structure of the pathogen *Streptococcus pyogenes* Sortase was solved, and transpeptidase activity tests were also established *in vitro*[196]. The findings offer a better understanding of the active site and all involved amino acids, showing an involved cysteine that forms a highly reactive thiol-ester intermediate. Additionally, the structure of Sortase A (SrtA) of *Staphylococcus aureus* was solved by trapping the enzyme in its catalytic intermediate, offering additional information about the mechanism, which is depicted in Figure 5[195,196]. This was done by synthesising an LPXTG analogue which forms a covalent complex with SrtA and mimics the thioacyl-based intermediate step. Further NMR-based[201,202] studies improved the structure determination and showed an eight-stranded β-barrel core with a long hydrophobic pocket. It was demonstrated, that SrtA recognises the LPXTG sorting signal through a large groove leading to the active site and binds it by closing and immobilising a loop.[195,196,203] In the first step, as seen in Figure 5, the enzyme recognises and binds the LPXTG recognition motif by breaking the T-G bond and forming a highly reactive thioacyl-linked protein-Sortase intermediate (LPXT-SrtA) through its cysteine (C184), with the help of the other two conserved H120 and R197 in the active site. In the second step, an N-terminal nucleophile, pentaglycine cross-bridge in the staphylococcal cell wall, attacks the thioacyl and the protein-T-GGGGG are attached covalently through a newly formed peptide bond, while the Sortase A is released and reduced back to its previous state.

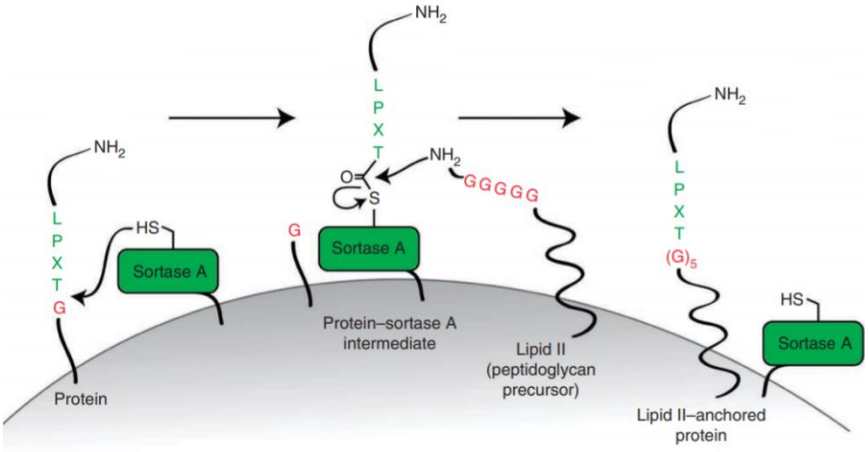

Figure 5: Mechanism of Sortase A ligation: 1) LPXTG-motif recognition and attack of the Sortase A cysteine 2) Formation of thioacyl-intermediate and subsequent attack of a free N-terminal Glycine, leading to breaking of thioacyl-bond and formation of a new stable peptide-bond 3) Ligated product and released Sortase A. Adapted from Guimaraes *et al.*, Site-specific C-terminal and internal loop labelling of proteins using Sortase-mediated reactions, Nat Protoc, 8, 1787-1799 (2013) with permission[204].

To employ this *in vitro*, reducing agents and glycine-rich motifs are used[205-207]. Further studies *in vitro* and *in vivo* of Sortase A found that it is a highly reactive and specific extracellular membrane-bound transpeptidase, easy to modify and study by a variety of different methods. Therefore, it became one of the most popular and well-studied Sortase enzymes[204,207,208]. The ligation is ATP independent and does not require any artificial target modifications, except for the LPXTG recognition motif, which can be added to either ligation-half and is independent of the residual protein sequence. One natural cofactor is Ca^{2+}, which stabilises the substrate binding-site and is beneficial for the reaction and increases the coupling yield through allosteric activation[209].

In recent years, SrtA-mediated protein ligation has been widely used for a plethora of protein modifications and tagging[207,210,211]. They include from N- and C-terminal site-specific labelling[212], the coupling of probes (e.g. biotin, fluorophores[213], carbohydrates, lipids), to multi-domain ligations of large complexes[214]. The enzyme was also used for NMR-based structural biological studies, to achieve selective segmented isotope labelling of multi-domain proteins[214]. In 2011 the Sortase A enzyme was greatly enhanced by Chen *et al*.[203] using it as a test system for a directed evolution strategy of bond-forming enzymes. In their study, the enzyme was evolved and screened for better catalytic activity through eight cycles of enzyme-mediated bioconjugation and fluorescence-activated cell sorting (FACS) in a yeast display. The resulting evolved Penta-mutant Sortase A (5M) was found to have five specific mutations (P94R, D160N, D165A, K190E, K196T) resulting in a 140-fold increased LPETG-coupling enzymatic activity.

Further screenings carried out by the same group in 2014 resulted in new Sortases that recognise two new specific LAXTG and LPXSG motifs, which can be utilised orthogonally and allow the simultaneous ligation of different substrates to their individual partners in one step[215]. Two further mutations E105K and E108A in the calcium binding-pocket have been further introduced, creating a calcium-independent hepta-mutant (7M), negating the problems of excessive calcium use during the ligation, which can be harmful to detergents or the ligation targets[209,216-218]. With these optimisations, there is no longer need for elevated reaction temperatures (37-42 °C) and long reaction times of several days, which can lead to unfolding and the destruction of the target protein structure and its stability. Also, the efficiency is highly improved, and therefore, the amount of proteins and enzyme required is reduced. Several recent *in vitro* techniques have been developed to push the possible ligation yields even more, for example, Ni-affinity-based ligation enhancement[219] or flow-based systems[205,206].

1.2 Bcl-xL and apoptosis

1.2.1 Cell Death and Bcl-2 Family members

What is it that tips the scales between life and death, and what ultimately determines the fate of a cell and possibly a whole organism? In most cases, broken down to a cellular or molecular level, the decisive factor can be just a small protein or its interplay with partner proteins in the cell[31,37-40,220,221]. Cell death can be categorised into two main classes: the uncontrolled and harmful necrosis and the tightly regulated programmed-cell death termed "apoptosis"[221,222]. For the latter, at least two such life-determining pathways were identified, that allow a regulated control of cell homeostasis and function. They can be categorised as extrinsic or intrinsic pathways**,** depending on the origin of the initiation signal and the protein machinery involved[221,223-225].

One of the leading protein families that orchestrate and initiate the intrinsic pathway is the B-cell lymphoma 2 (Bcl-2) protein family (Figure 6)[38,226,227]. The Bcl-2 family of proteins has been well-studied since the discovery of their first and founding member Bcl-2 in B-cell lymphomas 30 years ago. This led to the pursuit of other related partners and functionally similar proteins which is still ongoing[39,228,229]. So far, at least 20 proteins and several of their isoforms (created by alternative splicing[230]) were identified, creating the family of Bcl-2-like proteins, depicted in Figure 6[38,227]. It has been found that at least 12 of the known family members are tail-anchored with a TM domain either to the mitochondrial outer membrane (MOM) or endoplasmic reticulum (ER)[231]. They all share between one and four very similar, highly conserved structural domains called Bcl-2 homology (BH) domains (see Chapter 1.2.3). Though there are significant differences in some amino acid sequences throughout the Bcl-2 family members, their BH domains lead to a high structural homology of their globular folds, often referred to as the Bcl-2 core. A special category are a few pro-apoptotic proteins that contain just one BH3 domain, called "BH3-only" proteins (see Chapter 1.2.5), which has also been found in every other pro-apoptotic protein member so far[227,232-236].

While the numbers of Bcl-2 proteins and one of the interacting partners is continuously growing, a complex network and interplay of structurally similar proteins are revealed. This network is divided according to its two functions to induce (pro-apoptotic) or hinder (anti-apoptotic) the intrinsic apoptosis. It controls this tightly regulated, gradual cell death by either preventing or initiating the mitochondrial outer membrane permeabilisation (MOMP) through protein-protein interactions, which above all leads to the release of cytochrome c from the mitochondria[234,235,237].

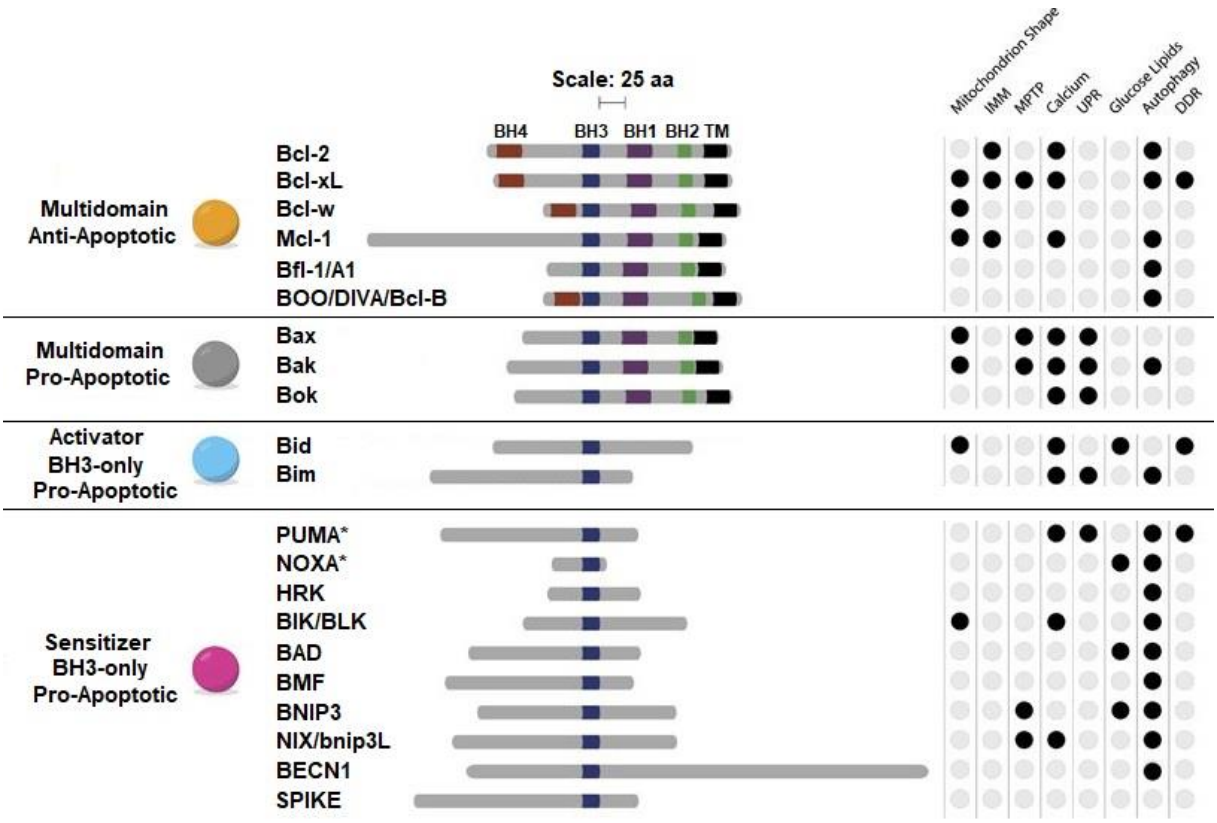

Figure 6: The classification of Bcl-2 Family of proteins, divided by apoptotic function and type. From top to bottom: multi-domain anti-apoptotic in yellow, multi-domain pro-apoptotic in grey, activator BH3-only pro-apoptotic in blue and sensitiser BH3-only pro apoptotic in purple. * Indicates BH3-only proteins which could also directly act as pro-apoptotic activators, supported by recent evidence. The size of the proteins and their type and number of BH-homology domains are indicated in the middle, additional transmembrane segments are indicated in black. In the right scheme indicated with dark circles are additional or alternative functions supported by recent evidence and studies. Adapted with permission from Gross, A. & Katz, S. G. Non-apoptotic functions of BCL-2 family proteins. Cell Death Differ 24, 1348-1358 (2017)[238].

It was shown, that cytochrome c deficient cells are resistant to intrinsic apoptosis and cannot activate other caspases, which are necessary for the process, making it the critical player [235,239]. The MOMP can be induced through several theorised pathways, on which there is a consensus, based on recent structural biological and *in vitro* studies.

Generally, MOMP happens if the anti-apoptotic proteins, as Bcl-2 or Bcl-xL, are inactivated or their function is blocked. This can happen through binding of blocking, so-called “sensitiser” BH3-only proteins (e.g. BAD) and if anti-apoptotic proteins are outnumbered through pro-apoptotic overexpression (rheostat model). Another possibility is that already preformed heterodimers of anti and pro-apoptotic proteins are dissociated through a competitive binding mechanism by binding of BH3-only sensitisers[38,40,227,234,240-242].

The latter would either release the previously bound pore-forming pro-apoptotic proteins from, e.g. Bcl-xL or Bcl-2, starting the pore-formation cascade or release bound BH3-only activators[241,242].

The other mode of action is that pro-apoptotic pore-forming proteins, such as Bak (Bcl-2 antagonist killer 1) or Bax (Bcl-2-associated x protein), are directly activated by BH3-only proteins (activators) or other already activated Bak and Bax ones[243], that have an exposed BH3-domain (see Chapter 1.2.4)[237,243-246]. This triggers their homodimerisation, following the formation of large oligomers that form lines, pores, and ruptures in the MOM, releasing its inner content[227,234,236,246,247]. It is assumed that once started this process cannot be reversed, as anti-apoptotic proteins are not able to disrupt formed oligomers or pores. The majority of these interactions, cascades, and mechanisms occur at or in the MOM[227,248] and depend on a lipid bilayer[241]. It has been shown that the membrane enables and facilitates changes in the Bcl-2 family, such as structural rearrangements and shifting binding affinities, which has a direct effect on the MOMP[241,249-251]. The release of the mitochondrial inner content allows cytochrome c to exit and bind to Apaf-1 in the cell and create a large apoptosome, which triggers further caspase activations and downstream events that lead to the controlled death of the cell[30,38,220].

In consequence, the Bcl-2 proteins and the inherent balance they gain from their network of interactions with each other can ultimately decide the fate of a cell. An imbalance, triggered by different stress signals or toxins, in favour of its pro-death family members, including Bax, Bak, BID, PUMA, leads to an induction of apoptosis. A shift of the equilibrium to cell-protective and anti-apoptotic proteins, e.g. Bcl-2, Bcl-xL, Mcl-1, Bcl-w, leads to overprotection from external or internal apoptotic stimuli, for example, nutrition or growth factor deficiency, DNA-damage, γ-radiation, and chemotherapy. Now, this overprotected cell is able to “cheat death” by shielding itself from the final effects and consequences of cellular stress and damage. If further mutations accumulate in this resilient cell, which leads, e.g. to uncontrolled growth or loss of communication with neighbouring cells, it may result in a very resistant and uncontrollable neoplasm, or even cancer[225]. Unsurprisingly, a defect of the apoptotic machinery has been found in over 50 % of human neoplasms[225]. Additionally, more than 85 % of follicular lymphomas have already been linked to translocation and overexpression of the Bcl-2 gene[252]. Such cancer types are therefore capable of avoiding a variety of cytotoxins, chemotherapeutics, and even advanced specific drug targeting, as the intrinsic pathway of apoptosis is then blocked. Their investigation and the search for their cause 30 years ago has led to the discovery of the Bcl-2 gene and the first link between Bcl-2 and tumour neogenesis.

While looking into the cause of follicular lymphomas, a gene translocation from chromosome eighteen to fourteen t(14;18) was commonly found[39,228,229,253,254]. It was shown that the Bcl-2 gene (18q21.3) is translocated to the immunoglobulin heavy chain (IGH) transcriptional enhancer, causing substantial overexpression[39,255]. In most cases, this is the primary event for tumorigenesis and as described, significantly increased anti-apoptotic Bcl-2 protein levels lead to resilient B-cells with a decreased sensitivity to apoptotic stimuli.

1.2.2 Bcl-xL structure and function

The human Bcl-x gene was discovered in 1993 by Boise *et al*.[256] together with two different isoforms (due to alternate splicing) with opposing functions, the 233 amino acid long (26 kDa) anti-apoptotic Bcl-xL (B-cell lymphoma-extra large) and the pro-apoptotic Bcl-xS. It was found that Bcl-xL shares about 45 % sequence identity with Bcl-2, but just 18-25 % with the folded multi-domain pro-apoptotic proteins. Therefore Bcl-xL has a very analogous structure and fold as Bcl-2[257] and inhibits apoptosis in a similar fashion[258,259]. Whereas Bcl-xS is missing its BH1 domain (residues 127-188 of Bcl-xL), making it the first pro-apoptotic protein with a fully conserved BH4 domain. A third distinct isoform and splice variant termed Bcl-xβ was found with modifications in the last 45 amino acids of Bcl-xL[260].

The structure of the apo soluble Bcl-xL domain, lacking the C-terminal helix Nr. 9 (α9), was solved by X-ray and NMR in 1996 by Muchmore *et al.*[258] and was the first structure of a Bcl-2 family protein soluble domain (Figure 7). It consists of a total of eight α-helices and a ~60 residue long and unstructured loop between helix α1 and α2. The centre bears two antiparallel and highly hydrophobic helices (α5, α6) surrounded by amphipathic helices α1, α2 and α7 on the one side, and α3 and α4 on the other, shielding this globular and solvent-accessible hydrophobic arrangement. Before helix α1 was identified as the BH4 domain of Bcl-xL, it was thought to stabilise the overall structure and fold[258].

More recent structural analysis and descriptions see helix α5 as a pivotal point and argue that all other helices are arranged around it, as depicted in Figure 7 on the right[261,262]. The resulting globular protein of highly homologous α-helical bundles comprises all 4 BH domains (BH1 parts of α4-α5, BH2 in α7-α8, BH3 in α2 and BH4 in α1)[234,258,263]. This unique fold (more recently termed “Bcl-2 core”[234,261,262]) is shared by anti-apoptotic Bcl-2 proteins and also pro-apoptotic Bak and Bax. It reveals a hydrophobic cleft, formed by BH1 and BH3-domains (α2-5) and capped by BH2 (mainly α8), referred to as the Bcl-2 family “BH3 binding groove”.

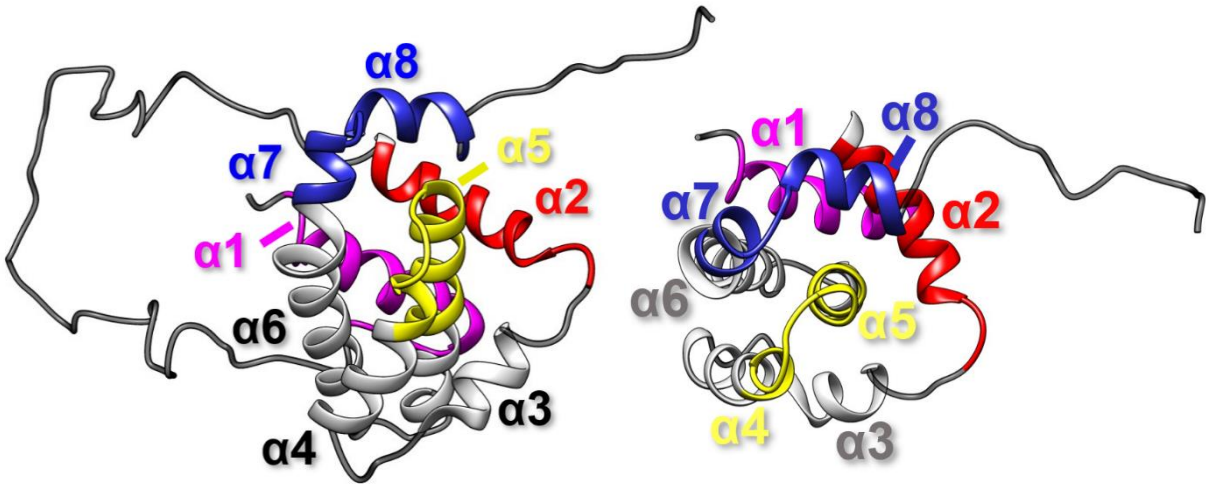

Figure 7: Depiction of the first NMR structure of a Bcl-xL without C-terminal helix α9, from PDB 1LXL[258]. The four BH domains are highlighted, BH1 in yellow, BH2 in dark blue, BH3 in red, lastly the BH4 (which was not determined at that point) in magenta in the background. Unstructured regions, as the flexible loop on the left and the C-terminus on the top are coloured in dark grey. On the right is the top view onto the α5 helix, part of BH1 in yellow. The flexible loop is deleted for better visualisation. The central position of α5 in the protein structure is clearly visible.

Remarkably, for Bcl-xL more parallel and tight arrangement of α3 and α4 has been found, whereas, for all other anti-apoptotic proteins, they adopt a V-shape[263]. This binding groove of, e.g. Bcl-2 and Bcl-xL, cannot only bind BH3-domains of pore-forming Bak and Bax and hinder them from oligomerising. It is also capable of binding sensitiser and activator BH3-only proteins, sequestering them and hindering a subsequent de-repression of other anti-apoptotic proteins, or in the latter case, direct activation of Bak or Bax (see Chapter 1.2.4). It was shown in the determined 3D-structure of Bax and Bcl-w, that their respective C-termini (α9) (membrane anchor) bind to their respective BH3-grooves and are thought to modulate their affinity for other Bcl-2 proteins, the membrane and in the case of Bax for its dimerisation[264-266]. It was also demonstrated, that the BH3 binding-affinities of Bcl-xL or Bcl-w are increased without the membrane anchor, which suggests that it shields the groove in both cases[265]. Furthermore, their transmembrane helix is thought to be released once in contact with the membrane or after activation by, e.g. BH3-only proteins, following a structural rearrangement, similar to that of Bax or Bak[234,261,263].

Though Bcl-2 and Bcl-xL exhibit nearly the same function in the cell, variances between both proteins in sequence and structure elucidate differences in their characteristics and their different binding affinities for BH3-only proteins[227,267].

So far, as only C-terminal truncated or mutated versions were studied, no full-length X-ray or NMR structures are available of Bcl-xL. Therefore, it is hard to predict how the native full-length structure would look like and how the highly hydrophobic α9 is arranged and possibly shielded from water exposure.

For biological assays or partner-protein binding studies, the truncated version has proven to be functional *in vitro* and in whole-cell assays[250,268], but the biological role and structure of the anchor remains unclear. Studies with Bax-Bcl-xL chimeras, e.g. containing the Bax soluble-domain with the Bcl-xL-TMH, showed that the helix of Bcl-xL is responsible for its membrane location[264]. Differences in α9 sequence and resulting structure, or lack of it, seem to influence the distribution and structure of the protein also for Bcl-2 and Bak, but its function in apoptosis is not clear. Removing the C-terminus of Bcl-xL results in a functional protein in whole-cell assays. However, binding to BH3-only proteins was found to be easier to disrupt by BH3-mimetics, and binding kinetics were altered[250].

Furthermore, most of the Bcl-2 family interaction studies also used peptides of the BH3-regions, instead of the full-length proteins (see Chapter 1.2.4). The experiments are typically performed at very high, physiologically irrelevant, concentrations and in the absence of membranes, or native lipids. This often leads to imprecise results and problems in defining the fundamental mechanisms of the Bcl-2 family proteins.

In functional studies with human breast cancer lines and mouse fibroblasts it was found, that Bcl-xL is about ten times more potent in inhibiting apoptosis in cells, that are exposed to identical cytotoxic stimuli, than Bcl-2[267]. Depending on the Bcl-xL location (either ER membrane or MOM) it showed qualitative and quantitative differences, compared to Bcl-2 and advanced responses to different kinds of drugs or stimuli. These findings, amongst others, attribute further mechanisms of action to Bcl-xL, which are not shared by Bcl-2. One of the mechanism differences is that Bcl-xL binds Bak and sequesters it, while Bcl-2 is not able to interact with one of the main two pore-formers[269]. Unsurprisingly, both proteins exhibit resistance to several chemotherapy agents and therefore their overexpression, especially for Bcl-xL, is generally associated with a poor prognosis in human cancer diagnosis[267,270-274]. Inactivating them and possibly other anti-apoptotic proteins, through mimicking the BH3-binding, has proven to be a successful strategy in fighting cancer and supporting chemotherapy against resistant tumours[232,273,275,276].

1.2.3 The function of the BH domains

Initially, through analysing and studying the sequence and later the structure of Bcl-2 two highly conserved and recurring sequence and structural motifs termed BH1 and BH2 were identified[277] and later also found in many other proteins (Bcl-2 like)[226,256,277-281]. A third motif (BH3) was first identified in Bak[280] and Bax[236], followed by every other pro-apoptotic protein. Also, the shorter and more unstructured ones were found to have the BH3-domain, where it was found to be the only one present (BH3-only proteins).

In anti-apoptotic proteins a triad of BH1-BH3 forms a highly hydrophobic groove that binds other BH3-domains of pro-apoptotic pore-forming partner proteins like Bax or Bak and BH3-only proteins. Binding them creates inactive heterodimers and inhibits or represses their activities. Binding tests showed that artificial[282], the own[283], or similar BH3-domains of anti-apoptotic proteins are also capable of binding to the groove. The binding studies indicated the possibility of homodimerisation or specifically targeted inactivation of anti-apoptotic Bcl-2 proteins[232,233,236,284]. These findings attribute a pivotal role to the BH3 domain as the mediator of the interplay between pro- and anti-apoptotic Bcl-2 family members. Mutations within BH1 or BH2 negate anti-apoptotic activity of Bcl-xL or Bcl-2 and hinder their binding to Bak or Bax and a subsequent heterodimerisation[258,277]. Therefore, it has been shown that both domains in synergy with BH3 are necessary for anti-apoptotic activity and hetero- or homodimerisation, which are the first step in hindering or inducing apoptosis, respectively. This BH1-BH3-dependent interaction and the opportunity to mimic or disturb it also offers the possibility for novel therapeutic drugs for cancer or impaired mitochondrial apoptosis treatment.

Finally, a fourth small helical domain (BH4) was determined in the N-terminal region of Bcl-2 and at least in several related anti-apoptotic proteins, Bcl-B[281], Bcl-rambo[285], Bcl-xL[258] and Bcl-w[265,266,286,287] and in the pro-apoptotic proteins such as Bcl-2-related ovarian killer protein homolog B (Bok), Bcl-xS (isoform of Bcl-xL) and Diva/Boo. Pore-forming Bak and Bax[227], to some extent, have an altered and similar version of BH4, with weak homology in this region. They are therefore considered to have only BH1-3 in most literature[38,288]. Further structural investigations and genome screenings showed that the BH4 motif is less amino acid sequence-specific but has a highly conserved structural motif[288,289]. Its functions are still under debate and not fully understood. It is thought not to have a direct role in the binding and dimerisation with Bcl-2 partner proteins, as BH4 deletion mutants of Bcl-2 or Bcl-xL were still able to make homodimers or heterodimers with other Bcl-2 proteins[290].

However, the anti-apoptotic function is mainly lost upon BH4 removal or substitution of its hydrophobic residues, suggesting non-canonical new apoptotic functions and alternative modes of actions outside the Bcl-2 family[290,291]. What has been proven so far, regarding the non-canonical role of Bcl-2 proteins, is that both pro- and anti-apoptotic proteins are also located at the ER membrane, some only under apoptotic conditions (see Figure 6). They can also be found at the contact surface between ER and OMM, called mitochondrial associated membrane (MAM)[227,275,292]. There they regulate and help with balancing the calcium homeostasis, ER stress and are therefore able to control autophagy and apoptosis by enhancing or blocking calcium-dependent signals from the ER. More recent reviews and studies of Bcl-2 proteins determined a role for the BH4 domain in binding different types of proteins, such as VDAC-1[293], Apaf-1[294], HIF-1/VEGF[295]. Direct involvement of the BH4 domain of Bcl-xL, Bcl-2, Mcl-1, Bax and Bak in the regulation of intracellular Ca^{2+}-signalling from the endoplasmic reticulum (ER), by interactions with the 1,4,5-trisphosphate receptor (IP3R) Ca^{2+}-channel, has been strongly implicated as well[227,292,296]. Also, the BH4 domain of Bcl-xL has been implicated in mitochondrial calcium signalling and uptake[293].

It has been shown that all anti-apoptotic proteins have at least BH1-BH3 domains important for binding and interaction, some an additional BH4 for non-canonical interactions. Whereas pro-apoptotic proteins always have at least the BH3 domain (e.g. BH3-only), which can be considered a death- or death-inducing domain[226,227,247]. A common feature in 12 of the unique structures is a hydrophobic domain located at the carboxy-terminus which acts as a membrane anchor. It also allows insertion and further dimerisation or oligomerisation at or in the membrane. Depending on its sequence and length, it may occupy and protect the BH3 binding groove and allow shuttling between cytosol and MOM of Bcl-2 proteins[38,227].

1.2.4 Bcl-xL and Bak/Bax

To understand the cytoprotective activity of Bcl-xL and the mechanism behind it, several X-ray and NMR structures were solved of its heterodimers with, e.g. Bak[297] or Bax[298] BH3-domains, one example is depicted in Figure 8. The first observation was that a flexible and unstructured loop (as the C-terminal helix 9) is not necessary for Bak and Bax binding. Removing the loop even increases the anti-apoptotic activity of Bcl-xL in solution and simplifies the model. Therefore, most structures and studies in solution were done with a truncated loop and a truncated C-terminus.

Structures of Bak and Bax BH3-complexes of Bcl-xL and other pro-survival proteins show that their BH3-ligand binds as an amphipathic helix in the Bcl-2 groove[263]. The binding grove, depicted in Figure 8, consists of the BH1-3 domains.

Looking at recent structures and studies of Bax[264,299,300] and Bak[244,301-304] showing their BH3 binding-mode and way of dimerisation, the structural similarities among the multi-motif pro- and anti-apoptotic counterparts become apparent and more transparent. These similarities strongly imply that the mechanism of action of the Bcl-2 family proteins is similar[234,244,299].

However, their specific binding affinities and preferred binding partners define their function and roles. So far, it is assumed that this is due to distinct variations in sequence and structure, leading to structural effects on their binding-pocket, such as altered geometry, electrostatic environment, or degree of occlusion by their membrane anchor[227,262].

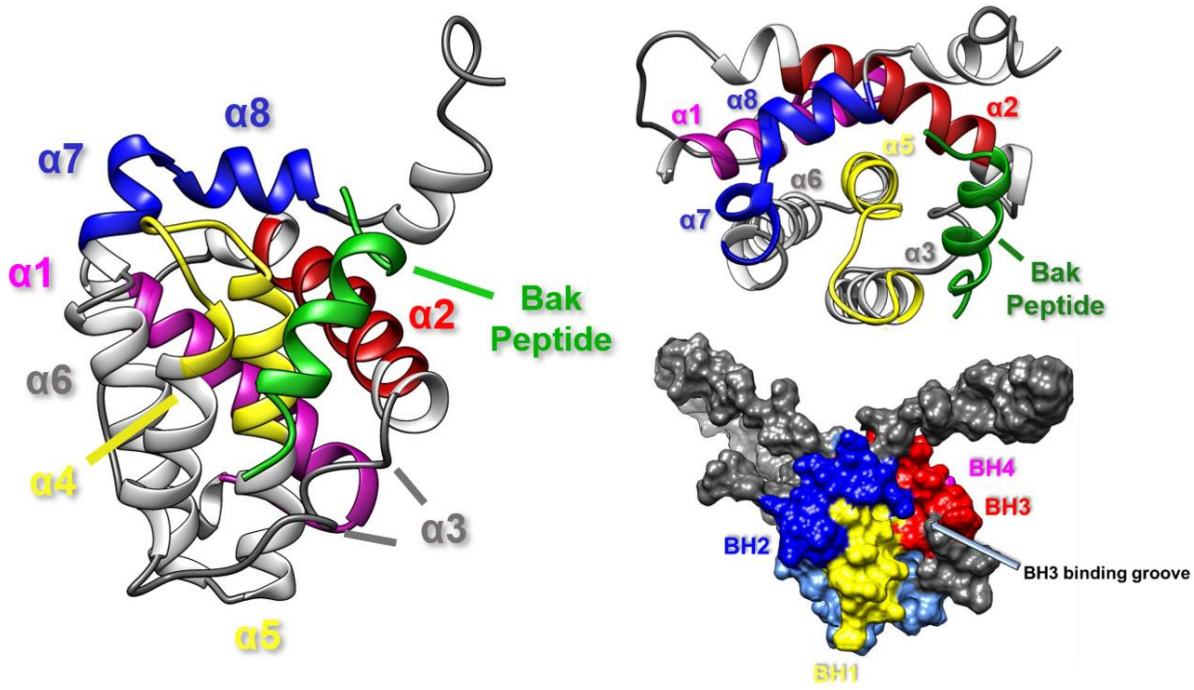

Figure 8: NMR structure of the first Bcl-xL complex with a Bak-BH3 peptide, in green, from the PDB NMR structure 1BXL[297]. For this study the loop and the C-terminal helix were deleted. BH domains are coloured as following, BH1 in dark blue, BH2 in yellow, BH3 in red and BH4 in magenta. On the top right is the top view onto helix five, positioned in the middle. The BH3-peptide is filling the groove and is surrounded by the BH1-3 domains, partially capped by the residual C-terminus. In the top view it is visible, how the central helix is completely shielded from all sides, stabilising the whole fold. Due to structural changes induced by the binding, the α3 helix next to the peptide is partially unfolded. On the bottom right is a depiction of the identified hydrophobic BH3 binding groove of the Bcl-2 family proteins from the PDB NMR structure 1LXL[258]. The C-terminus, which is pointing out, would have the TMH attached, which could partially close the groove and shield it from BH3-only proteins, or water.

Only through structural biological studies such variances could be identified and attributed to the three main respective roles of the Bcl-2 family[247,263,283].

New studies of full-length Bak (with altered C-terminus)[304] and Bax[264] in solution show that their BH3 binding groove is occupied or shielded by their respective C-terminal helix. However, under physiological conditions, inactive Bak monomers are permanently located in the membrane, and their α9 helices are inserted. This resembles the behaviour of apo Bcl-2, which has an unstructured TMH in solution, that leads to an unstable soluble state. For Bak, the structure of the native C-terminus could not be determined so far, or of the full-length native protein, for similar causes like for Bcl-2. Determining the reason for the Bak location-preference proves elusive, but most likely, the cause is similar to its counterpart Bcl-2.

By contrast, inactive Bax adopts the observed soluble structure also in healthy cells under normal conditions and is primarily found in the cytosol, similar to its counterpart Bcl-xL[305]. For Bax to insert into the membrane, an activator BH3-only protein needs to bind to the BH3 groove[237,242,246]. Binding this BH3-motif displaces the Bax N-terminal α1 helix and the α9 cap, and in the presence of a membrane, it inserts into the bilayer[246,306]. This results in active Bax to adopt an analogous conformation to that of inactive Bak or membrane-inserted Bcl-xL. It is not clear, if Bcl-xL exhibits the same mechanism of insertion. Chimeras of Bax with the Bcl-xL α9 showed different behaviour and were located inside the membrane in apo-form, implicating that the sequence and fold of the C-terminus are responsible for Bax different behaviour and cytosol distribution[264].

With this, two locations for Bcl-2 proteins have been suggested or observed respectively for two counteracting pairs, and an insertion mechanism was identified[246,247,305]. It was shown that the sequence and fold of the C-terminus determine the protein distribution and the occlusion of the BH3 groove. It is also postulated, that inactive Bak, Bax, and BID can release their BH3 domain in a membrane environment. Spontaneous activation of Bak or Bax might also occur in the presence of a membrane. Similar behaviour and spontaneous activation have also been observed for Bcl-xL[307-310]. Generally, this is possible if their globular fold is perturbed through external stimuli that expose their BH3-domain and hydrophobic core[243]. Such stimuli can be antibodies[311], small molecules[312,313], heat[314], changes in pH[315], or adding mild detergents[316]. This enables further oligomerisation and ascribes a pivotal role for the membrane bilayer and its lipids, for pro-apoptotic and Bcl-2 family function in general. At this interface, most of their interactions and conformational changes take place. One of them is the pore formation of activated Bak or Bax[237]. It was observed that they form dynamic pores, lines and arcs, which enlarge over time. The size and shape depend on their respective concentration. Recent studies show that activated Bak and Bax, consisting of a heterodimer with a BH3-activator,

first form homodimers with another Bak or Bax[227,243]. There are two different, symmetrical and asymmetrical, conformations possible.

How Bak and Bax transition from hetero- to a homodimer, and how these dimers oligomerise further and form larger complexes is still under debate[306]. Additionally, in what way Bcl-xL interferes and blocks this process at the membrane is still unclear. The general theory is that Bak and Bax dimers can pair with other dimers via weak affinity interactions, which is supported by the constant and proceeding enlargement of pores. Recent evidence points towards symmetrical dimers[227,243,306]. As it cannot be interrupted or stopped by anti-apoptotic proteins, this process seems to be the point of no return for the cell fate. Studying this process, and the role and mechanisms of Bcl-xL, is therefore of upmost importance to understand MOMP and ways, how to use it to our advantage through selective and specific drug targeting.

1.2.5 BH3-only Protein PUMA

Differentiating between BH3-only and other pro-apoptotic multi-motif proteins is not only based on their role in apoptosis but also their sequence (see Figure 9) and structure[233].

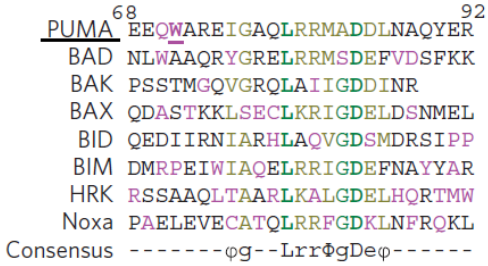

Figure 9: Comparison of different BH3-domain sequences of the Bcl-2 Family, colour-coded according to degree of conservation: Bold green, conserved; green, highly conserved; olive, partially conserved; purple, unique. BH3-consensus motif is indicated as: ϕ, hydrophobic residue; g, usually glycine, serine or alanine; L, highly conserved leucine; r, usually arginine or lysine; Φ, hydrophobic residue; D, aspartic acid; e, glutamic acid or aspartic acid. The unique Trp71 of PUMA BH3-domain, responsible for Bcl-xL unfolding and tight binding, and the residue numbers for PUMA are given at the top. Adapted from[317] with permission.

Except for BID, BH3-only proteins are characterised by their predominant intrinsically disordered structure. The exception is their BH3-domain which, upon binding to pro- or anti-apoptotic proteins, adopts an amphipathic alpha-helical structure[234,250]. In contrast, multi-motif Bcl-2 proteins are globularly folded and structured, excluding intrinsically disordered regions (IDRs), for example, the disordered flexible loop of Bcl-2 and Bcl-xL.

These significant structural and sequence differences of BH3-only proteins lead to their unique roles in apoptosis. One is the role of a derepressor, that binds and disrupts already formed heterodimers of anti- and pro-apoptotic Bcl-2 family members or occupies the anti-apoptotic BH3 groove (sensitiser) and hinders anti-apoptotic function[234]. This process does not directly form pores in the mitochondria. The other role is that of a direct activator of pro-apoptotic multi-motif proteins[232,233,241,244-246]. It is still under debate, how BH3-only proteins bind to the BH3 groove of Bak or Bax, and then get displaced by another Bax or Bak BH3-domain[234]. This mechanism seems to be necessary, as only Bak or Bax homodimers form pores during MOMP[234,237]. This is also supported by recent structures and studies of activated Bak or Bax homodimers, allowing to predict a mechanism of formation[243,299,301].

Consequently, high concentrations of activators should hinder pore formation and compete with other Bak or Bax for the same interaction site, which could not be observed in tests. Therefore, it is suggested, that BH3-only proteins leave the groove, once the pore-former is activated. That would attribute the role of a catalyst to the activator BH3-only proteins, which was already observed in several experiments with Bax.

While studying activator BH3-only proteins, it was found that they also bind to anti-apoptotic Bcl-2 family members[318]. Like sensitisers, this binding inactivates pro-life function and the anti-apoptotic protein. The binding usually occurs due to a conserved 13 residue sequence of the BH3-motif harbouring four main hydrophobic residues[234]. Interactions occur both through hydrophobic interactions and electrostatic ones between the conserved Bcl-2 core and the BH3-domain of the BH3-only protein[234,244,263,299,300,304,319]. Moreover, activator BH3-only proteins are supposed to induce the membrane-anchored form of anti-apoptotic proteins, e.g. Bcl-xL, analogous to the activation of Bax. Therefore, it is complicated to determine which interactions are predominant, and which family members inhibit each other first, under physiological or apoptotic conditions. For BH3-only proteins and anti-apoptotic ones, it seems to be related to their abundance and affinities in their membrane-bound or soluble state[250,318]. Also, small sequence alterations in the BH3-motif, between different BH3-only proteins, change their interaction and binding mode to pro- and anti-apoptotic proteins. The different BH3-squences lead to changes in the binding topology of Bcl-2 binding-partners, causing different specificities and BH3-only roles[319].

One of the most interesting and challenging BH3-only members is the p53 upregulated modulator of apoptosis (PUMA)[320]. The gene of PUMA encodes two different versions (PUMA-α and PUMA-β) which are both unstructured proteins in solution, with similar activities and function[246,317,318,320,321]. Their expression is induced after cell stress or damage in cells following p53 activation, that is a pivotal detector of DNA-damage or other stressors.

Furthermore, PUMA has been shown to bind to anti apoptotic Bcl-2 family proteins, especially Bcl-xL[263,317]. PUMA-binding releases Bcl-xL from pre-formed p53-Bcl-xL heterodimers and thereby enhances p53 function to activate Bax or Bak, leading to mitochondrial apoptosis[322]. Additionally, it sequesters Bcl-xL and blocks its function, further accelerating MOMP. Afterwards, the PUMA-Bcl-xL heterodimer is transferred to the mitochondrial outer membrane, if the anti-apoptotic partner is not already inserted. So far, it is controversial if PUMA is only a sensitiser BH3-only protein[240], as studies have shown that it is capable of binding to Bax[323] and introduce mitochondrial permeabilisation *in vitro*[246].

However, Chipuk *et al.*[324] have shown, through knockouts, that recombinant PUMA is not an activator of Bak or Bax and functions solely as a sensitiser. Unfortunately, those *in vitro* studies do not fully reflect apoptotic conditions in the cell, and PUMA seems to be involved in several different and overlapping pathways. What has been shown so far *in vivo* is that PUMA binds extremely strong to Bcl-xL with high affinity. Breaking up this formed heterodimer with BH3-mimeticks has been proven very difficult[250]. This complex is also responsible for the cell resistance to chemotherapeutics, since breaking it up with drugs would free PUMA and lead to more Bcl-xL sequestering. Until now, no molecule or drug could be designed that breaks up their tight complex and helps to block PUMA-bound Bcl-xL from exhibiting its function.

One reason for this can be found in the solved structure of the Bcl-xL complex with the PUMA-β BH3-domain (Figure 10)[317]. The study revealed, as expected, that PUMA is an intrinsically disordered protein, and that its BH3-domain folds into a helical shape upon binding. No huge differences in binding to Bcl-xL between full-length PUMA-β or its BH3-peptide only where observed. That is why mainly all structural studies were performed with the peptide only, and with binding-active truncated Bcl-xL, missing the flexible loop (ΔL) and its C-terminal α9 TMH (ΔC), termed Bcl-xLΔLΔC.

Apart from the classical BH3-domain binding to the BH3 groove, involving conserved residues amongst BH3-only proteins and Bcl-2 anti-apoptotic proteins, one more unique interaction was found. The aromatic sidechain of His113 in α3 of Bcl-xL and the unique Trp71 of PUMA (see Figure 10) show π-stacking effects. They are assumed to stabilise the structure and weaken the α2 and α3 helical structure of Bcl-xL, leading to partial unfolding as depicted in Figure 10, which has not been observed for other BH3-only protein complexes with Bcl-xL so far. Furthermore, PUMA abolishes the interactions of Bcl-xL-p53 upon binding, mainly through the His113-Trp71 interaction. In the *in vitro* studies, this interaction was linked to p53 dissociation and subsequent MOMP of isolated mitochondria, through non-canonical Bak and Bax activation involving p53.

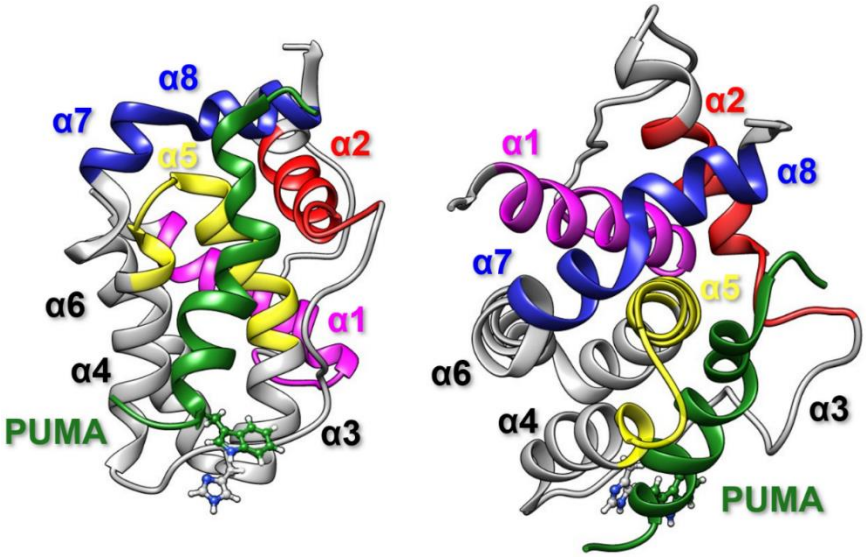

Figure 10: Ribbon representation of the lowest-energy structure of BcL-xLΔLΔC–PUMA(BH3) complex solved by NMR[317], with deleted loop and α9 of Bcl-xL (PDB: 2M04). Side view on the left showing the BH3 groove with the bound PUMA BH3-peptide in green. On the right, top view with α5 centred showing the triad interaction of the BH-domains, BH1 in yellow, BH2 in blue, BH3 in red and BH4 in magenta (not involved). The flexible residues of the C-terminus are cut out for better visualisation. The unique interaction between His113 (Bcl-xL) and Trp71 (PUMA-BH3), which (amongst others) is responsible for the unfolding of α3 of Bcl-xL, is highlighted.

Overall, the role of BH3-only proteins is to act as stress sensors and induce apoptosis through at least two distinct canonical pathways and one p53-dependent non-canonical one. They can be activated transcriptionally, translationally, and (or) post-translationally by different stimuli and trigger apoptosis upstream of Bak or Bax[250]. Like for Bak and Bax, their counterparts are anti-apoptotic proteins, e.g. Bcl-2 and Bcl-xL and it was found that the membrane and its surrounding is vital for the BH3-pathways. Impaired membrane localisation and attachment of Bcl-xL, through removed or altered C-terminus, was found to sensitise BH3-only interactions and improve impairment through medication in recent studies[250]

It was suggested, that the mechanism behind it comes from a lack of membrane integration and not from a soluble-state effect of the C-terminus, as BH3-binding is generally improved without it in solution. This offers new possibilities to drug and interfere in the interaction of Bcl-2 proteins with their associated membranes. Further structural studies of membrane-bound and full-length anti- and pro-apoptotic proteins are necessary to help in this process.

1.2.6 Post-translational modifications and caspase cleavage of Bcl-xL

Bcl-xL[325-327] is subjected to many post-translational modifications (PTMs) in its flexible loop region between α1 and α2, which mitigates or inhibits its anti-apoptotic function. A new study[327] investigated the effects of several different PTMs on Bcl-xL *in vitro*. Phosphorylation at S62 or deamidation of N52 and N56, turning both asparagine to aspartic acid, lead to a decrease in BH3 affinity. Furthermore, the interaction of the unstructured loop with its folded core was increased upon phosphorylation or deamidation, possibly shielding the groove.

Induced changes in conformation and fold of Bcl-xL were shown via NMR, that support this claim. This led to the conclusion that the unstructured loop of Bcl-xL plays an important PTM-driven allosteric role in regulating Bcl-xL function and thereby apoptosis.

Amongst phosphorylation sites, also a caspase cleavage-site was identified in Bcl-2 and Bcl-xL[327]. Both get cleaved by pro-inflammatory caspase 1[326] or by executioner caspase 3[325,328] during late apoptosis in the unstructured loop. Interestingly, the caspase cut enhances apoptosis, especially in the case of Bcl-xL.

There, the cut site was identified at Asp61, which would lead to the loss of the BH4 domain and to two cleavage products of approximately 12 and 16 kDa in size. Such cleavage products have already been identified *in vivo* and *in vitro*. They have been linked to neuronal death and changes in neuronal plasticity and play an important role in exocytosis[329-336]. It is controversial if the cut changes Bcl-xL into a pro-apoptotic protein because the possible loss of its BH4 domain makes it more similar to pro-apoptotic Bcl-2 family members. Another explanation would be that the BH4-domain is vital for further non-canonical interactions, which are negated after cleavage. Moreover, a caspase cut could change the Bcl-xL fold and structure in general, at least in the flexible and binding pocket region, altering its binding affinities to BH3-domains. This would offer an explanation without inverting the role of the anti-apoptotic protein.

Until now, no structural studies of caspase cleaved Bcl-xL have been reported so far. Only the final effect, enhancement of apoptosis, is known, but not the significant changes that occur in or around Bcl-xL.

1.3 Nuclear Magnetic Resonance Spectroscopy

NMR is a non-destructive structural biological technique which is used to obtain high-quality structures as well as dynamics of small molecules, or larger macromolecules, like proteins. Since NMR enables to measure at atomic resolution and yields information, e.g. about connectivity and chemical surrounding of atoms, bond angles, amount, purity and concentration of compounds, it is an optimal tool to study proteins and biomolecules in solution, in their native-like surrounding, and obtain high-quality protein dynamics and structures. Compared to the most abundant method in protein structure-determination so far, which is X-ray crystallography, NMR experiments yield more than snapshots of a protein conformation. NMR can also be used to determine structural changes in solution, e.g. upon ligand- or partner-protein binding, and unravel dynamics of structural elements, and give insights to the complex mechanism of the studied protein, its function and folding.

In recent years NMR has become one of the essential tools for ligand-optimisation and drug-compound screenings, as it also enables to study kinetics, binding affinities and specific interactions. For more detailed information and practical applications, the reader is referred to[337-340], and especially, to: Gordon S. Rule; T. Kevin Hitchens, Fundamentals of Protein NMR Spectroscopy, Springer Science & Business Media, 2006[341].

1.3.1 Basic principles

Similar to many spectroscopic techniques, in NMR, the emitted energy from an excited state which transitions back to its ground state is detected. However, in contrast to standard spectroscopic methods, which employ light and usually excite electronic states, NMR is based on nuclear spin excitation. This is possible since nuclei of an atom have a property called spin (as a simplification), or intrinsic angular momentum ($\vec{I}$)[337-340].

Since atoms are composed of nuclei and they may couple with each other, the atom's total angular momentum, or spin quantum number (I), depends on the ratio of neutrons and protons that compose them. While even-numbered nuclei have a spin quantum number of 0 (since their spins can couple) and are undetectable by NMR, odd-numbered nuclei have a half-integer or integer value.

Typically, for NMR spectroscopy of biomolecules and proteins, the most studied nuclei have a spin of ½, arising from an unpaired proton, which are ^{1}H, ^{15}N, ^{13}C, see table 1. Additionally, nuclei with an integer value, as deuterium (^{2}H) for example, are employed. Unfortunately, since neither ^{2}H, ^{15}N nor ^{13}C are abundant in nature, as shown in table 1, they have to be enriched through isotopic labelling. The labelling of a protein is also the main prerequisite for samples to be NMR-active. Due to its spin quantum number of 0, naturally occurring ^{12}C, for example, is not possible to be studied by NMR. Therefore, if employing recombinant protein expression, the host organism must be grown in isotopic rich media. As explained in Chapter 1.1.3, only *E. coli* can survive higher deuterium concentration and are ideal for isotopic labelling with high deuterium content, hence they were chosen as main expression host in the frame of this work.

Since the spin is quantised, it may occupy different energy states and is possible to be excited into higher ones. However, under normal conditions, the energy states have no preferred orientation or energy difference, which is termed degenerate. Nevertheless, due to the intrinsic angular momentum of nuclei, they possess also magnetic moment states, which is the basis for the magnetic moment μ of an atom[337,341]. The ratio of the magnetic moment to its angular momentum of a given atom is directly proportional and can be expressed as the gyromagnetic ratio γ by $\gamma = \frac{\mu}{I}$, which makes it a nucleus-specific factor or proportionality constant (see table 1).

This inherent property of a magnetic moment μ and its different magnetic spin states gives rise to the possibility to employ them for NMR.

Table 1. Properties of essential nuclei for Protein NMR adapted from[337]. The used nuclei for this thesis and standard protein-NMR are highlighted.

Nucleus	Spin quantum number *I*	Gyromagnetic ratio γ (10^7 $T^{-1}s^{-1}$)	Natural abundance [%]
^{1}H	**½**	**26.7522**	**99.99**
^{2}H	**1**	**4.1066**	**0.012**
^{14}N	1	1.934	99.63
^{15}N	**½**	**-2.7126**	**0.37**
^{13}C	**½**	**6.7283**	**1.07**

In an applied constant, strong and external magnetic field B_0 given in z-direction, the magnetic moments of the spins interact with it. This leads to two possible orientations in z-direction for ½ magnetic quantum numbers. One is with (+½, low energy state termed α) or against (-½, high energy state, termed β) the applied magnetic field (B_0).

These two orientations lead to two different states (α and β), thereby splitting into two different energy levels. This event is known as the Zeeman-effect.

The E of the magnetic moment in z-direction (μ_z) interacting with the magnetic field (B_0) can be described by[341]:

$$E = -\mu_z B_0 = -\gamma I_z B_0 = -\gamma m \hbar B_0$$

where I_z is the spin quantum number in z-direction, γ is the gyromagnetic ratio, m the magnetic quantum number and $\hbar$ is the reduced Planck constant ($\hbar = h/2\pi$). For every magnetic quantum number m, there are 2m+1 energy levels, which gives two energy levels for m = ½ atoms. Hence, for a nucleus, the energy difference ΔE can be described by[341]:

$$\Delta E = \gamma \hbar B_0$$

This shows that the difference of energy states depends mainly on the magnetic field, which is tuneable, and the inherent constant gyromagnetic ratio, that depends on the corresponding nucleus. The sensitivity of the NMR experiment depends on the intensity of the signal, which is proportional to the energy gap ΔE. Therefore, the sensitivity also depends on the magnetic field strength and the used nucleus, where a higher γ enhances the energy difference and thereby the signal.

Since ^1H has the highest gyromagnetic ratio of all atoms in a typical protein-NMR sample, it is consequently the preferred starting nucleus for excitation as well as for the final detection of signals.

As the spins have angular momentum and align to an applied external field, they precess around it with a certain angular frequency, termed Larmor-frequency (ω). Since energy can be described by $E = \hbar\omega$, concordantly the Larmor-frequency (ω), which also depends on the magnetic field and gyromagnetic ratio γ, can be described as following[341]:

$$\omega = \gamma B_0$$

The Boltzmann distribution can describe the population of the two (α and β) energy states in[341]:

$$\frac{N_\beta}{N_\alpha} e^{-\frac{\Delta E}{k_B T}}$$

where k_B is the Boltzmann constant and T the temperature. Unfortunately, since the energy difference is minimal at room temperature and at typical magnet strengths of 14.1 T (600 MHz Spectrometer) - 22.3 T (950 MHz Spectrometer), the population is almost evenly distributed. Just a few parts per million are in the ground state and can be excited.

In order to excite the residual respective nuclear spins in the ground state, the energy difference must be supplied. Typically, it is in the range of radio-frequency, and must match the magnitude of the respective Larmor frequency with[341]:

$$\nu = \omega = \gamma B_0$$

in order to reach resonance-conditions. ν is the supplied radio-frequency, ω the Larmor frequency and γ the gyromagnetic ratio and B_0 the applied magnetic field strength of the NMR magnet. Since the nucleus specific gyromagnetic ratio defines the order of magnitude of the frequency, it is possible to excite specific nuclei or different ones in a user-defined succession. So, upon application of a radio frequency (rf) pulse under resonance condition, the net spin magnetisation vector inclines away from the z-axis of the applied magnetic field (B_0).

As soon as the external rf pulse is stopped, the magnetic vector will try to align to the z-axis and reach its equilibrium state again. This (nuclear) magnetisation decay, from the tilted to the equilibrium state, gives rise to a so-called free induction decay (FID). Since the FID is a moving electromagnetic field, it induces a current in the NMR coils, which is recorded. This recorded spin-flipping, or energy transition, from the low (α) to the high (β) energy state yields specific and unique signals for every spin. Additionally, each nucleus (or spin) within an assembly resonates with a discrete frequency, dependent on its local electromagnetic field, usually given by its electron distribution. This frequency-shifting effect is termed chemical shift (CS). The CS allows to differentiate between the same type of nuclei, e.g. amongst all protons within a protein.

However, in order to analyse this signal frequency-dependent, first, it must be converted from this time-domain signal in a frequency-domain signal. This is done by a mathematical Fourier Transformation (FT).

1.3.2 Spin Relaxation

Spin Relaxation is induced by two distinct processes: T1 and T2 relaxation, by which an excited spin returns to equilibrium NMR magnetisation in z-direction after a pulse[337-341]. In NMR, this process may take up to several seconds, allowing for manipulation of the generated magnetisation by NMR pulse sequences, e.g. transfer the excited state to other nuclei before detection.

The ensemble of spins in one sample has a bulk magnetisation, which aligns according to the direction of the applied pulse (usually x or y).

The time it takes for the magnetisation to go back to the Boltzmann equilibrium in the z-direction is called T1 time or spin-lattice relaxation time[337-341]. It describes the re-alignment of the bulk magnetic moment to the external field in the z-direction. This longitudinal relaxation happens when the spins give their acquired excess energy to the surrounding (lattice). Since this process of converting NMR transitions from radio frequency to thermal energy is deficient, the resulting T1 relaxation takes a relatively long time. For proteins, it is in the one-second range, for smaller molecules it may take up to 10 seconds.

Another effect or relaxation pathway that happens after a pulse is T2 relaxation. Generally, the T2 relaxation is an entropic effect that describes the loss of coherent transverse magnetisation due to dephasing in the x,y plane. The dephasing does not affect the population of excited spins, as they do not return to thermal equilibrium. Only their phase coherence, or the loss of it, is affected. The time constant for this relaxation is also called T2.

1.3.3 The PRE-Effect and Practical Application

Since local magnetic fields may induce relaxation in nuclei, which are in proximity, this effect may be used to one's advantage[342]. Employing paramagnetic atoms or molecules with unpaired electrons, e.g. Gadolinium (Gd^{3+}) or stable radicals (spin-label), allows to selectively create regions with high local magnetic fields. Labelling specific regions in proteins with such a paramagnetic tag, also referred to as paramagnetic probes, leads to the magnetic dipolar interactions of the observed protein spins with the unpaired electrons of the tag. This results in increased relaxation rates (usually T1 and T2) of the observed spins around the paramagnetic tag, which leads to weakening or "bleaching" of their signals in a proximity-dependent matter (r^{-6}), as depicted in Figure 11[173]. This employed effect is called paramagnetic enhanced relaxation (PRE) and may yield additional orientational and structural information, of short to long distances up to 24-35 Å[342-345]. Once they are tagged with paramagnetic probes, binding to ligands, partner proteins, or membrane surfaces may be studied.

If a paramagnetic tag has an anisotropic distribution of its unpaired electrons, it has a resulting so-called magnetic susceptibility tensor[346]. This effect can be observed, for example, in Dy^{3+}

and Tb^{3+} ions[346-349]. The anisotropic tensor leads to an alignment of the tag to the external magnetic field, like a small bar magnet.

This alignment depends on the rigidity of the attached tag, the strength of the external magnetic field and the magnetic susceptibility tensor. The results can be the re-introduction of residual dipolar couplings (RDC), see chapter 1.3.4 RDC[342].

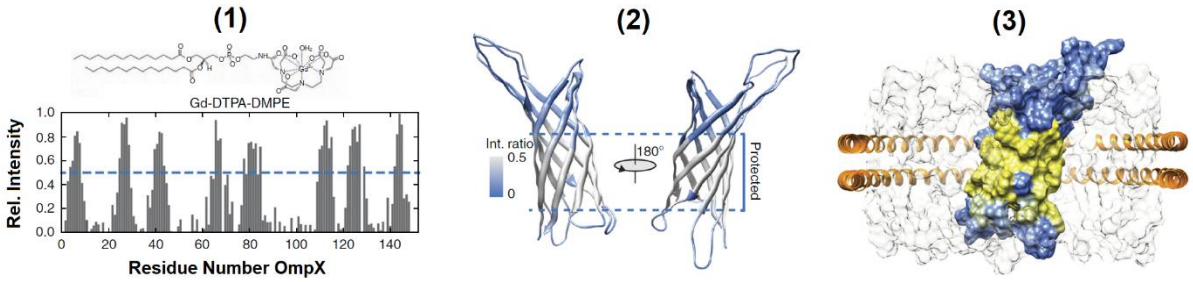

Figure 11: 1) Example of a Gd^{3+}-mediated PRE-effect in the NMR-spectra of OmpX in nanodiscs, where several lipids in the bilayer are with a Gd^{3+}-tag. The reduced intensities, through proximity to the tag, are assigned to the amino acid residues. 2) Mapping of the PRE-affected residues onto the OmpX structure. This way, residues which are outside of the bilayer can be determined. 3) Final positioning of OmpX inside of the bilayer according to the Gd^{3+}-exposed protein-residues, which are close or outside the bilayer surface, and the PRE-unaffected ones, which are buried inside the nanodisc. Adapted from Hagn *et al*.[173], with permission.

Additionally, alterations of the chemical shifts may be introduced to the sample-nuclei by contact to the anisotropic electron distribution of the paramagnetic tag, termed Pseudo-contact shifts (PCS)[342]. The PCS have an r^{-3} distance-dependence, compared to the r^{-6} dependence of the PRE-effect itself. This results in a more extensive experimental range to detect PCS of up to ~40 Å and gives rise to new additional structural information.

Through recent computational and biochemical advances, the PRE-method and the use of PCS became popular and well-established for a plethora of studies[342,347,350]. The study of structures of soluble proteins[351,352], membrane proteins[173,343,344,353-355], or larger complexes like protein-protein complexes[353,356,357] and protein-nucleic acid complexes[345,358] may be improved or facilitated using the PRE restraints. It is also possible to study different folding states of proteins[359,360].

1.3.4 The RDCs and their application in Protein NMR

As long as molecules tumble in solution, the studied system is undergoing isotropic tumbling and the probability of finding a molecule at a specific angle is averaged to zero. Nevertheless, if a molecule can be partially orientated, e.g. through lanthanide-tags or filamentous bacteriophage[173], a new bond-angle and orientation-dependent component, the residual dipolar coupling (RDC) can be re-introduced[347]. This contribution to the scalar coupling is caused by dipolar interaction between directly bound nuclei. The resulting RDCs present an additional splitting of the spectral lines, through the dipole-dipole coupling, as depicted in Figure 12.

The observed spin-spin coupling ω_{AB} for two nuclei A and B in the anisotropic case can be described by:

$$\omega_{AB} = D_{AB} + \pi J_{AB}$$

where D_{AB} is the secular part of the dipole-dipole interaction and J_{AB} the coupling constant. In turn, D_{AB} is given by:

$$D_{AB} = D_{MAX}\langle(3\cos^2\theta - 1)/2\rangle$$

where D_{MAX} is the dipole-dipole coupling constant, θ is the angle between the internuclear bond vector and the external magnetic field B_0. Here, the pointed brackets represent time or ensemble averaging.

Without artificial alignment through paramagnetic-tags or filamentous bacteriophages in solution, the term in the pointed brackets would average to zero. In solid-state NMR, where dipolar-couplings are impeding, this term can be averaged to zero when 54.74° is chosen for θ (called magic angle) while spinning the sample at high kilohertz rates.

The dipole-dipole coupling constant D_{MAX} is given by:

$$D_{max} = \frac{\mu_0 h \gamma_A \gamma_B}{8\pi^3 r_{AB}^3}$$

where μ_0 is the vacuum permeability, h is the Planck's constant, γ_A and γ_B are the gyromagnetic ratios of nuclei A and B, and r_{AB} is the distance between nuclei A and B, respectively. D_{MAX} is dependent on the bond-type, and generally in the magnitude of 10^3 Hz. Additionally, the value of D_{MAX} is determined by the distance between both coupled nuclei A and B. It decreases with the power of r^{-3}, like the PCS of paramagnetic tags.

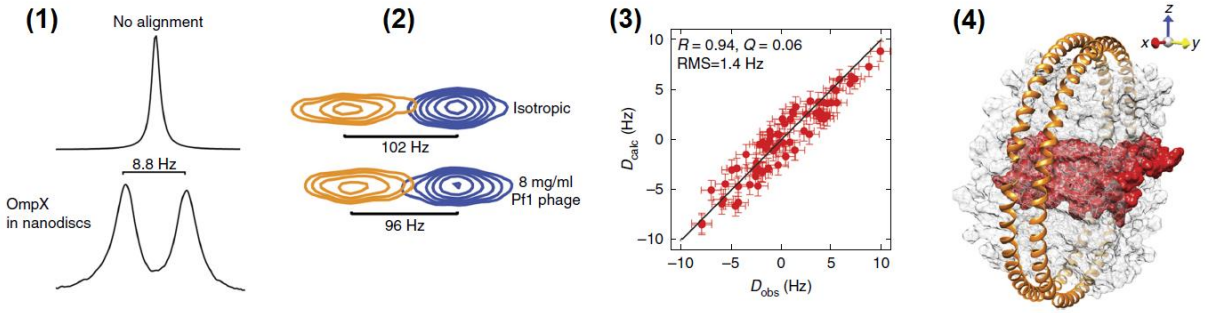

Figure 12: Example of RDCs used for structure refinement of OmpX in nanodiscs. (1) Quadrupolar splitting of the water resonance in a ^{2}H spectrum, introduced by a partial alignment of the NMR sample with Pf1-phage. (2) RDC effect in the spectrum. (3) A correlation plot of all obtained RDCs, where experimental RDCs (D_{obs}) and back-calculated RDCs from the available OmpX structure (D_{calc}) are compared, to quantify and estimate the quality of the structural calculations. (4) PRE calculations (Figure 11) helped to determine the position of OmpX in the nanodisc. Now combined with the obtained alignment tensor, form the RDC analysis, the orientation of the OmpX and nanodisc around it can be estimated. Adapted from Hagn *et al*.[173], with permission.

With this additional information about the bond angles and the total protein orientation, the structural NMR-based data of a protein may be complemented, as seen in Figure 12. Furthermore, obtained RDC's provide pivotal information about internal protein dynamics, over a wide range of timescales. RDSs can be used to study the orientation, binding or interaction, and folding of complexes or larger molecular assemblies.

1.3.5 Protein NMR and Assignment of Proteins

Through NMR spectroscopic studies of a protein, several different information may be obtained, that culminate into the creation of a new protein structure[337-341]. Such information may include chemical shifts, magnetic coupling of nuclei through bonds, or PRE and RDC studies. All of those employed NMR techniques (and data) help to determine and characterise the structure, orientation and dynamics of a protein, at atomic resolution and under native-like conditions.

In order to correctly determine which residues are directly connected with each other and assign them to their positions in the amino acid chain, one can measure spin-spin interactions that are mediated by the electrons in chemical bonds. These spin-spin interactions of connected atoms, usually with 1-3 bonds between them, are called scalar or J coupling.

The scalar interactions lead to splits of the NMR signals, into characteristic and assignable multiplets. Here, the spacing between those multiplets, referred to as J coupling constant correlates with the different nuclei (H, C, N) and the strength of their interaction.

In so-called 2D heteronuclear experiments (see Chapter 1.3.6), the magnetisation of the starting nucleus, usually ^{1}H, which is the most sensitive due to its high gyromagnetic ratio, is selectively transferred to attached nitrogen (^{15}N) or carbon (^{13}C) nuclei, and then transferred back for detection. The obtained correlations are characteristic for each amino acid type, usually the N-H amide-bond of the protein backbone, and some side-chains (containing nitrogen).

In subsequent experiments, called 3D, the magnetisation can be further transferred to a third nucleus. Usually, the first step is again from H to the neighbouring N, and then subsequently to the Cα or C=O connected carbons, and back from the nitrogen to the starting proton. This is established through a so-called INEPT (insensitive nuclei enhanced by polarisation transfer) sequence, displayed in Figure 14. By starting from the most sensitive nucleus, the proton, the transfer to the more insensitive nuclei can be performed to enhance their excited spin-states. In this example of a 3D series from ^{1}H to ^{15}N, finally to ^{13}C, the specific couplings and shifts of the carbons (to their respective side chains and groups) may be obtained. This gives rise to the possibility to determine which amino acid is the next following or preceding neighbour. With a series of 2D and 3D experiments, one can sequentially assign the backbone and side-chain resonances of a given protein. As mentioned before, additional information or structural restraints, that help to fill the gaps and refine the structural calculations, can be gained through additional experiments. The main source of structural information are short-distance couplings through space (5-6 Å), usually ^{1}H-^{1}H-couplings. They are useful, e.g. to assign close contacts secondary structure elements and long-distance tertiary structure elements. Short distance couplings employ dipolar cross-relaxation and enable to obtain contacts that are not mediated through direct bonds, but through space (close proximity). Selectively exciting one spin may transfer magnetisation to its dipolar-coupled neighbour, enhancing or decreasing its intensity. The transfer mechanism is termed the Nuclear Overhauser effect (NOE). By mapping these interactions and transfers of magnetisation, one can determine inter-atomic contacts and neighbours, to create a secondary or tertiary protein structure model. Further structural refinement is possible with complementary PRE or RDC experiments. The more different experiments and studies are done through NMR, employing preferably all different techniques and effects, the better and more native the resulting structure is.

1.3.6 TROSY Effect and Application of TROSY in Protein NMR

The Transverse relaxation-optimised spectroscopy (TROSY) is a 2D-[^{1}H,^{15}N]-NMR method, which uses the interference between dipolar couplings (DD) and chemical shift anisotropy (CSA) of nitrogen and proton[361]. Through the application of specific pulses, it is possible to selectively choose one component of the multiplet of an 2D NMR signal, where DD and CSA cancel each other out (TROSY effect), as depicted in Figure 13. Since both effects usually decrease the T2 time and therefore lead to line-broadening, the result of the TROSY-effect is an increase in both resolution and sensitivity of the heteronuclear NMR experiments.

Moreover, this method can be used to improve 3D experiments and help with obtaining more signals with higher resolution, which significantly improves, e.g., protein assignments carried out by NMR. In the original publication by Pervushin *et al.*[361] the linewidths of the 2D (^{1}H-^{15}N) experiments were reduced by 40-60 %.

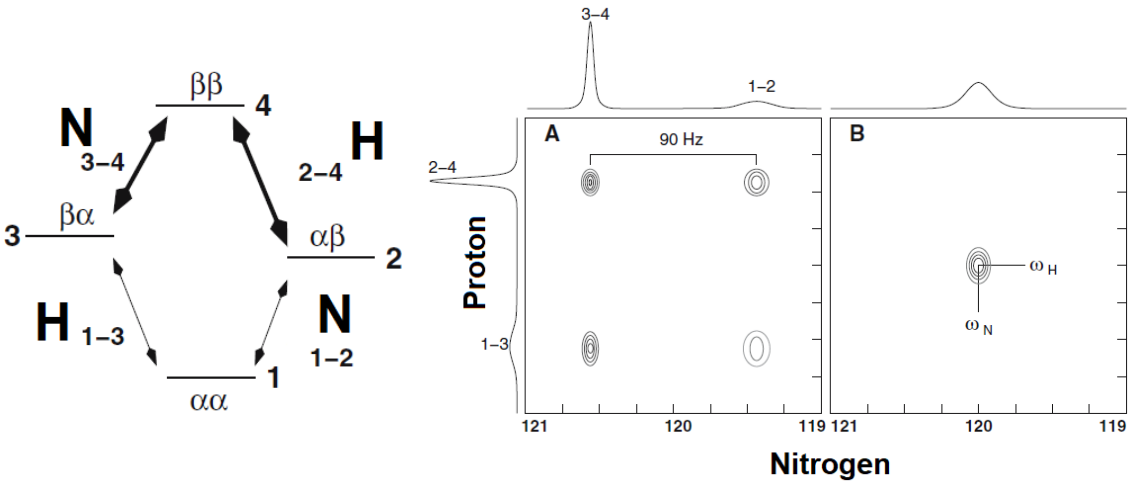

Figure 13: (1) Energy-level diagram for the coupled H and N spins. (2) In A) the obtained quartet from a coupled HSCQ is depicted, resulting from the missing decoupling and 180 ° pulse in the t1 period. The coupling of J_{NH}, usually 90 Hz, is visible as spacing. The desired TROSY peak is in the top left corner, with the narrowest line. On the top are the one-dimensional cross-sections in the ^{15}N-dimension (top) or ^{1}H-dimension (left), with the associated transitions from (1). In (B) is the standard HSQC peak, which is obtained through decoupling in t1 and t2. An average of all four linewidths is observed. Adapted from[341], page 334-335, with permission.

As seen in the pulse programs (Figure 14), in the beginning, both experiments transfer the proton polarisation to the nitrogen spin with an INEPT sequence. As described earlier, usually the sensitive ^{1}H serves as the starting point of most NMR pulse-programs.

Applying the INEPT sequence allows a more efficient transfer of the ^{1}H excited spin-states to the coupled ^{15}N or ^{13}C, than exciting the less sensitive nuclei directly.

Next, a chemical shift evolution period (t1) is applied, following two INEPT sequences, that transfer the magnetisation back to the ^{1}H for detection. However, in the TROSY experiment, three main differences can be observed in the pulse-program, that lead to the selection of the peak with the slowest T2 relaxation. Firstly, during the t1 period, no 180 ° proton pulse is applied. Consequently, the ^{1}H spin-state is not inverted, and the nitrogen magnetisation follows both transitions (1-2, 3-4) without mixing, which are highlighted in Figure 13.

Secondly, the nitrogen decoupling at the end of the sequence, highlighted in red in the HSQC pulse-program (Figure 14), is not applied. Therefore, the coupled nitrogen spin-state is not inverted during the acquisition, and the proton magnetisation may follow the 1-3 or 2-4 transition.

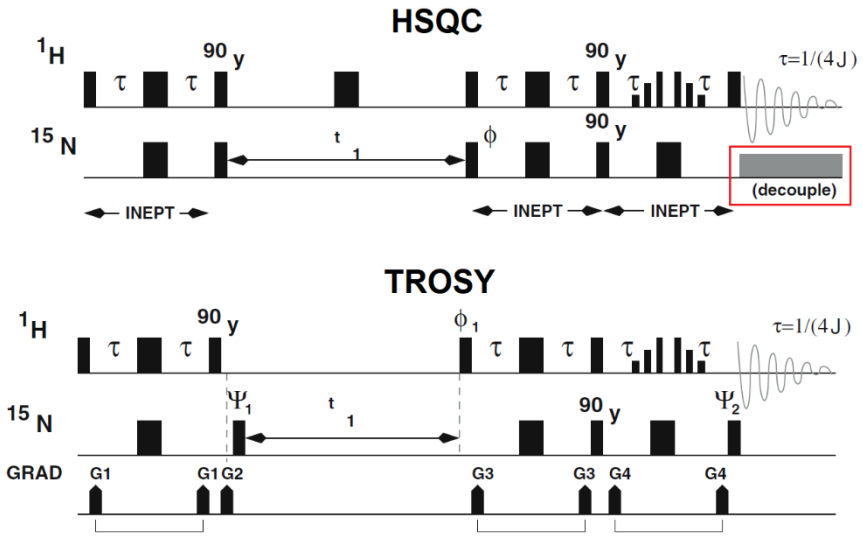

Figure 14: Depiction and comparison of the pulse-programs of a sensitivity enhanced HSQC (top) and a standard TROSY (bottom), where narrow bars represent 90 ° high-power pulses, wide bars 180 ° pulses, and the small six consecutive pulses at the end of the sequence are the WATERGATE water-suppression pulses. In both cases, the delay τ is set to 1/(4J). The decoupling period is marked in red, which is missing in the TROSY case. Adapted from[341], page 336, with permission.

Lastly, the depicted phase cycle selects for single quantum coherences during both t1 (3-4) and t2 (2-4) times. All other three possible transitions are cancelled.

1.4 Motivation and aim of the thesis

Bcl-xL is one of the key Bcl-2 family players in mitochondrial apoptosis and therefore an important drug target in cancer treatment. In recent years, its involvement in neuronal diseases or metastasis progression and survival has been discovered and studied. Further, it is known that Bcl-xL can be cleaved in its flexible loop, which leads to neuronal death or defects and an enhancement of apoptosis. If Bcl-xL becomes pro-apoptotic upon cleavage or its binding to other Bcl-2 proteins is impaired is not known. Up to now, there is no full-length structure of Bcl-xL or one in a native-like environment. This is mainly due to the fact, that there is no sufficient method for the production and handling of full-length tail-anchored proteins. Typically, Bcl-2 proteins are studied as transmembrane-truncated constructs, as the TMH is highly insoluble and leads to inclusion body formation during expression. Purifying of the full-length protein without the use of harsh detergent or other strong denaturants, which damage the soluble domain and impair its function, is nearly impossible.

Additionally, little is known about the influence and role of the membrane where Bcl-xL resides. Which structural changes and switches happen upon partner-protein binding in the membrane and how full-length Bcl-xL expedites its anti-apoptotic function is not fully understood.

The first objective of this work was to establish a method for the production of full-length Bcl-xL from two separately expressed parts, the TMH and the soluble domain. After incorporating the TMH in phospholipid nanodiscs, the next step is a Sortase A mediated ligation of the soluble domain, which yields the full-length protein in a native-like nanodisc.

Secondly, the next goal was to study the membrane-bound full-length Bcl-xL for the first time in a native-like membrane with the help of structural biological methods, mainly NMR. The final goal of the study is to obtain an NMR-based 3D protein structure in its native state and determine its orientation within the nanodisc.

Further, another aim was to identify the role of the membrane and the effect of its composition on the structure of Bcl-xLΔTM and full-length Bcl-xL. Additionally, determining the localisation at the membrane and the interaction of Bcl-xL with a binding partner (PUMA BH3-peptide) in presence of a membrane was aimed for.

Another goal, regarding the functionality and role of Bcl-xL, was the study of the caspase cleavage of the flexible loop and its effect on the protein. Mimicking of the cut was envisaged by inserting a thrombin cut site in the respective loop region.

Through NMR and fluorescence-based liposome assays an answer to the question, what happens to Bcl-xL and does it become pro-apoptotic and inserts into the membrane, was sought.

The final objective was to device a new method for the production of full-length tail-anchored proteins in *E. coli*. This was intended by co-expression of the chaperone Asna1/TRC40 or Get3 together with full-length Bcl-xL. This could allow a high yield production of the otherwise insoluble and aggregation-prone full-length Bcl-xL, or other tail-anchored proteins, as a soluble protein complex. Removal of Get3 or Asna1/TRC40 enables to transfer full-length Bcl-xL into various membrane mimetics, without the need of inclusion-body solubilisation and refolding and the use of harsh detergents.

2 Materials and Methods

2.1 Materials

2.1.1 Chemicals and Materials

All chemicals or materials, if not otherwise stated, were purchased in the highest possible purity grade from Alfa Aesar (Haverhill, USA), Amresco Inc. (Solon, USA), AppliChem GmbH (Darmstadt, DE), Asla biotech (Riga, Latvia), Avanti Polar Lipids, INC. (Alabaster, USA), Bio-Rad Laboratories (Hercules, USA), Biozym Scientifc GmbH (Hessisch Oldendrof, DE), Electrophoresis GmbH (Heidelberg, DE), Fisher Scientific Internatonal (Pittsburgh, USA), Invitrogen (Carlsbad, USA), Merck Millipore (Darmstadt, DE), Roche (Basel, CH), Santa Cruz Biotechnology (Dallas, USA), SERVA Carl Roth (Karlsruhe, DE), Sigma-Aldrich (St.Louis, USA), Thermo Fisher Scientific (Waltham, USA), VWR International (Radnor, USA).

2.1.2 Kits and Enzymes

Table 2: List of used kits and enzymes.

Kits	Companies (headquarters, country)
Gel and PCR Clean-Up System	Promega (Madison, USA)
Minipreps DNA Purification System	Promega (Madison, USA)
Mix & Go E. coli Transformation Kit	Zymo Research (Irvine, USA)
QuikChange Lightning Site-Directed Mutagenesis Kit	Agilent Technologies (Santa Clara, USA)

Enzymes	Companies (headquarters, country)
DNaseI, bovine pancreas	Roche (Basel, CH)
DpnI	Merck (Darmstadt, GER)
Lysozyme, chicken egg	Carl Roth (Karlsruhe, DE)
Pfu DNA Polymerase	Promega (Madison, USA)
TEV protease	Dr.Arie Geerlof (Helmholtz-Zentrum Munich)
Thrombin, bovine	Merck Millipore (Darmstadt, DE)

2.1.3 Instruments

Table 3: List of used instruments.

Instruments	Companies (headquarters, country)
Autoclave VX-150	Systec GmbH (Linden, DE)
Agarose gel caster 1704422 Mini-Sub Cell GT	Bio-Rad Laboratories (Hercules, USA)
CD spectrometer J-715 Spectropolarimeter	JASCO (Oklahoma City, USA)
Cell Density Meter WPA CO 8000	Biochrome Ltd (Cambridge, UK)
Centrifuge HET 1011	Andreas Hettich GmbH & Co. KG (Tuttlingen, DE)
Centrifuge Sorvall LYNX 6000	Thermo Fisher Scientific (Waltham, USA)
Centrifuge Rotor Fiberlite F9-6x1000 LEX	Thermo Fisher Scientific (Waltham, USA)
Centrifuge Rotor T29-8x50	Thermo Fisher Scientific (Waltham, USA)

Instruments	Companies (headquarters, country)
Diaphragm pump MD 1	VACUUBRAND GmbH + Co. KG (Wertheim, DE)
Dishwasher Miele Professional PG 8583 CD	Miele (Gütersloh, DE)
Freezer HERAfreeze HFU T	Thermo Fisher Scientific (Waltham, USA)
Gel electrophoresis Mini-Sub Cell GT Horizontal Electrophoresis System	Bio-Rad Laboratories (Hercules, USA)
Gel electrophoresis PowerPac, Basic Power Supply	Bio-Rad Laboratories (Hercules, USA)
Gel electrophoresis SE250 Mighty Small II Mini Vertical Protein Electrophoresis Unit	Hoefer Inc (Massachusetts, USA)
Heating block Analog Dry Block Heater	VWR International (Radnor, USA)
Homogenizer SilentCrusher M	Heidolph Instruments (Schwabach, DE)
Hotplate stirrer VMS-C7	VWR International (Radnor, USA)
Incubator Heratherm IGS60	Thermo Fisher Scientific (Waltham, USA)
Incubator Shaker Series Innova 40	New Brunswick Scientific (Edison, USA)
Incubator Shaker Series Innova 44	New Brunswick Scientific (Edison, USA)
Isothermal titration calorimeter, MicroCal PEAQ-ITC	Malvern Instruments (Malvern, UK)
Microcentrifuge Galaxy MiniStar C1400-RT	VWR International (Radnor, USA)
Microcentrifuge I R	Carl Roth (Karlsruhe, DE)
Mini Water Circulation Bath MCB-100	JASCO (Oklahoma City, USA)
Nutating Mixer	VWR International (Radnor, USA)
Nutating shaker Mini BioMixer 3D	Benchmark Scientific (Sayreville, USA)
PCR cycler Mastercycler nexus X2	Eppendorf (Hamburg, DE)
Peltier element PTC-348WI	JASCO (Oklahoma City, USA)

Instruments	Companies (headquarters, country)
Peltier element PTC-348WI	JASCO (Oklahoma City, USA)
pH bench meter FiveEasy FE20-ATC kit	Mettler Toledo (Columbus, USA)
Photometer NanoPhotometer N60	Implen GmbH (München, DE)
Pipette Controller accu-jet pro	Brand (Wertheim, DE)
Pipette Research plus	Eppendorf (Hamburg, DE)
Platform shaker Rotamax 120	Heidolph Instruments (Schwabach, DE)
Refrigerated heating circulator F 25	JULABO (Seelbach, DE)
Refrigerator CD615-E	Polar Refrigeration (Bristol, UK)
Refrigerator RK 6192 EX	Gorenje (Velenje, Slovenia)
Scale ATILON ATL-84-I	(Acculab) Sartorius AG (Göttingen, DE)
Scale Entris 2202–1S	Sartorius AG (Göttingen, DE)
Scale Pioneer PA114C Analytical Balance	Ohaus Corporation (Parsippany, USA)
SDS casting chamber Multiple Gel Caster	Hoefer Inc (Massachusetts, USA)
Sonifier S-250D	Branson Ultrasonics (Markham, Canada)
Spectrofluorometer FP-8300	JASCO (Oklahoma City, USA)
Stirrer big squid	IKA Werke GmbH & Co. KG (Staufen, DE)
Stirrer small squid	IKA Werke GmbH & Co. KG (Staufen, DE)
Table centrifuge Micro Star 17R	VWR International (Radnor, USA)
Table centrifuge 5424	Eppendorf (Hamburg, DE)
Table centrifuge 5424 R	Eppendorf (Hamburg, DE)
ThermoMixer C	Eppendorf (Hamburg, DE)
Ultrasonic bath Sonorex RK 103 H	BANDELIN electronic GmbH & Co. KG (Berlin, DE)

Instruments	Companies (headquarters, country)
Ultrasonic bath Sonorex RK 103 H	BANDELIN electronic GmbH & Co. KG (Berlin, DE)
UV Transilluminator Mini Benchtop M-10E	UVP (Upland, USA)
Vortex Mixer Analog	VWR International (Radnor, USA)
Western Blot Pierce Power Blot Cassette	Thermo Fisher Scientific (Waltham, USA)

2.1.4 Software

Table 4: List of used softwares.

Software, Version	Companies (headquarters, country)
Adobe Photoshop CS5	Adobe Systems Incorporated (San Jose, USA)
Adobe Illustrator CS5	Adobe Systems Incorporated (San Jose, USA)
Dynamics	Wyatt Technology Corporation (Santa Barbara, USA)
ExPASy - ProtParam tool	ExPASy Bioinformatics Resource Portal
ExPASy - Translate tool	ExPASy Bioinformatics Resource Portal
Jasco Spectra Manager	JASCO (Oklahoma City, USA)
MicroCal PEAQ-DSC software v1.30	Malvern Instruments (Malvern, UK)
MicroCal PEAQ-ITC software Analysis Software	Malvern Instruments (Malvern, UK)
Microsoft Office 2013	Microsoft Corporation (Redmond, USA)
Microsoft Office 365	Microsoft Corporation (Redmond, USA)

NMR-FAM Sparky 1.413	NMRFAM (Madison, USA)
OriginPro 9.0 (Academic)	OriginLab Corporation (Northampton, USA)
PDB	RCSB (New jersey, USA)
ProFit	(Quantum Soft, Uetikon am See, Switzerland)
ProtParam	National Center for Biotechnology Information (Bethesda, USA)
PyMOL 1.8.4.2	Schrödinger LLC (New York, USA)
Serial Cloner 2.6.1	Franck Perez, SerialBasics
UCSF Chimera	University of California, San Francisco
Unicorn 7.1	GE Healthcare (Chicago, USA)
Uniprot	SIB (Lausanne, CH)

2.1.5 Bacterial Strains

Table 5: *E. coli* strains used for molecular cloning and recombinant protein expression. *E. coli* NEB 5-alpha or XL10 gold were used for molecular cloning. The *E. coli* BL21 (DE3) cells were used for standard recombinant protein expression, while *E. coli* BL21 (DE3) pLysS and BL21-CodonPlus (DE3)-RIPL were used for additional expression tests.

Strains	**Genotype**	**Company**
E. coli BL21(DE3)	*fhuA2 [lon] ompT gal (λ DE3) [dcm] ΔhsdS λ DE3 = λ sBamHIo ΔEcoRI-B int::(lacI::PlacUV5::T7 gene1) i21 Δnin5*	New England Biolabs Incorporated (Massachusetts, USA)

Strains	Genotype	Company
E. coli BL21(DE3) pLysS	*F^- ompT gal dcm lon $hsdS_B(r_B^-m_B^-)$ λ(DE3 [lacI lacUV5-T7p07 ind1 sam7 nin5]) $[malB^+]_{K-12}(\lambda^S)$ pLysS[T7p20 ori_{p15A}](Cm^R)*	Agilent (Santa Clara, USA)
E. coli BL21-CodonPlus (DE3)-RIPL	*E. coli* B F^- *ompT hsdS*(r_B^- m_B^-) *dcm*+ Tet^r gal (DE3) *endA* Hte [*argU proL* Cam^r] [*argU ileY leuW* Strep/$Spec^r$]	Agilent (Santa Clara, USA)
E. coli NEB 5-Alpha	*fhuA2 Δ(argF-lacZ)U169 phoA glnV44 Φ80 Δ(lacZ)M15 gyrA96 recA1 relA1 endA1 thi-1 hsdR17*	New England Biolabs Incorporated (Massachusetts, USA)
E. coli XL10 gold	Tet^r Δ(mcrA)183 Δ(mcrCB-hsdSMR-mrr)173 endA1 supE44 thi-1 recA1 gyrA96 relA1 lac Hte [F´ proAB lacIqZΔM15 Tn10 (Tet^r) Amy Cam^r]*	Agilent (Santa Clara, USA)

2.1.6 Buffers, media and stock solutions

Lysogeny Broth (LB) liquid media, DYT media and LB agar plates were prepared according to standard protocols[362].

Antibiotic stock solutions

The following sterile antibiotic stock solutions (1000x) were used for the cultivation of *E. coli* and were stored at -20 °C.

IPTG stock solutions

1 M IPTG in H_2O (1: 1000), stored at -20 °C

LB-Medium

Tryptone	1 % (w/v)
Yeast extract	0.5 % (w/v)
NaCl	1 % (w/v)

DYT-Medium

Tryptone	1.6 % (w/v)
Yeast extract	1 % (w/v)
NaCl	0.5 % (w/v)

SOC-Medium

Glucose	20 mM
KCl	2.5 mM
$MgCl_2$	10 mM
$MgSO_4$	10 mM
NaCl	10 mM
Tryptone	2 % (w/v)
Yeast extract	0.5 % (w/v)

Antibiotic stock stolutions

Ampicillin (Amp)	100 mg/mL in H_2O
Carbenicillin (Carb)	50 mg/mL in H_2O
Chloramphenicol (Cam)	34 mg/mL in Isopropanol
Kanamycin A (Kana)	50 mg/mL in H_2O

Standard buffers for protein purification

Lysis Buffer

Tris pH 8.0	25-50 mM
NaCl	150-200 mM
EDTA	2 mM
PMSF	1 mM
Protease Inhibitor cocktail	1/40 mL
BME (optional for cysteins)	*5-10 mM*

Ni-NTA Buffer

Tris pH 8.0	20-30 mM
NaCl	100-200 mM
BME (optional for cysteins)	*5-10 mM*

MSP buffer

Tris pH 7.5/8	20 mM
NaCl	100 mM
EDTA	0.5 mM

Sortase Reaction Buffer

Tris pH 7.5/8.0	50 mM
NaCl	150 mM
$CaCl_2$	10/20 mM
BME	10 mM

NMR buffer		Thrombin cut buffer	
NaPi pH 7.0	20 mM	Tris pH 8.0-8.5	20 mM
NaCl	20-50 mM	NaCl	100 mM
EDTA	0.5 mM	$CaCl_2$	2-5 mM
DTT (optional)	*2-5 mM*		

2.2 Molecular biological and protein chemical methods

2.2.1 Polymerase chain reaction (PCR)

A polymerase chain reaction after Mullis *et al*.[363] was used to amplify target DNA sequences.

Table 6: Typical used mixture for a PCR

ddH_2O	39.39 µL
Phusion® Puffer (10x)	5 µL
10 mM dNTP-Mix	1 µL
DNA-template (50 ng/µL)	1 µL
Primer 1 (10 µmol/µL)	1.33 µL
Primer 2 (10 µmol/µL)	1.33 µL
DMSO (optional)	*1.5 µL*
+ Pfu-Polymerase	1 µL

The PCR was performed in the thermocycler with the following program, where the indicated temperatures (red) were chosen depending on the primer annealing temperatures, which were calculated using the OligoCalc tool[364].

95 °C, 2 min; 30x (95 °C, 30 sec; 58 °C, 20 sec; 68 °C, 3 min); 68 °C, 5 min; ∞ 10 °C

The following longer program with higher temperatures was applied, if the first one was not successful:

95 °C, 2 min; 30x (95 °C, 30 sec; 58 °C, 30 sec; 72 °C, 3 min); 72 °C, 5 min; ∞ 10 °C

The final PCR product was further purified and checked via an agarose gel electrophoresis and stored at -20 °C.

2.2.2 Agarose gel electrophoresis of DNA

For preparative and analytical separation of plasmids, PCR amplification products or DNA fragments, freshly prepared agarose gels (table 7) were used according to standard protocols[362]. The gel and chamber were filled with 1x TBE buffer and the DNA samples (50 µL) were mixed with 10 µL 6x DNA application buffer and applied separately with a 100 bp DNA marker as a reference. The electrophoresis was carried out at 180 V and 4 °C for 10-20 min, depending on the expected size of the DNA fragments. The visualisation of the DNA bands was made under UV light at 365 nm with a gel documentation system and desired bands were cut out and purified with the *Wizard SV Gel and PCR Clean-Up System*. DNA concentration was determined with the nanodrop UV/VIS spectrophotometer at a wavelength of 260 nm.

Table 7: Table of used buffers and solutions for an agarose gel electrophoresis.

Solutions and Buffers	Compositions
Agarose gel	1 % (w/v) Agarose
	TBE Puffer
	0,00006 % (v/v) DNA Stain Clear G
TBE-Puffer (10 X)	89 mM TRIS pH 8.2 - 8.5
	89 mM Boric acid
	2 mM EDTA
DNA loading buffer	30 % (v/v) glycerol
	0.25 % (w/v) bromophenol blue
	0.25 % (w/v) xylene cyanol FF

2.2.3 Restriction free cloning

To insert the amplified DNA constructs from the first PCR, restriction free (RF) cloning was employed as a cloning tool for the second step[362]. Therefore, the previously amplified inserts have specifically designed overhangs that are complementary to the chosen vector, usually a lab tested plasmid with high expression. To achieve a good cloning yield, typically a 10-fold molar excess of insert to plasmid were chosen, which leads to different required ddH_2O and Insert volumes for each reaction (table 8).

Table 8: Typical used mixture for the RF cloning

ddH_2O	X µL
Quik Change 10x Buffer	2.5 µL
XL dNTP-Mix	0.5 µL
Plasmid (50 ng)	1 µL
Insert in 10-fold excess	X µL
DMSO (optional)	*0.75 µL*
+ Quik Change Enzyme Mix	0.5 µL

The RF cloning was performed in the thermocycler with the following program, where the indicated temperatures (red) were chosen depending on the insert's melting temperature and stability of its overhang's secondary structure:

95 °C, 2 min; 8x (95 °C, 30 sec; 52-68 °C, 30 sec; 68 °C, 7 min); 20x (95 °C, 30 sec; 64 °C, 30 sec; 68 °C, 7 min); 68 °C, 10 min

After the reaction the product was digested at 37 °C for 1 h with Dpn1, to remove residual input plasmid. Finally, the digested product was transformed into the respective *E. coli* strand and appropriate antibiotics and plated.

2.2.4 Quik Change site directed mutagenesis

For minor changes to a DNA construct, e.g. point mutations or small insertions, a quick and simplified one step mutagenesis after Papworth *et al*.[365] is conducted. The one step (termed Quik Change (QC)) reaction does not require a PRC amplification step, but directly inserts the desired mutation in the given plasmid backbone. This was achieved by two designed primers, with overhangs that are complementary to the chosen beginning and end of the insertion point of the vector. To achieve a good cloning yield, typically a 10-fold molar excess of primers to plasmid was chosen.

Table 9: Typical used mixture for the QC mutagenesis.

ddH_2O	X µL
Quik Change 10x Buffer	2.5 µL
XL dNTP-Mix	0.5 µL
Plasmid (50 ng)	1 µL
Primer 1 (10 µmol/µL)	0.66 µL
Primer 2 (10 µmol/µL)	0.66 µL
DMSO (optional)	*0.75 µL*
+ Quik Change Enzyme Mix	0.5 µL

2.2.5 SDS-polyacrylamide gel electrophoresis (SDS-PAGE)

The SDS-PAGE for quality control and analysis of a protein expression and purification was performed according to Laemmli *et al*[366]. Dependent on the protein sample concentration, the protein sample was mixed 1:1 or 2:1 with SDS loading buffer and denaturated at 95 °C for 5 min. Test-purification and test-expression samples, as well as samples of unstable proteins were used uncooked, in order to avoid degradation and artefacts. For expression tests with hard to stain inclusion bodies the samples were sonicated for 20 sec and not cooked. 20 µL of the prepared mixtures were loaded in each pocket onto the gel together with a separate protein marker. The electrophoresis was conducted at a current of 50 mA per gel and for 30-35 min.

For staining, the gel was first cooked twice with double distilled water and subsequently heated with Protein Page blue staining solution and incubated for 5-15 min with it. The destaining was done with double distilled water and a gently applied paper tissue, until enough contrast was observable.

Table 10: Table of used buffers and solutions for the SDS gel electrophoresis.

Solutions and Buffers	**Compositions**
(6 %) Stacking gel	2 mL volume per gel
	58 % (v/v) ddH_2O
	15 % (v/v) Acrylamide (40 % solution)
	25 % (v/v) 0.5 M Tris pH 6.8
	1 % (v/v) SDS (10 % solution)
	1 % (v/v) APS (10 % solution)
	0.1 % (v/v) TEMED
(15 %) Separation gel	4 mL volume per gel
	71 % (v/v) ddH_2O
	37.5 % (v/v) Acrylamide (40 % solution)
	25 % (v/v) 1.5 M Tris pH 8.8
	1 % (v/v) SDS (10 % solution)
	1 % (v/v) APS (10 % solution)
	0.1 % (v/v) TEMED
2 x Laemmli buffer	0.02 % (w/v) Bromophenol blue
	20 % (v/v) glycerol
	15 % (v/v) β-Mercaptoethanol
	120 mM Tris pH 7.0
	10 % (w/v) SDS
SDS 10x loading and running buffer	2 M Glycine
	0.25 M Tris
	1 % (w/v) SDS

2.2.6 Transformation of *E. coli*

The transformation of all DNA vectors into chemically competent cells was performed by standard protocols of the respective manufacturer. 25-50 µL competent *E. coli* cells and 50 ng of plasmid DNA were mixed on ice and incubated for 15-30 min. The Cells were then heat-shocked for 45 sec at 42 °C, followed by a 2 min incubation on ice. Afterwards 200-500 µL SOC medium were added and the cells are transferred into the incubator at 37 °C for 45 to 60 min, in order to establish antibiotic resistance. Finally, cells were plated on LB agar plates containing the respective antibiotics or precultures (25 mL per L expression) were inoculated and incubated overnight at 37 °C. For each expression a fresh transformation and overnight preculture was done.

2.2.7 Isolation of plasmid DNA from *E. coli*

A 5-7 mL selective medium was inoculated with a single picked colony from an agar plate and incubated at least over 12 h at 37 °C under shaking. Then the culture was centrifuged at 3200 g and 4 °C for 10 min, yielding the desired cell pellet. The subsequent isolation of the plasmid DNA was achieved with the *Wizard Plus SV Minipreps DNA Purification Kit* according to the manufacturer's instructions[367]. The elution was carried out with 30-40 µL ddH_2O. After determining the concentration, the plasmid DNA was stored at -20 °C or kept at 4 °C for transformation or sequencing.

2.2.8 DNA sequencing

The sequencing of plasmids was carried out by GATC Biotech AG (Konstanz, Germany) and GENEWIZ Germany GmbH (Leipzig, Germany) according to the method of Sanger *et al*[368]. For this purpose, 7.5 µL plasmid DNA and 2.5 µL of the corresponding sequencing primer (T7 forward or reverse) were mixed in an Eppendorf tube. The results of the sequencing were compared with the corresponding entries in the database (UNIPROT).

2.2.9 Isothermal titration calorimetry (ITC)

ITC measurements were performed on a MicroCal PEAQ-ITC at 10, 20 or 25 °C with usually 15-20 titration steps, 1-2 µL per step. All injections had a spacing of 180 s and a filter period of 5 s. The reference power was set to 10 µcal/sec, the initial delay to 300 s and stirring speed to 750 rpm. Titration partners were dialysed in the same buffer before the measurement or if not possible, the ligand was dissolved in the dialysis buffer. The instrument was thoroughly washed beforehand and at least one successful water to water titration was done before each measurement. In general, the concentration of the ligand in the syringe was 200, 500 µM or 1 mM, while the concentration of the binding partner in the cell was 10-fold lower (20, 50 or 100 µM respectively). The data were fitted with the MicroCal software and plotted using ProFit.

2.2.10 Differential Scanning Calorimeter (DSC)

DSC measurements were performed on a Malvern MICROCAL PEAQ-DSC manual Differential Scanning Calorimetry from 4 to 100 °C with a scanning speed of 60 °C/h and typical protein concentrations of 10-20 µM (without nanodiscs around 0.25-0.5 mg/mL) and sample volumes of 130 µL. Before the first sample at least 3 water-water and then 3 buffer-buffer runs with the same settings were done, to ensure optimal thermal equilibrium of the instrument and assess its cleanliness. Between samples usually at least one buffer-buffer run was performed. Obtained thermograms were analysed with the supplied PEAQ-DSC software and calibrated by it in accordance to the determined and input concentrations (measured by UV-Vis).

2.2.11 Dynamic light scattering (DLS)

Dynamic light scattering (DLS) measurements were done on a DynaPro NanoStar instrument (Wyatt Technology) at 20 °C and a wavelength of 622.3 nm or 658 nm, with the help of Markus Fleisch and Melina Daniilidis.

The duration of each measurement were typically 5-15 seconds and 10 measurements per experiment were recorded to ensure accurate data. The obtained correlation functions were derived and converted to particle diameters with DYNAMICS software (Wyatt Technology Corporation).

2.2.12 Circular Dichroism Spectroscopy (CD)

CD spectra were recorded at 20 °C using a 0.1 cm path-length quartz cuvette (Helma AG, Mühlheim, Germany) with a sample volume of 280-300 µL on a JASCO J-715 Spectro-polarimeter. The samples were scanned from 260 to 190 nm with a total of five scans, with a scanning speed of 100 nm/min and a band width of 1.0 nm. Thermal transitions were recorded using variable temperature measurements with a scanning rate of 60 °C/h, a bandwidth of 2 nm and a response time and a delay time of 1 sec each. Therefore, the signal minimum at 220-222 nm (α-helical fold) or 219 nm (mixed topologies) was followed during the temperature scan in the range of 20 to 100 °C. If needed, reverse scans from 100 to 20 °C were recorded to evaluate the refolding properties of the proteins or their secondary structure elements. For each sample a CD spectrum was recorded at 20 °C prior and after thermal melting, in order to assess the loss of secondary structure and the amount of reversibility.

2.2.13 Formation of Liposomes and Pore-forming Assay

For the formation of outer mitochondrial membrane like liposomes (OMMLs) for a pore-forming assay or as membrane mimetic respective lipid mixtures of *E. coli* total lipids or DMPC, DMPG and cardiolipin were prepared from chloroform stocks (5 or 10 mM). For nickel supported pore-forming assays, typically 10 % w/w nickel-lipids were added (18:1 DGS-NTA(Ni)). Chloroform was evaporated using a stream of nitrogen and remaining solvent was subsequently removed by lyophilisation overnight. The dry lipid films were mixed with the respective buffers, depending on the experiment. After adjusting the concentration of the lipids, the mixture was subjected to 15-20 freeze (liquid N_2) and thaw cycles (hot water) until the mixture became clear or mildly turbid. Finally, liposomes were formed by pressing the obtained clear mixture through an extruder with a 0.2 µm membrane at least 21 times.

If dye-filled liposomes were used, they were subjected to two subsequent Sephadex (NAP-5 or NAP-25, GE Healthcare, Chicago, USA) gravity column purifications to remove excess non-included dye and reduce background fluorescence.

2.2.14 Fluorescence-based spectroscopy

Fluorescence labelling with 5(6)-Carboxyfluorescein *N*-hydroxysuccinimide ester (FAM)[369]

All solution and stocks containing any dye were always covered during this procedure with aluminium foil and protected from light. A 3 to 5-fold excess of FAM (dissolved in 100 % DMSO) to 100-200 µM protein in nitrogen/Tris-free Buffer of 20 mM NaPi pH 6.4 was added for 1-2 h at room temperature. Unreacted dye was quenched with 5 to 10-fold excess of 1 M Tris pH 8.0. The quenched dye was removed through 3 rounds of concentration and dilution (centricon exchange) in an Amicon Centricon with 10 kDa cut-off, followed by 1 to 2 NAP-5 column purifications. Also, dialysis followed by 2 NAP-5 columns is possible, if more time is available. Size exclusion chromatography cannot be performed, as the dye reacts with the bead-material of the column and colours it yellow, which is hardly reversible.

Alexa Fluor 488 (C_5 Maleimide) labelling[370,371]

All solution and stocks containing any dye were always covered during this procedure with aluminium foil and protected from light. 50-100 µM protein were dialysed into 10 mM Tris pH 7.0, 50 mM NaCl and 1 mM TCEP. 4 mM additional TCEP was added to the sample after dialysis for 30 min at room temperature, to ensure full reduction of the cysteine, prior tagging. Excess TCEP was removed via two rounds of centricon exchange. Alexa Fluor 488 was dissolved in 100 % DMSO and added dropwise in 10-fold excess to the protein and closed in an aluminium container. The reaction was allowed to proceed for 2 h at room temperature, and additionally over night at 4 °C. Excess dye was removed via dialysis at 4 °C for 4 h and 2 subsequent NAP-5 columns.

Fluorescence polarisation and FRET-based assays

Fluorescence polarisation and FRET-based assays were measured on a JASCO Spectrofluorometer FP-8300 equipped with a water bath cooling system, typically at 20 degree under stirring in a large (1000 µL), or for tests in a small (100 µL) quartz cuvette.

For FRET measurements a new nanodisc-based system was designed, where a rhodamine containing lipid (16:0 PE) was incorporated during nanodisc assembly with 2 lipids per leaflet. The corresponding FRET partner (Alexa Fluor 488) was attached according to standard protocols to a newly introduced cysteine 102Cys of Bcl-xLΔTM as in[372]. Typically, for each experiment 1 µM of rhodamine-nanodiscs and 50-100 nM of AF488-Bcl-xL were mixed and measured at 455 nm excitation and the emission was recorded from 470-700 nm, with a bandwidth of 5 nm for both excitation and emission.

For fluorescence polarisation (FP) measurements 100 nM N-terminally labelled Bcl-xLΔTM with carboxyfluorescein (CAF), was measured with increasing concentrations of empty nanodiscs from 1 to 200 µM, in 10 µM steps. This was done for varying lipid compositions with each sample in a triplicate.

FP measurements were done in a 100 µL quartz cuvette with excitation wavelengths of 494 nm, emission wavelengths of 525 nm, and respective bandwidths of 5 nm. The response time was adjusted to one second with medium sensitivity, to ensure a good signal to noise ratio. As a buffer a composition of 20 mM NaPi, 25 mM NaCl, 2 mM BME was chosen.

2.2.15 NMR Measurements

Sample Preparations and measurements

All NMR samples were measured in shigemi tubes with volumes of 300-400 µL and final D_2O contents of 5-7 % (v/v) for an ideal lock signal. All NMR experiments were done at TUM (Garching) and Helmholtz-Zentrum München (Neuherberg) and recorded on Bruker AvanceIII instruments equipped with cryogenic probes and operating at 600, 800, 900 and 950 MHz proton frequency. The measurement temperatures were usually 30 °C (303 K) and 37 °C (310 K), if not stated otherwise. Most of nanodisc screenings, nanodisc titrations and studies of full-length Bcl-xL samples in nanodiscs were done at a field strength of 900 and 950 MHz, to yield the best possible spectra for the large particles.

Depending on the concentrations, usually 32, 64, 96 or 128 scans were used and a minimum of 192 increments were recorded, to ensure a good spectral resolution. Samples of soluble Bcl-xL only, were higher concentrations (0.5-2 mM) are possible, were recorded with fewer scans (8-16), but with 256 increments.

Processing and analysing data

All spectra were processed with Topspin and analysed with SPARKY4, and NMRFAM-SPARKY. Visualisation, colouring of affected residues, and creation of pictures and plots was done with the help of PDB structures, in combination with Pymol 1.8.4.2, UCSF Chimera and Origin 2017 94G.

Assignments, structure calculations and RDCs

Backbone resonance assignments were done with TROSY-based triple resonance (3D) experiments. Further NOESY experiments were recorded at 40 or 45 °C (313 K, 318 K) with a mixing time of 200 ms. Following structure calculations were performed with Xplor-NIH[373] using standard protocols. 20 structures with the lowest restraint violation energies were used to get structural statistics of an ensemble. Further, a Ramachandran map analysis was performed employing the RAMPAGE webserver[374].

RDCs of full-length Bcl-xL in nanodiscs were obtained, determined and measured by employing two sets of 2D-TROSY and semi-TROSY[361] experiments. For this the experiments were recorded for the isotropic case or for the aligned case in the absence, or presence, of 8 mg/mL Pf1 phage (Asla Biotech, Riga, Latvia) respectively. Finally, the software PALES and MODULE2 were employed for fitting of the resulting RDC alignment tensor and its visualisation.

PRE measurements and data analysis

To obtain distance dependent paramagnetic relaxation enchantment (PRE) effects and data in the nanodisc system, gadolinium (Gd^{3+}) pre-loaded, or self-loaded PE-DTPA-DMPE-lipids, were used. During the nanodisc assembly, these Gd^{3+}-tagged lipids were employed in a ratio of 2 per leaflet (together with Bcl-xL-TMH or Fl-Bcl-xL).

In order to determine which lipid compositions are preferred by Bcl-xL (for nanodisc-Bcl-xL titrations) 4 PE-Gd^{3+}-DTPA lipids per leaflet for empty nanodiscs were employed.

Since Gadolinium cannot be stripped from its highly stable complex with EDTA or DTPA, always 2 equivalent samples from the same stocks with and without Gadolinium were prepared. To compare the PRE-effect through NMR measurements, an optimal d1 delay of 2 s was determined, by comparing recorded 1D spectra from 0.5-3 s, and used for all samples and reference samples. Sample concentrations were adjusted and matched, if possible, to simplify the comparison process. Number of scans and increments were optimised for Gd^{3+}-samples with the lowest intensity in a sample series and used for all sets of samples (e.g. +/- Gd^{3+} and +/- PUMA or +/- nanodiscs) throughout the experiment series, to gain the best spectral quality and PRE-effects. The obtained spectral intensities for each amino acid residue of each set of samples were compared by referencing them to at least one PRE-unaffected residue with highest intensity available in both samples, to obtain an intensity ratio of 0.0-1.0.

2.2.16 Small angle X-ray scattering (SAXS)

Measurements were performed by Dr. Ralf Stehle (TUM, SFB1035) with a Rigaku BioSAXS1000 Camera attached to a Rigaku HF007 microfocus rotating copper anode (40 kV, 30 mA). Transmissions were measured with a photo diode beamstop. q calibration was carried out with a silver behenate sample (Alpha Aeser). Samples were measured in eight 900 second frames which were compared to check for beam damage. The circular averaging and solvent subtraction were done by the SAXSLab software (v3.0.2). Two concentrations (x, y mg/mL) were measured from each sample in NMR buffer at 4 °C (below) and 30 °C (above the transition temperature of the nanodisc lipids) normalised to concentration and compared to exclude concentration dependent effects.[375]

Fits for the empty discs were carried out with the SasView 4.1.2 software with a core shell bicelle model.[376]

2.2.17 Mass spectrometry

Electrospray ionisation mass spectrometry (ESI-MS) measurements were performed on an LCQ-FLEET, equipped with a 3D ion trap for mass spectrometry (MS) analysis and a high-performance liquid chromatography (HPLC), with the kind help of Dr. Inguna Goba and Burghard Cordes.

MALDI TOF measurements were done by Florian Rührnößl and Gina Feind on a Bruker ultraflex TOF/TOF.

2.2.18 Size exclusion chromatography (SEC)

All SEC experiments were carried out with an Äkta purifier system (GE healthcare) equipped with a F9-R fraction collector. For analytical runs with nanodiscs, or protein and nanodiscs, an analytical Superdex 200 Increase 10/300 GL column of 24 mL bed volume was employed. Preparative runs and protein purifications were performed on a Superdex 75 10/300 GL with 120 mL bed volume (for proteins) and a HiLoad 16/600 Superdex 200pg with 120 mL bed volume for large nanodisc assmeblies. The columns were equilibrated and run in 50 mM Tris pH 8.0, 150 mM NaCl and optional 10 mM BME optional. The sample injection volume was 500-850 µL (Superdex 200) and 3-4.5 mL (Superdex 75), flow rates were 0.5 mL/min (Superdex 200) and 1.2 mL/min (Superdex 75 and 200pg). For NMR samples a buffer of 20 mM NaPi pH 7.0, 20-50 mM NaCl, (2-5 mM DTT optional), 0.5-1 mM EDTA was employed.

2.3 Protein and enzyme methods

2.3.1 Protein Expression and Purification

The common enzymes TEV protease[377] and Sortase A[214,378] as well as MSP1D1 and MSP1D1ΔH5[158,173] were purified according to previous protocols. TEV protease was however mainly supplied by Dr. Arie Geerlof (Helmholtz-Zentrum Munich).

Bcl-xL-TMH and GlycophorinA Expression and Purification

The Bcl-xL transmembrane helix (TMH) and GlycophorinA were produced in inclusion bodies as a N-terminal His_6-GB1-THR-Bcl-xL-TMH or His_6-GB1-THR-GlycophorinA-TMH fusion construct with a thrombin cut site (LVPR/GS).

Therefore, the respective pET15b vector was transformed in *E. coli* BL21 (DE3) cells in 25 mL LB supplied with 2 % glucose per liter main culture. The main culture was grown at 37 °C until an OD_{600} of 0.7. The induction of protein expression was done with 1 mM IPTG and the cells were incubated for another 5 hours at 37 °C. To produce [U-^{2}H,^{13}C,^{15}N]-Bcl-xL-TMH, the bacteria were grown in M9 medium, supplemented with 1 g/L [U-99 % ^{15}N]-NH_4Cl and 2 g/L [U-99 % ^{2}H,^{13}C]-glucose in 99 % D_2O (Euroisotope or Sigma-Aldrich). For labelled protein expression typically 6 h of expression was done, until a final OD of 1.2-1.4 (comparable to LB expression) was reached.

Purification of Bcl-xL-TM-GB1 and GlycophorinA-GB1

For lysis, typically a 1 L pellet was resuspended with a homogeniser in 40-45 mL lysis buffer (50 mM Tris pH 8.0, 100 mM NaCl, 1 mM PMSF, 2 mM EDTA, 1 protease inhibitor tablet) and incubated with lysozyme while stirring for 30 min at 4 °C. Afterwards the lysate was sonicated (30 min, 30 % amplitude, 10 min pulse length) and DNaseI was added together with 6 mM $MgCl_2$ for another 30 min while stirring at 4 °C.

To solubilise the inclusion bodies, 6 M guanidine hydrochloride (≥ 99.99 %) was added as a powder to the buffer, resulting in approx. 60-65 mL of (50 mM Tris pH 8.0, 100 mM NaCl, 6 M GdmCl = buffer A) and incubated for one hour at room temperature, whilst shaking or stirring. Remaining insoluble cell debris and lipids were spun down with 50000 g for 20 min.

The supernatant was sterile filtered (0.4 µM) and applied to 10-15 mL Ni-NTA resin (GE-Healthcare) equilibrated with buffer A using a gravity flow column and incubated for one hour at room temperature, whilst shaking or stirring. The lysate was reapplied, and the resin was washed with 10-12 column volumes (CV) buffer A and 5 CV of buffer A + 10 mM imidazole. Finally, the protein was eluted using buffer A containing 600-750 mM Imidazole (6-8 CV) and dialysed against 5 L of 20 mM Tris pH 7.5 in a 3.5 kDa MWCO dialysis tube. Higher imidazole contents (750 mM) allow faster elution in smaller volumes, leading to more precipitate protein and higher yields, as protein can also be found in the soluble part. The precipitated protein was then dissolved in typically 1-2 mL of 2-5 % SDS solution. Using 2 % SDS is more beneficial for following nanodisc assemblies, and was preferred. The concentration was determined through UV/Vis spectroscopy using the absorption at 280 nm and a calculated (ProtParam) extinction coefficient ε280 of 19940 (Bcl-xL-TMH-GB1) or 5500 for Bcl-xL-TMH and 14440 for GB1-His_6, or 15890 for GlycophorinA-GB1 and 1490 for GlycophorinA respectively.

Bcl-xL-soluble domain Expression and Purification

All Bcl-xL soluble domain variants (Bcl-xLΔTM, Bcl-xL-SOR, Bcl-xL-THR-ΔTM and Bcl-xL-THR-SOR) were expressed and purified the same way[379], as well as 102C cysteine variants of Bcl-xL. They were produced with a pET21a-Bcl-xL vector (or pET21a-Bak) in *E. coli* BL21 (DE3) cells according to previous protocols[258,297]. Protein expression was induced with 1 mM IPTG at 37 °C at an OD_{600} of 0.7-0.8, and then cells were cooled down to 20 °C and incubated overnight (12-16 h). To produce [U-^{2}H,^{13}C,^{15}N]-Bcl-xL variants, bacteria were grown in M9 medium supplemented with 1 g/L [U-99 % ^{15}N]-NH_4Cl and 2 g/L [U-99 % ^{2}H,^{13}C]-glucose in 99 % D_2O (Euroisotope or Sigma-Aldrich).

Purification of Bcl-xL soluble domain

For lysis, usually a 2 L pellet was resuspended with a homogeniser in 50 mL lysis buffer (50 mM Tris pH 8.0, 200 mM NaCl, 2 mM EDTA, 5 mM BME, 1 mM PMSF, 2 protease inhibitor tablets) and incubated with lysozyme for 30 min at 4 °C while stirring. Following sonication (30 min, 30 % amplitude, 10 min pulse length), DNaseI was added together with 6 mM $MgCl_2$ and the mixture was stirred for 30 min. Residual cell debris was spun down at 50000 g for 20 min, the supernatant was sterile filtered (0.4 µM) and applied to 10-15 mL of Ni-NTA resin (Ge Healthcare) equilibrated with 20 mM Tris pH 8, 200 mM NaCl, 5 mM BME (buffer A) using a gravity flow column and incubated for 30-45 min at 4 °C.

The Ni-NTA resin was washed with 10-15 CV of buffer A, 3-5 CV of buffer A with 10 mM imidazole and lastly the protein was eluted with 8 CV buffer A containing 350-400 mM imidazole. Following a dialysis against 2 L of buffer A in a 10 kDa MWCO cut-off, the protein solution was concentrated with an Amicon centrifugal device of 10 kDa MWCO (Millipore) to a volume of 5 mL and purified on a HiLoad 16/600 Superdex 75 pg size exclusion column (Ge Healthcare) equilibrated with calcium free Sortase Buffer (50 mM Tris pH 8.0, 150 mM NaCl, 10 BME) or NMR buffer (20 mM NaPi pH 7.0, 20-50 mM NaCL, 2 mM DTT, 0.5 mM EDTA). The concentration was determined through UV/Vis spectroscopy using the absorption at 280 nm and a calculated (ProtParam) extinction coefficient ε280 of 41940 (Bcl-xL-SOR, Bcl-xL-THR-SOR, Bcl-xLΔTM Bcl-xL-THR-ΔTM).

Bcl-xL-TMH Nanodisc assembly

Nanodiscs assemblies were done according to established protocols[158,166,173]. The CTD-MSPΔH5 protein and cholate-solubilised lipids (usually DMPC: DMPG = 3:1) were incubated with Bcl-xL-TMH-GB1 (solubilised in 2-5 % w/v or 70-173 mM SDS) in 20 mM Tris pH 7.5-8.0, 100 mM NaCl, 0.5 mM EDTA (MSP buffer) at a final cholate concentration of 20 mM and SDS concentration of 2.5-8.2 mM SDS. The MSP to TMH ratio was kept at 6:1 or 4:1, with 200 µM of MSP and 33 or 50 µM of TMH respectively. The optimal MSP to Lipid ratio was between 1:35-1:38 for the CTD-MSP1D1ΔH5 and was determined empirically by varying the lipid content to obtain a largely monodisperse SEC profile. After incubation at RT for 1.5 h, 0.7-0.8 g of washed biobeads (BB) were added per mL of assembly mixture (referring to 1 mL with an MSP concentration of 200 µM) and the suspension was shaken at room temperature for 3.5-4 h.

Afterwards, the biobeads were removed in an empty gravity flow column and washed twice with MSP pH 8.0 buffer. The flow through and wash was pooled, 0.5 mM $MgCl_2$ was added to quench residual EDTA. The mixture was incubated with 5 mL Ni-NTA resin while shaking, equilibrated in 20 mM Tris pH 8.0, 100 mM NaCl (Ni-NTA buffer), for 1 h at room temperature. The resin was washed with 10 CV of Ni-NTA buffer and 4 CV of Ni-NTA buffer with 10 mM Imidazole to remove excess empty nanodiscs. Finally, the filled nanodiscs were eluted with Ni-NTA buffer containing 500 mM imidazole. After dialysing in 20 mM Tris pH 8.0-8.4, 100 mM NaCl, the nanodiscs were concentrated to 1 mL volume and incubated with 5-10 units of thrombin and 2-5 mM $CaCl_2$ at 37 °C for 0.5-1 h. Subsequently, the nanodiscs containing the cut off GB1 and Bcl-xL-TMH in nanodiscs, were purified and separated on a ÄKTA PURE system using a Superdex 200 increase 10/300 GL size exclusion column (GE Healthcare).

For a consequent Sortase Ligation the column was equilibrated with 50 mM Tris pH 8.0, 150 mM NaCl, 10 mM BME (calcium free sortase buffer). For an NMR sample of TMH containing nanodiscs the column was equilibrated using 20 mM NaPi pH 7.0, 50 mM NaCl, 0.5 mM EDTA.

One homogeneous peak was pooled and concentrated using an Amicon centrifugal device of 30 kDa MWCO (Millipore). The concentration was determined through UV/Vis spectroscopy using the absorption at 280 nm and a calculated (ProtParam) extinction coefficient ε280 of 45300 (5500 for Bcl-xL-TMH and 2x 19940 for CTD-MSPΔH5) The overall yield was usually between 20-25 %.

Determining the number of helices per Nanodisc

To determine the number of helices per nanodisc, both fractions (TMH-nanodiscs and GB1) were pooled, and concentrations were determined via UV-Vis spectroscopy and their respective extinction coefficients. Once the SEC UV-absorption (mAU) were referenced to UV-Vis A280-values, the creation of an empiric formula was possible, that allows to calculate the helices in one nanodiscs, by comparing the ratio of cut-off GB1 and nanodiscs respectively. Advancing this formula allowed to determine this ratio just from the SEC UV-absorption data (areas of both peaks).

Sortase A mediated ligation

The sortase mediated ligation was accomplished with the more active but calcium dependent Sortase A enzyme Penta-mutant (P94R, D160N, D165A, K190E, K196T)[203]. All used nanodiscs at this point were made of MSP with a C-terminal His-tag (CTD-MSPΔH5), which has no N-terminal glycine after TEV cleavage, as otherwise the Sortase A will ligate the Bcl-xL-SOR to one of the two MSPs of the nanodiscs outside (preferred reaction).

Typically, the ligation setup was in a final volume of 500-1000 µL with starting concentrations between 100-200 µM Bcl-xL-TMH nanodiscs, 100-200 µM Bcl-xL-SOR and 5-10 µM Sortase A (ratios of 1 : 1 : 0.04-0.075) and 20 mM $CaCl_2$. The ligation mixture was put in a mini Slide-A-Lyzer dialysis tip with 10 kDa MWCO at room temperature (22-23 °C) in Sortase A buffer (50 mM Tris pH 8.0, 150 mM NaCl, 10 BME, 20 mM $CaCl_2$).

After 30 min ligation time, 1-2 equivalents of Bcl-xL-SOR were added resulting in a ratio of 1 : 2-3 : 0.04-0.075. If a ratio of 1 : 0.04 or 1 : 0.05 was used for Sortase A, another equivalent was added together with Bcl-xL-SOR to reach a ratio of 1 : 2-3 : 0.075.

After additional 30 min another equivalent of Bcl-xL-SOR is added, reaching a final ligation ratio of 1 : 3 : 0.075 or 1 : 4 : 0.1 respectively. After 30 min the ligation was stopped by the addition of 20 mM EDTA followed by an immediate reverse Ni-NTA chromatography. The flow through and wash fractions, containing the product, uncoupled discs and hydrolysed Bcl-xL-SOR without His-tag, were concentrated using an Amicon centrifugal device of 30 kDa MWCO (Millipore) and purified on an ÄKTA PURE system using a Superdex 200 increase 10/300 GL size exclusion column (24 mL bed volume). The first peak fractions (product) were pooled and concentrated (45-50 % overall yield, coupling yield 80-90 %). The concentration was determined through UV/Vis spectroscopy using the absorption at 280 nm and a calculated (ProtParam) extinction coefficient ε280 of 87240.

3 Results

3.1.1 Expression and purification of Bcl-xL transmembrane helix

Preliminary work by Joka Pipercevic yielded the His_6-GB1-THR-TMH fusion construct (Figure 15) and was the starting point for the optimisation of the expression and the purification of Bcl-xL-TMH. It was found that the helix is expressed in very low yield and purity, as the *E. coli* cells degrade such small helices easily during expression. A fusion construct that protects the helix allows working with it in detergent, and keeps it stable in solution was emphasised.

In recent years, the chain A of the immunoglobulin-binding domain of streptococcal protein G (GB1 domain), linked to the N-terminus of target proteins, was successfully established for protein production[95,96]. It was shown that GB1 enhances protein production (especially of human proteins) in *E. coli*. Also, the solubility and handling during purification are improved, and GB1 was shown to be more advantageous than many other fusion-tags.

Throughout this work, a particular focus was the purification and high purity of the final product. This enabled to study the helix in two different systems, detergent and nanodiscs, which is the focus of the Bcl-xL-TMH chapter.

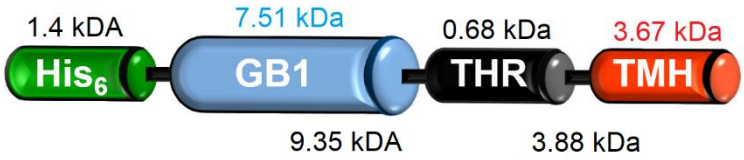

Figure 15: Depiction of the employed GB1 fusion construct (His_6-GB1-THR-TMH), with a thrombin cut site, indicated in bold, and an SG-linker (**LVPR/G**SG). In front of the His_6-tag are four amino acids (MSYY) responsible for the increased size of the tag. The overall size of the full construct is approximately 13.23 kDa, and the two parts after the thrombin cut are 9.35 and 3.88 kDa respectively. The Bcl-xL-TMH has three additional amino acids (35 instead of 32) because of the resulting GSG-linker.

Although the GB1-tag enhances solubility in most proteins, the Bcl-xL-TMH is very hydrophobic and therefore the construct is produced as inclusion-bodies by *E. coli*. The standard BL21(DE3) cell line produces the protein-construct in high yields and BL21(DE3)pLysS cells did not show any advantages. Expression at 30 °C for 1-12 h and 37 °C for 1-7 h showed that the lower temperature has no benefit than the higher one. As a conclusion, 4-5 h at 37 °C were chosen, as the yield did not change after 5 h.

For the purification, different inclusion-body purification-strategies were tried, see table 11. The highest yield and the best purity were obtained with a standard lysis, followed by the addition of 6 M of guanidine hydrochloride (≥ 99.99 % purity), as shown in materials and methods, and as can be seen in Figure 16. It was found that the GB1-Bcl-xL-TMH is not soluble in 1-8 M urea, or 8 M urea and different amounts of detergents (DPC or SDS), as seen in table 11.

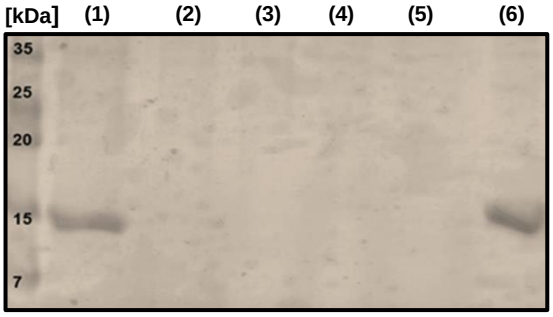

Figure 16: Coomassie stained SDS-PAGE-Gel of the Ni-NTA affinity chromatography of a standard GB1-Bcl-xL-TMH purification, with the 6 M guanidine hydrochloride approach. From left to right: (1) Lysate, (2) wash 1, (3) wash 2, (4) wash 3, (5) Imidazole (10 mM) wash, (6) Elution. The fusion-protein runs at 14-15 kDa, which is close to the calculated 13.23 kDa, and shows a monomer with high purity.

Good yields with a moderate to good purity were also obtained with a detergent-supported lysis and purification. Therefore, during (or after the standard lysis) the detergent of choice was added in high amount (1-2 % for DPC or 1 % for SDS). All following purification and nickel-affinity chromatography (Ni-NTA) steps were done with the respective detergent in the buffer. For elution, 0.2 % DPC (or 0.2 % SDS) were chosen, as this was found to be the maximum concentration of those detergents tolerated by thrombin.

Exchanging detergents (from SDS to DPC) was possible through Ni-NTA chromatography. However, once the helix is folded and the protein is in detergent micelles, the binding affinity to Ni^{2+} is heavily reduced.

Table 11: List of all employed detergents or denaturation agents, for purifications or solubility tests. It was found that harsh detergents (DPC, SDS) and guanidine chloride were the most suitable one.

Solubility Agent	Amount	Solubility
LDAO	0.5-10 %	Very low (50-100 µM)
DPC	0.2-0.5 %	Good (300-500 µM)
SDS	0.2-0.5 %	**Very good (1-2 mM)**
Urea	1-8 M	None
Urea + SDS/DPC	0.2-0.5 % SDS/DPC	Very low (50 µM)
Guanidine chloride	4-6 M	**Very good (1-2 mM)**

Overall, for most of this work, a combination of guanidine hydrochloride for purification, followed by SDS (0.2-0.5 %) for solubilisation and handling were chosen.

With this combination, the obtained yield per litre was 50-104 mg/L, as seen in table 12, for an unlabelled protein. Due to the high yield and other solubilised membrane proteins, it was found that it is critical to use a high amount of Ni-NTA slurry, in order to ensure proper binding. However, as SDS-solutions precipitate at low temperatures, the protein stock must be used up within one week, as multimerisation starts to occur over time (see Figure 17). That is also why no size exclusion chromatography could be performed with the SDS stock, as all ÄKTA-systems were cooled during this work.

Table 12: Optimised protein yields throughout this work for all three different labelling degrees used for the study of Bcl-xL-TMH. The average values, obtained from at least 5-fold expression and purifications, show that the yield drops by 38 % for a double-labelled protein and approximately by 87 % for a triple labelling. Comparing the maximum yields, the yield for the double labelled protein is less than 50 % of the unlabelled one. However, the average could not be determined for the triple-labelled construct, as it was expressed only once.

Labelling degree	Yield	Yield - Average
GB1-Bcl-xL-TMH	50-104 mg/L	77 mg/L
$^{2}H,^{15}N$ GB1-Bcl-xL-TM-H	45-50 mg/L	47.5 mg/L
$^{2}H,^{13}C,^{15}N$ GB1-Bcl-xL-TM-H	10 mg/L	-

After establishing the expression and purification, cutting His_6-GB1 off the TMH was the next step, in order to yield the native helix in detergent micelles and test the removal of the fusion-tag for further experiments and characterisations. Detergent-thrombin screenings showed that the limit is 0.15 % SDS, or 0.2 % DPC respectively, in the thrombin cut buffer (20 mM Tris pH 8.0-8.4, 100 mM NaCl, 2-5 mM $CaCl_2$). However, since SDS is easily precipitated by Ca^{2+} and the thrombin activity is lower in SDS presence, DPC was preferred for most detergent studies of Bcl-xL-TMH (see 4.1.2).

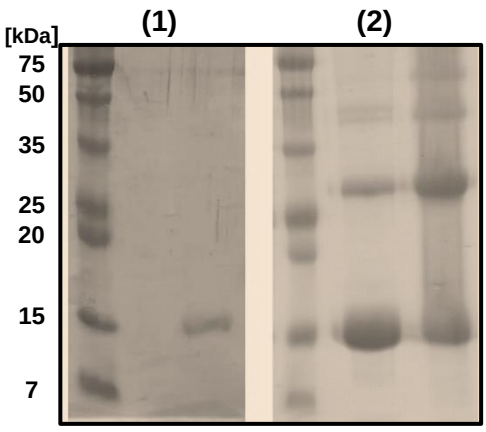

Figure 17: Comparison of Coomassie stained SDS-PAGE-Gels of the monomeric GB1-Bcl-xL-TMH (1) and its dimer- and trimerisation of the stock after several days in 2 % SDS (2). (1) An example of a fresh monomeric stock ($^{2}H,^{13}C,^{15}N$-GB1-Bcl-xL in 0.2 % DPC) with high purity, which runs at 15 kDa, besides being 13.23 kDa. The left Gel sample in (2) is cooked at 95 °C for 5 min, the right is uncooked. The stock starts to form dimers (band between 25-35 kDa, ~27-30 kDa), trimers (~40-45 kDa) and even higher-oligomers in the detergent solution.

3.1.2 Bcl-xL transmembrane helix in detergent and nanodisc

Bcl-xL transmembrane helix in detergent

In order to determine the structure of the native Bcl-xL-TMH in a phospholipid-bilayer, first the TMH needed to be reconstituted from detergent (DPC or SDS) into a nanodisc. Here, a method with several requirements was envisaged how to ensure a nanodisc assembly and subsequently remove the GB1 fusion-tag (see Figure 18). The first requirement is to obtain a homogeneous nanodisc-sample, where preferably only one helix is inserted. To achieve this, a 6 to 10-fold excess of membrane scaffold protein (MSP) and lipids was chosen, to ensure abundant nanodiscs are formed per helix. Furthermore, the buried helix inside the lipid bilayer of the nanodisc should still bind to Ni^{2+}-ions with the His_6-tag on its GB1-N-terminus, in order to remove the excess empty discs and residual assembly remains. An additional requirement is, that the thrombin cut site should be accessible for the thrombin-cleavage in the next step. Finally, the remaining linker must be long enough for a subsequent Sortase A ligation, as depicted in Chapter 3.1.5, in order to produce the full-length Bcl-xL.

Accordingly, lipids with a medium length (DMPC, 14:0, myristoyl) were chosen, and longer ones were also tested (POPC, 16:0-18:1, palmitoyl and oleoyl) to ensure an easy accessibility of all N-terminal residues.

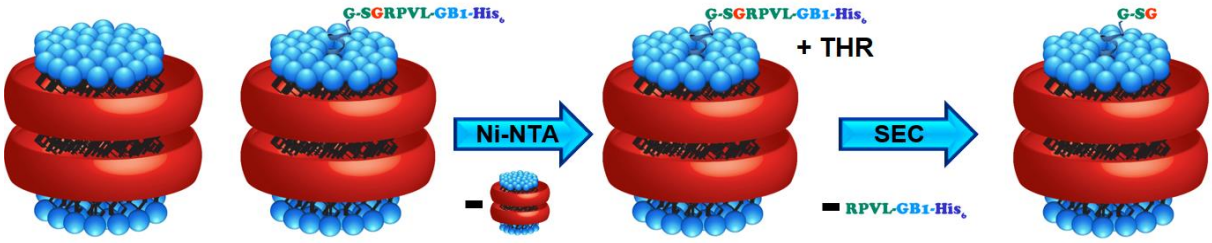

Figure 18: Schematic representation of the envisaged nanodisc assembly strategy, subsequent Ni-NTA purification with empty nanodisc-removal, followed by a thrombin cut and a size-exclusion chromatography to remove the His_6-GB1. The aim is to get a monomeric transmembrane helix into the nanodisc, to ensure sample homogeneity, and study the structure of the transmembrane helix in its native environment. The final goal is to get a monomeric full-length Bcl-xL after successful Sortase A ligation (see Chapter 3.1.5, Figure 34). Schematic nanodisc representation is adapted from[380].

Prior to nanodisc-assembly tests, the properties of the Bcl-xL-TMH in SDS (or DPC) were determined, and the purification and handling of the detergent system needed to be optimised for a successful nanodisc reconstitution. It was found that the thermal melting point of the helix in detergent (SDS and DPC) is so high, that it could not be determined via far-UV supported CD-spectroscopy with the given instrument heating range of 20-110 °C.

However, differential scanning calorimetry (DSC) was successfully performed, as the instrument thermal-range is up to 130 °C (Figure 19). Here, the transmembrane helix exhibited a melting point of 106.94 °C, while the onset was at 76 °C. As shown in Figure 17, if the purified protein was used within several days, a multimerisation of the TMH was avoided. It was found, that short sonication of 30 sec up to 2 min could reverse this process and homogenise the stock, without damaging the protein. These findings underline the stability of the system and its helical fold, also its robustness in terms of handling. These are good prerequisites for the single helix to successfully incorporate and refold into lipid bilayers.

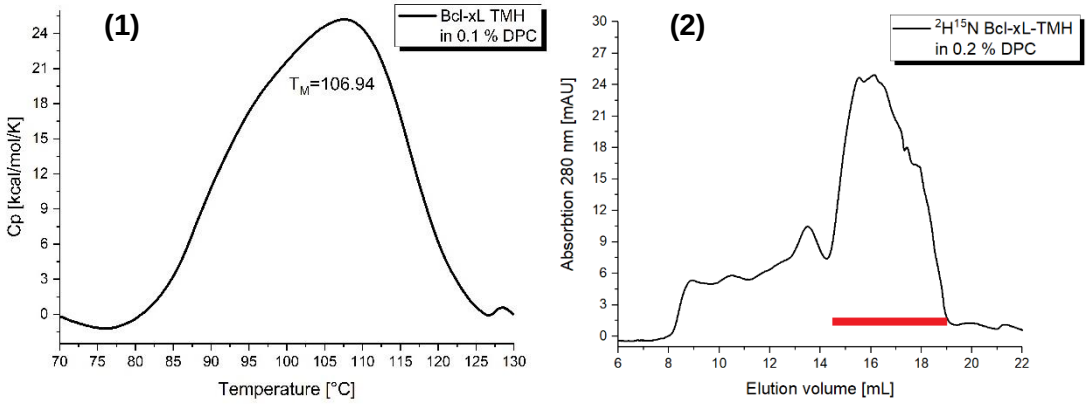

Figure 19: Differential scanning calorimetry (DSC) scan (1) and size exclusion chromatography (SEC) (2) of Bcl-xL-TMH in DPC. The DSC scan (kindly provided by Andrea Steiner) shows a broad melting range, from 77-127 °C, with an average melting point of 106.94 °C. The size exclusion chromatogram shows a large monomer peak (marked in red) at 16 mL, with a small preceding dimer peak at 13.5-14 mL, and larger oligomers from 8-13 mL.

Initial size exclusion chromatography (SEC) purification trials and subsequent NMR-studies of the ^2H,^{15}N-labelled Bcl-xL-TMH in 0.2 % DPC showed, that the cut-off GB1-tag is difficult to remove via size exclusion chromatography and it tails into the TMH-fractions, leading to high product loss. Furthermore, the highly soluble, small and flexible His_6-GB1-tag (9.35 kDa) produces very strong NMR signals, which overlay the one of the bigger helix-micelle particles of approximately 30-40 kDa. Therefore, thrombin-cut detergent samples were subjected to a reverse Ni-NTA chromatography, which successfully binds and removes the His_6-GB1 tag with high affinity. Subsequent SEC runs of the pure helix in 0.2 % DPC (Figure 19) exhibit mainly one broad peak at 16 mL, that corresponds to a monomer in a DPC micelle. A small amount of dimer-fraction is visible at 13-14 mL. Overall, the sample Is mainly monomeric and easy to separate from the dimer or higher oligomers. The indicated fractions containing the monomeric TMH in DPC were pooled and further studied by NMR (Figure 22).

To probe the homogeneity and assign the respective amino acids of the helix, two samples of uniformly labelled $^{2}H,^{15}N$-Bcl-xL-TMH and $^{2}H,^{13}C,^{15}N$-Bcl-xL-TMH were prepared. Both samples were measured with a 2D-[$^{1}H,^{15}N$]-TROSY spectra at 40 °C (313 K).

The 110 µM $^{2}H,^{15}N$-Bcl-xL-TMH in 400 mM DPC is depicted in Figure 22. As expected, the spectra show a folded α-helix with very narrow and well-resolved peaks, according to small and homogeneous particles (micelles), with monomeric Bcl-xL-TMH inside. This could also be confirmed by SDS-PAGE (Figure 16) and the SEC running behaviour and elution volume of the sample, as seen in Figure 19. Due to the sharp lines and the well-resolved spectra, a full assignment of the helix in DPC was possible.

Bcl-xL transmembrane helix in Nanodiscs

For nanodisc assemblies the shorter MSP1D1ΔH5 with a C-terminal His_6-tag was chosen, as bigger discs with MSP1D1 would favour the insertion of several helices per disc and possibly lead to inhomogeneous samples. Several lipids and lipid combinations with varying anionic content were probed during this work (Table 13) and their ratios were optimised empirically.

Table 13: Lipids and lipid mixes that were tested for nanodisc assemblies with GB1-Bcl-xL-TMH. All combinations were successful, though it was found that higher anionic content leads to a significant drop in assembly yield (below 5 %).

Lipids	Ratio [%]	Assembly
DMPC	100	Very good
DMPC/DMPG	75/25	Very good
DMPC/DMPG	50/50	Good
DMPC/DMPG	25/75	Bad
POPC	100	Very good
POPC/POPG	75/25	Very good
POPC/POPG	50/50	Good
DMPC/Cardiolipin	75/12.5	Very good
E. coli total lipids	100	Good

Neutrally charged POPC and DMPC, as well as their respective combination with anionic POPG or DMPG were successfully tested and found to work equally well. However, high anionic content of more than 50 % leads to high failure rates during nanodisc assembly, precipitations and a low overall assembly yield. Due to the presence of negative charge and a more native-like composition the ratio of 75 % DMPC and 25 % DMPG was chosen[381].

Several assembly methods were tested and optimised in parallel to the lipid composition, as can be seen in table 14. Since DPC does not dissolve the helix as good as SDS and as the overall assembly yield was better, SDS was chosen as a starting detergent for the reconstitution into nanodiscs and was mostly used during this work. Unfortunately, removing SDS and DPC is quite challenging, due to their big micelle size and their charge properties the detergents tend to bind to the dialysis membrane and cannot be easily removed with a 14-20 kDa cut off. Therefore, several different methods for SDS removal were devised, as shown in table 14. They include the addition of SDS-binding compounds. One compound is potassium chloride (KCl), which may precipitate SDS quickly, through a one-time addition, or slowly, through a dialysis-mediated exchange. Additionally, the use of β-cyclodextrin was probed, as it is shown to selectively bind and shuttle detergent molecules[382]. Typically, the dialysis was done in 5 L for at least 4 h and the buffer was exchanged between two to four times.

The biobeads-mediated standard nanodisc assembly was done in one or two steps, but always with a final amount of 0.7 g/mL assembly and 3-3.5 h incubation time.

Table 14: List of different employed methods and their cycle or compound amount that was used, for the reconstitution of GB1-Bcl-xL-TMH into nanodiscs and the successful removal of SDS.

Method used	Cycles or Amount used	Yield
Dialysis	2 to 4 in 5 L	< 1 %
Dialysis with β-Cyclodextrin in sample	2 to 4 in 5 L	< 10 %
Dialysis with KCl instead of NaCl	2 in 5 L	< 5 %
Dialysis with KCl precipitation beforehand	2 in 5 L	< 1 %
Biobeads	1 for 3 h	> 10 %
Biobeads	1/3 for 1 h, + 2/3 for 2 h	> 15 %
Biobeads	1/2 for 1.5 h, + 1/2 for 2 h	> 15 %

As depicted in table 14, all dialysis methods are inferior to biobeads-mediated nanodisc assemblies. Furthermore, due to several necessary buffer exchanges, the dialysis method takes several days, compared to 3-4 h of the biobeads technique. Further optimisations of the biobeads method showed that longer incubation times of 3.5-4 h and a step-wise addition is better, than the initial screening parameters. Overall yields of 15-20 % inserted helix can be achieved, calculated with one helix per nanodisc.

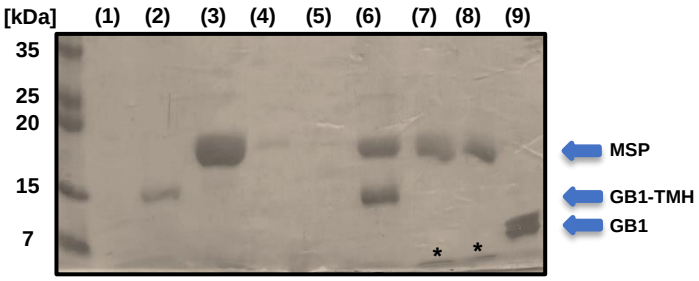

Figure 20: Exemplary Coomassie stained SDS-PAGE gel of a Ni-NTA purification of assembled nanodiscs and a subsequent thrombin-cut, followed by a size exclusion chromatography.(1) used biobeads, (2) $^{2}H,^{13}C,^{15}N$-GB1-Bcl-xL-TMH stock in DPC, (3) Ni-NTA flow-through, (4) and (5) the Ni-NTA wash, (6) elution of GB1-Bcl-xL-TMH nanodiscs, (7-8) TMH nanodiscs after SEC-purification, (9) cut-off GB1 after SEC-purification. The small and barely visible helix in (7) and (8) is marked with an asterisk.

The Ni-NTA purification was successfully established (Figure 20). The homogeneity of the assembled nanodiscs, their Ni-NTA purification and the thrombin-cut and subsequent removal of the GB1-tag was studied via SDS-PAGE (Figure 20), size-exclusion chromatography and dynamic-light scattering (DLS), as seen in Figure 21. Further mass-spectrometry analysis of the full GB1-Bcl-xL-TMH in nanodiscs, and the cut Bcl-xL-TMH in nanodisc, confirmed the successful assembly and full cut of the sample (Appendix, Chapter 6). Furthermore, the thrombin-cut also worked with long-chained lipids (POPC and POPG), which indicates that the linker is long enough for a following Sortase A ligation.

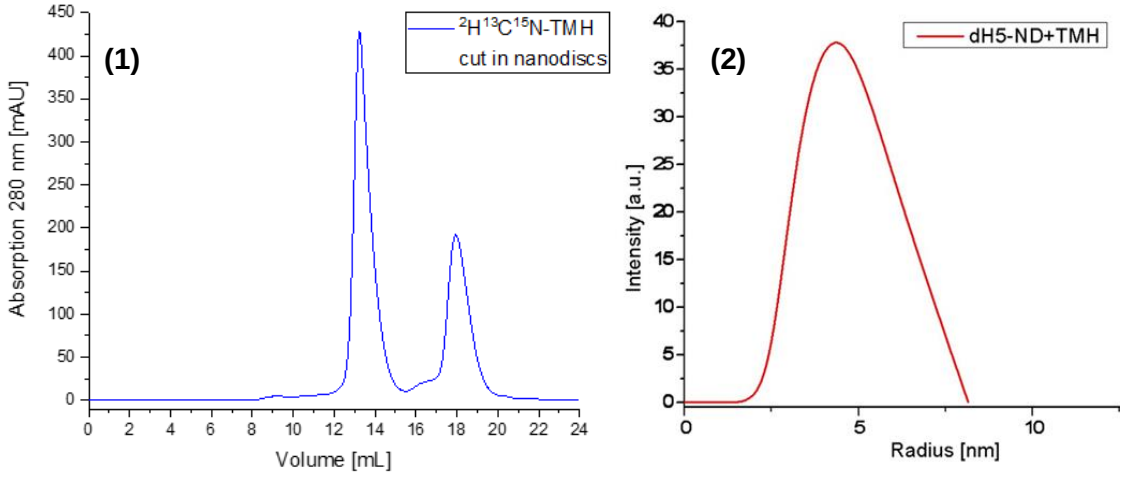

Figure 21: Size exclusion chromatography of $^{2}H,^{13}C,^{15}N$-Bcl-xL-TMH (13.24 mL) and its cut-off GB1-tag (17.94 mL) (1), and dynamic-light scattering (DLS) analysis (2) of the pooled nanodisc fraction. Both show a monomeric peak and a very homogeneous nanodisc sample. The elution volume of the S200a SEC-column of 13.24 mL corresponds to a standard MSP1D1ΔH5 nanodisc with the size of 8-10 nm in diameter. This finding is supported by the determined radius of 4.34 nm by DLS.

To assess the homogeneity and quality of the assembled TMH-nanodiscs, and to fully assign the respective amino acids, two samples of uniformly labelled $^{2}H,^{15}N$-Bcl-xL-TMH and $^{2}H,^{13}C,^{15}N$-Bcl-xL-TMH were prepared in MSP1D1ΔH5 nanodiscs. Deuterated (d_{54}) DMPC and DMPG lipids were used in the ratio 3 to 1.

A comparison between the nanodisc- and the detergent-sample is depicted in Figure 22. The 2D-[$^{1}H,^{15}N$]-TROSY spectra of the samples show 24-26 out of 35 residues, of which 32 are native and 3 are the GSG-linker. The low chemical shift dispersion could be correlated with an α-helical fold.

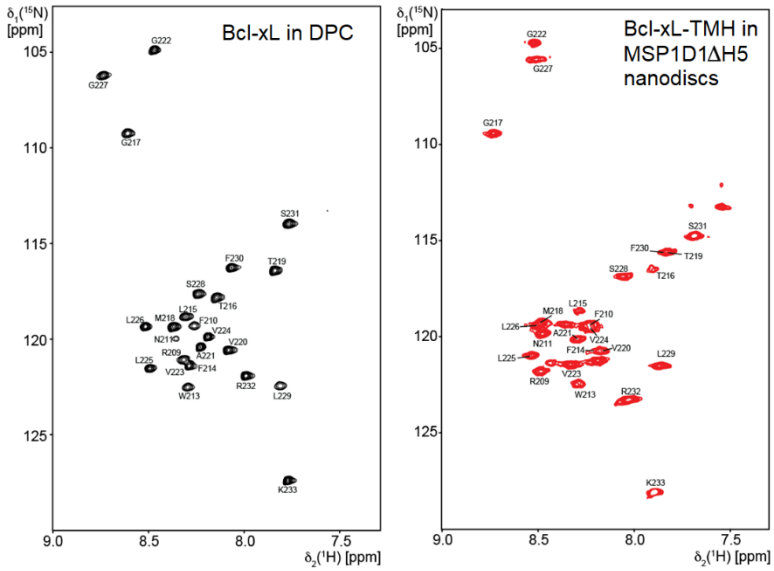

Figure 22: Comparison of two 2D-[$^{1}H,^{15}N$]-TROSY spectra of 110 µM $^{2}H,^{15}N$ Bcl-xL-TMH in 400 mM DPC (left) at 313 K, and 300 µM $^{2}H,^{13}C,^{15}N$ Bcl-xL-TMH in MSP1D1ΔH5 DMPC/DMPG (3:1) nanodiscs (right) at 315 K, W213 omitted for clarity. Assigned residues are indicated by the one-letter amino acid code with their respective amino-acid sequence number. Observable differences are several shifted residues, e.g. T219, G227, L229, F230, and also the TMH in nanodiscs shows broader peaks. This indicates a bigger and slower tumbling particle, which corresponds to a ~100 kDa nanodisc, compared to the ~30-40 kDa DPC micelles. Adapted from supplementary of[380] with permission.

Since the resolution and spread of the peaks was good, with almost no overlap, a full sequential resonance-assignment of the helix was possible in nanodiscs (Figure 23) using 2D-[$^{1}H,^{15}N$]-HSQC, 3D-tr-HNCO, 3D-tr-HNCA, 3D-tr-HNCACB, 2D-[$^{1}H,^{15}N$]-TROSY and 3D-tr-[$^{1}H,^{15}N$]-NOESY experiments for both membrane-mimetic systems. Through the 3D-NOESY experiments it was possible to gain structural information and structural restraints. These were used to determine and calculate a structure of the helix in nanodiscs, which is depicted in Figure 24 and Figure 26. The quality of the structure was very high with high accuracy and similarity between all calculated energy conformations, with a root-mean-square deviation (RMSD) of the backbone atomic positions of only 0.6 Å.

With the assigned residues and the obtained structure, the next step was to determine the position of the helix inside of the membrane-bilayer in the nanodisc, depicted in Figure 25. This was done by preparing a $^{2}H,^{15}N$-Bcl-xL-TMH sample in MSP1D1ΔH5 nanodiscs with DMPC an DMPG (3:1), where two lipids per leaflet were added with a Gd^{3+}-DTPA headgroup.

The distance-dependent PRE-effect of the Gd^{3+} allows to map the intensity-loss of the NMR signals to the respective proximity to the membrane surface, as depicted in Figure 25. The resulting signal-intensity loss was successfully mapped onto the amino-acid sequence of the helix, allowing to determine its position and orientation inside the nanodisc.

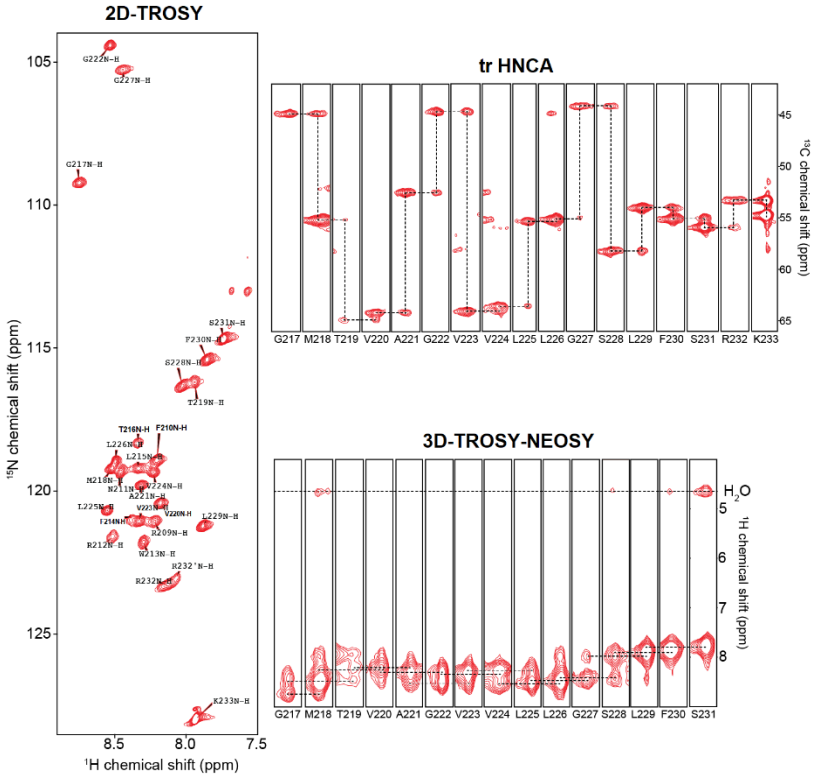

Figure 23: Assignment of 400 µM $^{1}H,^{13}C,^{15}N$-Bcl-xL-TMH in MSP1D1ΔH5 with deuterated d_{54}-DMPC/DMPG (3:1) nanodiscs at 318 K and 800 MHz field strength. On the left is a 2D-[$^{1}H,^{15}N$]-TROSY with 26 visible signals of 32 native amino acids (and 3 additional from the GSG linker), where all assigned backbone amide resonances are labelled in the spectrum. On the right top is an exemplary 3D-tr-HNCA-strip of the last 17 amino acids with the corresponding sequential walk. On the bottom right is the corresponding 3D-TROSY-NEOSY-strip, confirming close proximities and connections, visible in the tr-HNCA. The tryptophan W213 was omitted for better visualisation.

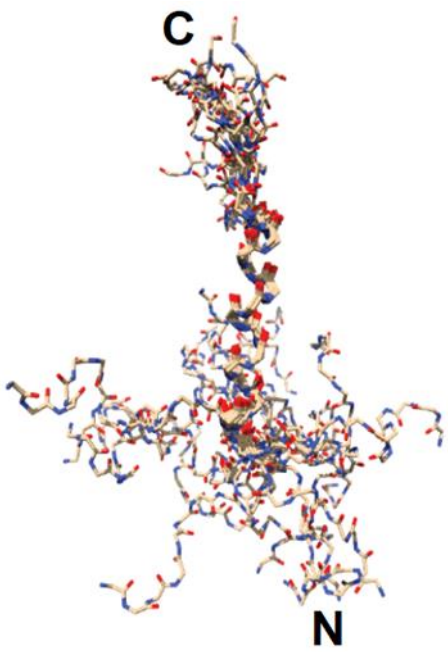

Figure 24: Depiction of the determined NMR-based 3D-structure of Bcl-xL-TMH in in MSP1D1ΔH5 nanodiscs with deuterated d_{54}-DMPC/DMPG (3:1) lipids. 20 of the most stable conformations are depicted, showing a stiff α-helix with a very flexible N-terminus, which is carrying the GSG linker. It was possible to determine the structure with a root-mean-square deviation (RMSD) of the atomic positions of 0.6 Å, which shows the high quality of the obtained structure. A representative depiction of this structure in a nanodisc is shown in Figure 26.

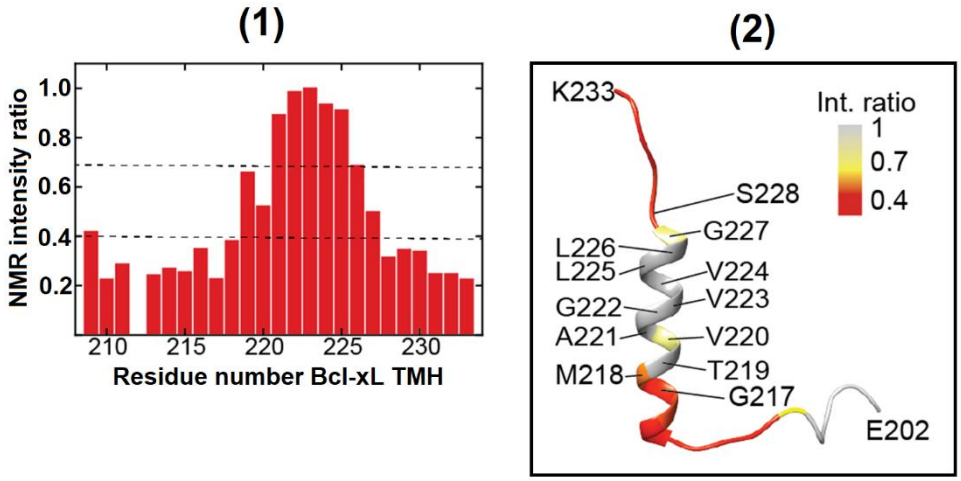

Figure 25: Depiction of the 2D-[^{1}H,^{15}N]-TROSY signal-intensity loss (1) of the ^{2}H,^{15}N-Bcl-xL-TMH sample in MSP1D1ΔH5 nanodiscs with DMPC an DMPG (3:1) doped with two Gd^{3+}-DTPA-DMPE lipids per leaflet, mapped onto the structure of the Bcl-xL-TMH (2). Most of the residues of the α-helix (219-226) are buried inside of the membrane bilayer and shielded from the PRE-effect of the Gd^{3+}-lipid-headgroup. Residues on both ends of the helix are pointing out of the membrane and are strongly affected. The longer and very flexible N-terminus is less affected at its end. Adapted from[380].

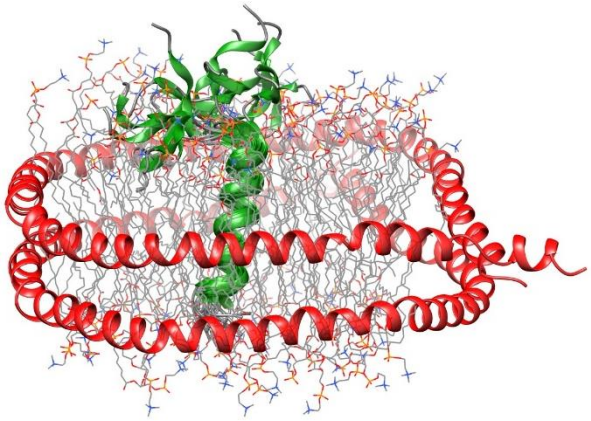

Figure 26: Depiction of the obtained 20 lowest-energy 3D-NMR-structures of Bcl-xL-TMH (PDB:6F46)[380] in green in MSP1D1ΔH5 nanodiscs. MSP1D1ΔH5 (MSP PDB: 2N5E) was used for the nanodisc depiction, where MSP is coloured red. The inserted amino-acids of the α-helix are more rigid and confined inside the bilayer, whilst the N and C terminus are pointing out and are more flexible.

3.1.3 Bcl-xL soluble domain – production and study of new variants

Purification protocols and chemical shift assignments for the Apo and PUMA-bound state soluble domain of Bcl-xL missing the C-terminal α9 helix (Bcl-xLΔTM) were already published[258,297,383]. However, several newly-designed constructs were used for this thesis, mainly the Bcl-xL-SOR with different buffer conditions, membrane mimetics (nanodiscs) or detergents. Therefore, additional 2D and 3D TROSY-based NMR-experiments were performed during this work, to assign the newly cloned variants, and assign changes upon PUMA or membrane binding. These new assignments are the basis for all NMR titration analysis with the Apo-form, nanodiscs, the BH3-peptides from Bak and PUMA, and other studies which are shown in this work.

Preliminary work by Joka Pipercevic with the soluble domain (solu) of Bcl-xL (Bcl-xLΔTM) and the full-length protein in a GST-fusion construct (GST-THR-Bcl-xL) showed, that the soluble domain is very sensitive with respect to detergent exposure, as seen in Figure 27. Harsh detergents as LDAO, DPC or SDS were irreversibly unfolding the structure. However, if working with the full-length protein, those are necessary to extract it from inclusion bodies, or keep the attached helix in solution. That is the reason why so far, just truncated Bcl-xL structures and studies of it are available.

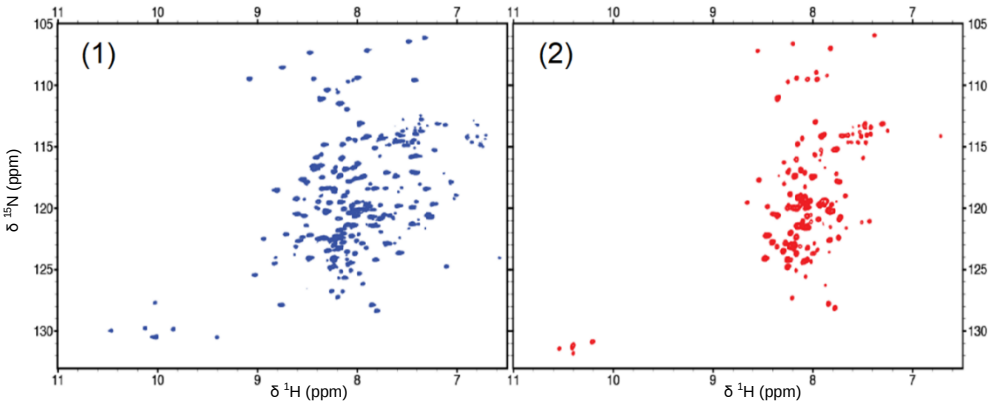

Figure 27: Comparison of two 2D-[^{1}H,^{15}N]-TROSY NMR spectra of ^{2}H,^{15}N-Bcl-xLΔTM in standard NMR buffer (1) and after treatment with LDAO (2). Under physiological NMR buffer conditions with 20 mM sodium phosphate (pH 7.0) and 50 mM NaCl, the protein shows a fully functional and tertiary fold, as published in literature[307,327]. Once the protein comes in contact with harsher detergents as LDAO (2), it loses its tertiary fold, as seen by several missing residues and the small spread of ca. 1.5 ppm, in comparison to 3 ppm in (1). This detergent sensibility is the reason why Bcl-xL cannot be handled as a full-length protein. Adapted from supplementary of[380] with permission.

Usually, for functional Bcl-xL studies and purifications with detergents only CHAPS seems feasible, according to literature, or even milder detergents[383,384]. This is however not feasible for handling the full-length protein, or the TMH. Therefore, we employed ligation of the Bcl-xL-TMH and Bcl-xL-solu through Sortase A, as depicted in Figure 34.

For the successful ligation and study of the soluble domain and its caspase-cleavage in the loop region (mimicked by a thrombin cleavage *in vitro*), several variants of the Bcl-xL soluble domain were cloned, expressed and purified, as depicted in Figure 28 and 29. The Sortase A motif Bcl-xL-variants were termed Bcl-xL-SOR, and the thrombin cut site containing variants Bcl-xL-THR respectively. Comparable yields to the TMH could be achieved through over-night expression at 20 °C and an optimised purification protocol, employing more Ni-NTA slurry, more washing steps and a size-exclusion chromatography (Figure 29) instead of the standard anion-exchange chromatography, as found in literature. Deviation from the protocol or long concentration steps yield a higher ratio of dimer and a significant drop in purity.

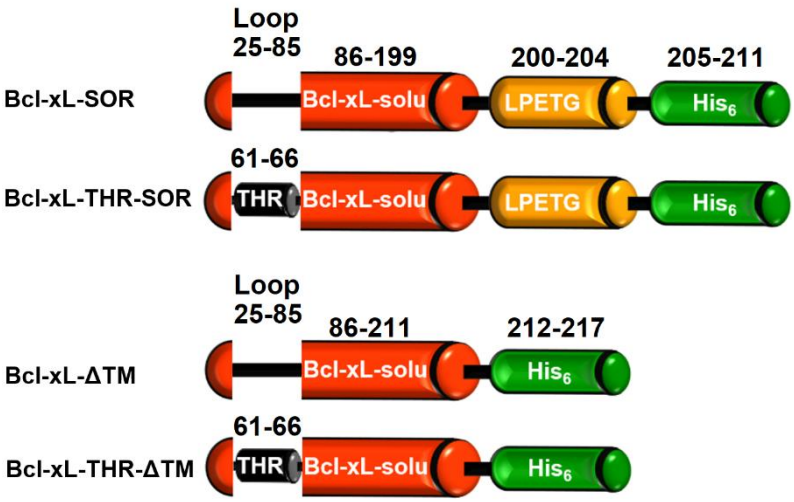

Figure 28: Depiction of the four different Bcl-xL soluble domain (solu) constructs with His_6-tag, from top to bottom: Bcl-xL-SOR with the Sortase A motif (LPETG), the native Bcl-xL-ΔTM, and their respective mutants with a thrombin cut site in the flexible loop. The native Bcl-xL-SOR has a shorter linker (6 amino acids) than the native Bcl-xL-ΔTM. Both, the Sortase A motif (LPETG) and the thrombin cut site (LVPRGS) were introduced through point mutations, which does not enlarge the respective constructs.

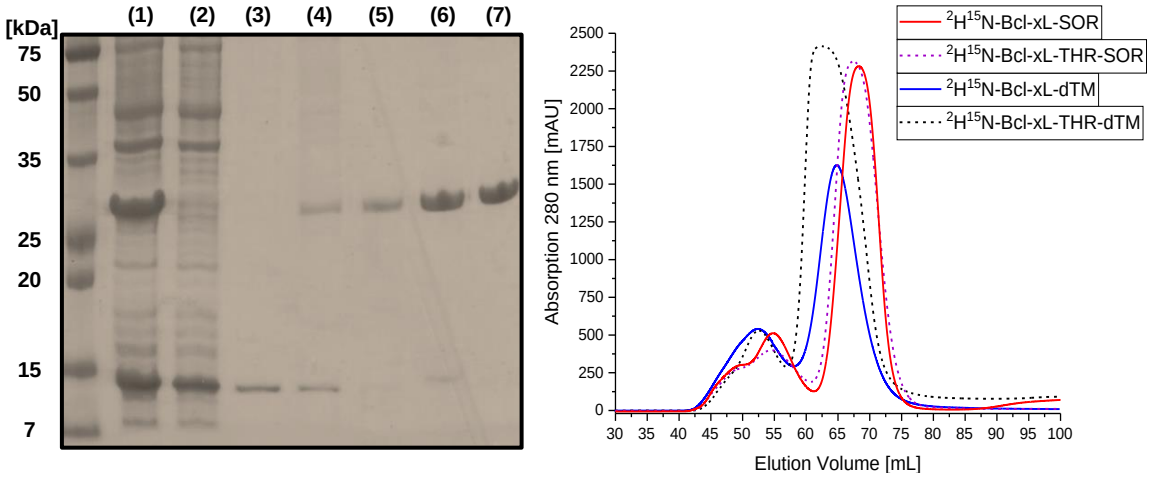

Figure 29: Coomassie stained SDS-PAGE gel (left) of an exemplary Ni-NTA purification of $^{2}H,^{13}C,^{15}N$-Bcl-xL-SOR, with (1) lysate, (2) flow-through of the Ni-NTA, (3) wash 1, (4) imidazole wash, (5) elution, (6) concentrated elution before SEC, (7) pooled monomer of the SEC. On the right are the corresponding size-exclusion chromatograms of all four different Bcl-xL soluble domain mutants. The standard Bcl-xL-SOR with the Sortase A motif in red (68.3 mL), its mutant with an additional thrombin cut site in the loop (Bcl-xL-THR-SOR) in dashed lilac (67.5 mL), the native soluble domain Bcl-xLΔTM in blue (64.9 mL), its respective thrombin mutant (Bcl-xL-THRΔTM) in dashed black (64 mL). The ΔTM-constructs have a six amino acid longer linker than the SOR-constructs and elute earlier due to their bigger size. The respective monomer yield is very high, between 80-90 % of the full size-exclusion chromatogram, compared to the dimer band between, e.g. 42-57.5 mL.

Table 15: Optimised protein yields throughout this work for all three different labelling degrees, used for the study of Bcl-xL-solu. The average values, obtained from at least 3-fold expression and purifications, show that the yield drops by 43 % for a double-labelled protein. For assignment, a $^{13}C,^{15}N$ double-labelled protein was expressed, as deuteration was not necessary. Expression in deuterium-free medium significantly improved yields, as can be expected. Different constructs and mutants yielded almost identical yields.

Labelling degree	Yield	Average
Bcl-xL-solu	70-80 mg/L	75 mg/L
$^{2}H,^{15}N$ Bcl-xL-solu	35-50 mg/L	42.5 mg/L
$^{13}C,^{15}N$ Bcl-xL-solu	50 mg/L	-

3.1.4 Study of the membrane interaction of Bcl-xL soluble domain

To study the interaction and affinity of the soluble domain of Bcl-xL (Bcl-xLΔTM) to membranes (nanodiscs), five different types of techniques were applied. Next to NMR-based titrations, also isothermal calorimetric titrations (ITC) were done and the samples were analysed with dynamic light scattering (DLS) to see, if a Bcl-xL-nanodisc species can be observed in solution. Additionally, a fluorescence resonance energy transfer (FRET) and a fluorescence polarisation (FP) based assay were established. For each method, nanodiscs with varying lipid compositions and anionic-content were screened (Table 16).

In order to use fluorescence or FRET-based assays, tagging of Bcl-xL was necessary. For the FRET-assay, the native cysteine at position C151 was mutated to an alanine and a new cysteine-residue was introduced at position 102, as successfully established in[372]. As an acceptor, a rhodamine-containing lipid was used for the nanodisc assembly, analogous to that of the liposome assay in[372]. Fluorescence polarisation was measured at the Bcl-xL-solu, where a standard N-terminal fluorescence tagging was sufficient.

Table 16: Lipids and lipid mixes that were tested for empty nanodiscs in combination with the soluble domain of Bcl-xL. The right table marked in bold with DMPC and cardiolipin (CL) was additionally screened with the FRET assay. For FRET based studies additionally two rhodamine-containing lipids (N-lissamine rhodamine B sulfonyl, 16:0, PE) per nanodisc-leaflet were added to each mixture.

Lipids	Ratio [%]
DMPC	100
DMPC/DMPG	75/25
DMPC/DMPG	50/50
DMPC/DMPG	25/75
DMPC/Cardiolipin	75/12.5

Lipids	Ratio [%]
DMPC	100
DMPC/CL	95/5
DMPC/CL	90/10
DMPC/CL	80/20

Isothermal calorimetry titrations (ITC) and dynamic light scattering (DLS) analysis

Dynamic light scattering analysis of Bcl-xL-solu alone, nanodiscs and both mixed together did not show a formation of a new distinct species or the enlargement of the nanodisc fraction. Furthermore, no information on affinities or preferred lipid composition could be obtained through this method.

Then Isothermal calorimetry titrations (ITC) was used to estimate the binding strength and binding affinities of Bcl-xL and respective nanodiscs. ITC measurements showed that the binding strength is too low to be measured at standard conditions, e.g. 20 µM of nanodiscs and 200 µM of Bcl-xL-solu at 20 or 25 °C. Lowering the measuring temperature to 10 °C and increasing said concentrations to 40 µM of nanodiscs and 400 µM of Bcl-xL showed that Bcl-xL binds weakly to anionic nanodiscs with 25 % of DMPG concentration (Figure 30), whereas a neutrally charged membrane with solely DMPC, or 75 % of DMPG and 25 % of DMPC, did not exhibit any binding at the given concentration.

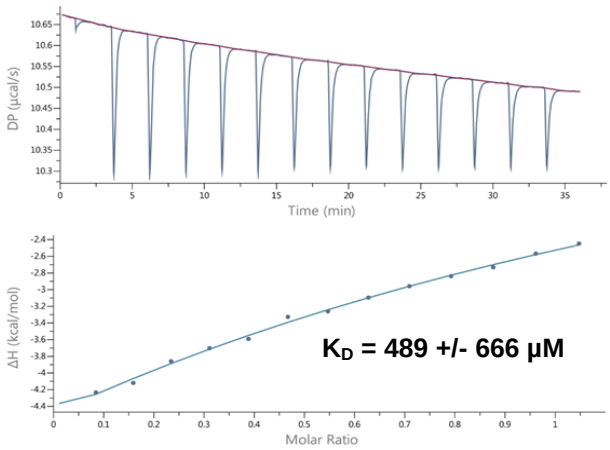

Figure 30: ITC titration of 400 µM Bcl-xL-solu and 40 µM of nanodiscs. The upper plot shows the titration steps and the reference power (DP) of the instrument, which is necessary to reach equilibrium after each titration step, the lower the fitted plot with the binding affinity (K_D).

Further increasing the concentrations of both compounds to 1350 or 1500 µM for Bcl-xL and 50 µM for the nanodiscs, showed that the binding affinity to DMPC nanodiscs is in the range of 1-4 mM, almost at the limit of detection (Figure 31). By contrast, Bcl-xL showed low micromolar affinity (9.2 +/- 6.2 µM) for 25 % DMPG and 75 % DMPC discs, while discs with a higher amount of DMPG (75 %) exhibited a low binding affinity similar to that of pure DMPC.

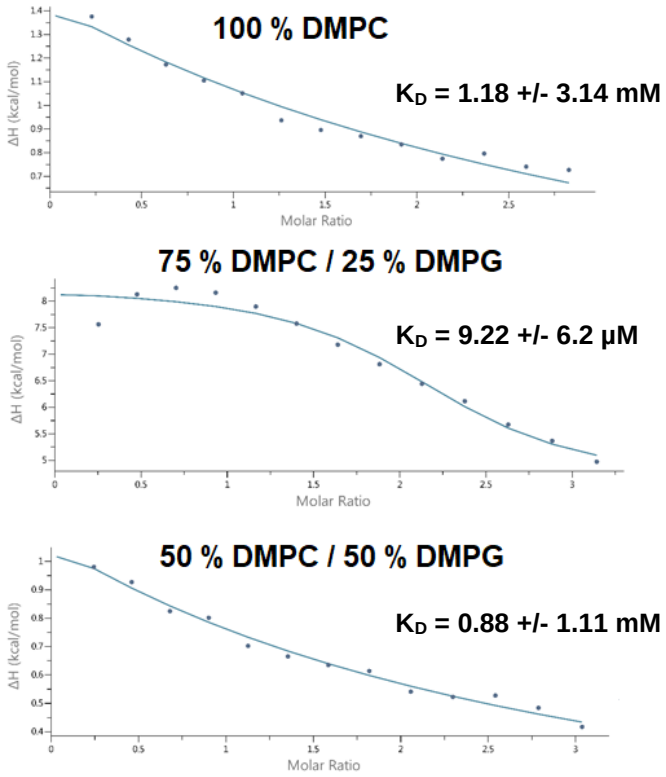

Figure 31: Three single ITC titration experiments of Bcl-xL-solu to nanodiscs with different lipid-compositions, 100 % DMPC, 75 % DMPC and 25 % DMPG, or 50 % DMPC and 50 % DMPG, showing the fitted titration plot and the binding affinity K_D. While Bcl-xL exhibits mM binding-affinity to 100 % DMPC or 50 % DMPC discs, the binding affinity for 75 % DMPC and 25 % DMPG nanodiscs is in the low micromolar range.

Fluorescence resonance energy transfer (FRET) and fluorescence polarisation (FP) assay

Vargas-Uribe *et al.*[372] demonstrated through a FRET-liposome based assay with different pH and varying lipid compositions that Bcl-xL-solu interacts with a negatively charged membrane at low (unphysiological) pH of 4-6. Furthermore, they found that Bcl-xL preferably binds to lipids or lipid surfaces with negatively charged headgroups with a minimum amount of 10 % anionic content. Higher amounts of negatively charged lipids (≥ 25 %) lead to a significant shift in the membrane surface potential and the pK_a of binding, as did also cardiolipin, which leads to a binding in the physiological range of 6.0-7.5. The study was based on single cysteine variants and tracking of one single amino acid in Bcl-xL at a time.

The Bcl-xL residues were 70, 102,110 or 175. It was found that all residues worked equally well, but 102 was preferred in their study.

To investigate the effect of the membrane and the lipid composition of the full-length Bcl-xL, first, the interaction of Bcl-xL-solu with a variety of differently composed NDs was studied, to identify preferred lipid compositions at pH 6.5-7.0. A special focus was set on screening the anionic lipid content and cardiolipin (table 16), as supported by the results of Vargas-Uribe *et al.*[372].

Therefore, analogous to the FRET-based liposome assay of Vargas-Uribe *et al.*[372] a FRET-based nanodisc-assay was designed, employing fluorescence labelled 102Cys-Bcl-xL (donor) and rhodamine labelled lipids (acceptor) in NDs. For that, several ND compositions were prepared with 0, 25 and 50 % anionic content in form of DMPG or 0, 5, 10 and 20 % cardiolipin, each containing additionally two rhodamine-containing lipids per ND leaflet. As cardiolipin is a double-lipid, its molar content equals the double molar amount of DMPG. The rhodamine-lipid serves as the acceptor, analogous to that of the FRET-based liposome assay.

Additionally, the pH dependence of the membrane interaction was screened within the physiological range of 6.0-7.5 in steps of 0.5. The newly introduced 102-cystein of Bcl-xLΔTM was tagged with pH-independent AlexaFlour488 or 5-Iodoacetamidofluorescein (5-IAF), to test both FRET-donors for their utility.

Both, the cardiolipin- and DMPG-content screening were done with AlexaFlour488, depicted in Figure 32, where it was found that already 5 % of cardiolipin increase the binding affinity of Bcl-xL to the nanodisc-membrane, measured with the drop of donor-intensity in a ratio of 0-1.0. Binding to the membrane increases the FRET from the donor (Bcl-xL) to the acceptor (membrane surface), thereby depleting the respective signal intensity of the donor. Higher amounts of cardiolipin further increased the overall donor-depletion of AlexaFluor488, from an average ratio of 0.193 for 0 % cardiolipin, to a ratio of 0.306 for 10 % cardiolipin, or a ratio of 0.332 for 20 % cardiolipin respectively. More importantly, Bcl-xL showed a higher binding affinity at the physiological pH of 7.0 or 7.5 to higher amounts of cardiolipin. A similar effect could not be observed for varying amounts of DMPG (data not shown), as the donor-depletion did not vary as strongly as for cardiolipin and was in the range of 100 % DMPC.

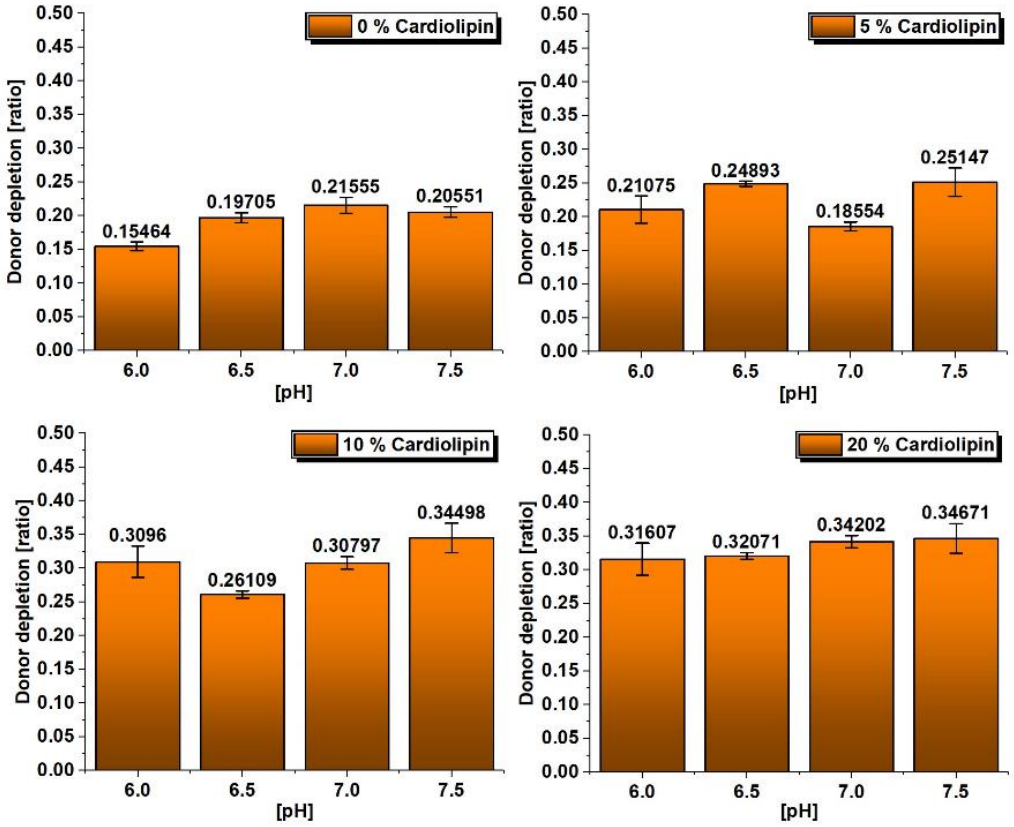

Figure 32: Depiction of the amount of donor-depletion (from Bcl-xL-solu) in the cardiolipin-content and pH screening, with rhodamine-labelled nanodiscs and AlexaFluor488 labelled Bcl-xL. The screened lipid compositions were with 0 %, 5 %, 10 % and 20 % cardiolipin content, for pH 6.0, 6.5, 7.0 and 7.5. The remaining lipids were the neutrally charged DMPC and two rhodamine-containing lipids per nanodisc-leaflet as FRET-acceptor. Measured was the donor depletion through FRET, which correlates to the amount of binding or affinity for a certain membrane surface. Higher cardiolipin content leads to a strong increase in donor depletion, peaking for 10 and 20 % cardiolipin content with 30-35 % depletion. The effect is almost independent of the sample pH, but a bit higher in the physiological range of pH 7.0-7.5.

Unfortunately, 5IAF showed a strong pH-dependence, and apart from that, high deviations between each sample and each reference. Concordantly, the calculated standard deviation and error were higher than the obtained donor depletion signal. So, it was found not to be applicable for this type of assay. Even for screening at one pH, the 5-IAF was very error prone and not useful. Its solubility was lower than that of AF488 and handling was found to be more difficult, as also tagging of the protein. Similar, the fluorescence-polarisation assay showed very high signal fluctuations and deviations between each sample, proving not to be reproducible. Moreover, it was found, that the N-terminal labelling with 5(6)-Carboxyfluorescein lead to very similar results for all employed lipid-compositions, showing very high affinities (10-30 nM). It was not possible to distinguish between different samples. A high affinity of the dye to the membrane was correlated.

NMR-based titrations

In order to study the interaction of Bcl-xL-solu and the respective NDs at atomic resolution for all amino acids and in sufficient concentrations for optimal binding NMR experiments and studies were conducted. Studying of the binding mode and affinity for differently charged membranes (table 16) was done with NMR-based titrations at pH 7.0, using for each sample 200 µM $^{2}H,^{15}N$-Bcl-xLΔTM and 300 µM of a respective nanodisc. For each nanodisc sample an equal sample (300 µM) with the same lipid composition, but with additional three Gd^{3+}-containing lipids (DTPA), was prepared and measured separately with 200 µM $^{2}H,^{15}N$-Bcl-xLΔTM. All samples or mixtures of $^{2}H,^{15}N$-Bcl-xLΔTM and the respective nanodiscs were split in half and measured with or without two equivalents of PUMA. The comparison of Gd^{3+}-containing and standard nanodiscs enabled to map the binding interface of Bcl-xL-solu and the respective membrane and quantify the binding-tendencies towards different membranes (Figure 33). Previously determined optimal cardiolipin concentrations of 10 % to 20 % by the FRET-based nanodisc-assay were also considered, besides DMPG/DMPC compositions. Therefore, a sample of 12.5 % cardiolipin (CL) and 75 % DMPC was used for the NMR-based titrations, as it corresponds roughly to the standard 25 % DMPG and 75 % DMPC by charge, since cardiolipin is a double lipid and negatively charged. This allows to directly compare cardiolipin and DMPG and see if other lipid properties besides charge (e.g. headgroup) have an influence on the membrane interaction of Bcl-xL.

As a reference for all titrations 200 µM $^{2}H,^{15}N$-Bcl-xLΔTM was measured with and without 2 molar equivalents of PUMA in the absence of nanodiscs.

The PRE-effect from Gd^{3+}-lipids on the labelled Bcl-xLΔTM leads to NMR signal intensity attenuation in a distance dependent matter that allowed to compare the effect amongst different types of membranes (Figure 33), by comparing the NMR intensities of Bcl-xL with NDs and Bcl-xL and the respective Gd^{3+}-ND counterpart. It was observed, that all measured lipid compositions of 100 % DMPC, 25 % DMPG/75 % DMPC, 50 % DMPG/50 % DMPC and 12.5 % CL/75 % DMPC show a PRE-effect in the hydrophobic BH3-binding groove in the apo state of Bcl-xL. The region of the attenuated signals and residues (mainly 105-140) is very selective and not due to random orientation, as it occurs in all samples and is mainly restricted to this region. While 100 % DMPC showed the lowest amount of NMR signal attenuation and therefore corresponding membrane-binding, 25 % DMPG exhibited a much stronger pronounced effect. Interestingly, 12.5 % CL exhibited the strongest PRE-effect, though it has the same charge properties as 25 % DMPG. This is in good agreement with the observed FRET-data, which indicated a much stronger membrane-binding to cardiolipin containing membranes than DMPG ones.

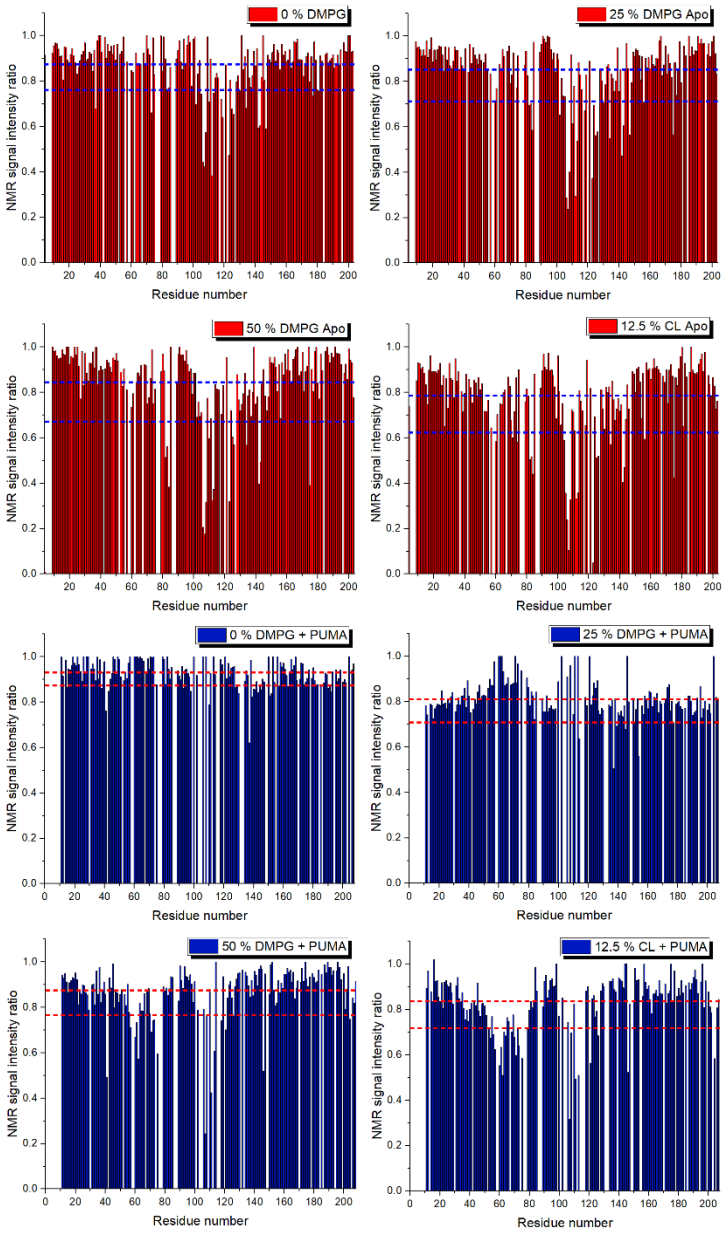

Figure 33: Depiction of the obtained $^{2}H,^{15}N$-Bcl-xLΔTM-NMR intensity plots from the 2D-[$^{1}H,^{15}N$]-TROSY NMR-based titration at 950 MHz of 200 µM $^{2}H,^{15}N$-Bcl-xLΔTM with 300 µM of each four different nanodiscs (top, in red), containing either 0 % DMPG lipids, 25 % DMPG, 12.5 % Cardiolipin or 50 % DMPG, referenced with their respective Gd^{3+}-containing equivalents plotted against the residue number of Bcl-xLΔTM. The top dashed line represents the average and the bottom dashed line average minus standard deviation. On the bottom in blue are the result of a subsequent PUMA addition to each individual sample. The membrane-binding of Apo Bcl-xLΔTM is quantified and visualised by the Gd^{3+} PRE-effect with the respective the membrane. While for 100 % DMPC (0 % DMPG) there is already a small membrane binding of Apo Bcl-xL-solu, the binding tendency towards the membrane increases with increasing negative charge, where cardiolipin (12.5 % CL) shows the highest amount, comparable to 50 % DMPG. When PUMA is added, the membrane binding is almost completely depleted for 0 % DMPG and 25 % DMPG, whereas the cardiolipin and 50 % DMPG sample still exhibit a strong membrane binding, though weaker than in Apo form.

Higher amounts of anionic lipids (50 % DMPG) exhibited an almost equally strong PRE-effect as 12.5 % CL and showed that lipid-headgroup charge is at least equally important as the composition of the lipid.

Upon PUMA BH3-peptide addition the PRE-effect is almost completely abrogated in the 100 % DMPC and 25 % DMPG samples, indicating a detachment of Bcl-xL from the membrane. The effect is also observable for all non-BH3 binding amino acids, which further indicates that this is not due to shielding from the Gd^{3+} by the added peptide. However, both the 12.5 % CL and 50 % DMPG sample did not exhibit such a strong effect after the addition of PUMA. Both spectra look almost identical with the same PRE-pattern, exhibiting the same membrane-binding-mode, just with slightly less overall signal intensity depletion. As with their strong membrane attachment in the apo state, both samples still exhibit an affinity or binding to the membrane even in a ligand-bound state.

In contrast to suggestions, that Bcl-xL might bind to or insert into the membrane upon ligand binding, the here obtained data shows the contrary. Nevertheless, these experiments only take into account the soluble domain. Therefore, the results cannot be completely transferred to the full-length protein, where the distance to the membrane may be shorter and more constant through the membrane anchor. The additional helix, which is usually truncated for Bcl-xL studies, could also lead to a different orientation on the membrane.

3.1.5 Sortase A ligation of full-length Bcl-xL

To obtain and study the full-length Bcl-xL in a native-like membrane environment a Sortase A mediated ligation method was envisaged (Figure 34) employing the optimised penta-mutant Sortase A[203]. It allows to assemble the protein from two separate parts, the membrane inserted helix in a nanodisc and the soluble domain. This circumvents the exposure of detergent to the soluble domain, while still employing the necessary harsh detergents for the separate purification of the transmembrane helix, as shown in Chapter 3.1.2. By separate and parallel expression and purification of both Bcl-xL-parts, the helix can be incorporated in its native surrounding, as established in Chapter 3.1.2. In the next step, the soluble domain can be ligated via Sortase A and the Bcl-xL Sortase A motif LPETG, as depicted in Figure 34.

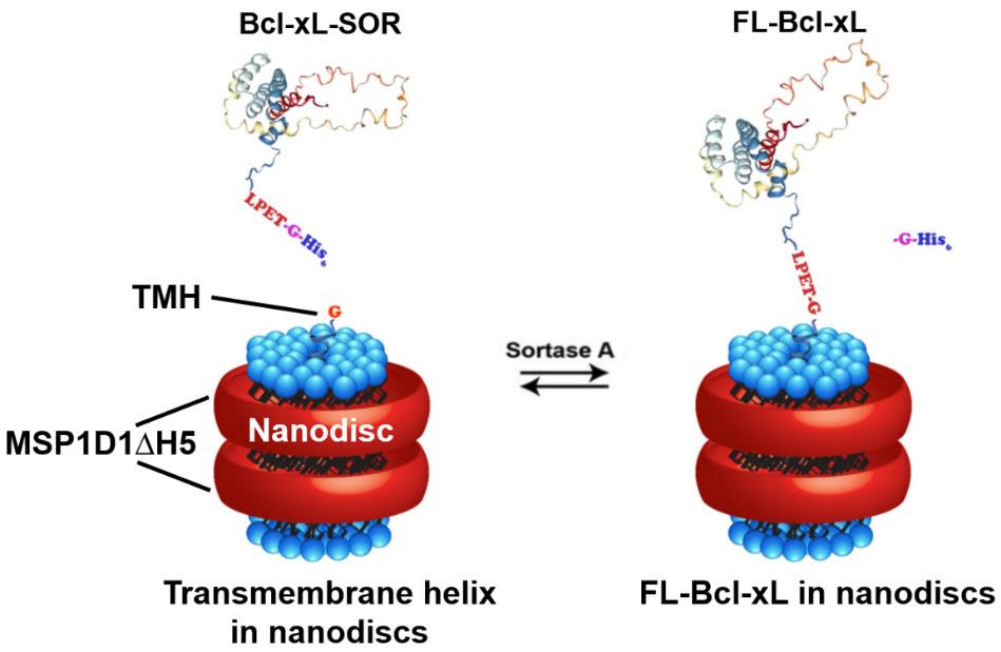

Figure 34: Schematic representation of the envisaged novel Sortase A ligation protocol for the production of full-length Bcl-xL in a native-like environment. After successful incorporation of the GB1-Bcl-xL-TMH into the nanodisc, the GB1 is cut off, leaving the reactive glycine (Figure 18, Chapter 3.1.2). After removal of GB1, the soluble domain with the Sortase A recognition site (Bcl-xL-SOR) is added together with the enzyme. The ligation yields the full-length protein in a nanodisc. Adapted from[380] with permission.

The Sortase A ligation was probed with test reactions at room temperature (22-23 °C) (Figure 35) using Bcl-xL-SOR and MSP1D1ΔH5, in order to find the optimal stochiometric ratios of the N- and C-terminal ligation partners and also the optimal Sortase A ratio, with respect to Bcl-xL. TEV cleaved MSP1D1ΔH5 (without a His_6-tag) was chosen as it is an abundant protein, big enough to see a successful ligation with Bcl-xL, and it harbours an N-terminal glycine necessary for the ligation.

As both proteins are soluble it was possible to perform the ligation in the absence of detergents and in high concentrations of 25 µM Sortase A, 50 µM for Bcl-xL-SOR and 50, 100, 250 and 400 µM for MSP1D1ΔH5 respectively. Ratios of 1 (Bcl-xL-SOR) : 1 MSP, 1:2, 1:5 and 1:8 were tested, with 0.5 equivalents of Sortase A, with respect to Bcl-xL. After mixing, a small amount of the ligation reaction was directly mixed with Laemmli Buffer and cooked for 5 min at 95 °C and taken as the start SDS-PAGE reference. Interestingly, the ligation proceeded so fast that the initial mixing state could not be trapped, except for the ratio 1:8. In all other SDS-PAGE samples (Figure 35, left) directly three bands could be observed, corresponding to the uncoupled MSP1D1ΔH5 (19.45 kDa) at approximately 17-19 kDA, Bcl-xL-SOR (23.5 kDa) which runs at 25 kDa and their ligation product at ca. 42-43 kDa.

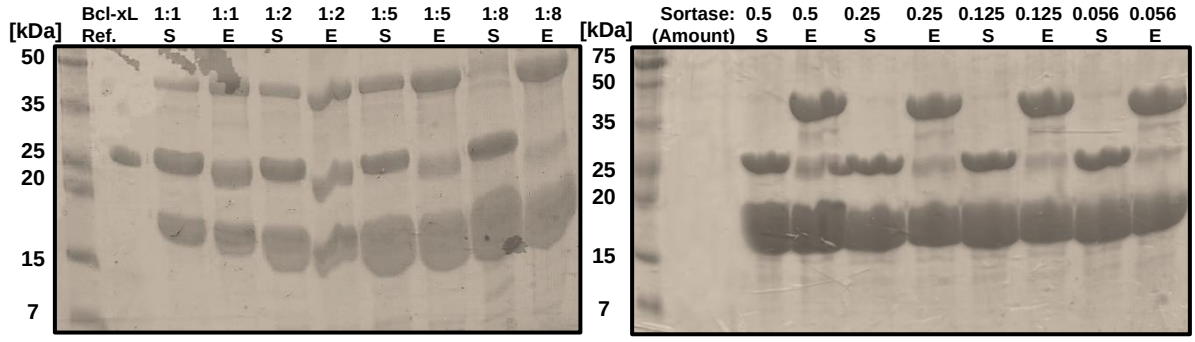

Figure 35: Coomassie stained SDS-PAGE gels of Sortase A test ligations with Bcl-xL-SOR (LPETG-motif, 23.5 kDa) and regular TEV cut MSP1D1ΔH5 without His_6-tag (19.45 kDa) with a free N-terminal glycine. On the left is the screening for optimal N- (Bcl-xL-SOR) to C-terminal (Glycine, MSP) ratio from 1 to 1, to 1 to 8, with 0.5 equivalent of Sortase A, where the start of the ligation is indicated as "S" and the end after 60 min as "E". For all ligation tests a successful ligation of both proteins was observed, already directly after mixing, by the appearance of the ca. 42-43 kDa product. Higher C-terminal amounts larger than 1:2 showed the highest final yield, indicated by the thick reaction product band at approximately 42 kDa and the missing, almost completely ligated Bcl-xL-SOR. On the right is the subsequent screening for an optimal Sortase A ratio from 0.5 to 0.056, with a 1:6 N- to C-terminus ratio. Ratios of Sortase A from 0.5 to 0.25 lead to a high amount of back reaction and an incomplete turnover of the coupling products (Bcl-xL-SOR). Lower stochiometric amounts of 0.056 showed the highest observed final yield.

For the slower proceeding 1 N- to 8 C-terminal ratio the highest yield was observed and almost no residual Bcl-xL-SOR was left, indicating no back-reaction and cleavage of the final product and an almost complete turnover of both ligation compounds. Since the reaction proceeded too fast under most conditions and the turnover of both coupling products seemed not optimal, the ratio of Sortase A was optimised in further test reactions. Here, a Bcl-xL-SOR to MSP ratio of 1:6 was chosen with of 0.5 to 0.056 molar equivalents of Sortase A respectively.

In all cases the starting point of the ligation was possible to be trapped by SDS-PAGE, and the reaction proceeded more controlled and quantitatively with decreasing Sortase A concentrations. The final yields of the coupling product were similar, as can be seen in Figure 35 (right), but the lowest ratio of 1 : 6 : 0.056 yielded the biggest protein-band in the SDS-PAGE together with the lowest residual Bcl-xL-SOR one. By choosing an excess of one reaction (C- or N-terminal) compound and a ratio of 1:20 or 1:25 of Sortase A to the reference ligation protein, the reaction was optimised. It was found that a stepwise addition of the excess ligation-partner is of benefit and increases the coupling yield, while suppressing a back-reaction (hydrolysing of the product). Shorter (0-1 h) or longer reaction times of greater than 12 h showed no further improvement in yield.

In the designed production of Fl-Bcl-xL the MSP1D1ΔH5 nanodiscs with DMPC and DMPG (3:1 ratio) containing Bcl-xL-TMH (TMH-ND) with the N-terminal glycine is the limiting factor and was thereby chosen as the reference ligation compound, while Bcl-xL-SOR was chosen to be added in the highest possible excess, through stepwise addition. Hence, there would be no later problems of separating a large excess of uncoupled nanodiscs and nanodiscs containing the full-length Bcl-xL. Additionally, excess unligated Bcl-xL-SOR harbours a His_6-tag and may therefore be recovered after successful ligation through Ni-NTA, while Bcl-xL-SOR that was hydrolysed in the back-reaction would lose the tag. As Sortase A (SOR) was proven to be extremely reactive, a ratio of 1 SOR to 20 TMH-ND was chosen (0.05 with respect to TMH-ND), to ensure a moderate reaction speed with higher overall yields. As a final starting ratio 1 TMH-ND : 1 Bcl-xL-SOR : 0.05 Sortase A was chosen, and after 30 min one more equivalent Bcl-xL-SOR was added to reach 1 : 2 : 0.05 respectively.

The progress of the ligation of Bcl-xL-SOR (23.5 kDa) to its TMH (3.67 kDa) could be followed by the appearance of the product (27.2 kDa) in the corresponding SDS-PAGE (Figure 36), while the TMH is used up in the process and slowly disappearing after approximately 1 h-1.5 h reaction time. After quenching the 20 mM $CaCl_2$ and therefore the reaction with 20 mM EDTA, an immediate Ni-NTA purfication removes the unligated Bcl-xL-SOR and the Sortase A enzyme both through their respective His_6-tag, while the full-length Bcl-xL in nanodiscs bears no affinity tag and is found in the flow through and wash fraction. A subsequent size-exclusion chromatography allows to separate unligated TMH-ND from Fl-Bcl-xL in ND and residual Bcl-xL-SOR which was hydrolysed during the ligation and bears no His_6-tag anymore (Figure 36 and Figure 37). The increase in hydrodynamic radius of the product was seen in the overlay of the SEC elution volumes of the educt (13.1 mL) and product (11.2 mL) in the S200a column and the respective analysis via dynamic light scattering, which showed a large increase of the particle radius and varified, together with mass spectromertry, the successful Sortase A ligation and production of the full-length Bcl-xL. Both DLS and Mass spectrometry analysis and the SDS PAGE of the final product show a clean an homogeneous sample and a successful ligation.

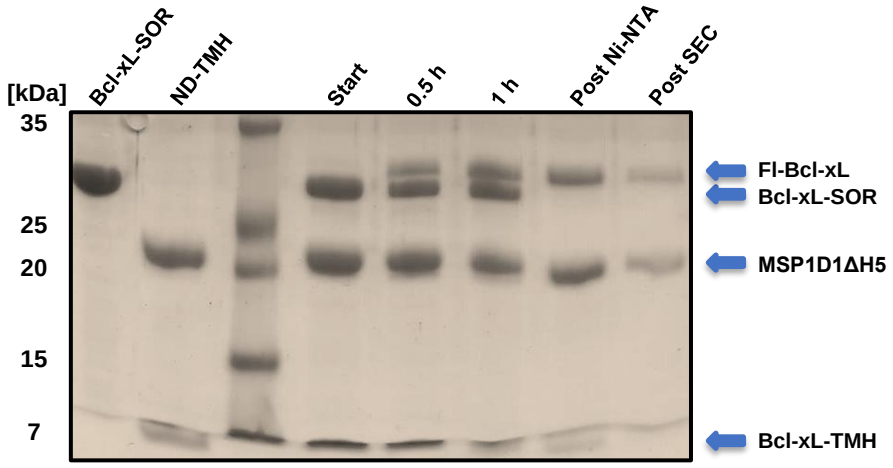

Figure 36: Exemplary Coomassie stained SDS-PAGE gel of the optimised stepwise Fl-Bcl-xL Sortase A ligation in MSP1D1ΔH5 (20 kDa single mass) nanodiscs with both educt references (Bcl-xL-SOR, 23.5 kDa and Bcl-xL-TM, 3.67 kDa in nanodiscs) on the left and the mixture, its subsequent reaction and purification on the right. After 0.5 h one more equivalent of Bcl-xL-SOR was added and already a thick product band (27.2 kDa expected) at approximately 30 kDa is visible, which further increases after 1 h. Bcl-xL-TMH is almost completely used up during the process, as its amount was kept constant. Further Ni-NTA purification separated the unreacted Bcl-xL-SOR and the Sortase A enzyme, enriching the nanodisc fraction in the Ni-NTA flow through. Through a final size exclusion column purification, the final product of Fl-Bcl-xL in nanodiscs was obtained, showing no residual and unligated TMH in nanodiscs. Adapted from[380] with permission.

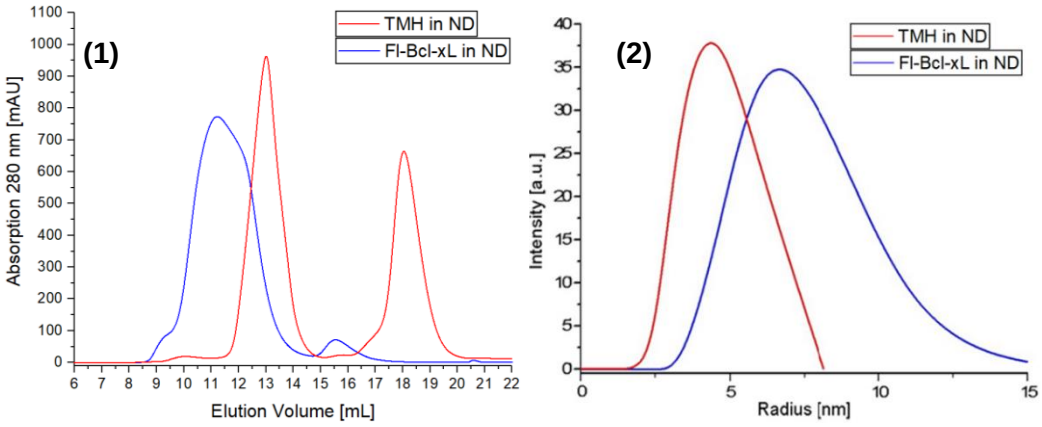

Figure 37: Overlay of the corresponding size-exclusion chromatograms (SEC) (1) of the unligated (educt) Bcl-xL-TMH in nanodiscs (TMH-ND) (13.1 mL) with the cut off GB1-tag (18.2 mL) in red and the full-length Bcl-xL protein (11.2 mL) in nanodiscs after Sortase A ligation and Ni-NTA purification in blue. The SEC shows an increase in hydrodynamic radius, represented by a decrease in elution volume of approximately 2 mL. Excess Bcl-xL-SOR can be separated and elutes at 15-16 mL. (2) Overlay of the respective dynamic-light scattering (DLS)[380] analysis of both main fractions (pooled) from TMH-ND or Fl-Bcl-xL in ND, which shows an increase in overall particle size and radius after Sortase A ligation.

3.1.6 Study of full-length Bcl-xL in nanodiscs

After establishing and optimising the Sortase A mediated ligation and production of Fl-Bcl-xL in MSP1D1ΔH5 nanodiscs, the full-length protein was further characterised and studied in its native-like environment. The purity, quality, folding and its functional property was studied via NMR spectroscopy, ITC (Figure 38) and CD spectroscopy (Figure 39), with and without its ligand PUMA. The ligand binding was used to assess its binding affinity, binding mode and the Bcl-xL functionality after the Sortase A mediated procedure and to compare them with the soluble domain (Bcl-xLΔTM or Bcl-xL-SOR) respectively. Therefore, fully $^{2}H,^{15}N$-labelled Fl-Bcl-xL and segmentally labelled Fl-Bcl-xL, where either the TMH or the soluble domain were $^{2}H,^{15}N$-labelled, were produced in MSP1D1ΔH5 nanodiscs with DMPC and DMPG lipids in 3:1 ratio.

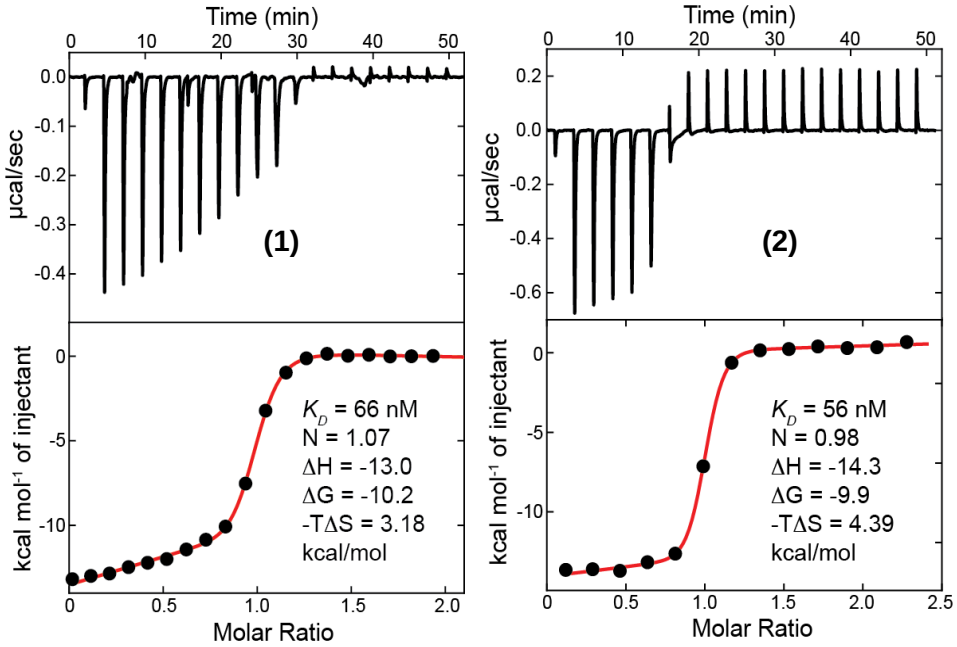

Figure 38: Depiction and comparison of the Isothermal titration calorimetry (ITC) probing the binding of PUMA BH3 peptide to Bcl-xL-solu (1) and Fl-Bcl-xL in MSP1D1ΔH5 nanodiscs (2). In both cases the binding affinity (K_D) is in the nanomolar range with very similar number of binding sites (N) and thermodynamic parameters. Adapted from[380] with permission.

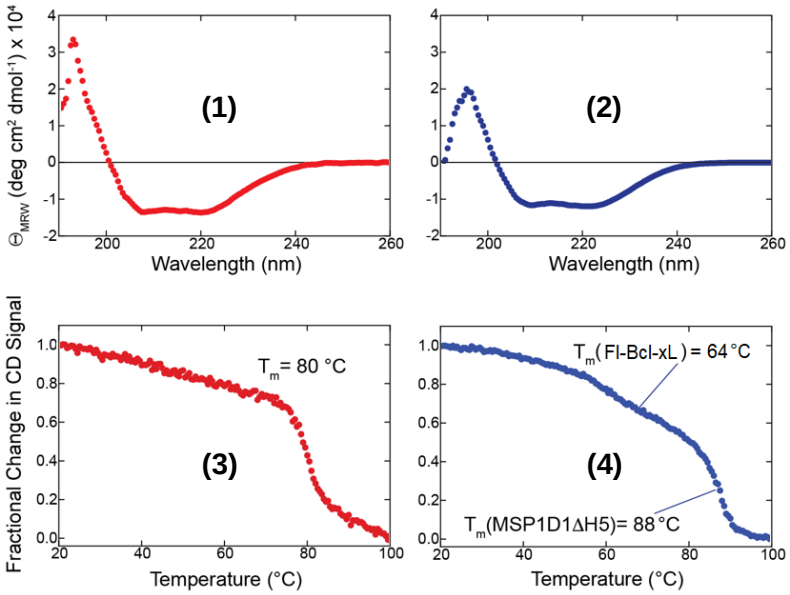

Figure 39: Depiction of the far-UV CD spectrum of Bcl-xL-solu in red (1) and Fl-Bcl-xL in MSP1D1ΔH5 nanodiscs in blue (2) and their respective thermal unfolding spectrum (3 and 4) recorded at 220 nm. Both proteins exhibit an expected α-helical fold and exhibit two distinct melting points of 80 °C for the soluble domain (3), while the full-length protein melts at 64 °C in the nanodisc, before the MSP-belt at 88 °C does. In the nanodisc spectrum (2) the contribution of both MSPs was subtracted, showing only the Fl-Bcl-xL. This was done by recording empty nanodiscs as a reference and subtracting the respective signal from the Fl-Bcl-xL-ND spectrum. Adapted from[380] with permission.

Furthermore, through analogous PRE experiments (Figure 43) as established for the membrane interaction of the soluble domain (Bcl-xLΔTM, Chapter 4.1.4) with Gd^{3+}-containing nanodisc leaflets and with additional RDC (2D-[^{1}H,^{15}N]-TROSY and 2D-[^{1}H,^{15}N]-semi-TROSY) NMR experiments (Figure 44) the influence of the membrane surface on the folding, flexibility and location of the Bcl-xL-solu and Bcl-xL-TMH in the full-length membrane embedded state was studied. Hence, for each PRE-sample one set of nanodisc with Gd^{3+}-DTPA-DMPE lipids and one without was assembled (with the Bcl-xL-TMH) and the soluble domain was ligated via the Sortase A method.

As the structure, location and orientation of the Bcl-xL-TMH in the nanodisc was already determined previously (see Chapter 4.1.2) the new PRE samples were segmentally labelled only at the soluble domain, to study its behaviour, binding mode and orientation and membrane localisation. The NMR signal intensities of the Fl-Bcl-xL in nanodiscs in Apo and PUMA bound state were analysed and compared with the ones from the Gd^{3+}-DTPA-DMPE lipid samples (Figure 43). Mapping the signal attenuation onto the structure of Bcl-xL-solu in the full-length sample (Figure 43) allowed to map the membrane proximity of each residue and visualise the position of Bcl-xL-solu and especially its BH3 binding groove.

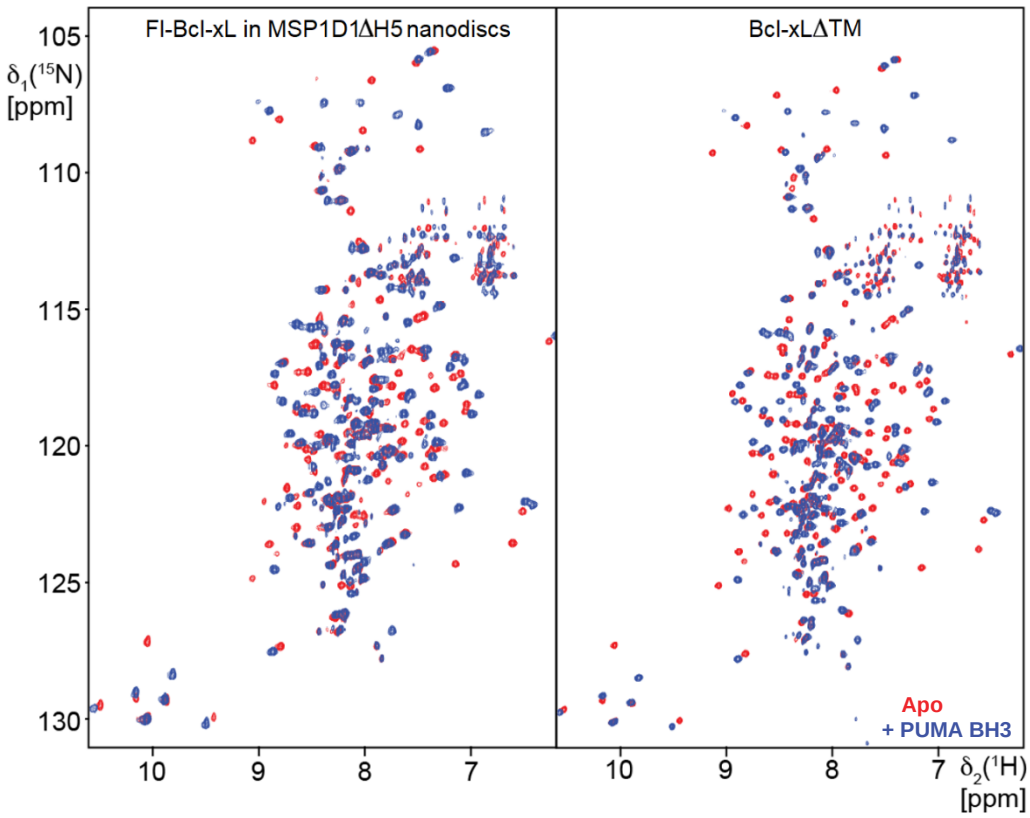

Figure 40: Comparison of 2D-[^{1}H,^{15}N]-TROSY experiments and NMR titrations of ^{2}H,^{15}N-Bcl-xLΔTM on the right or segmentally labelled ^{2}H,^{15}N-Fl-Bcl-xL (Bcl-xL-solu labelled only) in MSP1D1ΔH5 nanodiscs on the left with (red) and without (blue) PUMA BH3 peptide. Both spectra show a very similar fold and chemical shifts upon PUMA BH3 binding. However, the Fl-Bcl-xL exhibits slightly broader peaks, due to its attachment to the slow tumbling nanodisc. Adapted from[380] with permission.

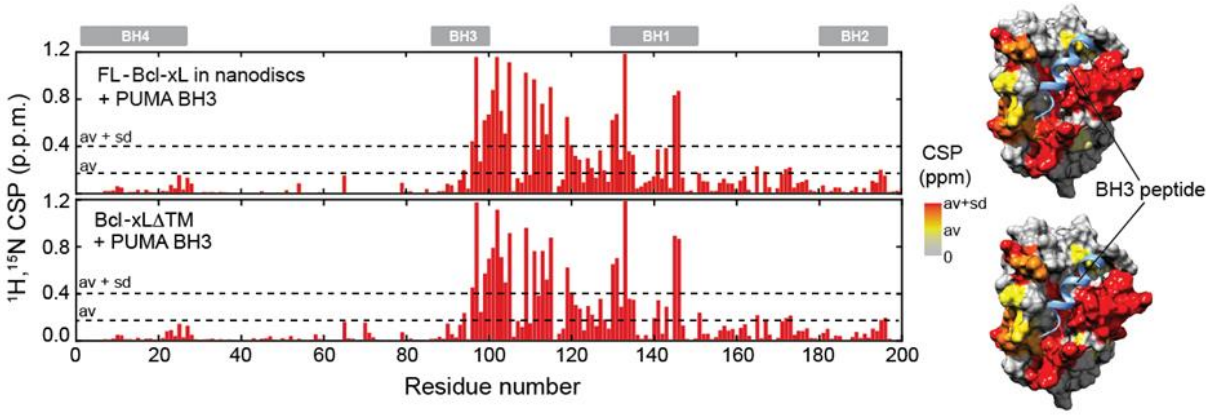

Figure 41: Depiction of obtained average CSP values upon PUMA addition from 2D-[^{1}H,^{15}N]-TROSY experiments with apo and PUMA-bound ^{2}H,^{15}N-Bcl-xLΔTM or segmentally labelled ^{2}H,^{15}N-Fl-Bcl-xL (Bcl-xL-solu labelled only) in MSP1D1ΔH5 nanodiscs, plotted against residue number in each case on the left. The resulting average (av) and average plus standard deviation (sd) are depicted as a dashed line. On the right are the respective CSP values colourcoded onto the structure of Bcl-xL showing the affected residues and the postion of the BH3 PUMA peptide. Both proteins exhibit the same mode of binding and the same affected residues upon PUMA addition. Adapted from[380] with permission.

Mapping the chemical shifts of the membrane-bound Fl-Bcl-xL sample (Figure 42) onto the Bcl-xL-solu shows the influence of the membrane and slight differences in the full-length protein.

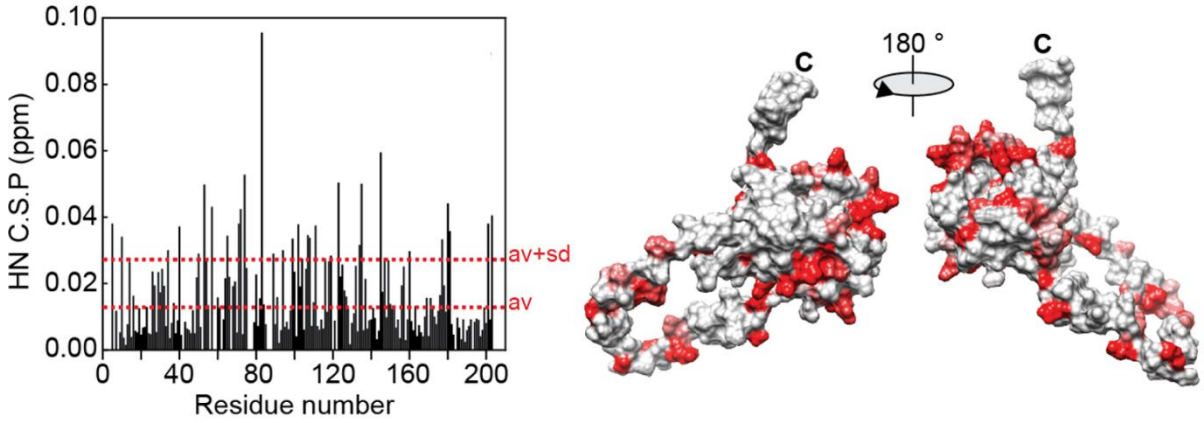

Figure 42: Depiction of obtained CSP values from 2D-[^{1}H,^{15}N]-TROSY experiments with Apo ^{2}H,^{15}N-Bcl-xLΔTM or segmentally labelled ^{2}H^{15}N-Fl-Bcl-xL (Bcl-xL-solu labelled only) in MSP1D1ΔH5 nanodiscs, plotted against residue number in each case on the left. The resulting average (av) and average plus standard deviation (sd) are depicted as a red dashed line. On the right are the respective CSP values colour coded onto the structure of Bcl-xL showing the affected residues due to the presence of a membrane surface.

For the H-N backbone RDC studies two sets of either TMH or Bcl-xL-solu labelled samples were measured with 8 mg/mL and without Pf1 phage (ASLA Biotech, Riga, Latvia) using 2D-TROSY and 2D-semi-TROSY experiments, which depict the H-N backbone amides of Bcl-xL. The obtained RDCs were used together with the PRE data, NOE-based NMR experimental data and previous data from Chapter 3.1.2 for the TMH, for structural refinement and production of a 3D-model of Fl-Bcl-xL in the membrane of a nanodisc (Figure 44).

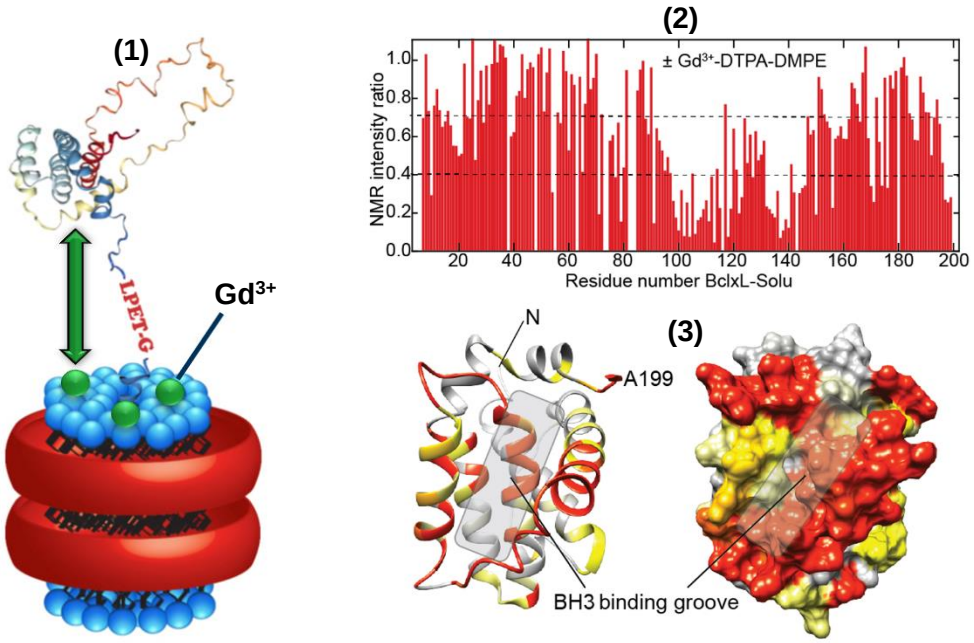

Figure 43: Depiction of (1) a Gd^{3+}-DPTA-DMPE lipid containing MSP1D1ΔH5 nanodisc model with the full-length Bcl-xL employed to probe the membrane location of Bcl-xL and the corresponding PRE-effect through proximity (green arrow). (2) The corresponding obtained NMR PRE-intensity ratio of segmentally $^{2}H,^{15}N$-labelled Fl-Bcl-xL (Bcl-xL-solu labelled only) in nanodiscs containing Gd^{3+}-DTPA-DMPE, with observable signal attenuation by Gd^{3+} proximity, compared to the Gd^{3+}-free reference. (3) Colour coding of the most affected residues onto the structure of Bcl-xL-solu, showing that the most affected residues lie with or around its BH3 binding groove. Adapted from[380] with permission.

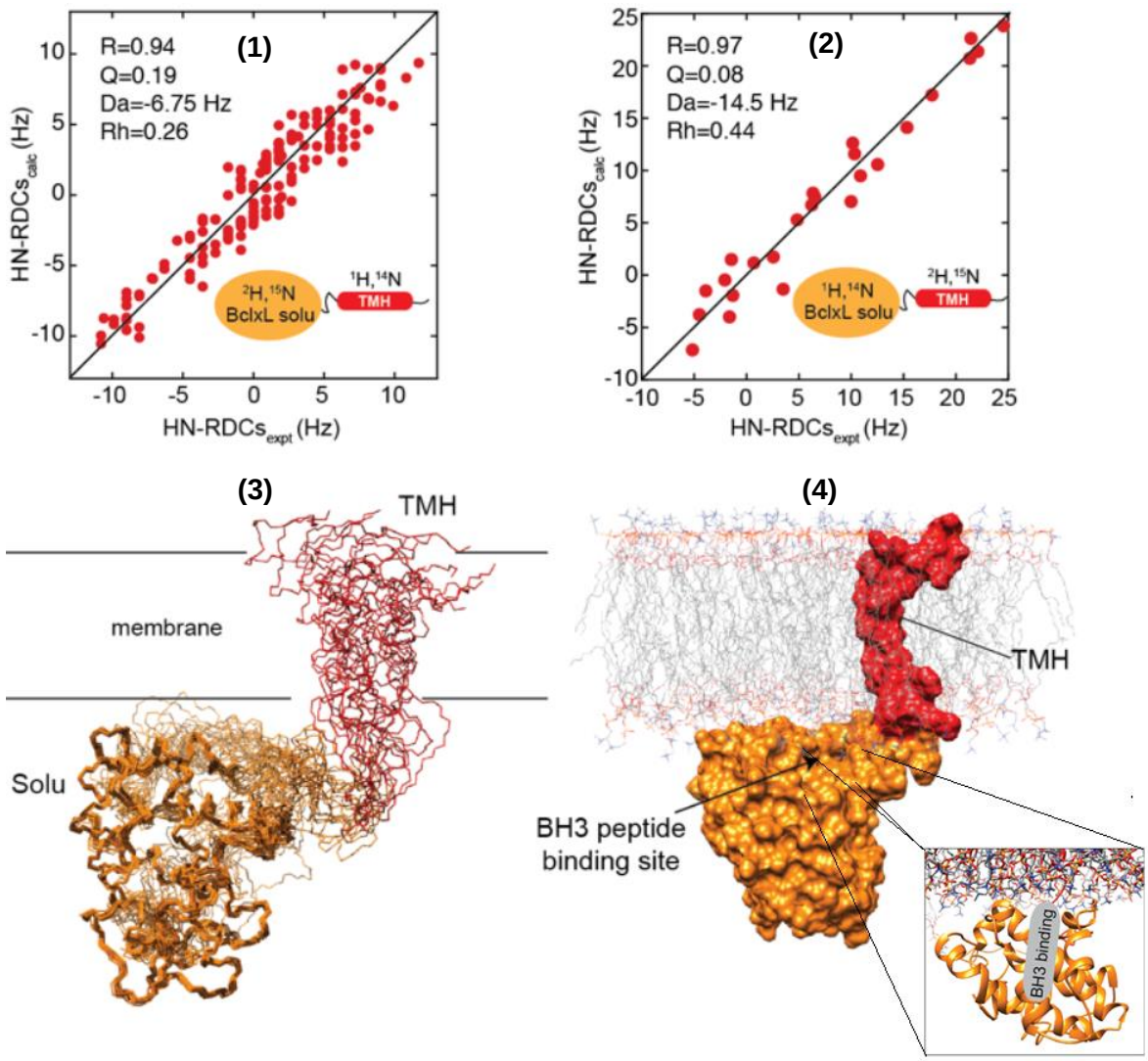

Figure 44: Depiction of the obtained and used RDC data (1, 2) from segmentally labelled ^{2}H,^{15}N-Fl-Bcl-xL (either TMH (2) or Bcl-xL-solu (1) labelled) in MSP1D1ΔH5 nanodiscs with and without Pf1 phage from 2D-[^{1}H,^{15}N]-TROSY and semi-TROSY experiments. The obtained RDCs are shown as a correlation plot between experimental and back-calculated backbone amide RDCs, where Da and Rh are the magnitude and rhombicity of the alignment tensor, R the correlation coefficient and Q the quality factor. The more rigid and membrane embedded helix shows less flexibility as seen from the little spread across the plot and good agreement between calculated and experimental data. The highly flexible Bcl-xL-solu (1), which is at the membrane surface, may move more freely in solution and exhibits a wider spread. The data was used for structure refinement of Fl-Bcl-xL, where (3) shows the relative orientation between both protein parts in the RDC-refined structure. (4) Depiction of the protein surface of both parts and their location with respect to the membrane. The BH3 binding site of Bcl-xL-solu is in close proximity to the membrane surface. Adapted from[380] with permission.

3.1.7 Modulation of membrane interaction of Fl-Bcl-xL by Lipids and PUMA

Up to now, little is known about the mechanisms and binding interactions of full-length Bcl-xL and its Bcl-2 partner proteins in the membrane environment, the interaction of Bcl-xL and the membrane-bilayer and its lipids. It has only been shown, that membrane-attached or anchored Bcl-2 proteins, like Bcl-xL, need a membrane to exert their full potential and interact with their partner proteins[241,249-251]. This *in vivo* finding could only be studied so far in heterogeneous liposome samples or assays with different lipid-compositions and truncated Bcl-xL-solu missing its native membrane-anchor[372]. Bcl-xL-solu has further been found to bind and interact with negatively charged lipids, that are also abundant in their native surrounding, the mitochondrial outer membrane[372,385].

It was previously demonstrated in Chapter 3.1.4 that Bcl-xL-solu interacts with different types of lipids and that the interaction is dependent on membrane charge and composition. Negatively charged lipids and especially cardiolipin were preferred by the soluble-domain. Further addition of the BH3-peptide of the binding partner PUMA in the same experiments showed a detachment from the membrane surface and hinted a possible mechanism of the membrane-interaction of Bcl-xL-solu and PUMA.

So far, the full-length protein and its membrane interaction were studied for the apo-state of Fl-Bcl-xL with 25 % DMPG/75 % DMPC nanodiscs in this work. The soluble-domain of the membrane-anchored protein proved to be loosely attached to the membrane surface, just as the previously studied Bcl-xL-solu alone. The BH3 binding groove and its surrounding was shown to be pointing towards the membrane-bilayer. However, the effect of PUMA-binding as well as the effect of different lipid compositions on the full-length protein has not been studied so far. A detailed insight into the importance of the membrane charge and composition, as well as a mechanistic insight into the conformational changes of Fl-Bcl-xL is still missing.

In order to make a detailed investigation, further unlabelled and segmentally labelled (Bcl-xL-solu labelled) $^{2}H,^{15}N$-Fl-Bcl-xL samples were prepared in MSP1D1ΔH5 nanodiscs with different lipid compositions to elucidate the influence of the membrane composition onto the protein and to better understand the membrane-effect on the structure and localisation of Bcl-xL-solu upon PUMA binding.

The NMR titration series with Bcl-xL-solu and empty nanodiscs with different lipid compositions in Chapter 3.1.4 indicated the lowest amount of Bcl-xL-solu binding to 100 % DMPC membranes, a very high one to 12.5 % cardiolipin (CL) with 75 % DMPC ones and the comparable (by charge) 25 % DMPG and 75 % DMPC.

As all full-length studies in the previous chapter the previous chapter were done with the common 25 % DMPG and 75 % DMPC combination, the composition with the best Bcl-xL-solu binding (12.5 % CL) and the lowest one (100 % DMPC, as a reference) were chosen to further investigate the effect of the lipids on the full-length sample and to compare all three different environments. A special focus was set on the effect of PUMA binding on the localisation of the Bcl-xL-solu, with respect to the membrane.

Therefore, analogous to the study of the full-length sample in 25 % DMPG/75 % DMPC from the previous chapter, two sets of segmentally labelled (Bcl-xL-solu labelled) $^{2}H,^{15}N$-Fl-Bcl-xL samples were prepared in MSP1D1ΔH5 nanodiscs. For each sample with the transmembrane helix of Bcl-xL in 100 % DMPC or 12.5 % CL nanodiscs, one corresponding sample with Gd^{3+}-DTPA-DMPE lipids (2 per leaflet) were prepared for the additional PRE-effect. That way, the localisation of Bcl-xL-solu and the binding to the membrane was studied, with respect to the different lipid composition (Figure 45).

The respective 2D-[$^{1}H,^{15}N$]-TROSY experiments of both apo samples show an almost identical fold and behaviour in both membrane environments (Appendix: Figure 74, 76) and also upon PUMA binding (Appendix: Figure 75, 77). The observed typical BH3-bound chemical shifts and the corresponding fold can be observed in both cases. However, in the PRE-based experiments (Figure 45) and the comparison between the respective standard with Gd^{3+}-containing samples, larger differences are observable. Since both full-length Bcl-xL samples in 100 % DMPC or 12.5 % CL are closely attached to the membrane by their respective helix, the PRE-effect is strong and evident in both cases, in comparison to the non-attached Bcl-xLΔTM study. However, still a stronger binding in the apo 12.5 % CL sample can be observed by a larger PRE-effect, compared to the amount of intensity depletion in the apo 100 % DMPC sample.

The average intensity value for the 12.5 % CL sample is lower and ten more residues are affected (below the top average dashed line) by the PRE effect, than in the 100 % DMPC case. The amount of strongly affected residues (below the bottom average minus standard deviation line) is identical in both cases and exhibits almost the same pattern, but with stronger depletion in the N- and C-terminal end of Bcl-xL-solu for in the 12.5 % CL sample. Also, in the PUMA BH3-peptide bound state more residues (three) are strongly affected in the 12.5 % CL nanodiscs than in the 100 % DMPC sample, but the total number (68) of all affected residues is the same. Nevertheless, the 12.5 % CL sample exhibits a stronger PRE-effect and membrane proximity in the N- and C-terminal region, especially in the sequence region of 20-30,150-160 and 185-205.

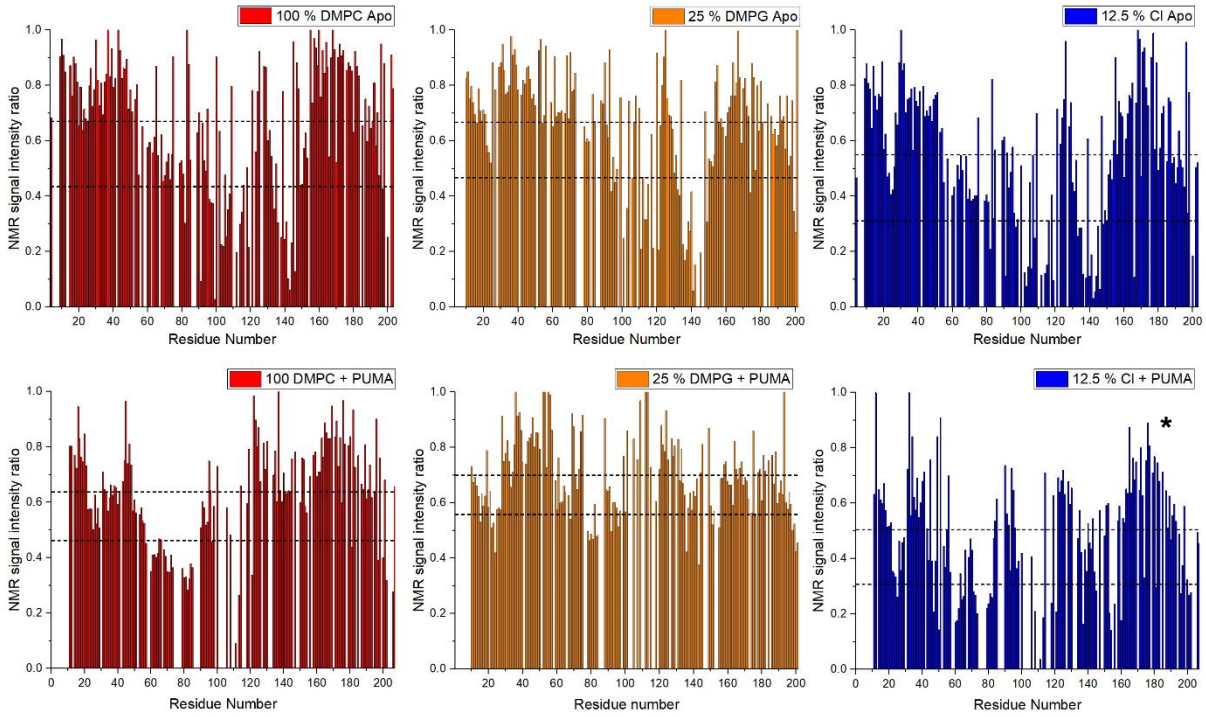

Figure 45: Depiction of the obtained PRE-based intensity plots from 2D-[^{1}H,^{15}N]-TROSY NMR-based experiments at 900 MHz field strength with 120-180 µM segmentally labelled ^{2}H,^{15}N-Fl-Bcl-xL (Bcl-xL-solu labelled) in MSP1D1ΔH5 nanodiscs containing either 100 % DMPC (red), 25 % DMPG and 75 % DMPC (orange), 12.5 % cardiolipin (CL) and 75 % DMPC (blue). On the top are the respective apo Fl-Bcl-xL plots and on the bottom the PUMA bound ones, where the top dashed line represents the average and the bottom dashed line average minus standard deviation. For each sample one corresponding paramagnetic tag (Gd^{3+}-DTPA-DMPE) containing one was prepared and compared with the reference. The Apo samples show a strong PRE-effect, where 100 % DMPC and 25 % DMPG exhibit almost the same amount, except for the C-terminus of 25 % DMPG and the region 135-155, which is more affected and shows a stronger membrane-binding. The 12.5 % CL shows the highest amount of intensity depletion in the Apo and PUMA-bound state, also visible by the lower average line. The 12.5 % CL PUMA BH3-bound sample is marked with an asterisk, as this sample showed quality problems. Upon PUMA BH3-binding all three sample still exhibit a strong PRE-effect in the flexible loop region (ca. 55-85), whereas the region around the BH3-binding site (residues 120-155) are not affected anymore.

Interestingly, the 100 % DMPC sample shows a strong binding of parts of the flexible loop (residues ca. 45-85 from 25-85) to the membrane surface in both states, but stronger in the PUMA bound one. This effect is also observable in the 12.5 % CL experiments, but less pronounced.

Overall, it was possible to obtain Fl-Bcl-xL PRE-intensity plots by comparing each Gd^{3+}-sample with the Gd^{3+}-free one for the respective membrane composition. In all three different apo samples for all studied lipid-compositions it was found that the soluble-domain of the full-length Bcl-xL is attached to the membrane via the same orientation.

All residues of the three BH1-3 domains (86-100 are BH3, 129-148 are BH1 and 180-195 are BH2) responsible for the formation of the BH3-binding groove are strongly affected, but especially the BH1 and BH3 domain of the protein. However, while the 12.5 % CL sample showed the highest signal intensity attenuation and membrane-binding, both the 100 % DMPC and 25 % DMPG sample exhibited similar and barely distinguishable results. Therefore, it can be assumed that in all cases the full-length protein is closely attached to the membrane by its respective helix and so the PRE-effect is strong and evident in all cases, contrary to the non-attached Bcl-xLΔTM study where the protein is not membrane-anchored. In the latter case, the soluble domain is held only by weak hydrophobic and electrostatic interactions which are dependent on the membrane charge and lipid headgroup, so the lipid surface appears to have a pivotal influence. It seems that in the full-length protein, the proximity through anchoring "forces" a membrane attachment, which can be expected form tail-anchored proteins, and differences are not so prominent for various lipids. Still, in both studies the cardiolipin sample exhibited the strongest membrane-binding and PRE-effect.

The effect of PUMA BH3 peptide on the membrane location of full-length Bcl-xL was also investigated in all three cases. Compared to the Bcl-xLΔTM titrations where the addition of PUMA almost completely removed Bcl-xL-solu from the membrane except in the 12.5 % CL case, for the full-length protein all three samples seemed to be still membrane-attached after binding of the ligand. It was found that residues 100-120 and the BH1 domain (129-148) are less affected by PRE upon PUMA binding, which can be explained by a light detachment or tilt of the soluble-domain away from the membrane surface. The flexible loop of all three samples (around the region 50-70) is still more prominently affected and seems to be in membrane proximity. Nevertheless, the loop is not involved in the PUMA binding and seems to play only a small regulatory role in BH3-ligand affinities[317].

In the PUMA-bound state, the cardiolipin sample is an exception as it shows (apart from the BH1 domain) still strongly affected residues and a membrane-attachment even after PUMA addition. This can be explained by the fact that this specific PUMA-bound sample was also used for different types of measurements beforehand and showed slight degradation and unfolding before this 2D-TROSY measurement. Both events can lead to a membrane-binding and distortion of the obtained PRE-data. Therefore, this sample was marked with an asterisk and excluded from deeper analysis and comparison, as it could only serve for an estimation.

Additionally, the effect of the membrane-composition and the effect of PUMA BH3-binding on the stability of the protein was studied via far UV-Vis CD (Figure 46). Surprisingly, both Fl-Bcl-xL in either 100 % DMPC or 12.5 % CL exhibited almost the same melting point between 64-65 °C as seen for the full-length study in 25 % DMPG (Figure 39).

Moreover, the addition of PUMA BH3 had no influence on the stability and thermal unfolding of the 100 % DMPC sample and just a small one in the 12.5 % CL. This is in contrast to the observation that PUMA increases the thermal unfolding temperature of Bcl-xL-solu and stabilises its structure. It seems that binding to the membrane surface leads to a strong destabilisation of Bcl-xL, or it favours its insertion at elevated temperatures.

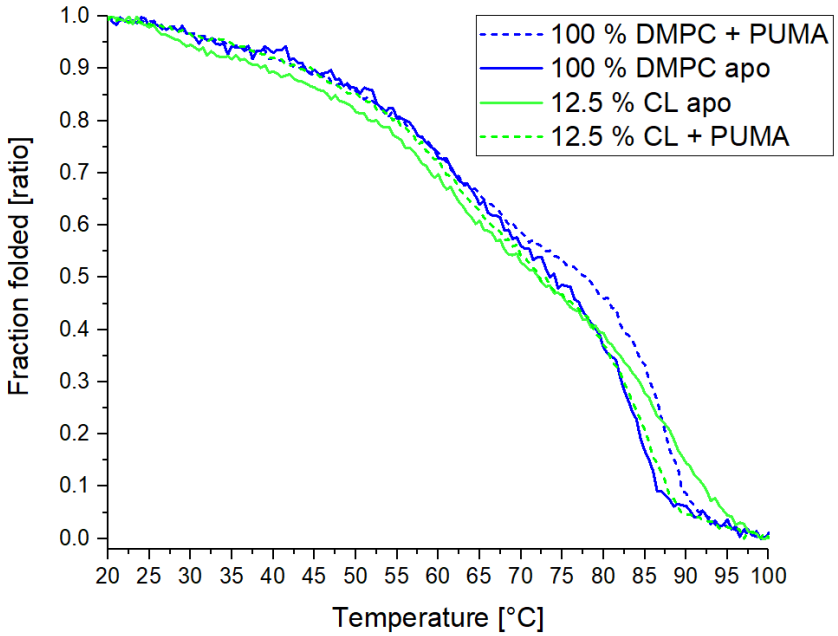

Figure 46: Far-UV-Vis Thermal unfolding measurements at 220 nm of Fl-Bcl-xL in either 100 % DMPC (blue) or 12.5 % CL/75 % DMPC (green) in the presence (dashed lines) or absence of PUMA. All full-length samples exhibit a melting temperature of ca. 64-65 °C, while the respective MSPs melt between 84-90 °C. No difference in protein stability was found in the presence of PUMA, except a small increase in the 12.5 % CL sample.

Apart from the NMR experiments, the attachment of Bcl-xL-solu to the membrane and its possible release upon PUMA binding was studied through small angle X-ray scattering (SAXS), in the full-length protein samples in nanodiscs (Figure 47). The SAXS experiments and their analysis were done by Dr. Ralf Stehle. For a successful calibration curve and fitting different concentration of unlabelled full-length samples of Fl-Bcl-xL (1.0-3.0 mg/mL) in either 100 % DMPC or 12.5 % Cl and 75 % DMPC MSP1D1ΔH5 nanodiscs were prepared. Several measurements were done for the respective apo and PUMA-bound forms, also for different concentrations at 4 °C (Figure 47, below lipid-phase transition) and 30 °C (above lipid-phase transition). Due to higher noise at 30 °C, the 4 °C measurements were considered for an adequate comparison of different samples at same concentrations. It was found, that 12.5 % Cl nanodiscs with apo Fl-Bcl-xL show a more compact structure and therefore a smaller maximal particle-radius than the respective apo 100 % DMPC sample (Figure 47) and smaller per distance distribution versus radius (pvr).

The same was observed for the PUMA-bound state of both different nanodiscs. Looking at the same sample, either 100 % DMPC or 12.5 % Cl, the maximum particle radius increases upon PUMA BH3 addition as does the per distance distribution versus radius (pvr). This indicates that the PUMA-bound form of the soluble domain is less membrane-attached and further away from the membrane, which enlarges the overall particle size.

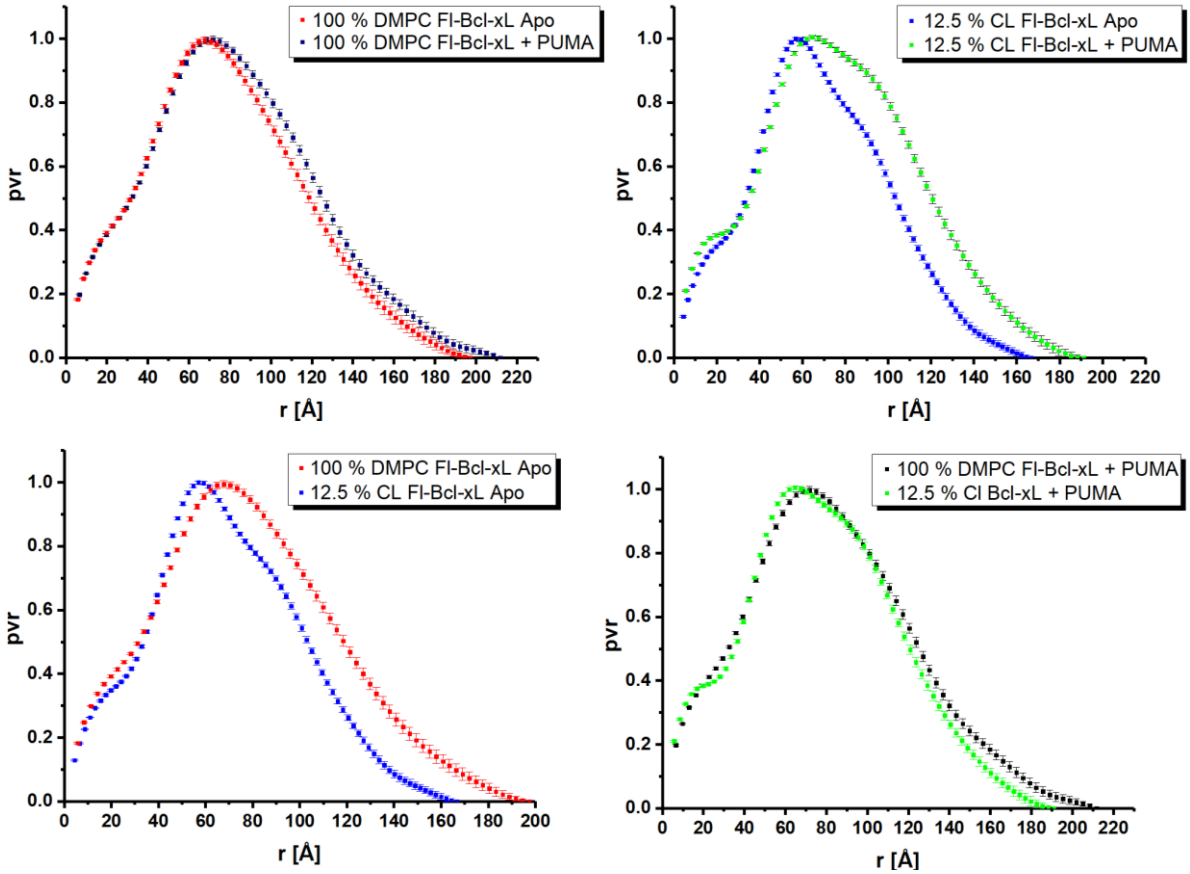

Figure 47: Small angle X-ray scattering (SAXS) analysis of apo or PUMA BH3-bound Fl-Bcl-xL in MSP1D1ΔH5 nanodiscs with either 100 % DMPC (red in apo-, black in PUMA-bound state) or 12.5 % cardiolipin (CL) and 75 % DMPC lipid composition (blue in apo-, green in PUMA-bound state) where pvr is the per distance distribution versus radius and r represents the radius of the measured particles. All cardiolipin samples in apo- or PUMA-bound state are larger than the respective 100 % DMPC samples. For each pair, the respective PUMA-bound state is larger than its apo-state.

This hints that Bcl-xL-solu of the membrane-anchored Fl-Bcl-xL detaches from the membrane upon PUMA addition and that overall, Bcl-xL-solu binds stronger to cardiolipin-containing membranes. This is in good agreement with the soluble-domain studies of Bcl-xLΔTM and the Fl-Bcl-xL PRE-based studies of this chapter.

3.1.8 Effect of caspase-like cut on Bcl-xL structure and function

The final outcome of the caspase cut in the flexible loop of Bcl-xL is known, which is an increased MOMP and cell death[325,327]. Unsurprisingly, the resulting ΔN-Bcl-xL was linked to pro-apoptotic stress and, amongst others, to neuronal cell death[329,330,332]. It is still controversial what happens to Bcl-xL after the cut and if the protein switches roles and becomes pro-apoptotic itself and inserts into the MOM, or if the mechanism for the increased apoptosis is different. It is further thought that a possible pro-apoptotic Bcl-xL could also form pores, analogous to Bak or Bax.

To elucidate this, two constructs were cloned and purified, Bcl-xL-THR-SOR and Bcl-xL-THRΔTM (Chapter 4.1.3), with a thrombin cut site in the flexible loop. Bcl-xL-THRΔTM was subjected to a test thrombin cut that mimics the native caspase cleavage in the flexible loop and the properties of the uncut and cut protein were studied. The cut one exhibits two distinct cut-product bands in the SDS gel of ca. 15 kDa and 10 kDa that correspond to the expected mass of both halves (Figure 48). Furthermore, the cut Bcl-xL-THRΔTM exhibits a 11.7 °C lower melting point in the circular dichroism (CD) thermal unfolding experiments and therefore a much lower stability than the uncut one (Figure 48).

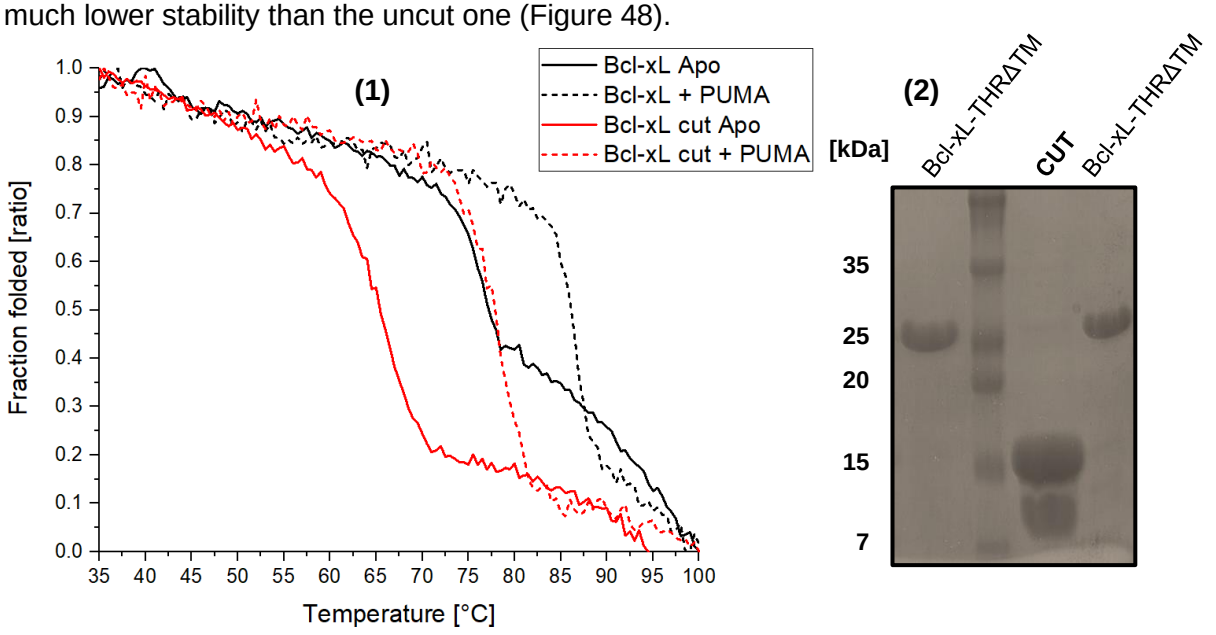

Figure 48: (1) Far-UV-Vis Thermal unfolding measurements at 220 nm of Bcl-xL-THRΔTM cut (red) or uncut apo (black) and PUMA BH3 peptide-bound form (dashed-line). Bcl-xL-THRΔTM exhibits an unfolding temperature of 77.2 °C in apo and 86.3 °C in PUMA BH3-bound form. The cut apo Bcl-xL has a much lower unfolding temperature of 65.5 °C and its unfolding temperature increases up to 77.8 °C upon PUMA BH3 peptide-binding, reaching a similar value to that of uncut apo Bcl-xL. (2) Exemplary Coomassie stained SDS-PAGE gel of the uncut and cut Bcl-xL-THRΔTM

Surprisingly, upon PUMA addition to either the uncut or cut Bcl-xL-solu, the melting temperature increases by 9.1 °C, or 12.3 °C respectively. This indicates a high amount of stability gain and a successful binding of the BH3 PUMA peptide to both the cut and uncut soluble domains and two functional o binding-competent proteins. Furthermore, the previously strongly destabilised cut Bcl-xL gains more stability (3.2 °C) from the PUMA binding.

Complementary 2D-[^{1}H,^{15}N]-TROSY NMR-based experiments with thrombin-cut and uncut labelled ^{2}H,^{15}N-Bcl-xL-THRΔTM were also performed (Figure 49). Additionally, mild detergents (CHAPS and Triton-X 100) and urea (1-8 M) were screened for their ability to remove the smaller cut product, which corresponds to the BH4-domain and N-terminal part of the soluble Bcl-xL domain by washing it off on a Ni-NTA column.

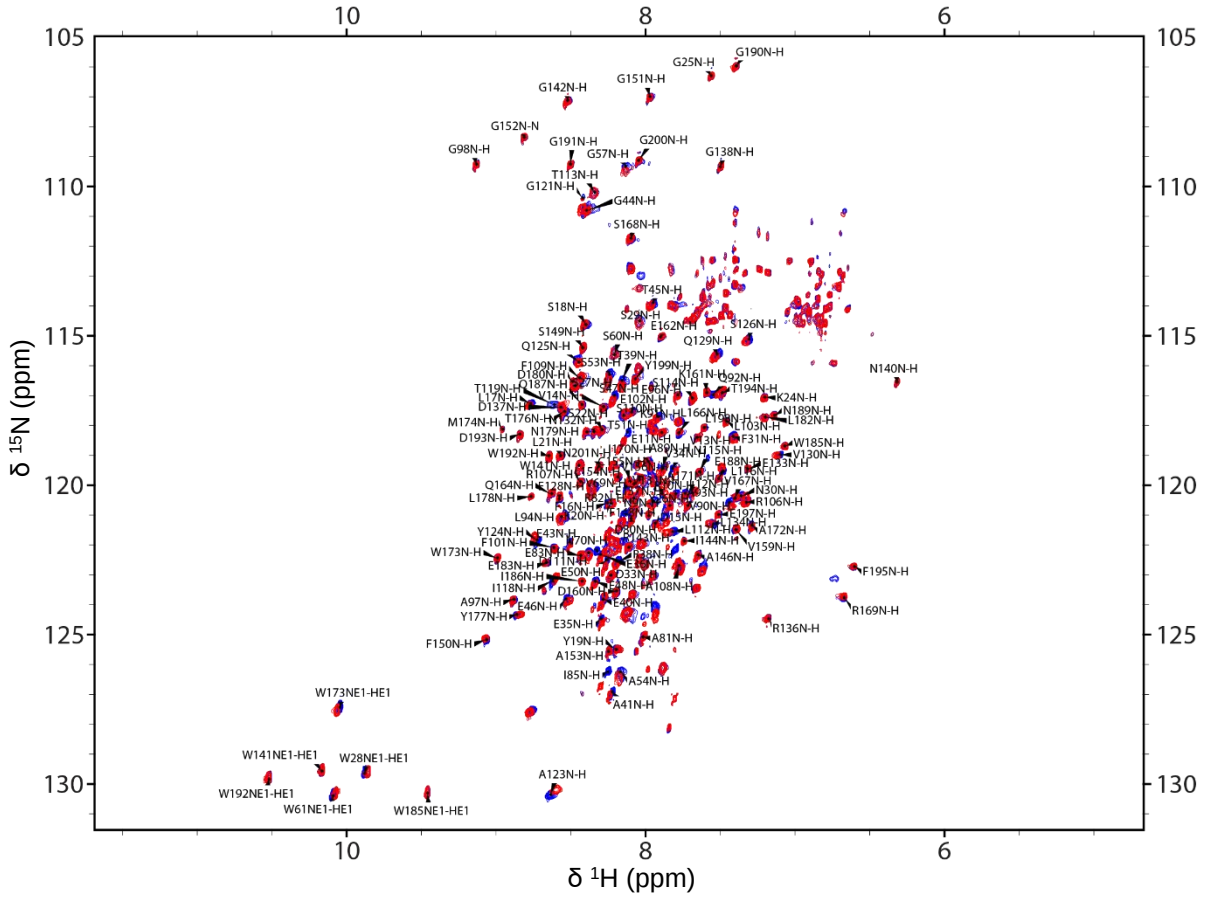

Figure 49: Overlay of 2D-[^{1}H,^{15}N]-TROSY experiments with uncut apo (blue) ^{2}H,^{15}N-Bcl-xL-THRΔTM and cut one (red). Mainly chemical shifts in the loop region, which are expected after a cut, are obtained and smaller once in the BH1 And BH3 domain.

It was found that neither both detergents, which are tolerated by Bcl-xL solu, are able to remove the BH4-domain, nor 1-6 M of urea. Upon concentrations of 7 M of urea or higher the protein unfolds, and both cut products can be separated on the Ni-NTA column. However, the remaining BH4-deficient Bcl-xL-solu cannot be further studied as it remains unfolded in solution, as seen in Figure 73 (Appendix).

The 2D-[^{1}H,^{15}N]-TROSY NMR-based experiments (Figure 49) show a similar fold and only slight chemical shifts upon thrombin-cut of Bcl-xL-solu (Figure 50) and the appearance of a new C and N-terminus. Upon PUMA BH3 peptide addition (Figure 51), the cut protein further shows the same behaviour in the NMR experiments as the uncut one and is able to bind the peptide regardless of the cut, as supported by the same stability increase (or larger) in the CD-based thermal unfolding experiments.

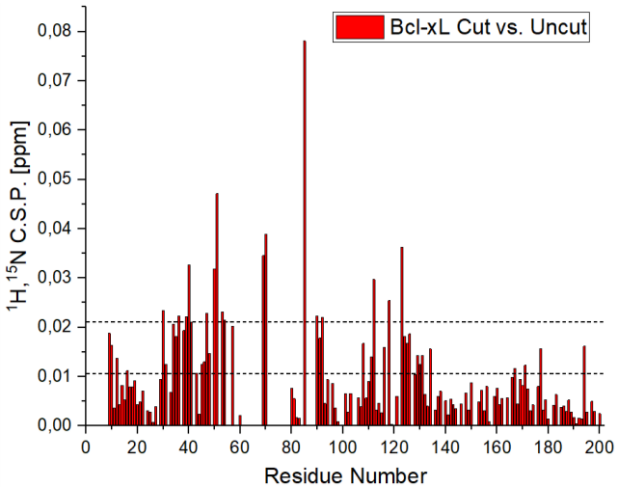

Figure 50: Obtained chemical shift perturbations (CSP) from the comparison of the 2D-[^{1}H,^{15}N]-TROSY spectra of cut and uncut ^{2}H,^{15}N-Bcl-xL-THRΔTM (Figure 49). Only a few residues (mainly) in the cut loop-region are affected (40-70) and the BH3 (86-100) and BH1 (129-148) region of the protein.

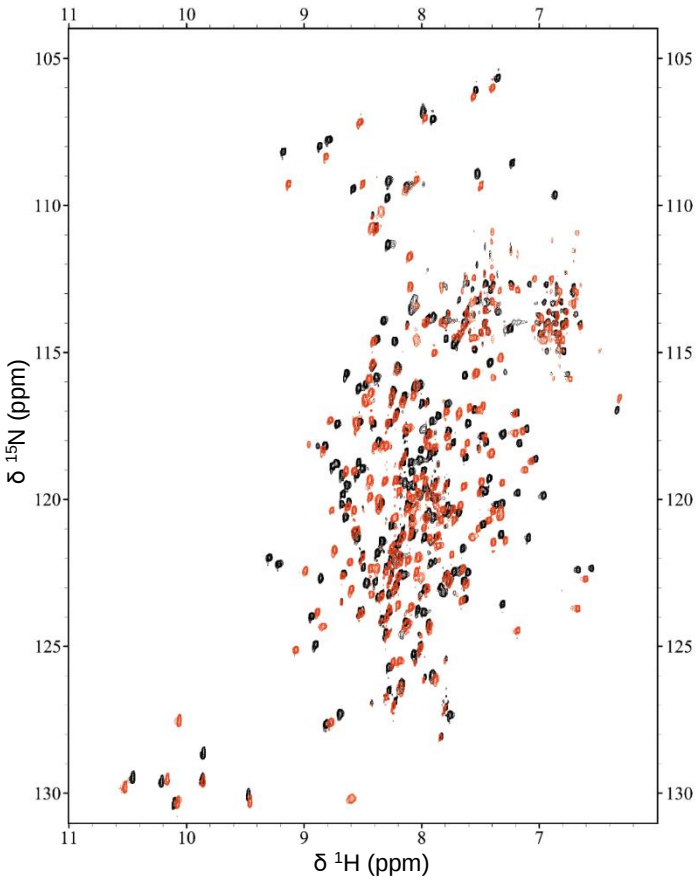

Figure 51: Overlay of 2D-[^{1}H,^{15}N]-TROSY experiments with cut apo (red) ^{2}H,^{15}N Bcl-xL-THRΔTM and cut one with Bak BH3 peptide (black). Mainly chemical shifts in the loop region, which are expected after a cut, are obtained and smaller once in the BH1 And BH3 domain.

In order to see if the cut induces structural changes in the apo or PUMA-bound state that leads to an insertion of the protein, 2D-[^{1}H,^{15}N]-TROSY NMR-based experiments were done with ^{2}H,^{15}N-Bcl-xL-THRΔTM in the presence of empty nanodiscs with two different lipid compositions (25 % DMPG with 75 % DMPC or *E. coli* total lipids) and their corresponding Gd^{3+}-DTPA-DMPE containing nanodiscs.

E. coli total lipids have an estimated composition of 57.5 % phosphatidylethanolamine, 15.1 % phosphatidylglycerol and 9.8 % of (*E. coli*) cardiolipin (double lipid), according to the manufacturer (Avanti Polar Lipids, INC.)[386]. With an overall net negative charge of about 31.6 %, cardiolipin and a high amount of phosphatidylethanolamine, this makes them an ideal substitute for the mitochondrial outer membrane, which is known to content varying amounts of cardiolipin and high amounts of phosphatidylethanolamine[381,387,388].

In the NMR experiments with both different lipid compositions (DMPC/DMPG or *E. coli* total lipids) no difference (membrane-related effects) were observed for uncut or cut Bcl-xL-solu, so the protein was bound in additional experiments via its His_6-tag to nanodisc with Ni^{2+}-NTA containing lipids and their respective Gd^{3+}-DTPA-DMPE containing counterparts. However, this fast membrane-attachment screening method - as an alternative for full-length Bcl-xL production - introduced several PRE-based signal attenuation artefacts in uncut Apo Bcl-xL-solu, which were also present in the cut one. Apart from this unexpected effect, no further PRE-based signal attenuation or changes in the NMR-spectrum of Bcl-xL-solu were observed upon thrombin cut. Subsequent binding of Bak-BH3 peptide did not induce any substantial changes in the NMR-spectrum or the localisation of the protein (PRE-effect) than the one that occur upon PUMA BH3-peptide binding. In none of the said NMR-experiments, the cut indicated any substantial changes in the protein fold, its binding capacity to BH3-peptides, or its localisation or insertion into the membrane.

Probing the relevance of the cut in apoptosis was done via a previously reported liposome-based fluorescence assay that allows detecting membrane pore-formation[389]. In our assay Bcl-xL-solu (cut or uncut) in combination with the soluble domain of Bak-solu and its activator tBID are studied in several triplicate experiment series (Figure 52) performed by Laura Sperl. Therefore, a fluorescent dye 8-aminonaphthalene-1,3,6-trisulfonic acid (ANTS) and its quencher *p*-xylene-bis-pyridinium bromide (DPX) are trapped in freshly prepared mitochondria-like liposomes, which can be released from the liposomes upon pore formation, causing a fluorescence signal.

In our studies, *E. coli* total lipids were chosen, as they showed a strong pore formation with activated Bak-solu alone (used as the reference). Intact and functional Bcl-xL-solu can interact with Bak-solu and hinder a pore formation of the inactivated or activated form (Figure 52). By employing 10 % of Ni^{2+}-NTA containing lipids, the membrane binding of Bak-solu and the respective Bcl-xL-solu is enhanced, which increases the efficiency of Bak oligomerisation and pore formation in the absence of Bcl-xL and further improves the assay.

In the said assay, the reference anti-apoptotic Bcl-xL-solu alone did not induce pore formation, neither did tBID, or Bcl-xL together with tBID (not shown). The pore-forming reference Bak-solu shows already a small basal pore-formation in the inactive state, while the tBID activated Bak-solu showed a high amount of pore-formation. Addition of equimolar or higher amounts of Bcl-xL leads to successful suppression of pore formation in the absence, or presence, of equimolar amounts of tBID. The thrombin cut Bcl-xL-solu did not exhibit a notably pore-formation on its own or any type of liposome leakage after addition, neither in the presence of tBID.

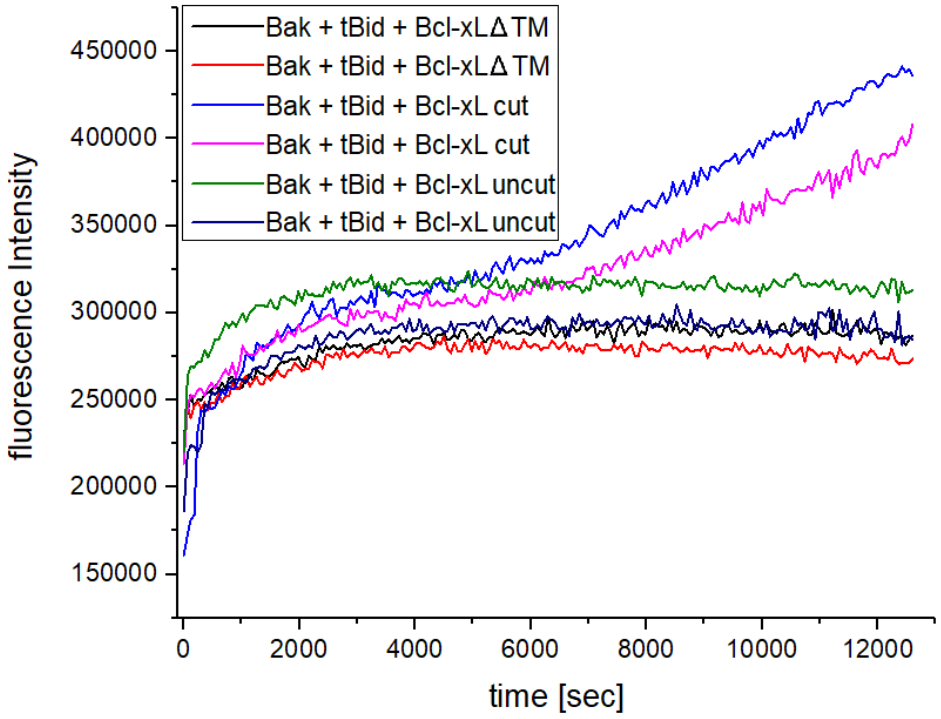

Figure 52: Depiction of the obtained fluorescence data (duplicates) from the pore-forming liposome assay performed by Laura Sperl with Bcl-xL-THRΔTM (cut and uncut), Bcl-xLΔTM as additional reference, Bak-solu, tBid and *E. coli* total lipid liposomes with 10 % Ni^{2+}-lipids. Bak-solu with uncut Bcl-xL-THRΔTM (dark-blue and green) or Bak-solu, uncut Bcl-xLTHRΔTM and tBid (red and black) do not form pores, and therefore the fluorescence reaches a plateau. Cut Bcl-xL can only stop the pore formation of Bak-solu and tBid (pink and blue) for about 90-100 min and then the pore formation starts, seen by the increase of fluorescence due to release of the dye from the liposomes. Bcl-xL-THRΔTM and Bcl-xL-ΔTM exhibit the same amount of anti-apoptotic activity and both stop a pore formation, which indicates no functional changes through the thrombin-cut site point mutations.

However, cut Bcl-xL-solu attenuates Bak-mediated pore-formation only for 90 min, after which the liposomes start to leak and exhibit a high amount of fluorescence, compared to intact ones. The final amount of formed pores and their fluorescence signal is less than the one for activated Bak-solu in absence of Bcl-xL-solu, but still higher than with intact Bcl-xL. This indicates an altered and deficient Bcl-xL-Bak-tBid interplay when Bcl-xL-solu is cut.

3.1.9 Asna1/Get3 co-expression and production of Fl-Bcl-xL

The successful and high-yield recombinant expression and production of native and functional full-length Bcl-2 proteins and tail-anchored proteins in general is the key ingredient that helps to access the full and native potential, the mechanisms and interactions of this complex network of proteins. Until now, only Bax and Bcl-w were expressed and studied as functional full-length proteins, which helped to understand the role of their C-termini[265,266]. Both proteins are distributed in the cytosol and are therefore accessible for *E. coli* expression. However, the toxic Bax is produced as fusion construct (chitin-binding domain) with extremely low yields of 0.25 mg/L culture. Furthermore, membrane-anchored native Bcl-xL and Bak have not been successfully produced as full-length proteins so far, without truncating or altering the sequence of them, as they seem to be too insoluble and/or interacting with the host membrane. Also, their recombinant yields of functional (altered) full-length protein is very low and not useful for most studies and structural biological methods.

Since the human Asna1/TRC40 and the yeast analogue Get3 function as selective binders and transporters of tail-anchored proteins, which keep them in solution, they could be employed as a co-expression system for toxic or insoluble tail-anchored proteins. This would offer the possibility to express tail-anchored and Bcl-2 proteins as full-length constructs and create a high-yield addition to the established Sortase A mediated approach (Chapter 4.1.5). The feasibility of Asna1 or Get3 has been shown in a small-scale expression that mainly focused on the insertion mechanism of the Asna1/Get3-tail-anchored protein complex and the Asna1 or Get3 protein. It was emphasised that Asna1 or Get3 could capture the Fl-Bcl-xL during co-expression and keep it in the solution instead of inclusion bodies and allow a fast and easy purification of the complex. Furthermore, once purified, Asna1 or Get3 could be removed and the Fl-Bcl-xL may be integrated or co-assembled into nanodiscs, or directly studied in detergent solution (Figure 53).

First, to test and optimise the co-expression of Asna1 with F-Bcl-xL or Get3 with Fl-Bcl-xL, the Bcl-xL was cloned into a pT5L/T7 vector as a Z-tag-fusion construct with a TEV cut site (in between) under the T7 promotor, supplied by Prof. Dr. Blanche Schwappach-Pignataro (University of Göttingen). Separately, the plasmid contains either Asna1 or Get3 as an MBP-fusion construct, with a TEV cut site in between, under the T5 promotor.

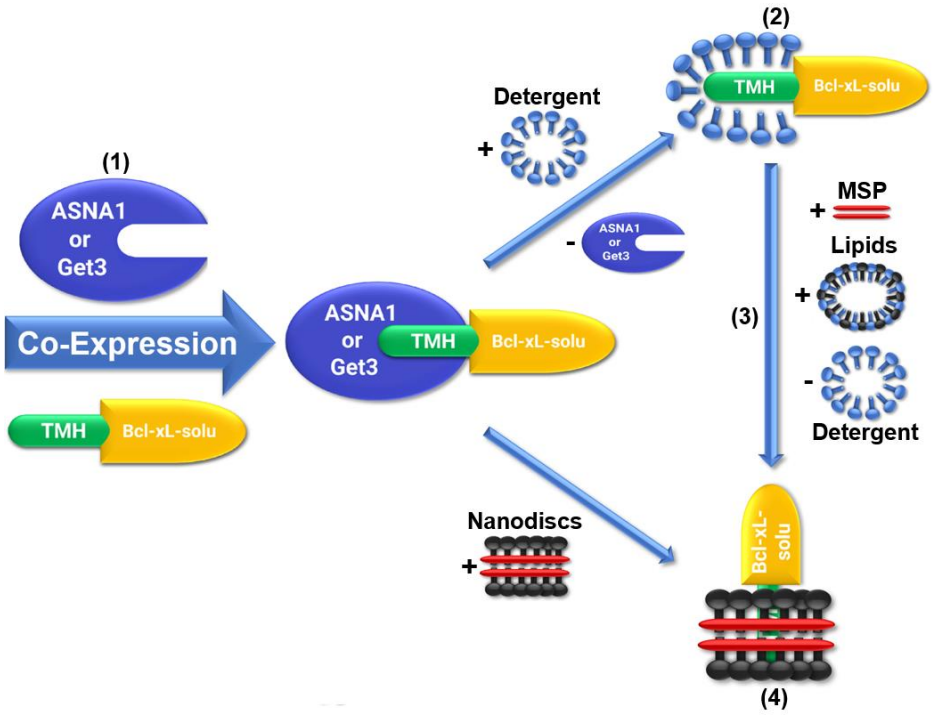

Figure 53. Depiction of the envisaged co-expression (1) of Asna1 or Get3 with Fl-Bcl-xL and the subsequent processing of the formed complex, either through detergent-mediated Asna1/Get3 removal (2) and/or (3) lipid- and MSP-mediated nanodisc assembly. (4) A further possibility is the addition of pre-formed nanodiscs to the purified Fl-Bcl-xL in detergent, which could lead to the integration of Fl-Bcl-xL.

As both are inducible by IPTG, an induction leads to the simultaneous expression of both target proteins and possibly a complex formation of the co-chaperon Asna1/Get3 and its tail-anchored target Fl-Bcl-xL.

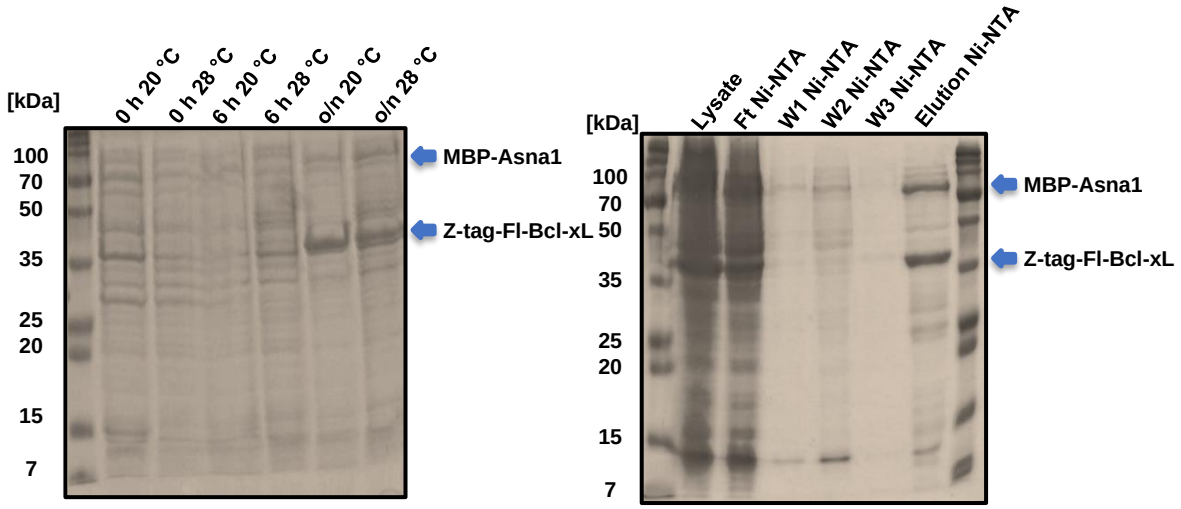

Figure 54: Representative Coomassie stained SDS-PAGE gel on the left of an MBP-fusion Asna1 and Z-tag fusion Fl-Bcl-xL co-expression test with 0.2 mM IPTG at 20 or 28 °C, followed by (2) a Ni-NTA purification. Hereunder both conditions, a successful expression and purification were possible.

Tested were BL21 cells with an induction using 0.2 or 1 mM IPTG at an optical density OD_{600} of 0.7-0.8. As expression temperature and time 20 °C or 28 °C over-night, 37 °C and 30 °C from 1 to 5 hours were tested (Figure 54) for Asna1-Fl-Bcl-xL and Get3-Fl-Bcl-xL respectively (Figure 55). As all conditions and IPTG concentrations showed a very high and quantitative expression, similar to that of Bcl-xL-solu, a faster expression of 37 °C and 4-5 h was chosen for future studies.

Overall Get3 showed a higher amount of expression and performed better in the subsequent Ni-NTA purification, or the detergent removal of Get3. Therefore, most studies were done with Get3.

The purification of the respective Fl-Bcl-xL complex was done via standard lysis, following a Ni-NTA gravity-flow purification (see Materials and Methods, 3.3.1). A quantitative and good purification could be achieved with this method and the complex was eluted and was further processed (Figure 55).

Detergent screenings to remove Get3 from Fl-Bcl-xL were done with CHAPS, Triton X-100, DDM, Brij-58 and DPC. For this, the complex was either added to a Ni-NTA gravity-column after successful purification, or it can also be done directly during the lysis and the first Ni-NTA (Figure 56).

Additionally, since Asna1 or Get3 need ATP/ADP and Mg^{2+} to function and exhibit a Zn^{2+} binding-site, an extra wash step with ATP and Mg^{2+} in 2-5 mM concentration was added in the Ni-NTA purification. It was found that this step or one with an additional 2 mM Zn^{2+} significantly increases the removal of Asna1/Get3 from its target. This way, for all tested detergents a quantitative purification and subsequent removal of the co-chaperon was established.

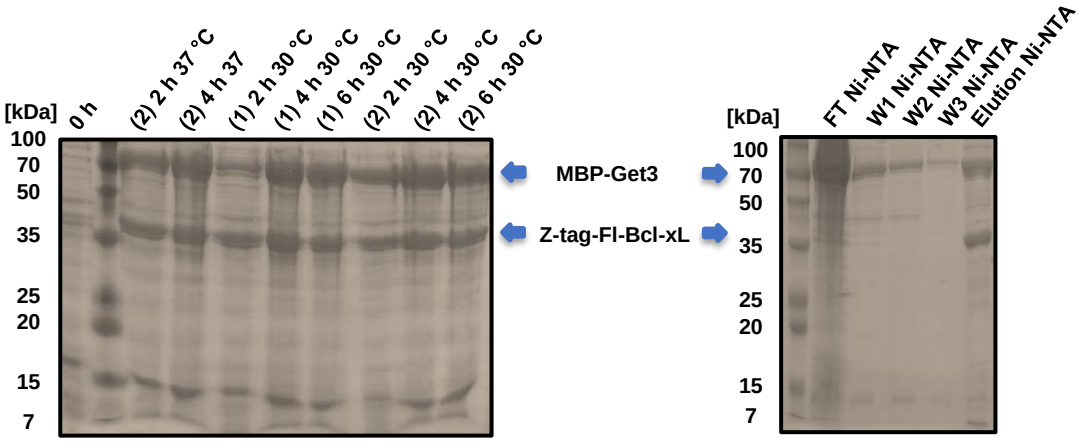

Figure 55: Representative Coomassie stained SDS-PAGE gel on the left of an MBP-fusion Get3 and Z-tag fusion Fl-Bcl-xL co-expression test with 0.2 mM IPTG, marked as (1), or 1 mM IPTG, marked as (2), for 6 h at 30 or 37 °C. On the right is the respective Ni-NTA purification of the protein-complex.

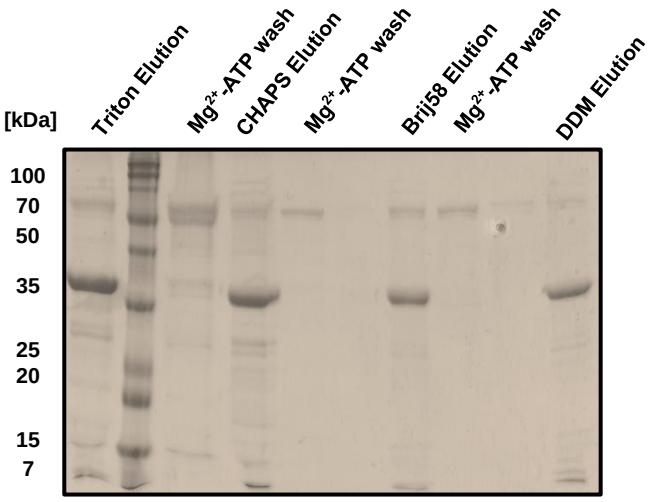

Figure 56: Representative Coomassie stained SDS-PAGE gel of different detergent-mediated MBP-Get3 removal screenings from the MBP-Get3 and His_6-Z-tag-Fl-Bcl-xL complex, using Ni-NTA chromatography with (left to right) Triton X-100, CHAPS, Brij58 and DDM. All detergents show a good separation, where CHAPS and DDM show the highest amount of separation and best final Fl-Bcl-xL purity.

The obtained Z-tag-Fl-Bcl-xL in detergent (CHAPS, Triton X-100, Brij-58, or DDM) was directly used for following nanodisc assemblies, employing either the dialysis or the biobeads method (0.7 g/mL). Bcl-xL-containing nanodiscs were separated by their His_6-tag via Ni-NTA from the empty nanodiscs, following a size-exclusion chromatography. Unfortunately, no successful incorporation of the full-length protein into phospholipid nanodiscs could be achieved with this setup and no Fl-Bcl-xL nanodiscs were obtained. Therefore, the Z-tag was TEV cleaved prior to the assembly and removed via Ni-NTA. The final purified Fl-Bcl-xL in detergent (CHAPS, DDM, Triton X-100) solution was used for analogous nanodisc assemblies with biobeads (0.7 g/mL) or through a dialysis supported method. Even without the Z-tag, this approach did not yield any Fl-Bcl-xL-containing nanodiscs and the protein could not be incorporated or transferred into nanodiscs.

A different approach using pre-formed empty nanodiscs (25 % DMPG and 75 % DMPC) with 5 mM ATP, 5 mM $MgCl_2$ and incubating them with Get3-Fl-Bcl-xL complex did not yield any inserted Fl-Bcl-xL in nanodiscs.

4 Discussion and Outlook

Expression, purification of Bcl-xL transmembrane helix (TMH) and study in detergent or nanodiscs

Before this work was started, there was almost no information about the C-terminus of Bcl-xL, as the structure and fold, or how it anchors Bcl-xL to the MOM. In order to obtain a 3D-structure of Bcl-xL and produce the full-length protein from two parts, this TMH was the starting point of the synthesis and structural studies of Bcl-xL. As small transmembrane proteins and helices are difficult to express without fusion tags[390], a new fusion-protein-construct was needed to facilitate a high-yield expression, such as GB1[95].

The expression with the His_6-GB1-tag was successfully established and showed high yields in unlabelled and ^{2}H,^{15}N-labelled samples. The straight forward purification leads to a monomeric and homogeneous product in detergent without further impurities. The cut and removal of GB1 was optimised in detergent or in nanodiscs (ND) and yielded a monomeric helix in the respective membrane-mimetic. After removal of the His_6-GB1-tag the TMH was successfully studied and assigned in DPC micelles.

The His_6-GB1-TMH was further successfully transferred from DPC or SDS into phospholipid MSP1D1ΔH5 ND (with a variety of different phospholipids), which was the first detrimental step for the production of Fl-Bcl-xL, and the structural studies of the TMH. Resulting GB1-TMH-ND were easily separated from excess empty ND via Ni-NTA chromatography. Even with longer chained lipids, as POPC and POPG, the thrombin cut site was readily accessible, and the removal of His_6-GB1 was possible via size-exclusion chromatography. This was an important step in order to be able to separate and later quantify the amount of cut-off GB1 per nanodiscs, so that the amount of helix per nanodisc can be back-calculated (see quantification of Bcl-xL below).
The homogeneity of the Bcl-xL-TMH in MSP1D1ΔH5 ND and the obtained results from the NMR experiments showed a successfully established purification and ND-assembly protocol for Bcl-xL-TMH-GB1 and subsequent removal of the tag.

The TMH was studied in MSP1D1ΔH5 ND via NMR, DSC and DLS. In nanodiscs, the helix was found to be a monomer (see quantification of Bcl-xL below). The TMH-ND were homogeneous and similar in hydrodynamic radius in the SEC and DLS to empty discs. As can be expected, it demonstrates that the helix is buried inside of the lipid bilayer, since Bcl-xL is known to be membrane-anchored. This is further supported by the NMR data.

Since the ND particle size did not increase and the obtained ND-TMH were homogeneous, high-quality 2D and 3D-NMR data were possible and a subsequent assignment of the TMH was done for all visible residues in the 2D. Employing paramagnetic Gd^{3+}-containing lipid headgroups allowed to get distance-dependent signal attenuation in the 2D-TROSY NMR spectra of the ND-TMH. Mapping them to the protein structure allowed to determine the relative position of the TMH in the ND. Additional 3D-NOESY experiments yielded high quality NOESY data which enabled to extract distance restraints for the TMH in the ND bilayer. Residues 214-229 exhibit clear amide-amide NOE cross-peaks which indicate a helical secondary structure and enabled to further calculate the first NMR structure of the Bcl-xL TMH (Figure 26). As expected, the obtained fold exhibits a flexible C- and N-terminus and a stiff helical core that is buried inside the lipid bilayer. These results are in good agreement with the known function and position of Fl-Bcl-xL, which is connected by a flexible loop to its TM-anchor[258,263,297]. The assignment and the results of this study are supported by a parallel study of Yao *et al.*[391], that was published during the course of this work. Their assignment, membrane integration and overall findings of the flexible C-terminus match the here presented results and are in good agreement with our data. It is also not proposed or expected, that Bcl-xL forms oligomers or multimers in the MOM. So, it is not surprising, that the helix is a rigid monomer in nanodiscs.

Overall, the established GB1-TMH expression, purification and transfer to detergent or nanodiscs proved to be a handy way to gain access to proteins, that are difficult to express or do so in low yields. The obtained homogeneous samples can be studied by a variety of different structural biological techniques to determine the properties and structure of a given target helix. The system was further transferred to Glycophorin A, VDAC-1 and small helices in our laboratory. In future experiments it could further be used to obtain and characterise the other missing Bcl-2 or different tail-anchored protein helices.

Quantification of Bcl-xL and Glycophorin A TMH per nanodisc

Quantification of the cut-off His_6-GB1 was possible by reverse Ni-NTA and by comparing the respective UV-Vis absorptions at 280 nm of the flow-through (ND-TMH) and the elution (His_6-GB1). This gave rise to the possibility to determine the number of inserted helices per ND and to further optimise the assembly conditions. For subsequent studies of homogeneous Bcl-xL-TMH, 1-1.2 helixes per ND were obtained. Additionally, this system was successfully transferred to the known dimeric Glycophorin A helix (His_6-GB1-GlycoA), which served as a reference, and VDAC1 (His_6-GB1-VDAC1).

In this work, the Glycophorin A was cloned into the GB1-vector, expressed and purified according to the Bcl-xL-TMH protocol. Furthermore, it was successfully transferred via the same conditions to MSP1D1 and the shorter MSP1D1ΔH5 ND. Compared to Bcl-xL (1-1.2) a ratio of 1.8-2.0 per ND was obtained for Glycophorin A, as expected from its known dimerisation behaviour[392]. The method allowed to calculate the MSP/ ND and TMH and GB1 ratios directly from the size-exclusion chromatograms and their UV-absorption at 280 nm. Since the small GB1 elutes separately at the end of the SEC run (16-18 mL), its quantification yields the exact number of respective TMHs. The residual ND UV-absorption at ca. 11-13 mL (in the S200a SEC) after subtraction of the TMH absorption, corresponds to the MSP-belt protein of the ND.

Overall, this method not only allows to quantify and study the oligomeric state of a protein in ND, but it also helps to optimise assembly conditions and thereby steer the amount of membrane proteins per ND in the desired direction.

Bcl-xL soluble domain – production, study of new variants and their membrane interaction

The soluble domain of Bcl-xL without the transmembrane anchor (Bcl-xLΔTM) was used for the first structure determination of the soluble Bcl-xL by Muchmore *et al*.[258] and without its loop for the first Bcl-2 heterodimer complex of Bcl-xL and a Bak BH3-peptide[297]. Both constructs show a properly functional and very similar behaviour as demonstrated, for example, with PUMA-BH3 binding studies[307]. Over the past decades, they have been both successfully established as the standard Bcl-xL construct of choice, since the full-length protein could not be produced in high yield or extensively studied so far. Preliminary production and studies by Yao *et al.* of Fl-Bcl-xL did not work in our hands[393].

The MOM and its lipids enable and facilitate structural changes and complex mechanism and interplay in the Bcl-2 family. Therefore, elucidating the interaction of Bcl-xL with differently composed membranes is of importance. It would allow to understand the role of the membrane and its individual lipids on the structure and function of Bcl-xL[241,249-251].

In order to produce full-length Bcl-xL via Sortase A mediated ligation and study the protein caspase-cleavage in the loop, mimicked by a thrombin cut site, several new Bcl-xL-solu variants were cloned, expressed and successfully studied in this work. For this, the Sortase A motif (LPET/G) was introduced at the C-terminus of the protein through five point-mutations and the linker (to the TMH) was shortened by six amino acids. An optional thrombin cut site (LVPR/GS) was introduced between amino acid 60-67 through six point-mutations, that was either cloned into the Bcl-xLΔTM or the Bcl-xL-SOR, for subsequent full-length studies.

All three new constructs Bcl-xL-SOR, Bcl-xL-THR-SOR, Bcl-xL-THRΔTM were successfully expressed and purified. All purified variants were mainly monomeric (≥ 90 %) and showed no dimerisation behaviour, just as Bcl-xLΔTM. No functional or structural alterations were found in NMR-based Apo studies and PUMA titrations. Also the thermal stability, measured by CD-spectroscopy, did not show notable differences. Further functional liposome assay studies with Bak-solu and tBid, or isothermal titration calorimetry (ITC) experiments with PUMA-BH3 peptide did not show any significant differences in their functional properties and the binding affinity was in the same low nanomolar range (data not shown). Concordantly, all three constructs were considered as native as Bcl-xLΔTM and used as references for respective experiments and screenings throughout this work.

Vargas-Uribe *et al.*[372] demonstrated through a FRET-liposome based assay with different pH and varying lipid compositions that Bcl-xL-solu interacts with a negatively charged membrane at low (unphysiological) pH of 4-6. Furthermore, they found that Bcl-xL preferably binds to lipids or lipid surfaces with negatively charged headgroups with a minimum amount of 10 % anionic content. Higher amounts of negatively charged lipids (≥ 25 %) lead to a significant shift in the membrane surface potential and the pK_a of binding, as did also cardiolipin, which leads to a binding in the physiological range of 6.0-7.5. Cardiolipin has been shown to influence binding of tBid to the MOM and has been implicated in the pore formation of Bax and Bak and proven to be necessary for many other mitochondrial proteins as well[387,388,394,395]. Nevertheless, the study of Vargas-Uribe *et al.* was based on single cysteine variants and tracking of one single amino acid in Bcl-xL at a time, which were either residue 70, 102,110 or 175. It was found that all residues worked equally well, but 102 was preferred in their study.

To investigate the effect of the membrane and the lipid on the full-length Bcl-xL, first, the interaction of Bcl-xL solu with a variety of differently composed NDs was studied, to identify preferred lipid compositions at pH 6.5-7.0. That way, the optimal lipid-composition for subsequent nanodisc assemblies was identified for future studies. A special focus was set on screening the anionic lipid content and cardiolipin, as supported by the results of Vargas-Uribe *et al.*[372].

First, the affinity of the membrane-binding of Bcl-xLΔTM was assessed by ITC, and the formation of possible membrane-attached species was studied by DLS. The ITC data suggest that the affinity is very low and barely measurable with the chosen method. While NDs with 0 % anionic content (100 % DMPC) showed a low millimolar binding affinity only at high concentrations of both components, for 25 % anionic content (25 % DMPG and 75 % DMPC) a weak micromolar binding was measured. Contrary to the findings of Vargas-Uribe *et al.*, which showed that even higher anionic content of up to 75 % increases the membrane binding

of Bcl-xL, for the 50 % samples a weaker affinity in the high micromolar range was obtained in the ITC study. However, due to the weakness of the membrane-interaction, the results were difficult to reproduce. Binding tendencies were mainly recorded, especially when all components were concentrated to the maximum possible amount (1.5 mM NDs and 150 µM Bcl-xL).

The DLS experiments with the corresponding mixtures of the ITC ones showed no new species and no change in the ND size (4-5 nm radius, as for TMH-ND or empty ND) upon Bcl-xL addition (data not shown). The data of both methods indicate that if there is a binding, it has a very high on/off rate or the affinity is too low for a stable complex formation.

Next, an analogous FRET-assay to that of Vargas-Uribe *et al.*[372] was devised, employing fluorescence labelled 102Cys-Bcl-xL (donor) and rhodamine labelled lipids (acceptor) in differently composed NDs instead of liposomes. Additionally, the pH dependence of the membrane interaction was screened within the physiological range of 6.0-7.5 in steps of 0.5. Mixtures of AF-Bcl-xL or 5IAF-Bcl-xL with the respective NDs exhibited FRET and a corresponding donor-signal depletion, which was followed and used as the indicator for membrane binding. Unfortunately, the 5IAF dye exhibited very high signal fluctuations and a strong pH-dependence, creating errors in the range of 10-15 %, making it impractical for this assay (data not shown).

For anionic DMPG from 0-50 % and pH 6.0-7.5 no large differences or tendencies in donor depletion were seen with AF-Bcl-xL (15-20 % donor depletion), indicating weak membrane binding and no attachment of Bcl-xL to the ND-membrane. This is supported by the data obtained from the ITC measurements and the findings by Vargas-Uribe *et al.*[372], that showed a membrane interaction only at pH 5.0 for such compositions up until a 75 % anionic content. However, such low pH ranges of 4.0-5.5 are not physiologically relevant, and the aim of this study is to determine the relevant effects at native-like conditions. Interestingly, the cardiolipin content had a bigger influence on the membrane binding and samples with 5 % CL already showed a significant increase in donor depletion, where 10 % and 20 % exhibited the maximum amount. Though with AF-Bcl-xL there were some deviations within the triplicate of samples, indicated as error bars, the error was within a 3-5 % range and allowed to determine definite trends and compare results. The membrane-binding affinity data of Bcl-xL indicate that cardiolipin has a higher impact than DMPG within the pH range of 6.0-7.5. This is in good agreement with previous experiments with Bak-solu, the pro-apoptotic counterpart of Bcl-xL, where it was shown that cardiolipin enhances its membrane binding and pore formation[396].

Nevertheless, only one amino acid of Bcl-xL could be studied by this assay simultaneously, which is not very informative compared to the full soluble protein. The maximum concentration that was possible to study by fluorescence was 1 µM NDs and 50 nm Bcl-xL, which is far too low for low-affinity binding studies. The ITC findings suggest using a much higher concentration within the millimolar range for NDs, which cannot be achieved with fluorescence labelled samples, as the obtained signal would lead to a signal overflow in the detector. That could also be one reason why no membrane binding was observed with 25 or 50 % DMPG content because the used concentrations were too low to determine a trend.

The established nanodisc-based FRET-assay was applicable for a fast screening of different conditions and does not rely on isotope-labelling. The rhodamine-labelled nanodiscs can be produced in high yield and proved to be highly stable and homogenous and advantageous compared to liposomes. Theoretically, after a successful titration, the samples can be separated via SEC and the nanodiscs and/or the target protein can be recycled, which is not possible for other purely lipid-based systems like liposomes. However, only one amino acid of the target-protein can be studied. The applied concentrations cannot be used for all sorts of interactions.

In order to study the interaction of Bcl-xL solu and the respective NDs at atomic resolution for all amino acids and in sufficient concentrations for optimal binding, NMR experiments were done using 200 µM $^{2}H,^{15}N$-Bcl-xLΔTM and 300 µM ND at 950 MHz field strength. As 10-20 % cardiolipin showed the highest amount of binding in the FRET assay, 12.5 % cardiolipin was chosen for the NMR titrations, as it corresponds to 25 % DMPG by charge, since it is a double lipid with negative net charge. This allows to directly compare cardiolipin and DMPG and see if other lipid properties (e.g. headgroup) have an influence on the membrane interaction of Bcl-xL. Additionally, the membrane-binding interface of Bcl-xLΔTM was determined and its orientation and location upon PUMA binding was studied using an identical set of NDs with Gd^{3+}-DTPA-DMPE lipids (ca. 4 per leaflet).

The PRE-effect from Gd^{3+}-lipids on the labelled Bcl-xLΔTM leads to NMR signal intensity attenuation in a distance dependent matter that allowed to compare the effect amongst different types of membranes, by comparing the NMR intensities of Bcl-xL with NDs and Bcl-xL and the respective Gd^{3+}-ND counterpart. It was observed, that all measured lipid compositions of 100 % DMPC, 25 % DMPG/75 % DMPC, 50 % DMPG/50 % DMPC and 12.5 % CL/75 % DMPC show a PRE-effect in the hydrophobic BH3-binding groove in the apo state of Bcl-xL. The region of the attenuated signals and residues (mainly 105-140) is very selective and not due to random orientation, as it occurs in all samples and is mainly restricted to this region.

While 100 % DMPC showed the lowest amount of NMR signal attenuation and therefore corresponding membrane-binding, 25 % DMPG exhibited a much stronger pronounced effect. Interestingly, 12.5 % CL exhibited the strongest PRE-effect, though it has the same charge properties as 25 % DMPG. This is in good agreement with the observed FRET-data, which indicated a much stronger membrane-binding to cardiolipin containing membranes than DMPG ones. Higher amounts of anionic lipids (50 % DMPG) exhibited an almost equally strong PRE-effect as 12.5 % CL and showed that lipid-headgroup charge is at least equally important as the composition of the lipids. However, such elevated values of negative charges are not present in the mitochondrial outer membrane, to the best of our knowledge[381], and were not considered for future studies (as well as the 75 % DMPG lipid composition) and merely used as an indicator for the importance of charge on the membrane-interaction.

Upon PUMA BH3-peptide addition the PRE-effect is almost completely abrogated in the 100 % DMPC and 25 % DMPG samples, indicating a detachment of Bcl-xL from the membrane. The effect is also observable for all non-BH3 binding amino acids, which further indicates that this is not due to shielding from the Gd^{3+} by the added peptide. However, both the 12.5 % CL and 50 % DMPG sample did not exhibit such a strong effect after the addition of PUMA. Both spectra look almost identical with the same PRE-pattern, exhibiting the same membrane-binding-mode, just with slightly less overall signal intensity depletion. As with their strong membrane attachment in the apo state, both samples still exhibit an affinity or binding to the membrane even in a ligand-bound state. This means that PUMA BH3 binding induces the removal of Bcl-xL-solu from neutrally or slightly negatively charged membranes, but this effect is not potent enough to counteract the strong binding of Bcl-xL-solu to highly negatively charged membranes of more than 50 %, or membranes with high cardiolipin contents of 12.5 % respectively. This could be explained by the fact that hydrophobic interactions and electrostatic interactions keep Bcl-xL at the mitochondrial membrane *in vivo* or *in vitro*. So, once the hydrophobic pocket is filled by a ligand the hydrophobic Bcl-xL membrane-interaction is lost, which leads to a detachment from neutrally charged lipids. However, if the charge properties or head groups allow a stronger electrostatic interaction, the protein stays in its native surrounding. In contrast to suggestions, that Bcl-xL might bind to or insert into the membrane upon ligand binding, the here obtained data shows the contrary. Nevertheless, these experiments only take into account the soluble domain. Therefore, the results cannot be completely transferred to the full-length protein, where the distance to the membrane may be shorter and more constant through the membrane anchor. The additional helix, which is usually truncated for Bcl-xL studies, could also lead to a different orientation on the membrane.

Sortase A ligation of full-length Bcl-xL and study of the Fl-Bcl-xL in nanodiscs

Previously reported methods of production of full-length tail-anchored proteins and Bcl-2 proteins rely on truncation of insoluble protein anchors[258], introduction of mutations in order to solubilise the target or change its properties[304], or the addition of various fusion-tags to the native protein[299,304]. Fusion-tagged full-length tail-anchored proteins express with very low yield and need to be solubilised with harsh detergents due to their hydrophobic membrane anchor (TMH). This leads to subsequent refolding, which additionally has a very low yield of correctly folded and functional protein and is even more difficult in the presence of an insoluble TMH. Afterwards, the target tail-anchored protein needs to be reconstituted into a membrane-mimetic system, e.g. nanodiscs, for following investigations, further decreasing the final yield. As current methods for the production of such membrane proteins are hampered by those difficulties and lead to very low yields, not compatible with many structural biological methods, we established the Sortase A ligation of full-length Bcl-xL, which can be transferred to other tail-anchored proteins.

After testing the optimal conditions for a test reaction with Bcl-xL-SOR (LPETG motif) and regular MSP1D1ΔH5 (N-terminal free glycine), it was determined that at least an excess of 6 to 1 of one component (LPETG motif or the free glycine) is necessary to quantitatively drive the reaction into the direction of the full-length product. Additionally, it was found that the evolved penta-mutant Sortase A in this thesis is far too potent and reactive and therefore, a small amount of 1/20 to 1/25 with respect to the reference educts is sufficient. Decreasing the Sortase A amount, increasing the ratio of at least 6:1 of both educts and a stepwise addition of the excess educt of choice proved to enhance the ligation yield.

These optimised conditions were transferred to the production of full-length Bcl-xL from the soluble domain Bcl-xL-SOR and the corresponding Bcl-xL-TMH in CTD-MSP1D1ΔH5 NDs with 25 % DMPG and 75 % DMPC lipids. It was found that ND-TMH was the limiting factor, so Bcl-xL-SOR was chosen to be used in excess of 3-4 and added in stepwise manner with 1 equivalent at a time over the course of 60-90 min.

The successful result of the Sortase A ligation was shown with various methods, including Coomassie stained SDS-PAGE gels, ESI-MS, DLS and NMR spectroscopy. Further, the successful progression can be seen by the diminishing amount of TMH which is used up during the ligation process, while more Bcl-xL-SOR is added stepwise leading its unchanged large educt band in the SDS-PAGE gel. The subsequent purification of the product was achieved by Ni-NTA and size exclusion chromatography (SEC, S200a), that showed an increase in hydrodynamic radius, leading to an elution volume of 11.8 mL compared to the educt ND-TMH

which runs (like empty NDs) at 13.5 mL. Since the inserted transmembrane helix did not change the hydrodynamic radius and therefore the elution volume of the large NDs, it can be assumed that the soluble domain of Bcl-xL is correctly attached to the helix and located outside of the ND on its membrane surface. The ligation was further verified by ESI-MS and (DLS). The latter also shows and confirms an increase of the particle size of the final purified product, as seen in the SEC profile. Surprisingly, the SEC data provided by Yao *et al.*[393] did not show any increase in the elution volume or hydrodynamic radius of their size exclusion profile of Fl-Bcl-xL attached to a nanodisc. This is contradictory, as an attached additional protein domain would increase said radius and lead to an earlier elution volume in the SEC. Nanodiscs with large inserted or attached proteins show an increase in elution volume, compared to empty nanodiscs, as well as nanodiscs with Ni-NTA lipids that are bound to a soluble domain via His_6-tag. This shows, a correctly folded Bcl-xL-solu which is attached outside on the membrane of the protein, and not inserted into it.

Far-UV CD spectroscopy was measured to probe the secondary structure content of Fl-Bcl-xL in NDs and compare it to Bcl-xL-SOR and determine if Bcl-xL-solu was still correctly folded after its successful ligation and purification. In the CD-spectra and thermal unfolding experiments of Fl-Bcl-xL in NDs the contribution of the two copies of helical MSP1D1ΔH5 was subtracted. Both, the Bcl-xL-solu and Fl-Bcl-xL spectra show that the protein retained its helical secondary structure in presence of the membrane and after the ligation and purification protocol. Appertaining thermal unfolding experiments showed that Fl-Bcl-xL unfolds at 64 °C and is less stable at a membrane surface in the ND than in solution (80 °C). The MSP-belt typically unfolds at 85-90°C and is well separated in the CD experiments from the FL-Bcl-xL transition. The similar Bak and Bax are known to interact with membranes and to insert at high temperatures[314], which could explain the drastically lower melting point of the product. In the study of Bcl-xLΔTM it was found that the soluble domain interacts with the membrane mainly through its hydrophobic pocket. So, additional hydrophobic interactions with the lipid-surface could favour an unfolding in the presence of lipids and explain the reduction in unfolding temperature and destabilisation of the protein structure. Additionally, the same effect on the melting temperature was observed for Bak-solu in the presence of membranes[396], further corroborating a successful membrane-interaction and highlighting the importance of the membrane surrounding.

The functional properties of Fl-Bcl-xL in NDs were tested the same as for the soluble domain and the Bcl-xL-solu NMR studies, by the titration with PUMA BH3 peptide. Comparing the obtained ITC titrations and binding affinities of Bcl-xL-solu (K_D of 66 nm) and Fl-Bcl-xL in NDs (K_D of 55 nm) with PUMA BH3 shows that both are very similar and there are no differences in

the overall thermodynamic properties (ΔG, ΔH, ΔS) of both titrations. That shows that the Fl-Bcl-xL is binding competent and functional in NDs and demonstrates that both samples exhibit a similar binding mode. Interestingly, for this Bcl-xL-PUMA interaction, the membrane does not seem to alter the binding-affinity for the PUMA-BH3 peptide and play a role on both protein interactions.

Several different NMR experiments and studies with fully $^{2}H,^{15}N$-labelled Fl-Bcl-xL and segmentally labelled one (TMH or Bcl-xL-solu were labelled) were done to elucidate and determine the structure, functionality and binding mode of the protein. The results were compared with the one of Bcl-xL-solu alone, to determine differences and similarities of the soluble domains in both cases and see the effect on the structure and function of Bcl-xL-solu in the full-length protein in a membrane environment.

Firstly, the chemical shift perturbations (CSP) upon PUMA BH3 binding in both scenarios were compared which showed almost indistinguishable CSP values in the same regions of the protein, indicating that the binding mode is identical in the presence of a membrane in the full-length example. Together with the ITC and CD-spectra, this confirms that the full-length protein is properly folded in proximity to the membrane and it is in a binding-competent state. Both 2D-[$^{1}H,^{15}N$]-TROSY spectra of Fl-Bcl-xL and Bcl-xL-solu with and without PUMA show almost the same fold and comparable chemical shifts, while the ND incorporated Fl-Bcl-xL has larger and broader peaks. As for the TMH in NDs, this is due to the slower tumbling of the ND in comparison to the protein (Bcl-xL-solu) alone. However, the line-broadening effect is not very strong compared to completely integrated proteins. So, it can be assumed that Bcl-xL-solu is more mobile and outside of the ND and in membrane proximity.

Secondly, the orientation and relative distance to the membrane surface of Bcl-xL-solu in the Fl-Bcl-xL was investigated with the same setup as for the Bcl-xLΔTM membrane-interaction study. One set of TMH-ND with MSP1D1ΔH5 was prepared with or without Gd^{3+}-DTPA-DMPE and Sortase A ligated to $^{2}H,^{15}N$-Bcl-xL-SOR, producing segmentally labelled Fl-Bcl-xL. The signal intensities were analysed for both samples and referenced with non-affected amino acids, creating relative intensities which can be compared to the Gd^{3+}-free sample, analogous to the Bcl-xLΔTM nanodisc study. The obtained PRE-data show a very similar result as for the membrane interaction of the soluble domain and empty NDs. The protein is in close proximity to the membrane and orientated with the BH3 binding site towards it. This specific signal attenuation and line broadening occurs in the same region, mainly at residues 91-117 (86-100 is the BH3 domain of Bcl-xL) and 133-140 (129-148 is the BH1 domain), which together with the SEC and DLS findings indicates that the soluble-domain is loosely attached to the membrane and not inserted in it, as can be expected from biological models of Bcl-xL.

Additionally, for each segmentally labelled Fl-Bcl-xL sample (either TMH or Bcl-xL-solu labelled) 2D-[^{1}H,^{15}N]-TROSY and semi-TROSY experiments were recorded at 40 °C or 45 °C in the presence and absence of 8 mg/mL Pf1 phage to get HN residual dipolar couplings (RDCs). With this supplementary data, the structure of Bcl-xL-solu was further refined.

The experimental HN-RDCs of the soluble domain were in very good agreement with the back-calculated ones. This shows that the structure of the soluble domain of Fl-Bcl-xL in nanodiscs is not massively altered compared to the one of Bcl-xLΔTM in solution. The HN-RDCs of the TMH of Fl-Bcl-xL were used to refine the structure of the TMH further, and they also exhibited an excellent agreement between experimental and back-calculated RDCs (R=0.98, Q=0.08). However, large differences in the magnitudes of the HN-RDCs of both protein-parts were observed. While the soluble-domain exhibits values between -12 and +12 Hz, the TMH one are from -6 to +24 Hz. The observed contrast may be due to different and specific orientations of the HN bond vectors relative to the magnetic field of both protein parts, caused by their different surrounding and relative orientation to the membrane surface. This is possible, as the TMH is more rigid and entrapped by the lipids and aligning together with the nanodisc, while the soluble domain could move freely around its anchor-point. This is reflected by the high tensor eigenvalues of the TMH compared to the one of the soluble domain. Since Bcl-xL-solu is more flexible and loosely attached, it has the possibility of higher relative motion with respect to the TMH-ND, which leads to reduced alignment (tensors) and smaller HN-RDC values. In order to take this into account, two separate alignment tensors were determined to refine the full-length protein structure.

To create a 3D NMR-based model of Fl-Bcl-xL in a ND, the NOE, RDC and chemical shift data of both parts were combined. The obtained bundle has a well-defined orientation between the TMH and Bcl-xL-solu and shows that the latter is orientated with its BH3 binding-groove towards the lipid surface. The determined orientation of the soluble domain would create a higher local concentration of the binding-pocket of Bcl-xL *in vivo* and *in vitro* and simplify and facilitate interactions with Bax or Bak. With this, our 3D-model depicts Fl-Bcl-xL in its native and active state and shows how the different binding partners could interact with each other in the MOM. Interestingly, the soluble domain of the full-length protein at the membrane has a very similar fold and structure as the one observed for the truncated construct. Future studies with this system could shine a light on how Fl-Bcl-xL binds Bak/Bax and hinders their pore formation as an inhibitor and also transfer this technique to other Bcl-2 family proteins.

Overall, the established Sortase A mediated ligation method was shown to be applicable for the production of tail-anchored proteins and further for the selective labelling of membrane proteins in NDs, which greatly helps with structural characterisation.

This novel method was successfully used to determine the first NMR-based 3D-structure of membrane-anchored Fl-Bcl-xL and further show how the protein is orientated with respect to the membrane. Also, for the first time the effect of the membrane on the full-length protein structure was studied in atomic resolution. Future experiments with this method could help to determine the unknown native and membrane-inserted structures of Bcl-2 proteins, e.g. Bak.

Generally, this method could be transferred to the production of other membrane-attached or inserted proteins and used to anchor them to the membrane and further study the influence of the lipid surface on the protein structure and function. The homogeneity and quality of the obtained product is high enough for a variety of structural biological methods and ligand-based studies, as demonstrated in this work. The Sortase A enzyme, as well as its ligation are very robust and not error prone[207,397]. This method shows for the first time its application to a membrane-inserted protein and its soluble domain and should also be transferrable to similar membrane-mimetic systems, e.g. SMALPS.

One disadvantage is the need for the introduction of the LPETG motif through points mutations which could alter the structure or function of the target. Further, a long enough linker and a free N-terminal glycine is needed, that can either span the nanodisc bilayer and/or facilitate the access to the active site of the Sortase A enzyme. Proteins like Bak do not have such a long linker in its sequence, where a LPETG motif could be inserted. Adding it would enhance the distance to the membrane and possibly alter its function. In our case the motif was in the C-terminal end of Bcl-xL-Solu and did not show any influence on both and helped to successfully determine its 3D-structure and behaviour in a membrane environment.

Membrane interaction of full-length Bcl-xL and effect of PUMA binding

Since it was previously demonstrated that Bcl-xL-solu interacts with different types of lipids and the interaction is dependent on the membrane charge and composition, the effects were further elucidated for the full-length protein. So far it was determined that Fl-Bcl-xL showed a membrane interaction in the 25 % DMPG/75 % DMPC nanodiscs and was loosely attached to the membrane surface, with the BH3 binding groove pointing towards it.

Two sets of segmentally labelled (^{2}H,^{15}N-Bcl-xL-solu) full-length Bcl-xL samples with either 100 % DMPC or 12.5 % CL were studied with 2D-[^{1}H,^{15}N]-TROSY experiments and also corresponding samples with inserted Gd^{3+}-DMPE-DTPA lipids for further 2D-[^{1}H,^{15}N]-TROSY-based PRE experiments. Additionally, two samples of unlabelled Fl-Bcl-xL in the same ND compositions were prepared for small angle X-ray (SAXS) studies of the size and shape of the protein-nanodisc particle.

As previously done for the 25 % DMPG sample, it was possible to obtain Fl-Bcl-xL NMR intensity plots by comparing each Gd^{3+}-sample with the Gd^{3+}-free one for the respective membrane composition. In all three different apo samples (for all studied lipid-compositions) it was found that the soluble-domain of the full-length Bcl-xL is attached to the membrane via the same orientation. All residues of the three BH1-3 domains (86-100 are BH3, 129-148 are BH1 and 180-195 are BH2) responsible for the formation of the BH3-binding groove are strongly affected, but especially the BH1 and BH3 domain of the protein. However, while the 12.5 % CL sample showed the highest signal intensity attenuation and membrane-binding, both the 100 % DMPC and 25 % DMPG sample exhibited similar and barely distinguishable results. Therefore, it can be assumed that in all cases the full-length protein is closely attached to the membrane by its respective helix and so the PRE-effect is strong and evident in all cases, contrary to the non-attached Bcl-xLΔTM study where the protein is not membrane-anchored. In the latter case, the soluble domain is held only by weak hydrophobic and electrostatic interactions which are dependent on the membrane charge and lipid headgroup, so the lipid surface appears to have a pivotal influence. It seems that in the full-length protein, the close proximity through anchoring “forces” a membrane attachment, which can be expected from tail-anchored proteins, and differences are not so prominent for various lipids. Still, in both studies the cardiolipin sample exhibited the strongest membrane-binding and PRE-effect.

It is important to note, that the Bcl-xL-solu in the full-length protein exhibits a notable binding to the membrane with its long unstructured loop, whose function is not completely clear. It is known to be the target of several post-translational modifications, that alter and regulate the activity of Bcl-xL[327]. Our data demonstrate that it could also be important for the interaction of Bcl-xL with the membrane, which could further keep the protein at its surface and enhance its activity. Studies with the truncated loop variant of Bcl-xL, e.g. used for the determination of the Bcl-xL Bak-BH3 structure could give more insight into this matter and show if the loop is necessary for a functional full-length protein in the membrane.

Another interesting observation of the full-length protein is that the first ~25 amino acids also seem to bind to the membrane to some extend. Liposome assay studies with tBid and Bak showed that a ΔBH4 deletion variant of Bcl-xL-solu (without the first 24 amino acids) exhibited a drastically decreased anti-apoptotic activity[389]. Our findings could offer an answer to this observation, to why the BH4 deletion reduces the function of Bcl-xL in presence of a membrane. Without it, the protein could be less attached and easier to remove from the membrane-surface. Also, full-length deletion variants could offer more insight into this matter.

The effect of PUMA BH3 peptide on the membrane location of full-length Bcl-xL was also investigated in all three membrane composition cases. Compared to the Bcl-xLΔTM titrations where the addition of PUMA almost completely removed Bcl-xL-solu from the membrane except in the 12.5 % CL case, for the full-length protein all three samples seemed to be still membrane-attached after binding of the ligand. It was found that residues 100-120 and the BH1 domain (129-148) are less affected by PRE upon PUMA binding, which can be explained by a light detachment or tilt of the soluble-domain away from the membrane surface. The flexible loop of all three samples (around the region 50-70) is still more prominently affected and seems to be in membrane proximity. Nevertheless, the loop is not involved in the PUMA binding and seems to play only a small regulatory role in this specific BH3-ligand affinity[317]. In the PUMA-bound state, the cardiolipin sample is an exception as it shows (apart from the BH1 domain) still strongly affected residues and a membrane-attachment even after PUMA addition. This can be explained by the fact that this specific PUMA-bound sample was also used for different types of measurements beforehand and showed slight degradation and unfolding before this 2D-[^{1}H,^{15}N]-TROSY measurement. Both events can lead to a membrane-binding and distortion of the obtained PRE-data. Therefore, this sample was marked with an asterisk and excluded from deeper analysis and comparison, as it could only serve for an estimation.

Additionally, the effect of the membrane-composition and the effect of PUMA BH3-binding on the stability of the protein was studied via far UV-Vis CD. Surprisingly, both Fl-Bcl-xL in either 100 % DMPC or 12.5 % CL exhibited almost the same melting point between 64-65 °C as seen for the full-length study in 25 % DMPG. Moreover, the addition of PUMA BH3 had no influence on the stability and thermal unfolding of the 100 % DMPC protein sample and just a slight increase on the 12.5 % one. This is in contrast to the observation that PUMA increases the thermal unfolding temperature of Bcl-xL-solu drastically by 5-7 °C and stabilises its structure. It seems that binding to the membrane surface leads to a strong destabilisation of Bcl-xL, or it favours its insertion at elevated temperatures.

SAXS measurements of the respective unlabelled apo Fl-Bcl-xL in either 100 % DMPC or 12.5 % CL nanodiscs showed that the DMPC sample exhibits a larger maximal radius and a higher per distance distribution versus radius (pvr). This indicates that the apo form of the soluble domain is less membrane-attached and further away from the membrane, which enlarges the particle radius. This was also observed in the PRE-experiments beforehand, where it was found that Bcl-xL binds stronger to cardiolipin-containing membranes in the apo form.

The same effect is also present in the PUMA bound state in both SAXS samples, but it is less pronounced. Compared to their apo state, both samples show a slight increase in size upon PUMA binding, corresponding to a detachment of the membrane surface as depicted in Figure 57. This is in good agreement with the previously determined PRE-data and the screening with the soluble domain only.

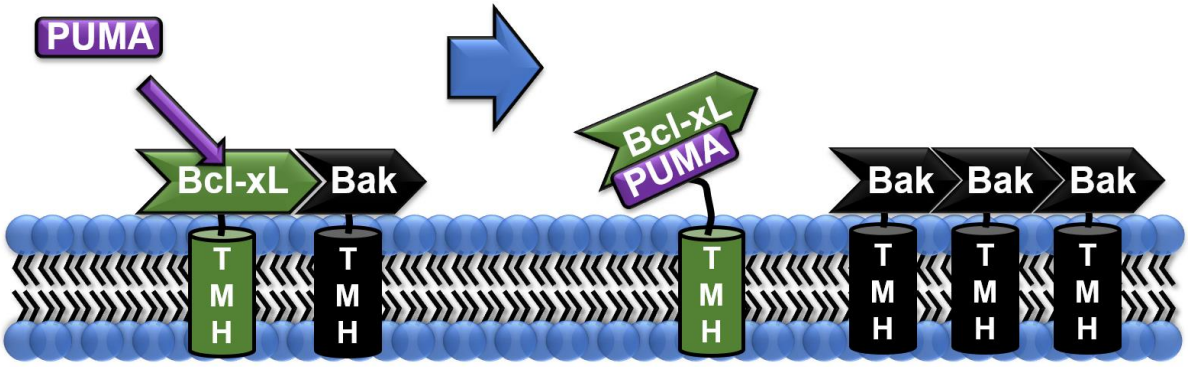

Figure 57: Depiction of the PUMA-BH3 (lilac) effect on the Bcl-xL (green) location and anti-apoptotic activity within its native membrane surrounding. PUMA binding occupies the BH3-groove and leads to structural changes within the Bcl-xL. Additionally, the soluble-domain of Bcl-xL is removed from the membrane surface and is now more loosely-attached. Both effects lead to a release of Bak and an inhibition of its anti-apoptotic function.

Overall, through NMR- and SAXS-based experiments it was observed that for the full-length membrane-anchored protein the membrane-composition plays a role on the location of Bcl-xL-solu. This effect was also observed for the single soluble domain of Bcl-xL before, but there the differences were more pronounced. This can be explained by the TMH-anchoring, which brings the soluble domain in close proximity to the lipid surface, where it can attach itself through hydrophobic interaction with its BH3 binding groove. The degree of interaction and attachment was higher for cardiolipin-containing lipid surfaces and much stronger for the apo state of the protein in all screened lipid compositions. While the addition of PUMA leads to an almost complete detachment of the membrane for the soluble domain, in the full-length protein this effect was on a lower scale and comparable to a tilt or light detachment of the soluble domain from the membrane (Figure 57). *In vivo*, such an effect would lead to a removal from the MOM and its inserted Bax or Bak proteins, which could lead to a severe reduction in the local concentration of Bcl-xL and a reduction of its cell-protective function. To the best of our knowledge, this study offers for the first time an insight into the mechanism involved in BH3-partner protein binding and its effect on the structure and location in Bcl-xL. Future studies with this system and Bcl-xL or Bak/Bax could reveal further interactions in the full-length scale and clarify the mechanisms behind their interactions.

Effect of caspase-like cut on Bcl-xL protein structure and function

The final outcome of the caspase cut in the flexible loop of Bcl-xL is known, which is an increased MOMP and cell death[325,327]. Unsurprisingly, the resulting ΔN-Bcl-xL was linked to pro-apoptotic stress and, amongst others, to neuronal cell death[329,330,332]. It is still controversial what happens to Bcl-xL after the cut and if the protein switches roles and becomes pro-apoptotic itself, or if the mechanism for the increased apoptosis is different. It is further thought that a possible pro-apoptotic Bcl-xL could also form pores, analogous to Bak or Bax.

In Bcl-xL-solu a new thrombin cut site was introduced at the caspase cleavage site (61-62) in the flexible loop and it was found, that the caspase-like thrombin cut strongly destabilises the structure and fold of Bcl-xL. This was determined by far-UV-Vis thermal unfolding measurements that showed that the thermal unfolding temperature of Bcl-xL of 76 °C drops to 65 °C upon cleavage. While binding of PUMA BH3 peptide increases the thermal unfolding temperature of Bcl-xL by 9 °C, the one of the cut protein rises by 12 °C (to 77.5 °C), which is in the same range as the uncut-apo or PUMA bound form. Therefore, it can be assumed that the cut protein is still able to function and bind BH3-peptides, which largely stabilises it to a similar level like its native form. This is not surprising, as the loop has been shown to have only a small effect on the protein function[297]. Removing it in Bcl-xL even increases the binding affinities for partner proteins. That means, that the cut does not completely abrogate the binding to other BH3 peptides.

2D-[^{1}H,^{15}N]-TROSY experiments did not show a large difference between the cut and uncut protein, except for the appearance of a new C- and N-terminus and small chemical shifts in the cut loop region. The most affected residues are in the proximity of the cut site, but also in the BH1 and BH3 region. This points out that the cut leads to a movement within these domains and that the protein structure is slightly distorted. That could also be one explanation, why the cut in the loop destabilises the whole protein and leads to a large drop in the thermal unfolding temperature of Bcl-xL.

The spectra of the BH3-bound form (Bak-BH3) are also very similar to the one of the uncut protein. So, it can be assumed that both BH3-bound Bcl-xL forms are similar in fold and binding behaviour and more interestingly, that the cut protein is functional.
The NMR and CD data show that BH3-peptide binding might induce a change in the structural conformation of cut Bcl-xL and revert it back to its native-like BH3-bound form. This model is supported by the drastic increase in melting temperature of the protein and by the highly similar NMR-spectrum to uncut BH3-bound Bcl-xL.

To see if the cleavage of Bcl-xL makes the protein pro-apoptotic and induces a pore formation or membrane insertion, cut Bcl-xL-solu was studied in the presence of nanodiscs. No significant changes were found in cut or uncut protein, apart from the membrane interaction observed in the previous study. Binding of Bcl-xL through its C-terminal His_6-tag to a nanodisc containing Ni^{2+}-DGS-NTA lipids did not show an insertion or a different behaviour upon cleavage at the membrane. Addition of either PUMA or Bak BH3-peptide showed the expected BH3-bound spectrum and no different behaviour in the presence of nanodiscs or a membrane.

To test and compare the biological function of Bcl-xL-solu and the cleaved one, a pore-forming liposome assay was done together with Bak-solu and tBid. It was found that the reference (data not shown) Bcl-xL alone or cut Bcl-xL do not form pores. As expected, Bcl-xL hinders the pore formation of Bak alone or Bak and tBid as shown in[242]. However, cut Bcl-xL interacts with Bak and tBid (or Bak alone) and also hinders their pore formation, but only for about 90 min. Afterwards, pore formation was detected, which was on a smaller scale than the one without Bcl-xL. This indicates an altered and deficient (but not abrogated) Bcl-xL-Bak-tBid interplay. Due to the 90 min lag-phase, it can be assumed that Bcl-xL is displaced or replaced in its formed protein-protein complex with either Bak or tBid, as depicted in Figure 58 and 59. Together with the NMR data, this demonstrates that cut Bcl-xL does not form pores or integrate itself into the membrane upon cleavage and is thereby not pro-apoptotic. However, its ability to form stable complexes with other pro-apoptotic proteins and to hinder pore formation is strongly reduced or impaired. This would attribute a role of Bcl-xL repression mechanism to the cleavage-site in the flexible loop. This has already been shown for other known post-translational modifications in the loop of Bcl-xL, which impair and weaken its affinities for pro-apoptotic proteins[327].

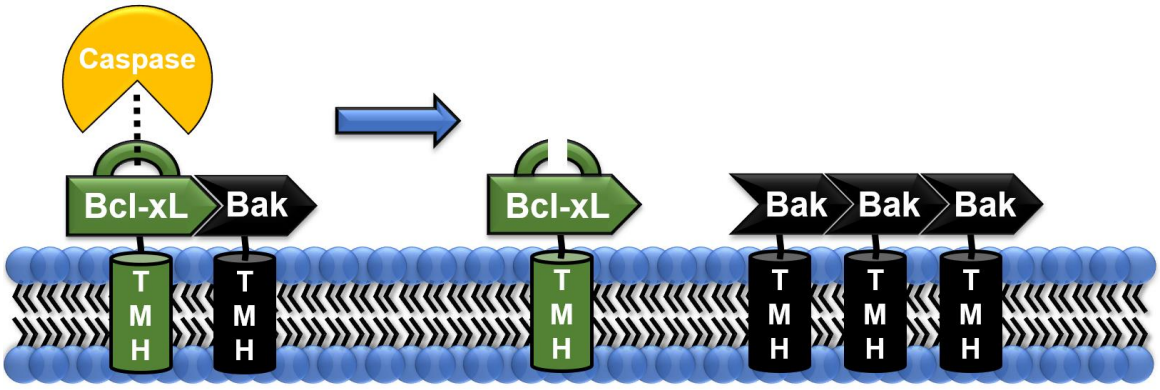

Figure 58: Depiction of the proposed effect of the caspase cut in the flexible loop of Bcl-xL (green) on its interaction with Bak (black). Cutting the loop leads to a slow release or insufficient binding of Bak, that then forms pores in the liposomes. Due to the forced binding of Bak to Ni-NTA-lipids the inactive Bak can also form pores. It is still under debate if inactive Bak leads to pore formation on its own.

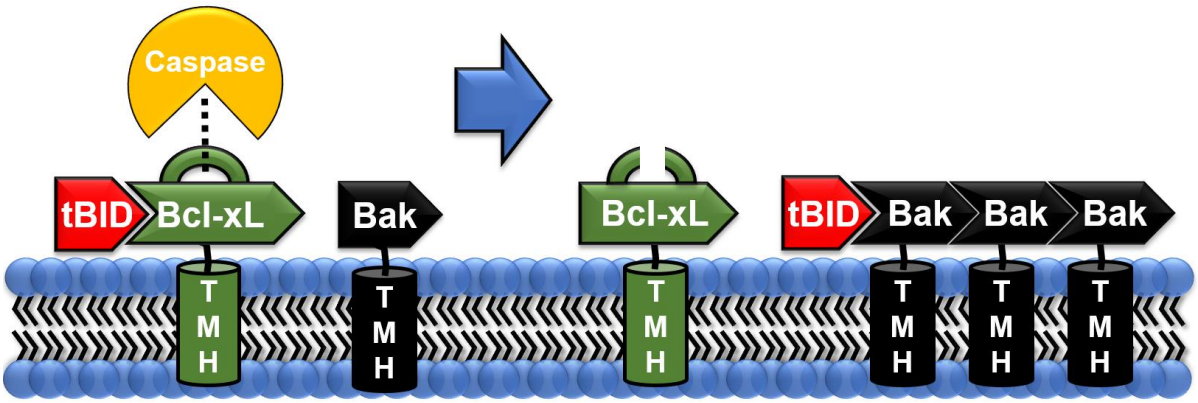

Figure 59: Depiction of the proposed effect of the caspase cut in the flexible loop of Bcl-xL (green) on its interaction with previously sequestered tBID (red) and inactive Bak (black). Cutting the loop leads to a slow release or insufficient binding of tBID which then activates Bak, leading to pore formation.

Our findings support the theory, that Bcl-xL does not become pro-apoptotic upon caspase cleavage, but its binding to Bak/tBid is impaired, leading to a significant loss in anti-apoptotic function. Future studies of Fl-Bcl-xL cut/uncut with Bak and tBid could shine a light on the detailed mechanism behind it and possibly, how to impair the function of Bcl-xL and mimic this caspase effect. This could then further pose a possible and susceptible mechanism for drug targeting, once more details are known.

Full-length Bcl-xL expression and production through Asna1/Get3 co-expression

The yeast chaperon Get3 and its human analogue Asna1 are known to specifically target tail-anchored (TA) proteins to the ER membrane[182-184,186,192]. The insertion mechanism of Asna1/Get3 and its target were studied regarding membrane-protein complex dependency. It was found that both the target protein and Asna1/Get3 can be co-expressed in a small scale, and they form stable and soluble complexes. In tests experiments, it was demonstrated that in the presence of other acceptor proteins, the target can be inserted *in vitro* into isolated native membranes.

However, trypsin treatment of the isolated membranes leads to abrogation of Asna1 insertion, which shows that acceptor proteins are necessary[183]. Also, for Get3, it has been found that Get4 and other partner-proteins are necessary for successful insertion of the TA target[189,193]. Since both protein systems (Asna1 and Get3) are known to bind specifically to tail-anchored proteins and keep them in solution, both are suitable chaperons for the (co) expression of such.

In this work, Asna1 or Get3 have been tested and established as such co-expression systems for tail-anchored proteins on Fl-Bcl-xL. The expression tests show a successful production of both separate proteins (Asna1-MBP or Get3-MBP fusion proteins) and Z-tag-Fl-Bcl-xL, that form a stable complex in *E. coli*. A straightforward and fast one-step Ni-NTA purification yielded the soluble protein-complex in high yield without losing product in insoluble inclusion bodies. The overall protein production and final sample yield is extremely high and even rivals that of Bcl-xL-solu. With this method the correctly folded and soluble Fl-Bcl-xL was accessed for the first time in high yield.

The separation of Asna1 or Get3 from its target Fl-Bcl-xL was successful with several different mild detergents, where CHAPS, Brij58 and DDM performed the best. This offers the possibility to produce and study Fl-Bcl-xL in a mild detergent without the need of inclusion-body purification and prior refolding with harsh detergents that would destroy the functionality and fold of Bcl-xL.

Subsequently, a reconstitution of Fl-Bcl-xL from DDM, CHAPS or Brij58 to MSP1D1ΔH5 nanodisc was tried with a biobeads or dialysis supported method. A subsequent Ni-NTA did not yield Bcl-xL-ND and the reconstitution was not possible with 100 % DMPC or 25 % DMPG and 75 % DMPC. Future studies could take into account different lipid compositions or different MSP-constructs, which were tested and identified in this work.

Additionally, it was screened if it is possible to insert Fl-Bcl-xL into pre-formed empty nanodiscs of said compositions directly, by switching Get3 or Asna1 into an open conformation with the addition of Mg^{2+} and ATP/ADP. As demonstrated in the study of Gristick *et al.*[189] and Kuboto *et al.*[193] it seems that even with ATP/ADP and Mg^{2+} Get3 or Asna1 are not able to release and insert their target into an artificial membrane which is lacking their partner proteins. Longer incubation or elevated temperatures did not help the process also in our case. Unfortunately, high amounts of detergent (to help the release) cannot be used in this case, as they would disassemble the nanodiscs. However, it could be possible to reconstitute the Fl-Bcl-xL from detergent into lipids/liposomes firstly and then assemble nanodiscs with the mixture. In case that future studies do not lead to successful insertion of Fl-Bcl-xL into nanodiscs, the Sortase A method can be used and the Get3/Asna1 co-expression for obtaining high amounts of Fl-Bcl-xL for other (mild) detergent-based studies. Kale *et al.*[383] have successfully demonstrated that Bcl-2 proteins are functional in mild detergents (CHAPS) and may be used, for example, for fluorescence-based methods. This method would offer a mild alternative for the production and reconstitution of Fl-Bcl-xL in mild detergents.

Overall, the here established Get3/Asna1-mediated co-expression method for the production of tail-anchored proteins was successfully established. A quick Ni-NTA purification yields the stable and soluble Get3/Asna1-Fl-Bcl-xL complex, which can also be directly separated by mild detergents and ATP/Mg^{2+}. For Fl-Bcl-xL, it was not possible to reconstitute the protein into nanodiscs and study the obtained product from this method and compare it to the Sortase A-mediated ligation one.

However, this co-expression method was further successfully established in our laboratory for the production of also toxic or hardly accessible helices or tail-anchored proteins, as an addition to the GB1-based expression that did not work in the Fl-Bcl-xL case. Furthermore, with this method it was possible to reconstitute several different types of proteins into nanodiscs. Future studies will determine if this is also possible for full-length Bcl-xL or other Bcl-2 proteins and could offer an alternative to the Sortase A mediated ligation, without altering the sequence of the protein.

5 References

1 Bernstein, F. C. *et al.* The protein data bank: A computer-based archival file for macromolecular structures. *Journal of Molecular Biology* **112**, 535-542 (1977).

2 Fox, N. K., Brenner, S. E. & Chandonia, J. M. SCOPe: Structural Classification of Proteins--extended, integrating SCOP and ASTRAL data and classification of new structures. *Nucleic Acids Res* **42**, D304-309 (2014).

3 Orengo, C. A. *et al.* CATH – a hierarchic classification of protein domain structures. *Structure* **5**, 1093-1109 (1997).

4 Murzin, A. G., Brenner, S. E., Hubbard, T. & Chothia, C. SCOP: a structural classification of proteins database for the investigation of sequences and structures. *J Mol Biol* **247**, 536-540 (1995).

5 Holm, L., Ouzounis, C., Sander, C., Tuparev, G. & Vriend, G. A database of protein structure families with common folding motifs. *Protein Sci* **1**, 1691-1698 (1992).

6 Yeagle, P. L. The Membranes of Cells (Third Edition). **10**, 219-269 (2016).

7 Bill, R. M. *et al.* Overcoming barriers to membrane protein structure determination. *Nat Biotechnol* **29**, 335-340 (2011).

8 Stillwell, W. An Introduction to Biological Membranes, Composition, Structure and Function (Second Edition). **6**, 89-110 (2016).

9 White, S. H. Biophysical dissection of membrane proteins. *Nature* **459**, 344-346 (2009).

10 Shen, H. H., Lithgow, T. & Martin, L. Reconstitution of membrane proteins into model membranes: seeking better ways to retain protein activities. *Int J Mol Sci* **14**, 1589-1607 (2013).

11 Rawlings, A. E. Membrane proteins: always an insoluble problem? *Biochem Soc Trans* **44**, 790-795 (2016).

12 Almen, M. S., Nordstrom, K. J., Fredriksson, R. & Schioth, H. B. Mapping the human membrane proteome: a majority of the human membrane proteins can be classified according to function and evolutionary origin. *BMC Biol* **7**, 50 (2009).

13 Krogh, A., Larsson, B., von Heijne, G. & Sonnhammer, E. L. Predicting transmembrane protein topology with a hidden Markov model: application to complete genomes. *J Mol Biol* **305**, 567-580 (2001).

14 Uhlen, M. *et al.* Proteomics. Tissue-based map of the human proteome. *Science* **347**, 1260419 (2015).

15 Luckey, M. Membrane Structural Biology With Biochemical and Biophysical Foundations (Second Edition). 1 (2014).

16 Deisenhofer, J., Epp, O., Miki, K., Huber, R. & Michel, H. Structure of the protein subunits in the photosynthetic reaction centre of Rhodopseudomonas viridis at 3Å resolution. *Nature* **318**, 618-624 (1985).

17 Henderson, R. *et al.* Model for the structure of bacteriorhodopsin based on high-resolution electron cryo-microscopy. *Journal of Molecular Biology* **213**, 899-929 (1990).

18 Caterina, M. J. *et al.* The capsaicin receptor: a heat-activated ion channel in the pain pathway. *Nature* **389**, 816-824 (1997).

19 McKemy, D. D., Neuhausser, W. M. & Julius, D. Identification of a cold receptor reveals a general role for TRP channels in thermosensation. *Nature* **416**, 52-58 (2002).

20 Kaupp, U. B. Olfactory signalling in vertebrates and insects: differences and commonalities. *Nat Rev Neurosci* **11**, 188-200 (2010).

21 Julius, D. & Basbaum, A. I. Molecular mechanisms of nociception. *Nature* **413**, 203-210 (2001).

22 Overington, J. P., Al-Lazikani, B. & Hopkins, A. L. How many drug targets are there? *Nat Rev Drug Discov* **5**, 993-996 (2006).

23 Yin, H. & Flynn, A. D. Drugging Membrane Protein Interactions. *Annu Rev Biomed Eng* **18**, 51-76 (2016).

24 Snyder, J. C. *et al.* A rapid and affordable screening platform for membrane protein trafficking. *BMC Biol* **13**, 107 (2015).

25 Macarron, R. *et al.* Impact of high-throughput screening in biomedical research. *Nat Rev Drug Discov* **10**, 188-195 (2011).

26 Arkin, M. R. & Wells, J. A. Small-molecule inhibitors of protein-protein interactions: progressing towards the dream. *Nat Rev Drug Discov* **3**, 301-317 (2004).

27 Wells, J. A. & McClendon, C. L. Reaching for high-hanging fruit in drug discovery at protein-protein interfaces. *Nature* **450**, 1001-1009 (2007).

28 Marsh, D., Horvath, L. I., Swamy, M. J., Mantripragada, S. & Kleinschmidt, J. H. Interaction of membrane-spanning proteins with peripheral and lipid-anchored membrane proteins: perspectives from protein-lipid interactions (Review). *Mol Membr Biol* **19**, 247-255 (2002).

29 Garber, E. A. E. & Margoliash, E. Interaction of cytochrome c with cytochrome c oxidase: An understanding of the high- to low-affinity transition. *Biochimica et Biophysica Acta (BBA) - Bioenergetics* **1015**, 279-287 (1990).

30 Jiang, X. & Wang, X. Cytochrome C-mediated apoptosis. *Annu Rev Biochem* **73**, 87-106 (2004).

31 Yang, J. Prevention of Apoptosis by Bcl-2: Release of Cytochrome c from Mitochondria Blocked. *Science* **275**, 1129-1132 (1997).

32 Liu, X., Kim, C. N., Yang, J., Jemmerson, R. & Wang, X. Induction of Apoptotic Program in Cell-Free Extracts: Requirement for dATP and Cytochrome c. *Cell* **86**, 147-157 (1996).

33 Mayor, S. & Riezman, H. Sorting GPI-anchored proteins. *Nat Rev Mol Cell Biol* **5**, 110-120 (2004).

34 Blobel, G. Intracellular protein topogenesis. *Proc Natl Acad Sci U S A* **77**, 1496-1500 (1980).

35 Entova, S., Billod, J. M., Swiecicki, J. M., Martin-Santamaria, S. & Imperiali, B. Insights into the key determinants of membrane protein topology enable the identification of new monotopic folds. *Elife* **7** (2018).

36 Allen, K. N., Entova, S., Ray, L. C. & Imperiali, B. Monotopic Membrane Proteins Join the Fold. *Trends Biochem Sci* **44**, 7-20 (2019).

37 Rojas-Rivera, D. & Hetz, C. TMBIM protein family: ancestral regulators of cell death. *Oncogene* **34**, 269-280 (2015).

38 Adams, J. M. & Cory, S. The Bcl-2 protein family: arbiters of cell survival. *Science* **281**, 1322-1326 (1998).

39 Vaux, D. L., Cory, S. & Adams, J. M. Bcl-2 gene promotes haemopoietic cell survival and cooperates with c-myc to immortalize pre-B cells. *Nature* **335**, 440-442 (1988).

40 Youle, R. J. & Strasser, A. The BCL-2 protein family: opposing activities that mediate cell death. *Nat Rev Mol Cell Biol* **9**, 47-59 (2008).

41 Goodman, K. M. *et al.* Molecular basis of sidekick-mediated cell-cell adhesion and specificity. *Elife* **5** (2016).

42 Tang, H. *et al.* Architecture of cell-cell adhesion mediated by sidekicks. *Proc Natl Acad Sci U S A* **115**, 9246-9251 (2018).

43 Prossnitz, E. R. & Barton, M. The G-protein-coupled estrogen receptor GPER in health and disease. *Nat Rev Endocrinol* **7**, 715-726 (2011).

44 Warne, T. *et al.* Structure of a beta1-adrenergic G-protein-coupled receptor. *Nature* **454**, 486-491 (2008).

45 Duy, D., Soll, J. & Philippar, K. Solute channels of the outer membrane: from bacteria to chloroplasts. *Biol Chem* **388**, 879-889 (2007).

46 Kojima, S. & Nikaido, H. Permeation rates of penicillins indicate that Escherichia coli porins function principally as nonspecific channels. *Proc Natl Acad Sci U S A* **110**, E2629-2634 (2013).

47 Husted, A. S., Trauelsen, M., Rudenko, O., Hjorth, S. A. & Schwartz, T. W. GPCR-Mediated Signaling of Metabolites. *Cell Metab* **25**, 777-796 (2017).

48 Apetoh, L. *et al.* Toll-like receptor 4-dependent contribution of the immune system to anticancer chemotherapy and radiotherapy. *Nat Med* **13**, 1050-1059 (2007).

49 O'Neill, L. A., Golenbock, D. & Bowie, A. G. The history of Toll-like receptors - redefining innate immunity. *Nat Rev Immunol* **13**, 453-460 (2013).

50 Buchanan, S. β-Barrel proteins from bacterial outer membranes: structure, function and refolding. *Current Opinion in Structural Biology* **9**, 455-461 (1999).

51 Schulz, G. E. β-Barrel membrane proteins. *Current Opinion in Structural Biology* **10**, 443-447 (2000).

52 Vinothkumar, K. R. & Henderson, R. Structures of membrane proteins. *Q Rev Biophys* **43**, 65-158 (2010).

53 Henderson, R. & Unwin, P. N. T. Three-dimensional model of purple membrane obtained by electron microscopy. *Nature* **257**, 28-32 (1975).

54 Rosenbaum, D. M. *et al.* GPCR engineering yields high-resolution structural insights into beta2-adrenergic receptor function. *Science* **318**, 1266-1273 (2007).

55 Hauser, A. S., Attwood, M. M., Rask-Andersen, M., Schioth, H. B. & Gloriam, D. E. Trends in GPCR drug discovery: new agents, targets and indications. *Nat Rev Drug Discov* **16**, 829-842 (2017).

56 Wall, M. A. *et al.* The structure of the G protein heterotrimer Gi alpha 1 beta 1 gamma 2. *Cell* **83**, 1047-1058 (1995).

57 Linder, M. E. *et al.* Lipid modifications of G proteins: alpha subunits are palmitoylated. *Proc Natl Acad Sci U S A* **90**, 3675-3679 (1993).

58 Wedegaertner, P. B., Wilson, P. T. & Bourne, H. R. Lipid modifications of trimeric G proteins. *J Biol Chem* **270**, 503-506 (1995).

59 Faller, M., Niederweis, M. & Schulz, G. E. The structure of a mycobacterial outer-membrane channel. *Science* **303**, 1189-1192 (2004).

60 Trias, J., Jarlier, V. & Benz, R. Porins in the cell wall of mycobacteria. *Science* **258**, 1479-1481 (1992).

61 Schleiff, E. *et al.* Prediction of the plant beta-barrel proteome: a case study of the chloroplast outer envelope. *Protein Sci* **12**, 748-759 (2003).

62 Misra, R. Assembly of the beta-Barrel Outer Membrane Proteins in Gram-Negative Bacteria, Mitochondria, and Chloroplasts. *ISRN Mol Biol* **2012**, 708203 (2012).

63 Fairman, J. W., Noinaj, N. & Buchanan, S. K. The structural biology of beta-barrel membrane proteins: a summary of recent reports. *Curr Opin Struct Biol* **21**, 523-531 (2011).

64 Cavalier-Smith, T. The Simultaneous Symbiotic Origin of Mitochondria, Chloroplasts, and Microbodies. *Annals of the New York Academy of Sciences* **503**, 55-71 (1987).

65 Martin, W. & Herrmann, R. G. Gene transfer from organelles to the nucleus: how much, what happens, and Why? *Plant Physiol* **118**, 9-17 (1998).

66 Gray, M. W. Mitochondrial Evolution. *Science* **283**, 1476-1481 (1999).

67 Schwartz, W. Lynn Margulis, Origin of Eukaryotic Cells. Evidence and Research Implications for a Theory of the Origin and Evolution of Microbial, Plant, and Animal Cells on the Precambrian Earth. XXII u. 349 S., 89 Abb., 49 Tab. New Haven-London 1970: Yale University. *Zeitschrift für allgemeine Mikrobiologie* **13**, 186-186 (2007).

68 Bishop, R. E. Structural biology of membrane-intrinsic beta-barrel enzymes: sentinels of the bacterial outer membrane. *Biochim Biophys Acta* **1778**, 1881-1896 (2008).

69 Cowan, S. W. *et al.* Crystal structures explain functional properties of two E. coli porins. *Nature* **358**, 727-733 (1992).

70 Schirmer, T., Keller, T., Wang, Y., Jurg P. Rosenbusch. Structural Basis for Sugar Translocation Through Maltoporin Channels at 3.1 A Resolution. *Science* **267**, 512-514 (1995).

71 Nakae, T. Identification of the outer membrane protein of E.coli that produces transmembrane channels in reconstituted vesicle membranes. *Biochemical and Biophysical Research Communications* **71**, 877-884 (1976).

72 Carolyn M. Ott, V. R. L. Integral membrane protein biosynthesis: why topology is hard to predict. *Journal of Cell Science* **115**, 2003-2009 (2002).

73 Midgett, C. R. & Madden, D. R. Breaking the bottleneck: eukaryotic membrane protein expression for high-resolution structural studies. *J Struct Biol* **160**, 265-274 (2007).

74 Tate, C. G. Practical considerations of membrane protein instability during purification and crystallisation. *Methods Mol Biol* **601**, 187-203 (2010).

75 Sachs, J. N. & Engelman, D. M. Introduction to the membrane protein reviews: the interplay of structure, dynamics, and environment in membrane protein function. *Annu Rev Biochem* **75**, 707-712 (2006).

76 Singer, S. J. & Nicolson, G. L. The fluid mosaic model of the structure of cell membranes. *Science* **175**, 720-731 (1972).

77 Engelman, D. M. Membranes are more mosaic than fluid. *Nature* **438**, 578-580 (2005).

78 Aceti, D. J. *et al.* Expression platforms for producing eukaryotic proteins: a comparison of E. coli cell-based and wheat germ cell-free synthesis, affinity and solubility tags, and cloning strategies. *J Struct Funct Genomics* **16**, 67-80 (2015).

79 Drew, D., Lerch, M., Kunji, E., Slotboom, D. J. & de Gier, J. W. Optimization of membrane protein overexpression and purification using GFP fusions. *Nat Methods* **3**, 303-313 (2006).

80 Miroux, B. & Walker, J. E. Over-production of proteins in Escherichia coli: mutant hosts that allow synthesis of some membrane proteins and globular proteins at high levels. *J Mol Biol* **260**, 289-298 (1996).

81 Grisshammer, R. & Tate, C. G. Overexpression of integral membrane proteins for structural studies. *Q Rev Biophys* **28**, 315-422 (1995).

82 Hockney, R. C. Recent developments in heterologous protein production in Escherichia coli. *Trends in Biotechnology* **12**, 456-463 (1994).

83 Hartmann, L., Kugler, V. & Wagner, R. Expression of Eukaryotic Membrane Proteins in Pichia pastoris. *Methods Mol Biol* **1432**, 143-162 (2016).

84 Brooks, C. L., Morrison, M. & Joanne Lemieux, M. Rapid expression screening of eukaryotic membrane proteins in Pichia pastoris. *Protein Sci* **22**, 425-433 (2013).

85 Trometer, C. & Falson, P. Mammalian membrane protein expression in baculovirus-infected insect cells. *Methods Mol Biol* **601**, 105-117 (2010).

86 Civjan, N. R., Bayburt, T. H., Schuler, M. A. & Sligar, S. G. Direct solubilization of heterologously expressed membrane proteins by incorporation into nanoscale lipid bilayers. *Biotechniques* **35**, 556-560, 562-553 (2003).

87 Thomas, J. A. & Tate, C. G. Quality control in eukaryotic membrane protein overproduction. *J Mol Biol* **426**, 4139-4154 (2014).

88 Andrell, J. & Tate, C. G. Overexpression of membrane proteins in mammalian cells for structural studies. *Mol Membr Biol* **30**, 52-63 (2013).

89 Henrich, E., Dotsch, V. & Bernhard, F. Screening for lipid requirements of membrane proteins by combining cell-free expression with nanodiscs. *Methods Enzymol* **556**, 351-369 (2015).

90 Noireaux, V., Bar-Ziv, R. & Libchaber, A. Principles of cell-free genetic circuit assembly. *Proc Natl Acad Sci U S A* **100**, 12672-12677 (2003).

91 Madin, K., Sawasaki, T., Ogasawara, T. & Endo, Y. A highly efficient and robust cell-free protein synthesis system prepared from wheat embryos: plants apparently contain a suicide system directed at ribosomes. *Proc Natl Acad Sci U S A* **97**, 559-564 (2000).

92 Spirin, A. S., Baranov, V. I., Ryabova, L. A., Ovodov, S. Y. & Alakhov, Y. B. A continuous cell-free translation system capable of producing polypeptides in high yield. *Science* **242**, 1162-1164 (1988).

93 Shi, T., Zhang, L., Li, Z., Newton, I. P. & Zhang, Q. Expression, purification and renaturation of truncated human integrin beta1 from inclusion bodies of Escherichia coli. *Protein Expr Purif* **107**, 13-19 (2015).

94 Wingfield, P. T., Palmer, I. & Liang, S. M. Folding and Purification of Insoluble (Inclusion Body) Proteins from Escherichia coli. *Curr Protoc Protein Sci* **78**, 6 5 1-30 (2014).

95 Hammarstrom, M., Woestenenk, E. A., Hellgren, N., Hard, T. & Berglund, H. Effect of N-terminal solubility enhancing fusion proteins on yield of purified target protein. *J Struct Funct Genomics* **7**, 1-14 (2006).

96 Huth, J. R. *et al.* Design of an expression system for detecting folded protein domains and mapping macromolecular interactions by NMR. *Protein Sci* **6**, 2359-2364 (1997).

97 Garavito, R. M. & Ferguson-Miller, S. Detergents as tools in membrane biochemistry. *J Biol Chem* **276**, 32403-32406 (2001).

98 Lee, S. C. *et al.* A method for detergent-free isolation of membrane proteins in their local lipid environment. *Nat Protoc* **11**, 1149-1162 (2016).

99 Prive, G. G. Detergents for the stabilization and crystallization of membrane proteins. *Methods* **41**, 388-397 (2007).

100 Hanson, M. A. *et al.* A specific cholesterol binding site is established by the 2.8 A structure of the human beta2-adrenergic receptor. *Structure* **16**, 897-905 (2008).

101 Matz, C., A. Jonas. Micellar complexes of human apolipoprotein A-I with phosphatidyl cholines and cholesterol prepared from cholate lipid dispersions. *J. Biol. Chem.* **257**, 4535-4540 (1982).

102 Gao, Y., Cao, E., Julius, D. & Cheng, Y. TRPV1 structures in nanodiscs reveal mechanisms of ligand and lipid action. *Nature* **534**, 347-351 (2016).

103 Heo, W. D. *et al.* PI(3,4,5)P3 and PI(4,5)P2 lipids target proteins with polybasic clusters to the plasma membrane. *Science* **314**, 1458-1461 (2006).

104 Bjorkholm, P. *et al.* Identification of novel sphingolipid-binding motifs in mammalian membrane proteins. *Biochim Biophys Acta* **1838**, 2066-2070 (2014).

105 Gupta, K. *et al.* The role of interfacial lipids in stabilizing membrane protein oligomers. *Nature* **541**, 421-424 (2017).

106 Park, M. J. *et al.* SH2 Domains Serve as Lipid-Binding Modules for pTyr-Signaling Proteins. *Mol Cell* **62**, 7-20 (2016).

107 Wu, W., Shi, X. & Xu, C. Regulation of T cell signalling by membrane lipids. *Nat Rev Immunol* **16**, 690-701 (2016).

108 Seddon, A. M., Curnow, P. & Booth, P. J. Membrane proteins, lipids and detergents: not just a soap opera. *Biochim Biophys Acta* **1666**, 105-117 (2004).

109 Linke, D. Detergents: An Overview. *Methods in Enzymology* **463**, 604-616 (2009).

110 Tanford, C. & Reynolds, J. A. Characterization of membrane proteins in detergent solutions. *Biochimica et Biophysica Acta (BBA) - Reviews on Biomembranes* **457**, 133-170 (1976).

111 Makino, S., Reynolds, J. A. & Tanford, C. The binding of deoxycholate and Triton X-100 to proteins. *J Biol Chem* **248**, 4926-4932 (1973).

112 Helenius, A. & Simons, K. Solubilization of membranes by detergents. *Biochimica et Biophysica Acta (BBA) - Reviews on Biomembranes* **415**, 29-79 (1975).

113 Helenius, A., McCaslin, D. R., Fries, E. & Tanford, C. Properties of detergents. *Methods Enzymol* **56**, 734-749 (1979).

114 Kessi, J. *et al.* Short-chain phosphatidylcholines as superior detergents in solubilizing membrane proteins and preserving biological activity. *Biochemistry* **33**, 10825-10836 (1994).

115 le Maire, M., Champeil, P. & Møller, J. V. Interaction of membrane proteins and lipids with solubilizing detergents. *Biochimica et Biophysica Acta (BBA) - Biomembranes* **1508**, 86-111 (2000).

116 Hjertén, S., Sparrman, M. & Liao, J.-l. Purification of membrane proteins in SDS and subsequent renaturation. *Biochimica et Biophysica Acta (BBA) - Biomembranes* **939**, 476-484 (1988).

117 Hjelmeland, L. M., Nebert, D. W. & Osborne, J. C. Sulfobetaine derivatives of bile acids: Nondenaturing surfactants for membrane biochemistry. *Analytical Biochemistry* **130**, 72-82 (1983).

118 Lee, S. Y., Lee, A., Chen, J. & MacKinnon, R. Structure of the KvAP voltage-dependent K+ channel and its dependence on the lipid membrane. *Proc Natl Acad Sci U S A* **102**, 15441-15446 (2005).

119 Guan, L., Smirnova, I. N., Verner, G., Nagamori, S. & Kaback, H. R. Manipulating phospholipids for crystallization of a membrane transport protein. *Proc Natl Acad Sci U S A* **103**, 1723-1726 (2006).

120 Hiller, S. *et al.* Solution structure of the integral human membrane protein VDAC-1 in detergent micelles. *Science* **321**, 1206-1210 (2008).

121 Ujwal, R. & Bowie, J. U. Crystallizing membrane proteins using lipidic bicelles. *Methods* **55**, 337-341 (2011).

122 De Angelis, A. A. & Opella, S. J. Bicelle samples for solid-state NMR of membrane proteins. *Nat Protoc* **2**, 2332-2338 (2007).

123 Durr, U. H., Gildenberg, M. & Ramamoorthy, A. The magic of bicelles lights up membrane protein structure. *Chem Rev* **112**, 6054-6074 (2012).

124 Laursen, T. *et al.* Characterization of a dynamic metabolon producing the defense compound dhurrin in sorghum. *Science* **354**, 890-893 (2016).

125 Denisov, I. G., McLean, M. A., Shaw, A. W., Grinkova, Y. V. & Sligar, S. G. Thermotropic phase transition in soluble nanoscale lipid bilayers. *J Phys Chem B* **109**, 15580-15588 (2005).

126 Caffrey, M. A lipid's eye view of membrane protein crystallization in mesophases. *Current Opinion in Structural Biology* **10**, 486-497 (2000).

127 Landau, E. M. & Rosenbusch, J. P. Lipidic cubic phases: a novel concept for the crystallization of membrane proteins. *Proc Natl Acad Sci U S A* **93**, 14532-14535 (1996).

128 Parmar, M. *et al.* Using a SMALP platform to determine a sub-nm single particle cryo-EM membrane protein structure. *Biochim Biophys Acta Biomembr* **1860**, 378-383 (2018).

129 Oluwole, A. O. *et al.* Formation of Lipid-Bilayer Nanodiscs by Diisobutylene/Maleic Acid (DIBMA) Copolymer. *Langmuir* **33**, 14378-14388 (2017).

130 Ravula, T., Ramadugu, S. K., Di Mauro, G. & Ramamoorthy, A. Bioinspired, Size-Tunable Self-Assembly of Polymer-Lipid Bilayer Nanodiscs. *Angew Chem Int Ed Engl* **56**, 11466-11470 (2017).

131 Yasuhara, K. *et al.* Spontaneous Lipid Nanodisc Fomation by Amphiphilic Polymethacrylate Copolymers. *J Am Chem Soc* **139**, 18657-18663 (2017).

132 Breyton, C., Pucci, B. & Popot, J. L. Amphipols and fluorinated surfactants: Two alternatives to detergents for studying membrane proteins in vitro. *Methods Mol Biol* **601**, 219-245 (2010).

133 Popot, J. L. Amphipols, nanodiscs, and fluorinated surfactants: three nonconventional approaches to studying membrane proteins in aqueous solutions. *Annu Rev Biochem* **79**, 737-775 (2010).

134 Zhong, Z., Yan, J. & Zhao, Y. Cholic acid-derived facial amphiphiles with different ionic characteristics. *Langmuir* **21**, 6235-6239 (2005).

135 Chae, P. S. *et al.* Maltose-neopentyl glycol (MNG) amphiphiles for solubilization, stabilization and crystallization of membrane proteins. *Nat Methods* **7**, 1003-1008 (2010).

136 Tribet, C., Audebert, R. & Popot, J. L. Amphipols: polymers that keep membrane proteins soluble in aqueous solutions. *Proc Natl Acad Sci U S A* **93**, 15047-15050 (1996).

137 Chien, C. H. *et al.* An Adaptable Phospholipid Membrane Mimetic System for Solution NMR Studies of Membrane Proteins. *J Am Chem Soc* **139**, 14829-14832 (2017).

138 Flayhan, A. *et al.* Saposin Lipid Nanoparticles: A Highly Versatile and Modular Tool for Membrane Protein Research. *Structure* **26**, 345-355 e345 (2018).

139 Popovic, K., Holyoake, J., Pomes, R. & Prive, G. G. Structure of saposin A lipoprotein discs. *Proc Natl Acad Sci U S A* **109**, 2908-2912 (2012).

140 Bayburt, T. H., Grinkova, Y. V. & Sligar, S. G. Self-Assembly of Discoidal Phospholipid Bilayer Nanoparticles with Membrane Scaffold Proteins. *Nano Letters* **2**, 853-856 (2002).

141 Jonas, A. Reconstitution of high-density lipoproteins. *Methods in Enzymology* **128**, 553-582 (1986).

142 Jonas, A., J. H. Wald, K. L. H. Toohill, E. S. Krul, K. Kezdy. Apolipoprotein A-1 structure and lipid properties in homogeneous, recombinant spherical and discoidal high-density lipoproteins. *J. Biol. Chem.* **265**, 22123-22129 (1990).

143 Jonas, A., K. Kezdy, J. H. Wald. Defined apolipoprotein A-I conformations in reconstituted high density lipoprotein discs. *J. Biol. Chem.* **264**, 4818-4824 (1989).

144 Denisov, I. G., Grinkova, Y. V., Lazarides, A. A. & Sligar, S. G. Directed self-assembly of monodisperse phospholipid bilayer Nanodiscs with controlled size. *J Am Chem Soc* **126**, 3477-3487 (2004).

145 Wlodawer A, S. J., Chung BH, Chiovetti R Jr, Weinstein JN. High-density lipoprotein recombinants: evidence for a bicycle tire micelle structure obtained by neutron scattering and electron microscopy. *FEBS Letters* **104**, 231–235 (1979).

146 Li, Y., Kijac, A. Z., Sligar, S. G. & Rienstra, C. M. Structural analysis of nanoscale self-assembled discoidal lipid bilayers by solid-state NMR spectroscopy. *Biophys J* **91**, 3819-3828 (2006).

147 Shih, A. Y., Denisov, I. G., Phillips, J. C., Sligar, S. G. & Schulten, K. Molecular dynamics simulations of discoidal bilayers assembled from truncated human lipoproteins. *Biophys J* **88**, 548-556 (2005).

148 Kontush, A. C., J. M. High-Density Lipoproteins: Structure, Metabolism, Function, and Therapeutics. *Wiley & Sons: Hoboken NJ* (2012).

149 Kontush, A. *et al.* Structure of HDL: particle subclasses and molecular components. *Handb Exp Pharmacol* **224**, 3-51 (2015).

150 Carlson, J. W., Jonas, A. & Sligar, S. G. Imaging and manipulation of high-density lipoproteins. *Biophysical Journal* **73**, 1184-1189 (1997).

151 Wald, J. H., Coormaghtigh, E., De Meutter, J., Ruysschaert, J. M. & Jonas, A. Investigation of the lipid domains and apolipoprotein orientation in reconstituted high density lipoproteins by fluorescence and IR methods. *J Biol Chem* **265**, 20044-20050 (1990).

152 Bayburt, T. H., Carlson, J. W. & Sligar, S. G. Reconstitution and imaging of a membrane protein in a nanometer-size phospholipid bilayer. *J Struct Biol* **123**, 37-44 (1998).

153 Joseph W. Carlson, T. B., Stephen G. Sligar. Nanopatterning Phospholipid Bilayers. *Langmuir* **16**, 3927-3931 (2000).

154 Grinkova, Y. V., Denisov, I. G. & Sligar, S. G. Engineering extended membrane scaffold proteins for self-assembly of soluble nanoscale lipid bilayers. *Protein Eng Des Sel* **23**, 843-848 (2010).

155 Rogers, D. P. *et al.* Truncation of the amino terminus of human apolipoprotein A-I substantially alters only the lipid-free conformation. *Biochemistry* **36**, 288-300 (1997).

156 Pourmousa, M. *et al.* Tertiary structure of apolipoprotein A-I in nascent high-density lipoproteins. *Proc Natl Acad Sci U S A* **115**, 5163-5168 (2018).

157 Bibow, S. *et al.* Solution structure of discoidal high-density lipoprotein particles with a shortened apolipoprotein A-I. *Nat Struct Mol Biol* **24**, 187-193 (2017).

158 Hagn, F., Etzkorn, M., Raschle, T. & Wagner, G. Optimized phospholipid bilayer nanodiscs facilitate high-resolution structure determination of membrane proteins. *J Am Chem Soc* **135**, 1919-1925 (2013).

159 Mei, X. & Atkinson, D. Crystal structure of C-terminal truncated apolipoprotein A-I reveals the assembly of high density lipoprotein (HDL) by dimerization. *J Biol Chem* **286**, 38570-38582 (2011).

160 Bayburt, T. H. & Sligar, S. G. Self-assembly of single integral membrane proteins into soluble nanoscale phospholipid bilayers. *Protein Sci* **12**, 2476-2481 (2003).

161 Bayburt, T. H., Grinkova, Y. V. & Sligar, S. G. Assembly of single bacteriorhodopsin trimers in bilayer nanodiscs. *Arch Biochem Biophys* **450**, 215-222 (2006).

162 Cheetham, P. S. J. Removal of Triton X-100 from aqueous solution using amberlite XAD-2. *Analytical Biochemistry* **92**, 447-452 (1979).

163 Denisov, I. G., Schuler, M. A. & Sligar, S. G. Nanodiscs as a New Tool to Examine Lipid-Protein Interactions. *Methods Mol Biol* **2003**, 645-671 (2019).

164 Denisov, I. G. & Sligar, S. G. Nanodiscs in Membrane Biochemistry and Biophysics. *Chem Rev* **117**, 4669-4713 (2017).

165 Nasr, M. L. *et al.* Covalently circularized nanodiscs for studying membrane proteins and viral entry. *Nat Methods* **14**, 49-52 (2017).

166 Miehling, J., Goricanec, D. & Hagn, F. A Split-Intein-Based Method for the Efficient Production of Circularized Nanodiscs for Structural Studies of Membrane Proteins. *Chembiochem* **19**, 1927-1933 (2018).

167 Ly, S. *et al.* Quantifying interactions of a membrane protein embedded in a lipid nanodisc using fluorescence correlation spectroscopy. *Biophys J* **106**, L05-08 (2014).

168 Ye, X., McLean, M. A. & Sligar, S. G. Conformational equilibrium of talin is regulated by anionic lipids. *Biochim Biophys Acta* **1858**, 1833-1840 (2016).

169 Autzen, H. E. *et al.* Structure of the human TRPM4 ion channel in a lipid nanodisc. *Science* **359**, 228-232 (2018).

170 Efremov, R. G., Gatsogiannis, C. & Raunser, S. Lipid Nanodiscs as a Tool for High-Resolution Structure Determination of Membrane Proteins by Single-Particle Cryo-EM. *Methods Enzymol* **594**, 1-30 (2017).

171 Marty, M. T., Das, A. & Sligar, S. G. Ultra-thin layer MALDI mass spectrometry of membrane proteins in nanodiscs. *Anal Bioanal Chem* **402**, 721-729 (2012).

172 Rouck, J. E., Krapf, J. E., Roy, J., Huff, H. C. & Das, A. Recent advances in nanodisc technology for membrane protein studies (2012-2017). *FEBS Lett* **591**, 2057-2088 (2017).

173 Hagn, F., Nasr, M. L. & Wagner, G. Assembly of phospholipid nanodiscs of controlled size for structural studies of membrane proteins by NMR. *Nat Protoc* **13**, 79-98 (2018).

174 https://www.sigmaaldrich.com/catalog/product/sigma/msp14?lang=en&region=US. (2019).

175 Josts, I. *et al.* Conformational States of ABC Transporter MsbA in a Lipid Environment Investigated by Small-Angle Scattering Using Stealth Carrier Nanodiscs. *Structure* **26**, 1072-1079 e1074 (2018).

176 Maric, S. *et al.* Stealth carriers for low-resolution structure determination of membrane proteins in solution. *Acta Crystallogr D Biol Crystallogr* **70**, 317-328 (2014).

177 Dang, S. *et al.* Cryo-EM structures of the TMEM16A calcium-activated chloride channel. *Nature* **552**, 426-429 (2017).

178 Marcink, T. C. *et al.* MT1-MMP Binds Membranes by Opposite Tips of Its beta Propeller to Position It for Pericellular Proteolysis. *Structure* **27**, 281-292 e286 (2019).

179 Beilharz, T., Egan, B., Silver, P. A., Hofmann, K. & Lithgow, T. Bipartite signals mediate subcellular targeting of tail-anchored membrane proteins in Saccharomyces cerevisiae. *J Biol Chem* **278**, 8219-8223 (2003).

180 Borgese, N., Brambillasca, S. & Colombo, S. How tails guide tail-anchored proteins to their destinations. *Curr Opin Cell Biol* **19**, 368-375 (2007).

181 Mateja, A. *et al.* The structural basis of tail-anchored membrane protein recognition by Get3. *Nature* **461**, 361-366 (2009).

182 Farkas, A., De Laurentiis, E. I. & Schwappach, B. The natural history of Get3-like chaperones. *Traffic* **20**, 311-324 (2019).

183 Favaloro, V., Vilardi, F., Schlecht, R., Mayer, M. P. & Dobberstein, B. Asna1/TRC40-mediated membrane insertion of tail-anchored proteins. *J Cell Sci* **123**, 1522-1530 (2010).

184 Favaloro, V., Spasic, M., Schwappach, B. & Dobberstein, B. Distinct targeting pathways for the membrane insertion of tail-anchored (TA) proteins. *J Cell Sci* **121**, 1832-1840 (2008).

185 Stefanovic, S. & Hegde, R. S. Identification of a targeting factor for posttranslational membrane protein insertion into the ER. *Cell* **128**, 1147-1159 (2007).

186 Schuldiner, M. *et al.* The GET complex mediates insertion of tail-anchored proteins into the ER membrane. *Cell* **134**, 634-645 (2008).

187 Suloway, C. J., Chartron, J. W., Zaslaver, M. & Clemons, W. M., Jr. Model for eukaryotic tail-anchored protein binding based on the structure of Get3. *Proc Natl Acad Sci U S A* **106**, 14849-14854 (2009).

188 Mateja, A. *et al.* Structure of the Get3 targeting factor in complex with its membrane protein cargo. *Science* **347**, 1152-1155 (2015).

189 Gristick, H. B. *et al.* Crystal structure of ATP-bound Get3-Get4-Get5 complex reveals regulation of Get3 by Get4. *Nat Struct Mol Biol* **21**, 437-442 (2014).

190 Chang, Y. W. *et al.* Interaction surface and topology of Get3-Get4-Get5 protein complex, involved in targeting tail-anchored proteins to endoplasmic reticulum. *J Biol Chem* **287**, 4783-4789 (2012).

191 Wang, F., Chan, C., Weir, N. R. & Denic, V. The Get1/2 transmembrane complex is an endoplasmic-reticulum membrane protein insertase. *Nature* **512**, 441-444 (2014).

192 Powis, K. *et al.* Get3 is a holdase chaperone and moves to deposition sites for aggregated proteins when membrane targeting is blocked. *J Cell Sci* **126**, 473-483 (2013).

193 Kubota, K., Yamagata, A., Sato, Y., Goto-Ito, S. & Fukai, S. Get1 stabilizes an open dimer conformation of get3 ATPase by binding two distinct interfaces. *J Mol Biol* **422**, 366-375 (2012).

194 Bozkurt, G. *et al.* Structural insights into tail-anchored protein binding and membrane insertion by Get3. *Proc Natl Acad Sci U S A* **106**, 21131-21136 (2009).

195 Suree, N. *et al.* The structure of the Staphylococcus aureus sortase-substrate complex reveals how the universally conserved LPXTG sorting signal is recognized. *J Biol Chem* **284**, 24465-24477 (2009).

196 Race, P. R. *et al.* Crystal structure of Streptococcus pyogenes sortase A: implications for sortase mechanism. *J Biol Chem* **284**, 6924-6933 (2009).

197 Mazmanian, S. K., Liu, G., Ton-That, H. & Schneewind, O. Staphylococcus aureus sortase, an enzyme that anchors surface proteins to the cell wall. *Science* **285**, 760-763 (1999).

198 Pishesha, N., Ingram, J. R. & Ploegh, H. L. Sortase A: A Model for Transpeptidation and Its Biological Applications. *Annu Rev Cell Dev Biol* **34**, 163-188 (2018).

199 Cascioferro, S., Totsika, M. & Schillaci, D. Sortase A: an ideal target for anti-virulence drug development. *Microb Pathog* **77**, 105-112 (2014).

200 Zhang, J. *et al.* Antiinfective therapy with a small molecule inhibitor of Staphylococcus aureus sortase. *Proc Natl Acad Sci U S A* **111**, 13517-13522 (2014).

201 Ilangovan, U., Ton-That, H., Iwahara, J., Schneewind, O. & Clubb, R. T. Structure of sortase, the transpeptidase that anchors proteins to the cell wall of Staphylococcus aureus. *Proc Natl Acad Sci U S A* **98**, 6056-6061 (2001).

202 Chen, J. L. *et al.* 3D Structure Determination of an Unstable Transient Enzyme Intermediate by Paramagnetic NMR Spectroscopy. *Angew Chem Int Ed Engl* **55**, 13744-13748 (2016).

203 Chen, I., Dorr, B. M. & Liu, D. R. A general strategy for the evolution of bond-forming enzymes using yeast display. *Proc Natl Acad Sci U S A* **108**, 11399-11404 (2011).

204 Guimaraes, C. P. *et al.* Site-specific C-terminal and internal loop labeling of proteins using sortase-mediated reactions. *Nat Protoc* **8**, 1787-1799 (2013).

205 Witte, M. D. *et al.* Site-specific protein modification using immobilized sortase in batch and continuous-flow systems. *Nat Protoc* **10**, 508-516 (2015).

206 Policarpo, R. L. *et al.* Flow-based enzymatic ligation by sortase A. *Angew Chem Int Ed Engl* **53**, 9203-9208 (2014).

207 Dai, X., Böker, A. & Glebe, U. Broadening the scope of sortagging. *RSC Advances* **9**, 4700-4721 (2019).

208 Theile, C. S. *et al.* Site-specific N-terminal labeling of proteins using sortase-mediated reactions. *Nat Protoc* **8**, 1800-1807 (2013).

209 Ugur, I. *et al.* Ca2+ binding induced sequential allosteric activation of sortase A: An example for ion-triggered conformational selection. *PLoS One* **13**, e0205057 (2018).

210 Antos, J. M. *et al.* Site-Specific Protein Labeling via Sortase-Mediated Transpeptidation. *Curr Protoc Protein Sci* **89**, 15 13 11-15 13 19 (2017).

211 Antos, J. M., Truttmann, M. C. & Ploegh, H. L. Recent advances in sortase-catalyzed ligation methodology. *Curr Opin Struct Biol* **38**, 111-118 (2016).

212 Antos, J. M. *et al.* Site-specific N- and C-terminal labeling of a single polypeptide using sortases of different specificity. *J Am Chem Soc* **131**, 10800-10801 (2009).

213 Petrache, A. I., Machin, D. C., Williamson, D. J., Webb, M. E. & Beales, P. A. Sortase-mediated labelling of lipid nanodiscs for cellular tracing. *Mol Biosyst* **12**, 1760-1763 (2016).

214 Freiburger, L. *et al.* Efficient segmental isotope labeling of multi-domain proteins using Sortase A. *J Biomol NMR* **63**, 1-8 (2015).

215 Dorr, B. M., Ham, H. O., An, C., Chaikof, E. L. & Liu, D. R. Reprogramming the specificity of sortase enzymes. *Proc Natl Acad Sci U S A* **111**, 13343-13348 (2014).

216 Jeong, H. J., Abhiraman, G. C., Story, C. M., Ingram, J. R. & Dougan, S. K. Generation of Ca2+-independent sortase A mutants with enhanced activity for protein and cell surface labeling. *PLoS One* **12**, e0189068 (2017).

217 Hirakawa, H., Ishikawa, S. & Nagamune, T. Ca2+ -independent sortase-A exhibits high selective protein ligation activity in the cytoplasm of Escherichia coli. *Biotechnol J* **10**, 1487-1492 (2015).

218 Hirakawa, H., Ishikawa, S. & Nagamune, T. Design of Ca2+-independent Staphylococcus aureus sortase A mutants. *Biotechnol Bioeng* **109**, 2955-2961 (2012).

219 David Row, R., Roark, T. J., Philip, M. C., Perkins, L. L. & Antos, J. M. Enhancing the efficiency of sortase-mediated ligations through nickel-peptide complex formation. *Chem Commun (Camb)* **51**, 12548-12551 (2015).

220 Thornberry, N. A. & Lazebnik, Y. Caspases: enemies within. *Science* **281**, 1312-1316 (1998).

221 Green, D. R. & Reed, J. C. Mitochondria and apoptosis. *Science* **281**, 1309-1312 (1998).

222 Kerr, J. F., Wyllie, A. H. & Currie, A. R. Apoptosis: a basic biological phenomenon with wide-ranging implications in tissue kinetics. *Br J Cancer* **26**, 239-257 (1972).

223 Evan, G. & Littlewood, T. A matter of life and cell death. *Science* **281**, 1317-1322 (1998).

224 Ashkenazi, A. & Dixit, V. M. Apoptosis control by death and decoy receptors. *Current Opinion in Cell Biology* **11**, 255-260 (1999).

225 Hotchkiss, R. S., Strasser, A., McDunn, J. E. & Swanson, P. E. Cell death. *N Engl J Med* **361**, 1570-1583 (2009).

226 Rech de Laval, V., Deleage, G., Aouacheria, A. & Combet, C. BCL2DB: database of BCL-2 family members and BH3-only proteins. *Database (Oxford)* **2014**, bau013 (2014).

227 Kale, J., Osterlund, E. J. & Andrews, D. W. BCL-2 family proteins: changing partners in the dance towards death. *Cell Death Differ* **25**, 65-80 (2018).

228 Tsujimoto, Y. & Croce, C. M. Analysis of the structure, transcripts, and protein products of bcl-2, the gene involved in human follicular lymphoma. *Proc Natl Acad Sci U S A* **83**, 5214-5218 (1986).

229 Cleary, M. L., Smith, S. D. & Sklar, J. Cloning and structural analysis of cDNAs for bcl-2 and a hybrid bcl-2/immunoglobulin transcript resulting from the t(14;18) translocation. *Cell* **47**, 19-28 (1986).

230 Brett, D., Pospisil, H., Valcarcel, J., Reich, J. & Bork, P. Alternative splicing and genome complexity. *Nat Genet* **30**, 29-30 (2002).

231 Wattenberg, B., Lithgow, T. Targeting of C-Terminal (Tail)-Anchored Proteins: Understanding how Cytoplasmic Activities are Anchored to Intracellular Membranes. *Traffic* **2**, 66-71 (2001).

232 Letai, A. *et al.* Distinct BH3 domains either sensitize or activate mitochondrial apoptosis, serving as prototype cancer therapeutics. *Cancer Cell* **2**, 183-192 (2002).

233 Huang, D. C. S. & Strasser, A. BH3-Only Proteins—Essential Initiators of Apoptotic Cell Death. *Cell* **103**, 839-842 (2000).

234 Moldoveanu, T., Follis, A. V., Kriwacki, R. W. & Green, D. R. Many players in BCL-2 family affairs. *Trends Biochem Sci* **39**, 101-111 (2014).

235 Tait, S. W. & Green, D. R. Mitochondria and cell death: outer membrane permeabilization and beyond. *Nat Rev Mol Cell Biol* **11**, 621-632 (2010).

236 Zha, H., Aime-Sempe, C., Sato, T. & Reed, J. C. Proapoptotic protein Bax heterodimerizes with Bcl-2 and homodimerizes with Bax via a novel domain (BH3) distinct from BH1 and BH2. *J Biol Chem* **271**, 7440-7444 (1996).

237 Wei, M. C. *et al.* Proapoptotic BAX and BAK: a requisite gateway to mitochondrial dysfunction and death. *Science* **292**, 727-730 (2001).

238 Gross, A. & Katz, S. G. Non-apoptotic functions of BCL-2 family proteins. *Cell Death Differ* **24**, 1348-1358 (2017).

239 Li, K. *et al.* Cytochrome c Deficiency Causes Embryonic Lethality and Attenuates Stress-Induced Apoptosis. *Cell* **101**, 389-399 (2000).

240 Willis, S. N. *et al.* Apoptosis initiated when BH3 ligands engage multiple Bcl-2 homologs, not Bax or Bak. *Science* **315**, 856-859 (2007).

241 Shamas-Din, A. *et al.* tBid undergoes multiple conformational changes at the membrane required for Bax activation. *J Biol Chem* **288**, 22111-22127 (2013).

242 Lovell, J. F. *et al.* Membrane binding by tBid initiates an ordered series of events culminating in membrane permeabilization by Bax. *Cell* **135**, 1074-1084 (2008).

243 Dewson, G. *et al.* To trigger apoptosis, Bak exposes its BH3 domain and homodimerizes via BH3:groove interactions. *Mol Cell* **30**, 369-380 (2008).

244 Moldoveanu, T. *et al.* BID-induced structural changes in BAK promote apoptosis. *Nat Struct Mol Biol* **20**, 589-597 (2013).

245 Sarosiek, K. A. *et al.* BID preferentially activates BAK while BIM preferentially activates BAX, affecting chemotherapy response. *Mol Cell* **51**, 751-765 (2013).

246 Kim, H. *et al.* Stepwise activation of BAX and BAK by tBID, BIM, and PUMA initiates mitochondrial apoptosis. *Mol Cell* **36**, 487-499 (2009).

247 Petros, A. M., Olejniczak, E. T. & Fesik, S. W. Structural biology of the Bcl-2 family of proteins. *Biochim Biophys Acta* **1644**, 83-94 (2004).

248 Chi, X., Kale, J., Leber, B. & Andrews, D. W. Regulating cell death at, on, and in membranes. *Biochim Biophys Acta* **1843**, 2100-2113 (2014).

249 Vasquez Montes, V. & Ladokhin, A. S. Lipid Modulation of the Activator-Independent Membrane Insertion and Refolding of the Apoptotic Inhibitor Bcl-xL. *Biophysical Journal* **116** (2019).

250 Pecot, J. *et al.* Tight Sequestration of BH3 Proteins by BCL-xL at Subcellular Membranes Contributes to Apoptotic Resistance. *Cell Rep* **17**, 3347-3358 (2016).

251 Leber, B., Lin, J. & Andrews, D. W. Still embedded together binding to membranes regulates Bcl-2 protein interactions. *Oncogene* **29**, 5221-5230 (2010).

252 Correia, C. *et al.* Emerging understanding of Bcl-2 biology: Implications for neoplastic progression and treatment. *Biochim Biophys Acta* **1853**, 1658-1671 (2015).

253 Bakhshi, A. *et al.* Cloning the chromosomal breakpoint of t(14;18) human lymphomas: clustering around Jh on chromosome 14 and near a transcriptional unit on 18. *Cell* **41**, 899-906 (1985).

254 Cleary, M. L. & Sklar, J. Nucleotide sequence of a t(14;18) chromosomal breakpoint in follicular lymphoma and demonstration of a breakpoint-cluster region near a transcriptionally active locus on chromosome 18. *Proc Natl Acad Sci U S A* **82**, 7439-7443 (1985).

255 Galteland, E. *et al.* Translocation t(14;18) and gain of chromosome 18/BCL2: effects on BCL2 expression and apoptosis in B-cell non-Hodgkin's lymphomas. *Leukemia* **19**, 2313-2323 (2005).

256 Boise, L. H. *et al.* bcl-x, a bcl-2-related gene that functions as a dominant regulator of apoptotic cell death. *Cell* **74**, 597-608 (1993).

257 Petros, A. M. *et al.* Solution structure of the antiapoptotic protein bcl-2. *Proc Natl Acad Sci U S A* **98**, 3012-3017 (2001).

258 Muchmore, S. W. *et al.* X-ray and NMR structure of human Bcl-xL, an inhibitor of programmed cell death. *Nature* **381**, 335-341 (1996).

259 Chao, D. T. *et al.* Bcl-XL and Bcl-2 repress a common pathway of cell death. *J Exp Med* **182**, 821-828 (1995).

260 Ban, J., Eckhart, L., Weninger, W., Mildner, M. & Tschachler, E. Identification of a human cDNA encoding a novel Bcl-x isoform. *Biochem Biophys Res Commun* **248**, 147-152 (1998).

261 Luna-Vargas, M. P. & Chipuk, J. E. The deadly landscape of pro-apoptotic BCL-2 proteins in the outer mitochondrial membrane. *FEBS J* **283**, 2676-2689 (2016).

262 Chipuk, J. E., Moldoveanu, T., Llambi, F., Parsons, M. J. & Green, D. R. The BCL-2 family reunion. *Mol Cell* **37**, 299-310 (2010).

263 Lee, E. F. & Fairlie, W. D. The Structural Biology of Bcl-xL. *Int J Mol Sci* **20** (2019).

264 Suzuki, M., Youle, R. J. & Tjandra, N. Structure of Bax. *Cell* **103**, 645-654 (2000).

265 Denisov, A. Y. *et al.* Solution structure of human BCL-w: modulation of ligand binding by the C-terminal helix. *J Biol Chem* **278**, 21124-21128 (2003).

266 Hinds, M. G. *et al.* The structure of Bcl-w reveals a role for the C-terminal residues in modulating biological activity. *EMBO J* **22**, 1497-1507 (2003).

267 Fiebig, A. A., Zhu, W., Hollerbach, C., Leber, B. & Andrews, D. W. Bcl-XL is qualitatively different from and ten times more effective than Bcl-2 when expressed in a breast cancer cell line. *BMC Cancer* **6**, 213 (2006).

268 Srivastava, R. K., Mi, Q. S., Hardwick, J. M. & Longo, D. L. Deletion of the loop region of Bcl-2 completely blocks paclitaxel-induced apoptosis. *Proc Natl Acad Sci U S A* **96**, 3775-3780 (1999).

269 Willis, S. N. *et al.* Proapoptotic Bak is sequestered by Mcl-1 and Bcl-xL, but not Bcl-2, until displaced by BH3-only proteins. *Genes Dev* **19**, 1294-1305 (2005).

270 Dunne, P. D. *et al.* Bcl-xL as a poor prognostic biomarker and predictor of response to adjuvant chemotherapy specifically in BRAF-mutant stage II and III colon cancer. *Oncotarget* **9**, 13834-13847 (2018).

271 Yoshimine, S. *et al.* Prognostic significance of Bcl-xL expression and efficacy of Bcl-xL targeting therapy in urothelial carcinoma. *Br J Cancer* **108**, 2312-2320 (2013).

272 Olopade O. I., A. M. O., Safa A. R., Hagos F, Mick R, Thompson C. B., Recant W. M. Overexpression of BCL-x protein in primary breast cancer is associated with high tumor grade and nodal metastases. *Cancer J. Sci. Am.* **3**, 230-237 (1997).

273 Lessene, G., Czabotar, P. E. & Colman, P. M. BCL-2 family antagonists for cancer therapy. *Nat Rev Drug Discov* **7**, 989-1000 (2008).

274 Choi, S. *et al.* Bcl-xL promotes metastasis independent of its anti-apoptotic activity. *Nat Commun* **7**, 10384 (2016).

275 Leber, B., Geng, F., Kale, J. & Andrews, D. W. Drugs targeting Bcl-2 family members as an emerging strategy in cancer. *Expert Rev Mol Med* **12**, e28 (2010).

276 Lee, E. F. *et al.* BCL-XL and MCL-1 are the key BCL-2 family proteins in melanoma cell survival. *Cell Death Dis* **10**, 342 (2019).

277 Yin, X. M., Oltvai, Z. N. & Korsmeyer, S. J. BH1 and BH2 domains of Bcl-2 are required for inhibition of apoptosis and heterodimerization with Bax. *Nature* **369**, 321-323 (1994).

278 Kozopas, K. M., Yang, T., Buchan, H. L., Zhou, P. & Craig, R. W. MCL1, a gene expressed in programmed myeloid cell differentiation, has sequence similarity to BCL2. *Proc Natl Acad Sci U S A* **90**, 3516-3520 (1993).

279 Lin, E. Y., Orlofsky, A., Berger, M. S. & Prystowsky, M. B. Characterization of A1, a novel hemopoietic-specific early-response gene with sequence similarity to bcl-2. *J Immunol* **151**, 1979-1988 (1993).

280 Chittenden, T. *et al.* A conserved domain in Bak, distinct from BH1 and BH2, mediates cell death and protein binding functions. *EMBO J* **14**, 5589-5596 (1995).

281 Ke, N., Godzik, A. & Reed, J. C. Bcl-B, a novel Bcl-2 family member that differentially binds and regulates Bax and Bak. *J Biol Chem* **276**, 12481-12484 (2001).

282 Lee, E. F. *et al.* A novel BH3 ligand that selectively targets Mcl-1 reveals that apoptosis can proceed without Mcl-1 degradation. *J Cell Biol* **180**, 341-355 (2008).

283 Lee, E. F. *et al.* The functional differences between pro-survival and pro-apoptotic B cell lymphoma 2 (Bcl-2) proteins depend on structural differences in their Bcl-2 homology 3 (BH3) domains. *J Biol Chem* **289**, 36001-36017 (2014).

284 Czabotar, P. E. *et al.* Structural insights into the degradation of Mcl-1 induced by BH3 domains. *Proc Natl Acad Sci U S A* **104**, 6217-6222 (2007).

285 Kataoka, T. *et al.* Bcl-rambo, a novel Bcl-2 homologue that induces apoptosis via its unique C-terminal extension. *J Biol Chem* **276**, 19548-19554 (2001).

286 Print, C. G. *et al.* Apoptosis regulator bcl-w is essential for spermatogenesis but appears otherwise redundant. *Proc Natl Acad Sci U S A* **95**, 12424-12431 (1998).

287 Gibson, L. *et al.* bcl-w, a novel member of the bcl-2 family, promotes cell survival. *Oncogene* **13**, 665-675 (1996).

288 Aouacheria, A., Rech de Laval, V., Combet, C. & Hardwick, J. M. Evolution of Bcl-2 homology motifs: homology versus homoplasy. *Trends Cell Biol* **23**, 103-111 (2013).

289 Gabellini, C., Trisciuoglio, D. & Del Bufalo, D. Non-canonical roles of Bcl-2 and Bcl-xL proteins: relevance of BH4 domain. *Carcinogenesis* **38**, 579-587 (2017).

290 Huang, D. C., Adams, J. M. & Cory, S. The conserved N-terminal BH4 domain of Bcl-2 homologues is essential for inhibition of apoptosis and interaction with CED-4. *EMBO J* **17**, 1029-1039 (1998).

291 Hirotani, M., Zhang, Y., Fujita, N., Naito, M. & Tsuruo, T. NH2-terminal BH4 domain of Bcl-2 is functional for heterodimerization with Bax and inhibition of apoptosis. *J Biol Chem* **274**, 20415-20420 (1999).

292 Monaco, G., Vervliet, T., Akl, H. & Bultynck, G. The selective BH4-domain biology of Bcl-2-family members: IP3Rs and beyond. *Cell Mol Life Sci* **70**, 1171-1183 (2013).

293 Monaco, G. *et al.* The BH4 domain of anti-apoptotic Bcl-XL, but not that of the related Bcl-2, limits the voltage-dependent anion channel 1 (VDAC1)-mediated transfer of pro-apoptotic Ca2+ signals to mitochondria. *J Biol Chem* **290**, 9150-9161 (2015).

294 Pan, G., O'Rourke, K. & Dixit, V. M. Caspase-9, Bcl-XL, and Apaf-1 form a ternary complex. *J Biol Chem* **273**, 5841-5845 (1998).

295 Trisciuoglio, D. *et al.* Involvement of BH4 domain of bcl-2 in the regulation of HIF-1-mediated VEGF expression in hypoxic tumor cells. *Cell Death Differ* **18**, 1024-1035 (2011).

296 Rong, Y. P., Barr, P., Yee, V. C. & Distelhorst, C. W. Targeting Bcl-2 based on the interaction of its BH4 domain with the inositol 1,4,5-trisphosphate receptor. *Biochim Biophys Acta* **1793**, 971-978 (2009).

297 Sattler, M. *et al.* Structure of Bcl-xL-Bak peptide complex: recognition between regulators of apoptosis. *Science* **275**, 983-986 (1997).

298 Czabotar, P. E. *et al.* Mutation to Bax beyond the BH3 domain disrupts interactions with pro-survival proteins and promotes apoptosis. *J Biol Chem* **286**, 7123-7131 (2011).

299 Czabotar, P. E. *et al.* Bax crystal structures reveal how BH3 domains activate Bax and nucleate its oligomerization to induce apoptosis. *Cell* **152**, 519-531 (2013).

300 Robin, A. Y. *et al.* Crystal structure of Bax bound to the BH3 peptide of Bim identifies important contacts for interaction. *Cell Death Dis* **6**, e1809 (2015).

301 Brouwer, J. M. *et al.* Bak core and latch domains separate during activation, and freed core domains form symmetric homodimers. *Mol Cell* **55**, 938-946 (2014).

302 Moldoveanu, T. *et al.* The X-ray structure of a BAK homodimer reveals an inhibitory zinc binding site. *Mol Cell* **24**, 677-688 (2006).

303 Alsop, A. E. *et al.* Dissociation of Bak alpha1 helix from the core and latch domains is required for apoptosis. *Nat Commun* **6**, 6841 (2015).

304 Leshchiner, E. S., Braun, C. R., Bird, G. H. & Walensky, L. D. Direct activation of full-length proapoptotic BAK. *Proc Natl Acad Sci U S A* **110**, E986-995 (2013).

305 Hsu, Y. T., Wolter, K. G. & Youle, R. J. Cytosol-to-membrane redistribution of Bax and Bcl-X(L) during apoptosis. *Proc Natl Acad Sci U S A* **94**, 3668-3672 (1997).

306 Uren, R. T., Iyer, S. & Kluck, R. M. Pore formation by dimeric Bak and Bax: an unusual pore? *Philos Trans R Soc Lond B Biol Sci* **372** (2017).

307 Follis, A. V. *et al.* PUMA binding induces partial unfolding within BCL-xL to disrupt p53 binding and promote apoptosis. *Nature Chemical Biology* **9**, 163-168 (2013).

308 Feng, Y. *et al.* Bcl-xL forms two distinct homodimers at non-ionic detergents: implications in the dimerization of Bcl-2 family proteins. *J Biochem* **143**, 243-252 (2008).

309 Denisov, A. Y., Sprules, T., Fraser, J., Kozlov, G. & Gehring, K. Heat-induced dimerization of BCL-xL through alpha-helix swapping. *Biochemistry* **46**, 734-740 (2007).

310 O'Neill, J. W., Manion, M. K., Maguire, B. & Hockenbery, D. M. BCL-XL dimerization by three-dimensional domain swapping. *J Mol Biol* **356**, 367-381 (2006).

311 Iyer, S. *et al.* Identification of an activation site in Bak and mitochondrial Bax triggered by antibodies. *Nat Commun* **7**, 11734 (2016).

312 Pritz, J. R. *et al.* Allosteric sensitization of proapoptotic BAX. *Nat Chem Biol* **13**, 961-967 (2017).

313 Brahmbhatt, H., Uehling, D., Al-Awar, R., Leber, B. & Andrews, D. Small molecules reveal an alternative mechanism of Bax activation. *Biochem J* **473**, 1073-1083 (2016).

314 Pagliari, L. J. *et al.* The multidomain proapoptotic molecules Bax and Bak are directly activated by heat. *Proc Natl Acad Sci U S A* **102**, 17975-17980 (2005).

315 Cartron, P. F., Oliver, L., Mayat, E., Meflah, K. & Vallette, F. M. Impact of pH on Bax alpha conformation, oligomerisation and mitochondrial integration. *FEBS Lett* **578**, 41-46 (2004).

316 Hsu, Y. T. & Youle, R. J. Nonionic detergents induce dimerization among members of the Bcl-2 family. *J Biol Chem* **272**, 13829-13834 (1997).

317 Follis, A. V. *et al.* PUMA binding induces partial unfolding within BCL-xL to disrupt p53 binding and promote apoptosis. *Nat Chem Biol* **9**, 163-168 (2013).

318 Chen, L. *et al.* Differential targeting of prosurvival Bcl-2 proteins by their BH3-only ligands allows complementary apoptotic function. *Mol Cell* **17**, 393-403 (2005).

319 Kvansakul, M. & Hinds, M. G. Structural biology of the Bcl-2 family and its mimicry by viral proteins. *Cell Death Dis* **4**, e909 (2013).

320 Nakano, K. & Vousden, K. H. PUMA, a Novel Proapoptotic Gene, Is Induced by p53. *Molecular Cell* **7**, 683-694 (2001).

321 Kim, H. *et al.* Hierarchical regulation of mitochondrion-dependent apoptosis by BCL-2 subfamilies. *Nat Cell Biol* **8**, 1348-1358 (2006).

322 Follis, A. V. *et al.* The DNA-binding domain mediates both nuclear and cytosolic functions of p53. *Nat Struct Mol Biol* **21**, 535-543 (2014).

323 Edwards, A. L. *et al.* Multimodal interaction with BCL-2 family proteins underlies the proapoptotic activity of PUMA BH3. *Chem Biol* **20**, 888-902 (2013).

324 Chipuk, J. E. *et al.* Mechanism of apoptosis induction by inhibition of the anti-apoptotic BCL-2 proteins. *Proc Natl Acad Sci U S A* **105**, 20327-20332 (2008).

325 Fujita, N., Nagahashi, A., Nagashima, K., Rokudai, S. & Tsuruo, T. Acceleration of apoptotic cell death after the cleavage of Bcl-XL protein by caspase-3-like proteases. *Oncogene* **17**, 1295-1304 (1998).

326 Clem, R. J. *et al.* Modulation of cell death by Bcl-XL through caspase interaction. *Proc Natl Acad Sci U S A* **95**, 554-559 (1998).

327 Follis, A. V. *et al.* Regulation of apoptosis by an intrinsically disordered region of Bcl-xL. *Nat Chem Biol* **14**, 458-465 (2018).

328 Kirsch, D. G. *et al.* Caspase-3-dependent cleavage of Bcl-2 promotes release of cytochrome c. *J Biol Chem* **274**, 21155-21161 (1999).

329 Park, H. A. & Jonas, E. A. DeltaN-Bcl-xL, a therapeutic target for neuroprotection. *Neural Regen Res* **12**, 1791-1794 (2017).

330 Park, H. A. *et al.* Inhibition of Bcl-xL prevents pro-death actions of DeltaN-Bcl-xL at the mitochondrial inner membrane during glutamate excitotoxicity. *Cell Death Differ* **24**, 1963-1974 (2017).

331 Li, H. *et al.* A Bcl-xL-Drp1 complex regulates synaptic vesicle membrane dynamics during endocytosis. *Nat Cell Biol* **15**, 773-785 (2013).

332 Ofengeim, D. *et al.* N-terminally cleaved Bcl-xL mediates ischemia-induced neuronal death. *Nat Neurosci* **15**, 574-580 (2012).

333 Alavian, K. N. *et al.* Bcl-xL regulates metabolic efficiency of neurons through interaction with the mitochondrial F1FO ATP synthase. *Nat Cell Biol* **13**, 1224-1233 (2011).

334 Berman, S. B. *et al.* Bcl-x L increases mitochondrial fission, fusion, and biomass in neurons. *J Cell Biol* **184**, 707-719 (2009).

335 Hickman, J. A., Hardwick, J. M., Kaczmarek, L. K. & Jonas, E. A. Bcl-xL inhibitor ABT-737 reveals a dual role for Bcl-xL in synaptic transmission. *J Neurophysiol* **99**, 1515-1522 (2008).

336 Jonas, E. A. *et al.* Proapoptotic N-truncated BCL-xL protein activates endogenous mitochondrial channels in living synaptic terminals. *Proc Natl Acad Sci U S A* **101**, 13590-13595 (2004).

337 Cavanagh, J. F., W. J.; Palmer, A. G.; Rance, M.; Skelton, N. J. Protein NMR Spectroscopy: Principles and Practice. *Elsevier* (2006).

338 Levitt, M. H. Spin Dynamics: Basics of Nuclear Magnetic Resonance, 2nd Ed. *John Wiley & Sons* (2008).

339 Keeler, J. Understanding NMR spectroscopy. *John Wiley & Sons Ltd* (2011).

340 Lian, G. R. L.-Y. Protein NMR Spectroscopy: Practical Techniques and Applications. *John Wiley & Sons Ltd* (2011).

341 Hitchens, G. S. R. T. K. Fundamentals of Protein NMR Spectroscopy. *Springer Science & Business Media* (2006).

342 Clore, G. M. & Iwahara, J. Theory, practice, and applications of paramagnetic relaxation enhancement for the characterization of transient low-population states of biological macromolecules and their complexes. *Chem Rev* **109**, 4108-4139 (2009).

343 Liang, B., Bushweller, J. H. & Tamm, L. K. Site-directed parallel spin-labeling and paramagnetic relaxation enhancement in structure determination of membrane proteins by solution NMR spectroscopy. *J Am Chem Soc* **128**, 4389-4397 (2006).

344 Roosild, T. P. *et al.* NMR structure of Mistic, a membrane-integrating protein for membrane protein expression. *Science* **307**, 1317-1321 (2005).

345 Iwahara, J., Schwieters, C. D. & Clore, G. M. Ensemble approach for NMR structure refinement against (1)H paramagnetic relaxation enhancement data arising from a flexible paramagnetic group attached to a macromolecule. *J Am Chem Soc* **126**, 5879-5896 (2004).

346 Bertini, I., Janik, M. B., Lee, Y. M., Luchinat, C. & Rosato, A. Magnetic susceptibility tensor anisotropies for a lanthanide ion series in a fixed protein matrix. *J Am Chem Soc* **123**, 4181-4188 (2001).

347 Peters, F. *et al.* Cys-Ph-TAHA: a lanthanide binding tag for RDC and PCS enhanced protein NMR. *J Biomol NMR* **51**, 329-337 (2011).

348 Su, X. C., McAndrew, K., Huber, T. & Otting, G. Lanthanide-binding peptides for NMR measurements of residual dipolar couplings and paramagnetic effects from multiple angles. *J Am Chem Soc* **130**, 1681-1687 (2008).

349 Allegrozzi, M. *et al.* Lanthanide-Induced Pseudocontact Shifts for Solution Structure Refinements of Macromolecules in Shells up to 40 Å from the Metal Ion. *Journal of the American Chemical Society* **122**, 4154-4161 (2000).

350 Opina, A. C. *et al.* Analysis of the isomer ratios of polymethylated-DOTA complexes and the implications on protein structural studies. *Dalton Trans* **45**, 4673-4687 (2016).

351 Donaldson, L. W. *et al.* Structural characterization of proteins with an attached ATCUN motif by paramagnetic relaxation enhancement NMR spectroscopy. *J Am Chem Soc* **123**, 9843-9847 (2001).

352 Battiste, J. L. & Wagner, G. Utilization of site-directed spin labeling and high-resolution heteronuclear nuclear magnetic resonance for global fold determination of large proteins with limited nuclear overhauser effect data. *Biochemistry* **39**, 5355-5365 (2000).

353 Card, P. B., Erbel, P. J. & Gardner, K. H. Structural basis of ARNT PAS-B dimerization: use of a common beta-sheet interface for hetero- and homodimerization. *J Mol Biol* **353**, 664-677 (2005).

354 Fang, Z. *et al.* Inhibition of K-RAS4B by a Unique Mechanism of Action: Stabilizing Membrane-Dependent Occlusion of the Effector-Binding Site. *Cell Chem Biol* **25**, 1327-1336 e1324 (2018).

355 Mazhab-Jafari, M. T. *et al.* Membrane-dependent modulation of the mTOR activator Rheb: NMR observations of a GTPase tethered to a lipid-bilayer nanodisc. *J Am Chem Soc* **135**, 3367-3370 (2013).

356 Gross, J. D. *et al.* Ribosome Loading onto the mRNA Cap Is Driven by Conformational Coupling between eIF4G and eIF4E. *Cell* **115**, 739-750 (2003).

357 Mahoney, N. M., Rastogi, V. K., Cahill, S. M., Girvin, M. E. & Almo, S. C. Binding Orientation of Proline-Rich Peptides in Solution: Polarity of the Profilin−Ligand Interaction. *Journal of the American Chemical Society* **122**, 7851-7852 (2000).

358 Varani, L. *et al.* The NMR structure of the 38 kDa U1A protein - PIE RNA complex reveals the basis of cooperativity in regulation of polyadenylation by human U1A protein. *Nat Struct Biol* **7**, 329-335 (2000).

359 Bertoncini, C. W. *et al.* Release of long-range tertiary interactions potentiates aggregation of natively unstructured alpha-synuclein. *Proc Natl Acad Sci U S A* **102**, 1430-1435 (2005).

360 Felitsky, D. J., Lietzow, M. A., Dyson, H. J. & Wright, P. E. Modeling transient collapsed states of an unfolded protein to provide insights into early folding events. *Proc Natl Acad Sci U S A* **105**, 6278-6283 (2008).

361 Pervushin, K., Riek, R., Wider, G. & Wuthrich, K. Attenuated T2 relaxation by mutual cancellation of dipole-dipole coupling and chemical shift anisotropy indicates an avenue to NMR structures of very large biological macromolecules in solution. *Proc Natl Acad Sci U S A* **94**, 12366-12371 (1997).

362 Michael R. Green, J. S. Molecular Cloning: A Laboratory Manual (Fourth Edition). (2012).

363 Mullis, K. *et al.* Specific enzymatic amplification of DNA in vitro: the polymerase chain reaction. *Cold Spring Harb Symp Quant Biol* **51 Pt 1**, 263-273 (1986).

364 Kibbe, W. A. OligoCalc: an online oligonucleotide properties calculator. *Nucleic Acids Res* **35**, W43-46 (2007).

365 Braman, J., Papworth, C. & Greener, A. Site-directed mutagenesis using double-stranded plasmid DNA templates. *Methods Mol Biol* **57**, 31-44 (1996).

366 Laemmli, U. K. Cleavage of structural proteins during the assembly of the head of bacteriophage T4. *Nature* **227**, 680-685 (1970).

367 https://www.promega.de/-/media/files/resources/protcards/wizard-plus-sv-minipreps-dna-purification-system-quick-protocol.pdf?la=en (accessed 17.11.2019).

368 Sanger, F. & Coulson, A. R. A rapid method for determining sequences in DNA by primed synthesis with DNA polymerase. *Journal of Molecular Biology* **94**, 441-448 (1975).

369 Kyrychenko, A., Posokhov, Y. O., Rodnin, M. V. & Ladokhin, A. S. Kinetic intermediate reveals staggered pH-dependent transitions along the membrane insertion pathway of the diphtheria toxin T-domain. *Biochemistry* **48**, 7584-7594 (2009).

370 https://www.thermofisher.com/order/catalog/product/A10254 (Accessed: 03.09.2019).

371 https://assets.thermofisher.com/TFS-Assets/LSG/manuals/mp00003.pdf (Accessed: 03.09.2019).

372 Vargas-Uribe, M., Rodnin, M. V. & Ladokhin, A. S. Comparison of membrane insertion pathways of the apoptotic regulator Bcl-xL and the diphtheria toxin translocation domain. *Biochemistry* **52**, 7901-7909 (2013).

373 Schwieters, C. D., Kuszewski, J. J., Tjandra, N. & Marius Clore, G. The Xplor-NIH NMR molecular structure determination package. *Journal of Magnetic Resonance* **160**, 65-73 (2003).

374 Lovell, S. C. *et al.* Structure validation by Calpha geometry: phi,psi and Cbeta deviation. *Proteins* **50**, 437-450 (2003).

375 Petoukhov, M. V. *et al.* New developments in the ATSAS program package for small-angle scattering data analysis. *J Appl Crystallogr* **45**, 342-350 (2012).

376 Doucet, M. C., Jae Hie; Alina, Gervaise; Bakker, Jurrian; Bouwman, Wim; Butler, Paul; Campbell, Kieran; Gonzales, Miguel; Heenan, Richard; Jackson, Andrew; Juhas, Pavol; King, Stephen; Kienzle, Paul; Krzywon, Jeff; Markvardsen, Anders; Nielsen, Torben; O'Driscoll, Lewis; Potrzebowski, Wojciech; Ferraz Leal, Ricardo; Richter, Tobias; Rozycko, Piotr; Snow, Tim; Washington, Adam. SasView Version 4.2.1 http://doi.org/10.5281/zenodo.2561236.

377 Tropea, J. E., Cherry, S. & Waugh, D. S. Expression and purification of soluble His(6)-tagged TEV protease. *Methods Mol Biol* **498**, 297-307 (2009).

378 Wu, Z., Hong, H., Zhao, X. & Wang, X. Efficient expression of sortase A from Staphylococcus aureus in Escherichia coli and its enzymatic characterizations. *Bioresour Bioprocess* **4**, 13 (2017).

379 Hagn, F. *et al.* BclxL changes conformation upon binding to wild-type but not mutant p53 DNA binding domain. *J Biol Chem* **285**, 3439-3450 (2010).

380 Raltchev, K., Pipercevic, J. & Hagn, F. Production and Structural Analysis of Membrane-Anchored Proteins in Phospholipid Nanodiscs. *Chemistry* **24**, 5493-5499 (2018).

381 Horvath, S. E. & Daum, G. Lipids of mitochondria. *Prog Lipid Res* **52**, 590-614 (2013).

382 Degrip, W. J., Vanoostrum, J. & Bovee-Geurts, P. H. Selective detergent-extraction from mixed detergent/lipid/protein micelles, using cyclodextrin inclusion compounds: a novel generic approach for the preparation of proteoliposomes. *Biochem J* **330 (Pt 2)**, 667-674 (1998).

383 Kale, J., Chi, X., Leber, B. & Andrews, D. Examining the molecular mechanism of bcl-2 family proteins at membranes by fluorescence spectroscopy. *Methods Enzymol* **544**, 1-23 (2014).

384 Rajan, S. *et al.* Structural transition in Bcl-xL and its potential association with mitochondrial calcium ion transport. *Sci Rep* **5**, 10609 (2015).

385 Vasquez-Montes, V. *et al.* Lipid-modulation of membrane insertion and refolding of the apoptotic inhibitor Bcl-xL. *Biochimica et Biophysica Acta (BBA) - Proteins and Proteomics* **1867**, 691-700 (2019).

386 https://avantilipids.com/product/100500 (Accessed 14.11.2019).

387 Bottinger, L., Ellenrieder, L. & Becker, T. How lipids modulate mitochondrial protein import. *J Bioenerg Biomembr* **48**, 125-135 (2016).

388 Chu, C. T. *et al.* Cardiolipin externalization to the outer mitochondrial membrane acts as an elimination signal for mitophagy in neuronal cells. *Nat Cell Biol* **15**, 1197-1205 (2013).

389 Billen, L. P., Kokoski, C. L., Lovell, J. F., Leber, B. & Andrews, D. W. Bcl-XL inhibits membrane permeabilization by competing with Bax. *PLoS Biol* **6**, e147 (2008).

390 Itaya, M., Brett, I. C. & Smith, S. O. Synthesis, purification, and characterization of single helix membrane peptides and proteins for NMR spectroscopy. *Methods Mol Biol* **831**, 333-357 (2012).

391 Yao, Y. *et al.* Characterization of the membrane-inserted C-terminus of cytoprotective BCL-XL. *Protein Expr Purif* **122**, 56-63 (2016).

392 Trenker, R., Call, M. E. & Call, M. J. Crystal Structure of the Glycophorin A Transmembrane Dimer in Lipidic Cubic Phase. *J Am Chem Soc* **137**, 15676-15679 (2015).

393 Yao, Y. *et al.* Conformation of BCL-XL upon Membrane Integration. *J Mol Biol* **427**, 2262-2270 (2015).

394 Gonzalvez, F. *et al.* tBid interaction with cardiolipin primarily orchestrates mitochondrial dysfunctions and subsequently activates Bax and Bak. *Cell Death Differ* **12**, 614-626 (2005).

395 Lutter, M. *et al.* Cardiolipin provides specificity for targeting of tBid to mitochondria. *Nat Cell Biol* **2**, 754-761 (2000).

396 Landeta, O. *et al.* Reconstitution of proapoptotic BAK function in liposomes reveals a dual role for mitochondrial lipids in the BAK-driven membrane permeabilization process. *J Biol Chem* **286**, 8213-8230 (2011).

397 Ritzefeld, M. Sortagging: a robust and efficient chemoenzymatic ligation strategy. *Chemistry* **20**, 8516-8529 (2014).

6 Appendix

6.1.1 Protein Constructs

pET28a His_6-TEV-MSP1D1ΔH5

Protein Sequence:

MGSS**HHHHHH**ENLYFQ/G**STFSKLREQLGPVTQEFWDNLEKETEGLRQEMSKDLEEVKAKVQPYL DDFQKKWQEEMELYRQKVEPLGEEMRDRARAHVDALRTHLAPYSDELRQRLAARLEALKENGGA RLAEYHAKATEHLSTLSEKAKPALEDLRQGLLPVLESFKVSFLSALEEYTKKLNTQ**

Number of amino acids:	184
Molecular weight:	21468.12
Ext. coefficient @280 nm:	19940

After TEV cut:

GSTFSKLREQLGPVTQEFWDNLEKETEGLRQEMSKDLEEVKAKVQPYLDDFQKKWQEEMELYRQ KVEPLGEEMRDRARAHVDALRTHLAPYSDELRQRLAARLEALKENGGARLAEYHAKATEHLSTLS EKAKPALEDLRQGLLPVLESFKVSFLSALEEYTKKLNTQ

Number of amino acids:	168
Molecular weight:	19488.01
Ext. coefficient @280 nm:	18450

TEV cut site: **ENLYFQ/G**

His_6-tag: **HHHHHH**

pET21a MSP1D1ΔH5-TEV-His_6 "CTD-MSP1D1ΔH5"

Protein Sequence:

M**STFSKLREQLGPVTQEFWDNLEKETEGLRQEMSKDLEEVKAKVQPYLDDFQKKWQEEMELYRQ KVEPLGEEMRDRARAHVDALRTHLAPYSDELRQRLAARLEALKENGGARLAEYHAKATEHLSTLS EKAKPALEDLRQGLLPVLESFKVSFLSALEEYTKKLNTQ**ENLYFQ/G**GNNAAAESRKGQERLE**HHH HHH

Number of amino acids: 197

Molecular weight: 22948.72

Ext. coefficient @280 nm: 19940

After TEV cut:

M**STFSKLREQLGPVTQEFWDNLEKETEGLRQEMSKDLEEVKAKVQPYLDDFQKKWQEEMELYRQ KVEPLGEEMRDRARAHVDALRTHLAPYSDELRQRLAARLEALKENGGARLAEYHAKATEHLSTLS EKAKPALEDLRQGLLPVLESFKVSFLSALEEYTKKLNTQ**ENLYFQ

Number of amino acids: 174

Molecular weight: 20357.01

Ext. coefficient @280 nm: 19940

TEV cut site: **ENLYFQ/G**

His_6-tag: **HHHHHH**

pET21a Bcl-xL-SOR-His_6

Protein Sequence:

M**SQSNRELVVDFLSYKLSQKGYSWSQFSDVEENRTEAPEGTESEMETPSAINGNPSWHLADSPAV**
NGATGHSSSLDAREVIPMAAVKQALREAGDEFELRYRRAFSDLTSQLHITPGTAYQSFEQVVNELF
RDGVNWGRIVAFFSFGGALCVESVDKEMQVLVSRIAAWMATYLNDHLEPWIQENGGWDTFVELYG
NNALPETGGHHHHHH

Number of amino acids: 211

Molecular weight: 23631.01

Ext. coefficient @280 nm: 41940

Bcl-xL-solu:
M**SQSNRELVVDFLSYKLSQKGYSWSQFSDVEENRTEAPEGTESEMETPSAINGNPSWHLADSPAV**
NGATGHSSSLDAREVIPMAAVKQALREAGDEFELRYRRAFSDLTSQLHITPGTAYQSFEQVVNELF
RDGVNWGRIVAFFSFGGALCVESVDKEMQVLVSRIAAWMATYLNDHLEPWIQENGGWDTFVELYG
NNA

Sortase recognition motif site: **LPETG**

His_6-tag: **HHHHHH**

After Sortase ligation – full-lenght Bcl-xL with TMH Helix:

M**SQSNRELVVDFLSYKLSQKGYSWSQFSDVEENRTEAPEGTESEMETPSAINGNPSWHLADSPAV**
NGATGHSSSLDAREVIPMAAVKQALREAGDEFELRYRRAFSDLTSQLHITPGTAYQSFEQVVNELF
RDGVNWGRIVAFFSFGGALCVESVDKEMQVLVSRIAAWMATYLNDHLEPWIQENGGWDTFVELYG
NNALPETGSGESRKGQERFNRWFLTGMTVAGVVLLGSLFSRK

Number of amino acids: 238

Molecular weight: 26548.51

Ext. coefficient @280 nm: 47470

pET21a Bcl-xL-THR-SOR-His_6

Protein Sequence:

M**SQSNRELVVDFLSYKLSQKGYSWSQFSDVEENRTEAPEGTESEMETPSAINGNPSWHLA**LVPR/G**SGATGHSSSLDAREVIPMAAVKQALREAGDEFELRYRRAFSDLTSQLHITPGTAYQSFEQVVNELFR DGVNWGRIVAFFSFGGALCVESVDKEMQVLVSRIAAWMATYLNDHLEPWIQENGGWDTFVELYGN NA**LPETG**G**HHHHHH**

Number of amino acids: 213

Molecular weight: 23887.36

Ext. coefficient @280 nm: 41940

Sortase recognition motif site: **LPETG**

His_6-tag: **HHHHHH**

Thrombin cut site: **LVPR/GS**

Thrombin cut:

Part1:

M**SQSNRELVVDFLSYKLSQKGYSWSQFSDVEENRTEAPEGTESEMETPSAINGNPSWHLA**LVPR

Number of amino acids: 64

Molecular weight: 7261.94

Part2:

GSGATGHSSSLDAREVIPMAAVKQALREAGDEFELRYRRAFSDLTSQLHITPGTAYQSFEQVVNEL FRDGVNWGRIVAFFSFGGALCVESVDKEMQVLVSRIAAWMATYLNDHLEPWIQENGGWDTFVELY GNNALPETG**G**HHHHHH**

Number of amino acids: 147

Molecular weight: 16413.22

pET21a Bcl-xLΔTM-His_6

Protein Sequence:

**MSQSNRELVVDFLSYKLSQKGYSWSQFSDVEENRTEAPEGTESEMETPSAINGNPSWHLADSPAV
NGATGHSSSLDAREVIPMAAVKQALREAGDEFELRYRRAFSDLTSQLHITPGTAYQSFEQVVNELF
RDGVNWGRIVAFFSFGGALCVESVDKEMQVLVSRIAAWMATYLNDHLEPWIQENGGWDTFVELYG
NNAAAESRKGQERLEHHHHHH**

Number of amino acids: 217

Molecular weight: 24431.88

Ext. coefficient @280 nm: 41940

Difference compared to Bcl-xL-SOR: **AAESRKGQERLE**

His6-tag: **HHHHHH**

pET21a Bcl-xL-THR-ΔTM-His_6

Protein Sequence:

**MSQSNRELVVDFLSYKLSQKGYSWSQFSDVEENRTEAPEGTESEMETPSAINGNPSWHLALVPR/G
SGATGHSSSLDAREVIPMAAVKQALREAGDEFELRYRRAFSDLTSQLHITPGTAYQSFEQVVNELFR
DGVNWGRIVAFFSFGGALCVESVDKEMQVLVSRIAAWMATYLNDHLEPWIQENGGWDTFVELYGN
NAAAESRKGQERLEHHHHHH**

Number of amino acids: 217

Molecular weight: 24431.88

Ext. coefficient @280 nm: 41940

Thrombin cut site: **LVPR/GS**

Difference compared to Bcl-xL-SOR: **AAESRKGQERLE**

His_6-tag: **HHHHHH**

pET15b His_6-GB1-THR-Bcl-xL-TMH

Protein Sequence:

MSYYHHHHHHDYDIPTTAMEYKLILNGKTLKGETTTEAVDAATAEKVFKQYANDNGVDGE
WTYDDATKTFTVTEIPTTLVPR/GSGESRKGQERFNRWFLTGMTVAGVVLLGSLFSRK

Number of amino acids: 117

Molecular weight: 13200.74

Ext. coefficient @280 nm: 19940

Thrombin cut site: **LVPR/GS**

GB1:
MEYKLILNGKTLKGETTTEAVDAATAEKVFKQYANDNGVDGEWTYDDATKTFTVTEIPTT

His_6-tag: **HHHHHH**

Bcl-xL-TMH: **ESRKGQERFNRWFLTGMTVAGVVLLGSLFSRK**

pET15b His_6-GB1-THR-GlycophorinA-TMH

DNA Sequence, *E. coli* codon optimised:

Atgtcgtactaccatcaccatcaccatcacgattacgatatcccaacgaccgccatggagtacaagcttatcctgaacggtaaaa
ccctgaaaggtgaaaccaccaccgaagctgttgacgctgctaccgcggaaaaagttttcaaacagtacgctaacgacaacggt
gttgacggtgaatggacctacgacgacgctaccaaaaccttcacggtaaccgaaatcccaacgaccctggttccgcgtggttctg
gttctggaagcgaaccggaaattaccctgattatttttggtgttatggcaggtgttattggtaccattctgctgattagctatggtattcgtc
gtctgattaaaaaatga

Protein Sequence:

MSYYHHHHHHDYDIPTTAMEYKLILNGKTLKGETTTEAVDAATAEKVFKQYANDNGVDGE
WTYDDATKTFTVTEIPTTLVPR/GSGSGSEPEITLIIFGVMAGVIGTILLISYGIRRLIKK

Number of amino acids: 120

Molecular weight: 13289.05

Ext. coefficient @280 nm: 15930

Thrombin cut site: **LVPR/GS**

His_6-tag: **HHHHHH**

GB1:

MEYKLILNGKTLKGETTTEAVDAATAEKVFKQYANDNGVDGEWTYDDATKTFTVTEIPTT

Glycophorin A: **SEPEITLIIFGVMAGVIGTILLISYGIRRLIKK**

pET29 Sortase A-His_6 P94R, D160N, D165A, K190E, K196T

Protein Sequence:

M**QAKPQIPKDKSKVAGYIEIPDADIKEPVYPGPATREQLNRGVSFAEENESLDDQNISIAGHTFIDRP NYQFTNLKAAKKGSMVYFKVGNETRKYKMTSIRNVKPTAVEVLDEQKGKDKQLTLITCDDYNEETG VWETRKIFVATEVKLE**HHHHHH

Number of amino acids:	156
Molecular weight:	17853.14
Ext. coefficient @280 nm:	14440

pT5L_T7-MBP-TEV-Asna1 and Z-tag-TEV-Fl-Bcl-xL

MBP-TEV-Asna1

M**KIEEGKLVIWINGDKGYNGLAEVGKKFEKDTGIKVTVEHPDKLEEKFPQVAATGDGPDIIFWAHDR FGGYAQSGLLAEITPDKAFQDKLYPFTWDAVRYNGKLIAYPIAVEALSLIYNKDLLPNPPKTWEEIPA LDKELKAKGKSALMFNLQEPYFTWPLIAADGGYAFKYENGKYDIKDVGVDNAGAKAGLTFLVDLIK NKHMNADTDYSIAEAAFNKGETAMTINGPWAWSNIDTSKVNYGVTVLPTFKGQPSKPFVGVLSAGI NAASPNKELAKEFLENYLLTDEGLEAVNKDKPLGAVALKSYEEELAKDPRIAATMENAQKGEIMPNI PQMSAFWYAVRTAVINAASGRQTVDEALKDAQTNSSSG**ENLYFQ/GS**MAAGVAGWGVEAEEFEDA PDVEPLEPTLSNIIEQRSLKWIFVGGKGGVGKTTCSCSLAVQLSKGRESVLIISTDPAHNISDAFDQKF SKVPTKVKGYDNLFAMEIDPSLGVAELPDEFFEEDNMLSMGKKMMQEAMSAFPGIDEAMSYAEVM RLVKGMNFSVVVFDTAPTGHTLRLLNFPTIVERGLGRLMQIKNQISPFISQMCNMLGLGDMNADQLA SKLEETLPVIRSVSEQFKDPEQTTFICVCIAEFLSLYETERLIQELAKCKIDTHNIIVNQLVFPDPEKPCK MCEARHKIQAKYLDQMEDLYEDFHIVKLPLLPHEVRGADKVNTFSALLLEPYKPPSAQ**

Number of amino acids:	728
Molecular weight:	80486.03
Ext. coefficient @280 nm:	88280

MBP:

MKIEEGKLVIWINGDKGYNGLAEVGKKFEKDTGIKVTVEHPDKLEEKFPQVAATGDGPDIIFWAHDR FGGYAQSGLLAEITPDKAFQDKLYPFTWDAVRYNGKLIAYPIAVEALSLIYNKDLLPNPPKTWEEIPA LDKELKAKGKSALMFNLQEPYFTWPLIAADGGYAFKYENGKYDIKDVGVDNAGAKAGLTFLVDLIK NKHMNADTDYSIAEAAFNKGETAMTINGPWAWSNIDTSKVNYGVTVLPTFKGQPSKPFVGVLSAGI NAASPNKELAKEFLENYLLTDEGLEAVNKDKPLGAVALKSYEEELAKDPRIAATMENAQKGEIMPNI PQMSAFWYAVRTAVINAASGRQTVDEALKDAQTNSSSG

TEV cut site: **ENLYFQ/G**

Asna1:

M**AAGVAGWGVEAEEFEDAPDVEPLEPTLSNIIEQRSLKWIFVGGKGGVGKTTCSCSLAVQLSKGRE SVLIISTDPAHNISDAFDQKFSKVPTKVKGYDNLFAMEIDPSLGVAELPDEFFEEDNMLSMGKKMMQ EAMSAFPGIDEAMSYAEVMRLVKGMNFSVVVFDTAPTGHTLRLLNFPTIVERGLGRLMQIKNQISPFI SQMCNMLGLGDMNADQLASKLEETLPVIRSVSEQFKDPEQTTFICVCIAEFLSLYETERLIQELAKCK IDTHNIIVNQLVFPDPEKPCKMCEARHKIQAKYLDQMEDLYEDFHIVKLPLLPHEVRGADKVNTFSAL LLEPYKPPSAQ**

T5 promotor (pQE) His_6-Z-tag-TEV-Fl-Bcl-xL

M**G**HHHHHHHHHH**GSNKFNKEQQNAFYEILHLPNLNEEQRNAFIQSLKDDPSQSANLLAEAKKLND AQAPKVAMNKFNKEQQNAFYEILHLPNLNEEQRNAFIQSLKDDPSQSANLLAEAKKLNDAQAPKVA MSG**ENLYFQ/G**TM**SQSNRELVVDFLSYKLSQKGYSWSQFSDVEENRTEAPEGTESEMETPSAINGN PSWHLADSPAVNGATGHSSSLDAREVIPMAAVKQALREAGDEFELRYRRAFSDLTSQLHITPGTAY QSFEQVVNELFRDGVNWGRIVAFFSFGGALCVESVDKEMQVLVSRIAAWMATYLNDHLEPWIQEN GGWDTFVELYGNNAAAESRKGQERFNRWFLTGMTVAGVVLLGSLFSRK**

Number of amino acids: 375

Molecular weight: 42268.94

Ext. coefficient @280 nm: 51910

His_6-tag: **HHHHHH**

TEV cut site: **ENLYFQ/G**

Z-tag:

GSNKFNKEQQNAFYEILHLPNLNEEQRNAFIQSLKDDPSQSANLLAEAKKLNDAQAPKVAMNKFNK EQQNAFYEILHLPNLNEEQRNAFIQSLKDDPSQSANLLAEAKKLNDAQAPKVAMSG

Fl-Bcl-xL:

M**SQSNRELVVDFLSYKLSQKGYSWSQFSDVEENRTEAPEGTESEMETPSAINGNPSWHLADSPAV**
NGATGHSSSLDAREVIPMAAVKQALREAGDEFELRYRRAFSDLTSQLHITPGTAYQSFEQVVNELF
RDGVNWGRIVAFFSFGGALCVESVDKEMQVLVSRIAAWMATYLNDHLEPWIQENGGWDTFVELYG
NNAAAESRKGQERFNRWFLTGMTVAGVVLLGSLFSRK

pT5L_T7 promotor-MBP-tev-Get3 Fl-Bcl-xL

MBP-TEV-Get3

MKIEEGKLVIWINGDKGYNGLAEVGKKFEKDTGIKVTVEHPDKLEEKFPQVAATGDGPDIIFWAHDR
FGGYAQSGLLAEITPDKAFQDKLYPFTWDAVRYNGKLIAYPIAVEALSLIYNKDLLPNPPKTWEEIPA
LDKELKAKGKSALMFNLQEPYFTWPLIAADGGYAFKYENGKYDIKDVGVDNAGAKAGLTFLVDLIK
NKHMNADTDYSIAEAAFNKGETAMTINGPWAWSNIDTSKVNYGVTVLPTFKGQPSKPFVGVLSAGI
NAASPNKELAKEFLENYLLTDEGLEAVNKDKPLGAVALKSYEEELAKDPRIAATMENAQKGEIMPNI
PQMSAFWYAVRTAVINAASGRQTVDEALKDAQTNSSSGENLYFQ/GSM**DLTVEPNLHSLITFTTHK**
WIFVGGKGGVGKTTSSCSIAIQMALSQPNKQFLLISTEPAHNLSDAFGEKFGKDARKVTGMNNLSC
MEIDPSAALKDMNDMAVSRANNNGSDGQGDDLGSLLQGGALADLTGSIPGIDEALSFMEVMKHIKR
QEQGEGETFDTVIFDTAPTGHTLRFLQLPNTLSKLLEKFGEITNKLGPMLNSFMGAGNVDISGKLNE
LKANVETIRQQFTDPDLTTFVCVCISEFLSLYETERLIQELISYDMDVNSIIVNQLLFAENDQEHNCKRC
QARWKMQKKYLDQIDELYEDFHVVKMPLCAGEIRGLNNLTKFSQFLNKEYNPITDGKVIYELEDKE

Number of amino acids:	734
Molecular weight:	81121.08
Ext. coefficient @280 nm:	88155

MBP:

MKIEEGKLVIWINGDKGYNGLAEVGKKFEKDTGIKVTVEHPDKLEEKFPQVAATGDGPDIIFWAHDR
FGGYAQSGLLAEITPDKAFQDKLYPFTWDAVRYNGKLIAYPIAVEALSLIYNKDLLPNPPKTWEEIPA
LDKELKAKGKSALMFNLQEPYFTWPLIAADGGYAFKYENGKYDIKDVGVDNAGAKAGLTFLVDLIK
NKHMNADTDYSIAEAAFNKGETAMTINGPWAWSNIDTSKVNYGVTVLPTFKGQPSKPFVGVLSAGI
NAASPNKELAKEFLENYLLTDEGLEAVNKDKPLGAVALKSYEEELAKDPRIAATMENAQKGEIMPNI
PQMSAFWYAVRTAVINAASGRQTVDEALKDAQTNSSSG

TEV cut site: **ENLYFQ/G**

Get3:

M**DLTVEPNLHSLITFTTHKWIFVGGKGGVGKTTSSCSIAIQMALSQPNKQFLLISTEPAHNLSDAFGE KFGKDARKVTGMNNLSCMEIDPSAALKDMNDMAVSRANNNGSDGQGDDLGSLLQGGALADLTGS IPGIDEALSFMEVMKHIKRQEQGEGETFDTVIFDTAPTGHTLRFLQLPNTLSKLLEKFGEITNKLGPML NSFMGAGNVDISGKLNELKANVETIRQQFTDPDLTTFVCVCISEFLSLYETERLIQELISYDMDVNSIIV NQLLFAENDQEHNCKRCQARWKMQKKYLDQIDELYEDFHVVKMPLCAGEIRGLNNLTKFSQFLNK EYNPITDGKVIYELEDKE**

6.1.2 Oligonucleotides

Bcl-xL into pT5L_T7-MBP-tev-Asna1WT_HZZtevStx5op

Primer 1:

CAGGAGAAAACCTTTATTTTCAGGGTACCATGTCTCAGAGCAACCGGGAGCTG

Primer 2:

Reverse complement:

CGAGTGCGGCCGCAAGCTTTCATTTCCGACTGAAGAGTGAGCCCAG

Insertion of Get3 into pT5L_T7-MBP-tev-Asna1WT_HZZtevBclxL (Replacing Asna1)

Primer 1:

GCAGACTAATTCGAGCTCGGGTGAAAACCAGGGATCCATGGATTTAACCGTGG

Primer 2:

Reverse complement:

CAGGAGTCCAAGCTCAGCTAATTAAGCTTCTATTCCTTATCTTCTAACT

Bcl-xL-R102C

Primer 1:

GTTTGAACTGCGGTACTGCCGGCCATTCAGTGACC

Primer 2:

Reverse complement:

GGTCACTGAATGCCCGGCAGTACCGCAGTTCAAAC

Bcl-xL-C151A

Primer 1:

CCTTCGGCGGGGCACTGGCTGTGGAAAGCGTAGACAAGG

Primer 2:

Reverse complement:

CCTTGTCTACGCTTTCCACAGCCAGTGCCCCGCCGAAGG

Bcl-xL-LVPRGS- Thrombin cut site between 61-62

Primer 1:

CCCATCCTGGCACCTGGCACTGGTTCCGCGTGGTTCTGGAGCCACTGGCCACAGC

Primer 2:

Reverse complement:

GCTGTGGCCAGTGGCTCCAGAACCACGCGGAACCAGTGCCAGGTGCCAGGATGGG

Glycophorina A

E. coli optimised gene made as a primer-pair (1,2), amplified with the second set of primers (3,4) for overhangs and inserted into GB1-THR-Bcl-xL-TMH replacing Bcl-xL-TMH.

Primer 1:

AGCGAACCGGAAATTACCCTGATTATTTTTGGTGTTATGGCAGGTGTTATTGGTACCATT
CTGCTGATTAGCTATGGTATTCGTCGTCTGATTAAAAAA

Primer 2:

Reverse complement:

TTTTTTAATCAGACGACGAATACCATAGCTAATCAGCAGAATGGTACCAATAACACCTGCCATAAC
ACCAAAAATAATCAGGGTAATTTCCGGTTCGCT

Primer 3:

CTGGTTCCGCGTGGTTCTGGTTCTGGAAGCGAACCGGAAATTACCCTG

Primer 4:

CTTTGTTAGCAGCCGGATCTCATTTTTTAATCAGACGACGAATACCATAG

CTD-MSP1D1ΔH5

Primer 1:

GTTTAACTTTAAGAAGGAGATATACATATGAGCACCTTTAGCAAACTGCGTG

Primer 2:

CGGCTGCTGCATTGTTCCCGCCCTGAAAATACAGGTTTTCCTGGGTGTTCAGTTTTTTGGTATAC

6.1.3 Mass Spectrometry

Bcl-xLΔTM

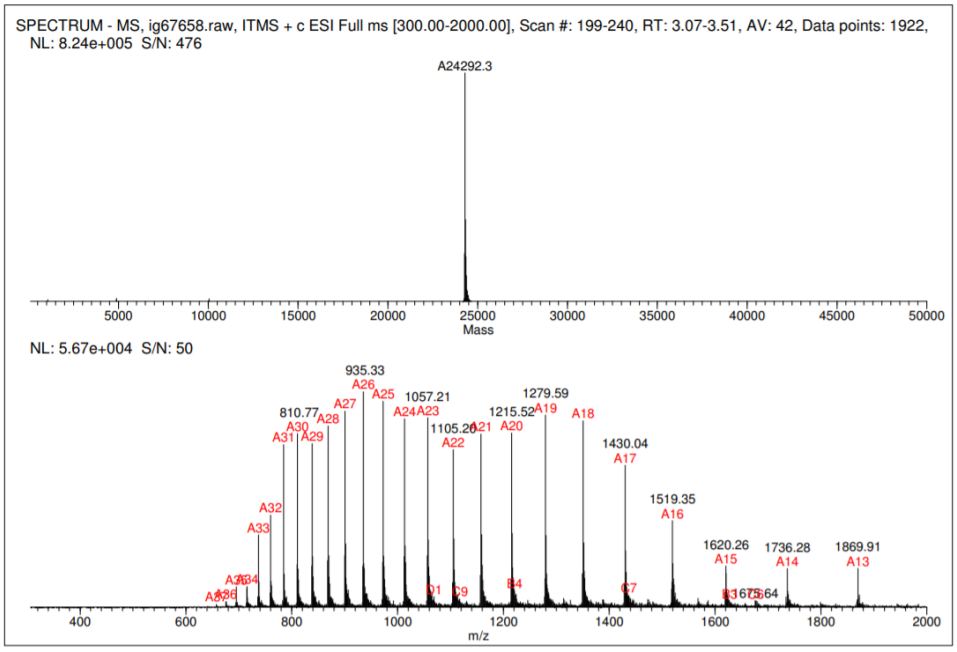

Figure 60: Electron spray ionisation mass spectrometry analysis of Bcl-xLΔTM with expected mass of 24300.7 Da and measured of 24292.3 Da.

Bcl-xL-SOR

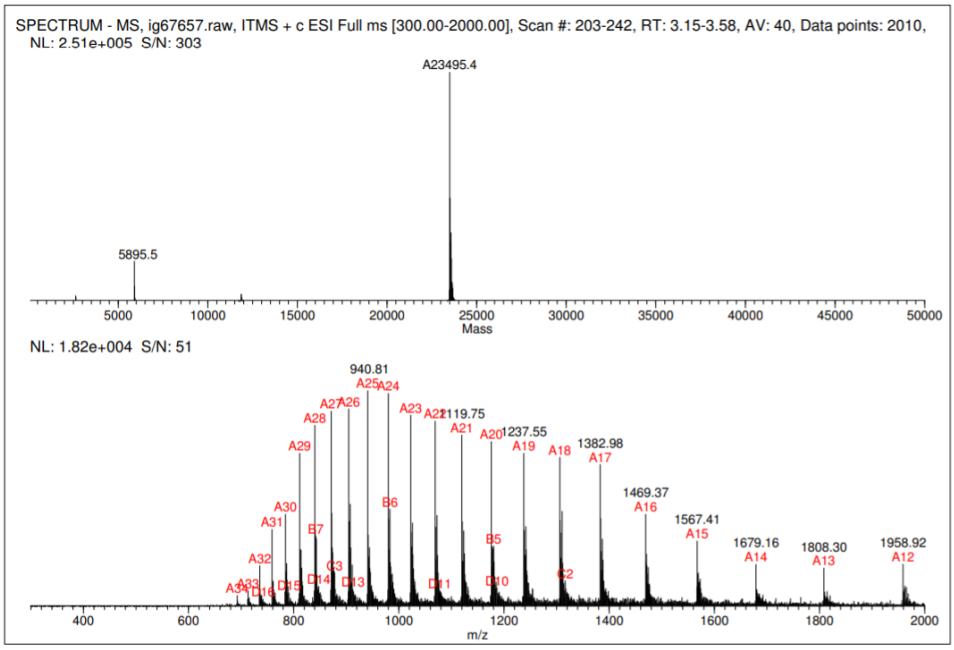

Figure 61: Electron spray ionisation mass spectrometry analysis of Bcl-xL-SOR with expected mass of 23499.8 Da and measured of 23495.4 Da. The 5895.5 corresponds to a different charge (4).

Bcl-xL TMH cut in nanodiscs:

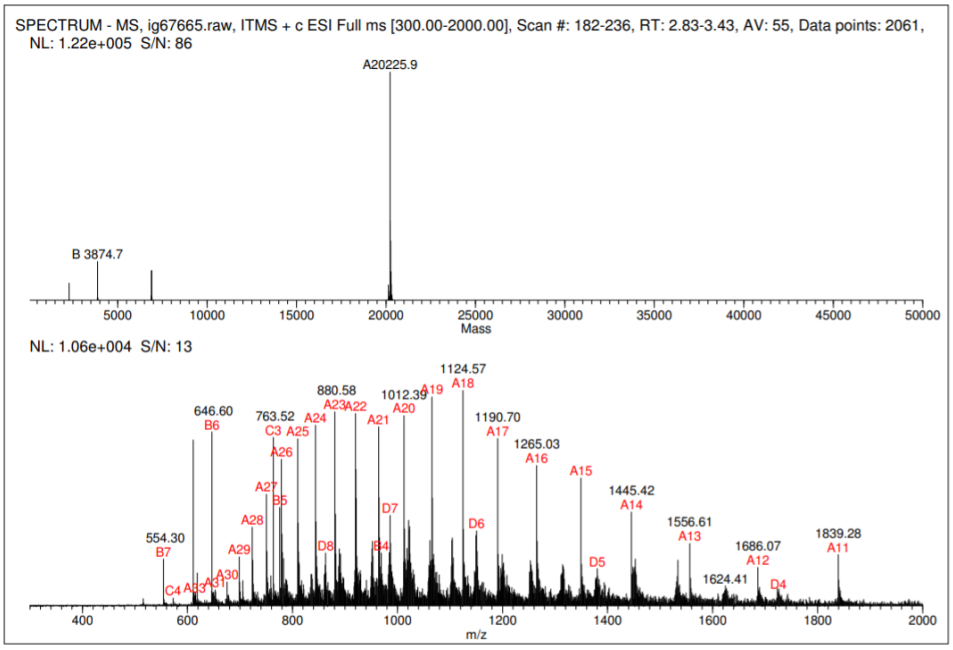

Figure 62: Electron spray ionisation mass spectrometry analysis of Bcl-xL TMH in CTD-MSP1D1ΔH5 nanodiscs. The TMH expected mass is 3872.5 Da and measured was 3874.7 Da, while the MSP has an expected mass of 20225.8 Da and determined were 20225.9 Da.

Fl-Bcl-xL in 12.5 % CL and 75 % DMPC nanodiscs (unlabelled sample for SAXS)

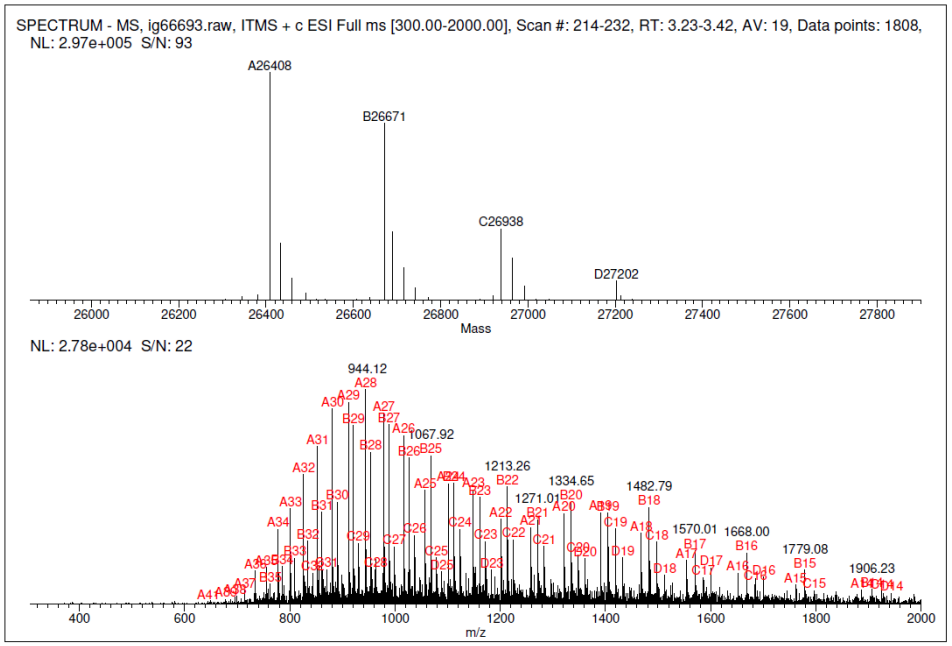

Figure 63a: Electron spray ionisation mass spectrometry analysis of full-length Bcl-xL obtained through the Sortase A method in CTD-MSP1D1ΔH5 nanodiscs with 12.5 % CL and 75 % DMPC lipids. The Fl-Bcl-xL has an expected mass of 26417.31 Da, while 26408-27202 Da were determined. The deviation lies within the error range of the instrument, as a protein within a nanodisc is difficult to measure in ESI and gives rise to a low signal and high noise. The MSP has an expected mass of 20225.8 Da and determined were 20223.2 Da, see Figure 63 b.

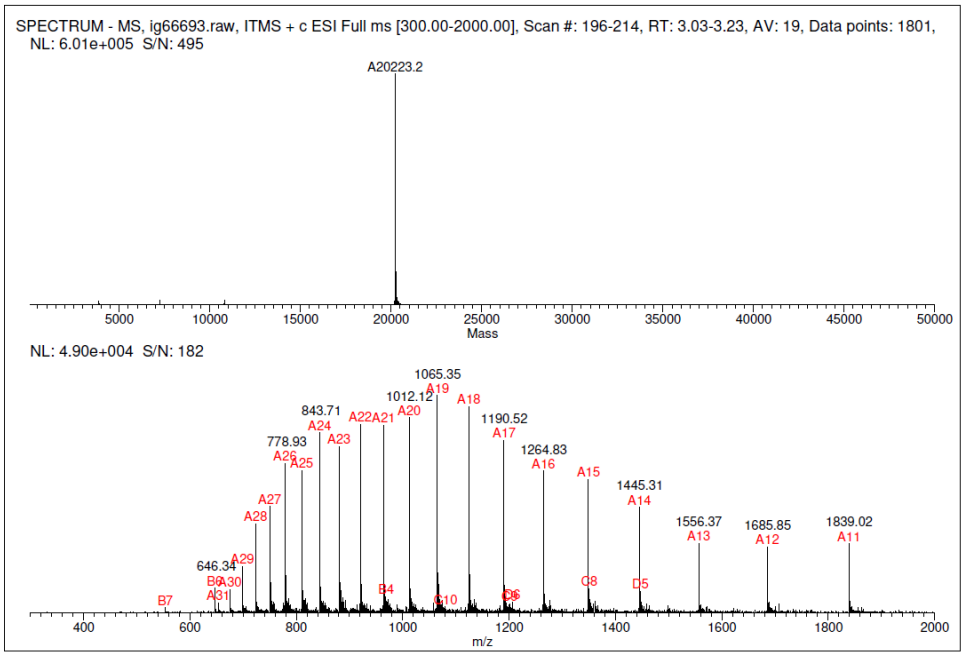

Figure 63 b: The MSP has an expected mass of 20225.8 Da and determined were 20223.2 Da.

Fl-Bcl-xL in 100 % DMPC nanodiscs (unlabelled sample for SAXS)

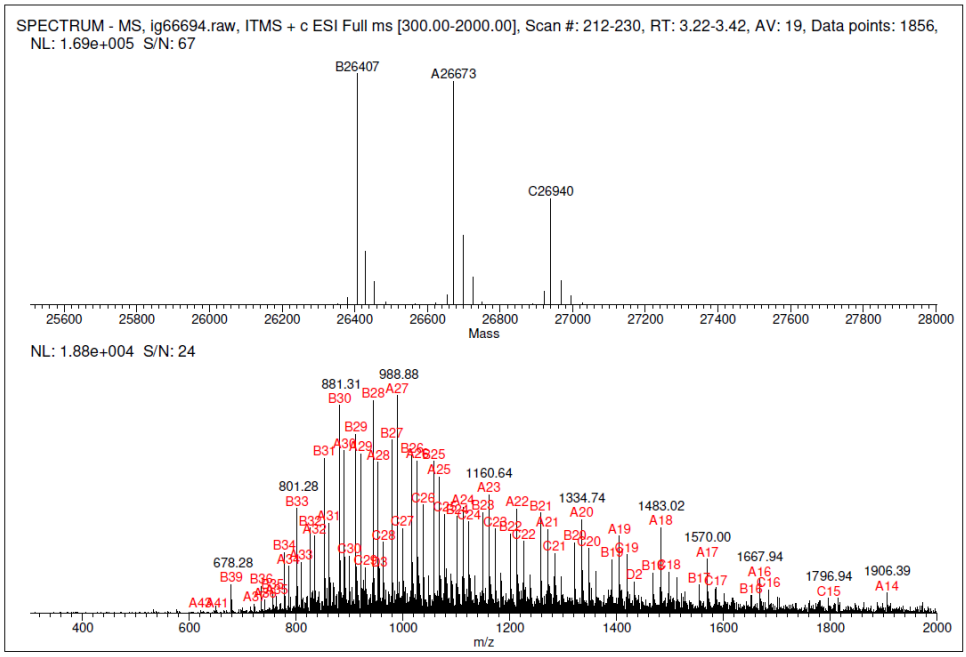

Figure 64: Electron spray ionisation mass spectrometry analysis of full-length Bcl-xL obtained through the Sortase A method in CTD-MSP1D1ΔH5 nanodiscs with 100 % DMPC lipids. The Fl-Bcl-xL has an expected mass of 26417.31 Da, while 26407-26940 Da were determined. The deviation lies within the error range of the instrument, as a protein within a nanodisc is difficult to measure in ESI and gives rise to a low signal and high noise. The MSP has an expected mass of 20225.8 Da and determined were 20223.2 Da.

6.1.4 NMR Spectra

Bcl-xLΔTM - empty nanodisc titrations

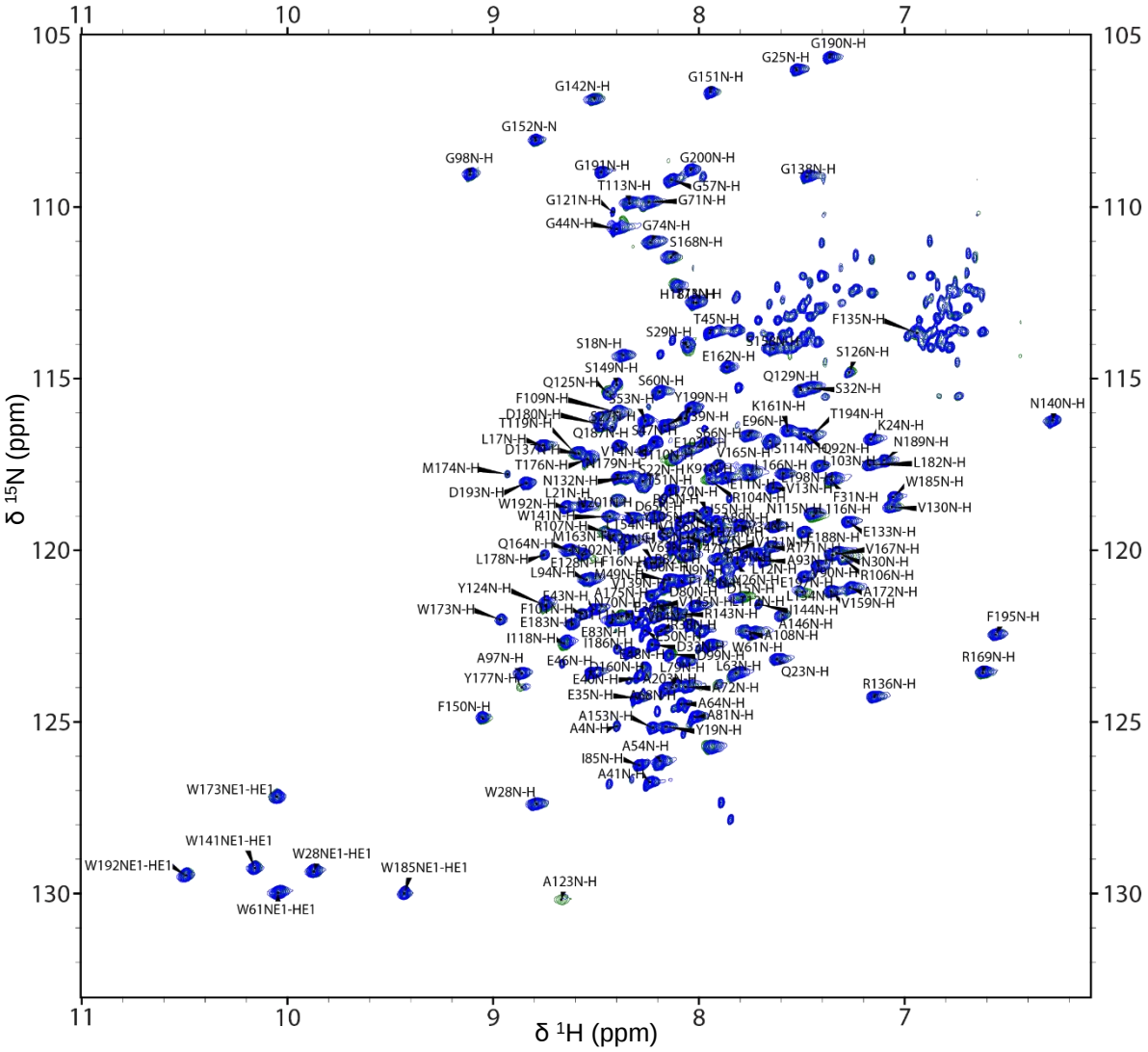

Figure 65: Overlay of 2D-[^{1}H,^{15}N]-TROSY of 200 µM ^{2}H,^{15}N-Bcl-xLΔTM with 300 µM 25 % DMPG / 75 % DMPC nanodiscs (green) and 300 µM Gd^{3+}-containing 25 % DMPG / 75 % DMPC nanodiscs (blue). Assignments of Bcl-xLΔTM are indicated by the one letter amino acid code and the respective sequence position.

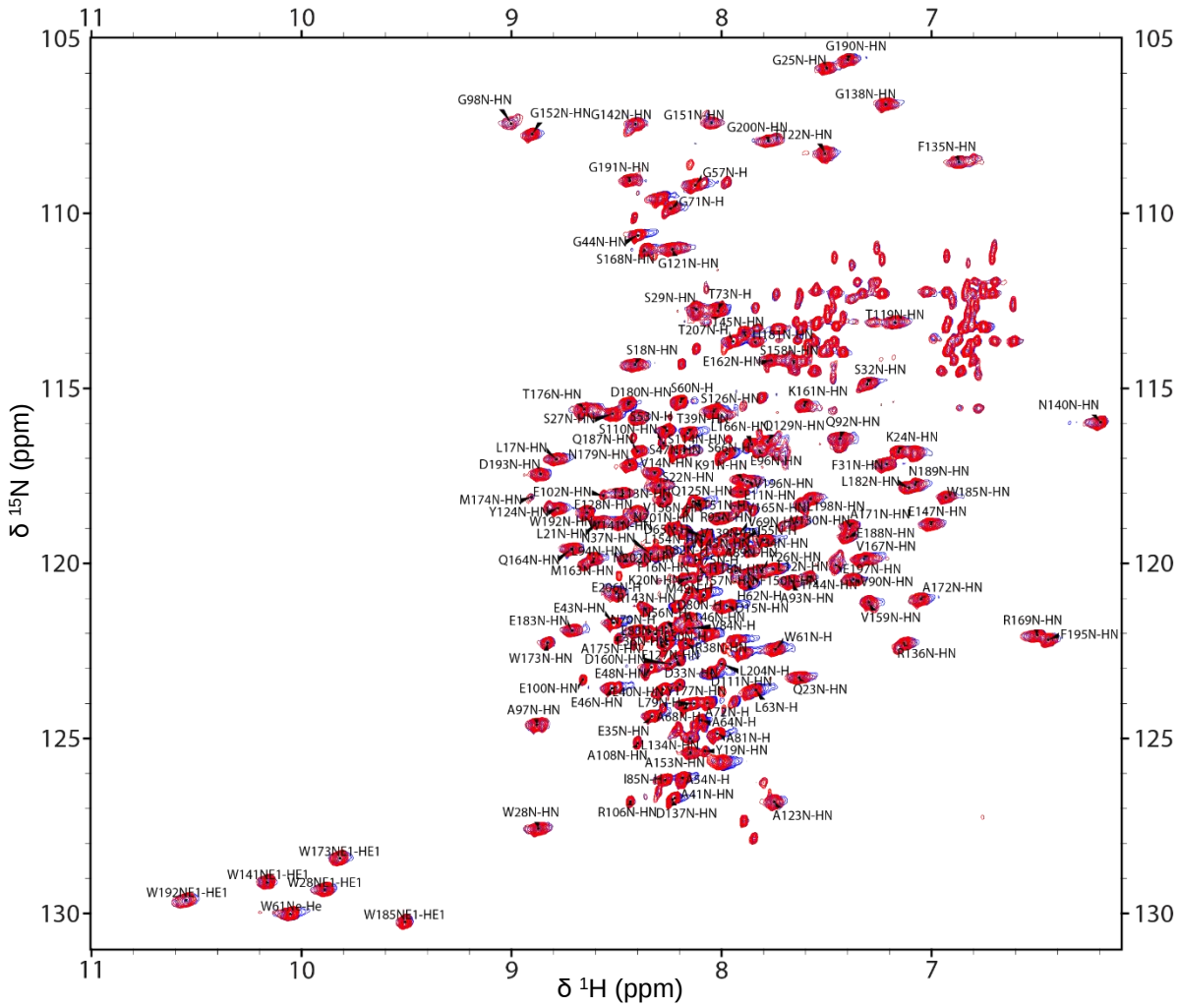

Figure 66: Overlay of 2D-[^{1}H,^{15}N]-TROSY of 200 µM PUMA-BH3 bound ^{2}H,^{15}N-Bcl-xLΔTM with 300 µM 25 % DMPG / 75 % DMPC nanodiscs (blue) and 300 µM Gd^{3+}-containing 25 % DMPG / 75 % DMPC nanodiscs (red). Assignments of Bcl-xLΔTM are indicated by the one letter amino acid code and the respective sequence position.

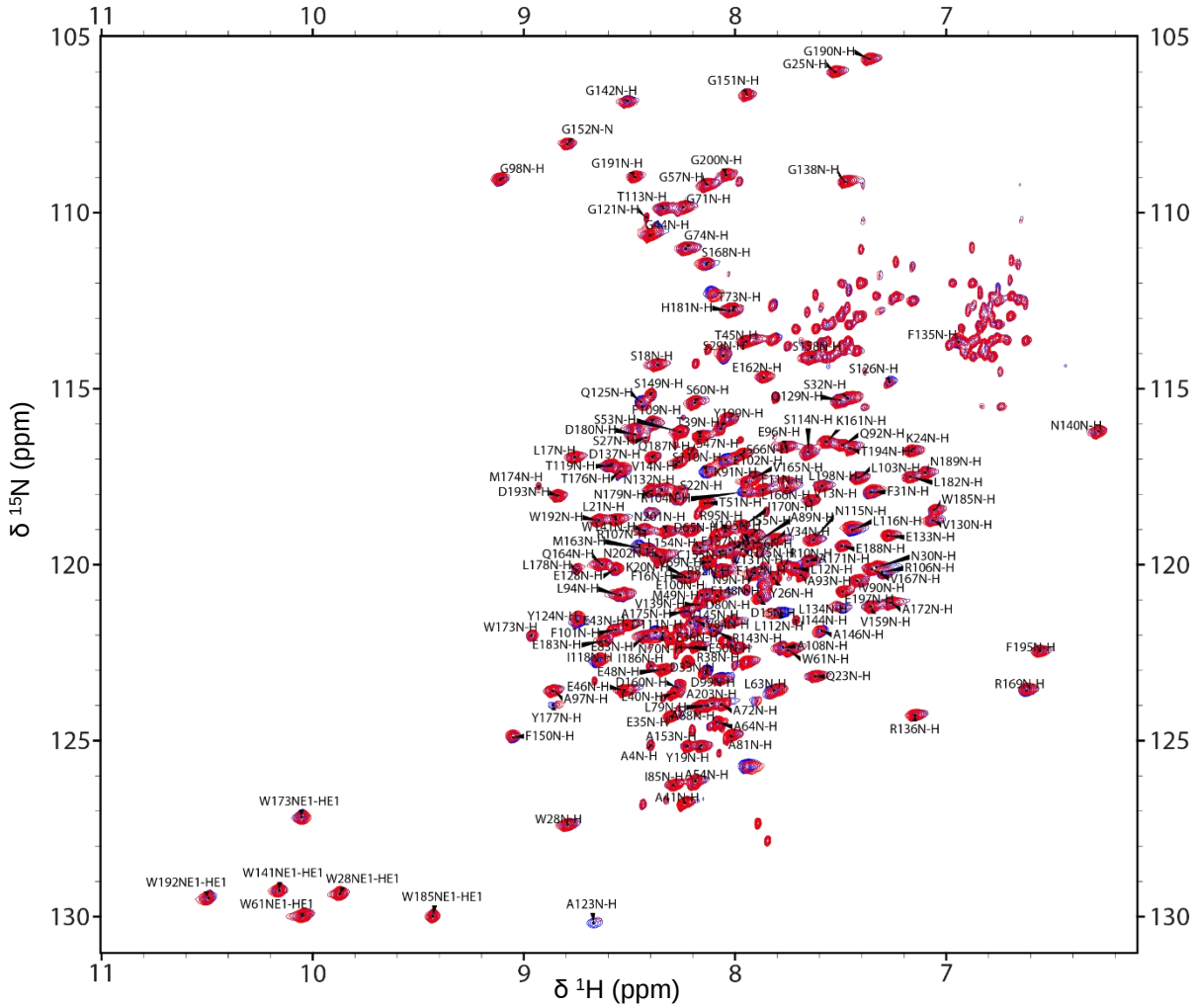

Figure 67: Overlay of 2D-[^{1}H,^{15}N]-TROSY of 200 µM ^{2}H,^{15}N-Bcl-xLΔTM with 300 µM 50 % DMPG / 50 % DMPC nanodiscs (blue) and 300 µM Gd^{3+}-containing 50 % DMPG / 50 % DMPC nanodiscs (red). Assignments of Bcl-xLΔTM are indicated by the one letter amino acid code and the respective sequence position.

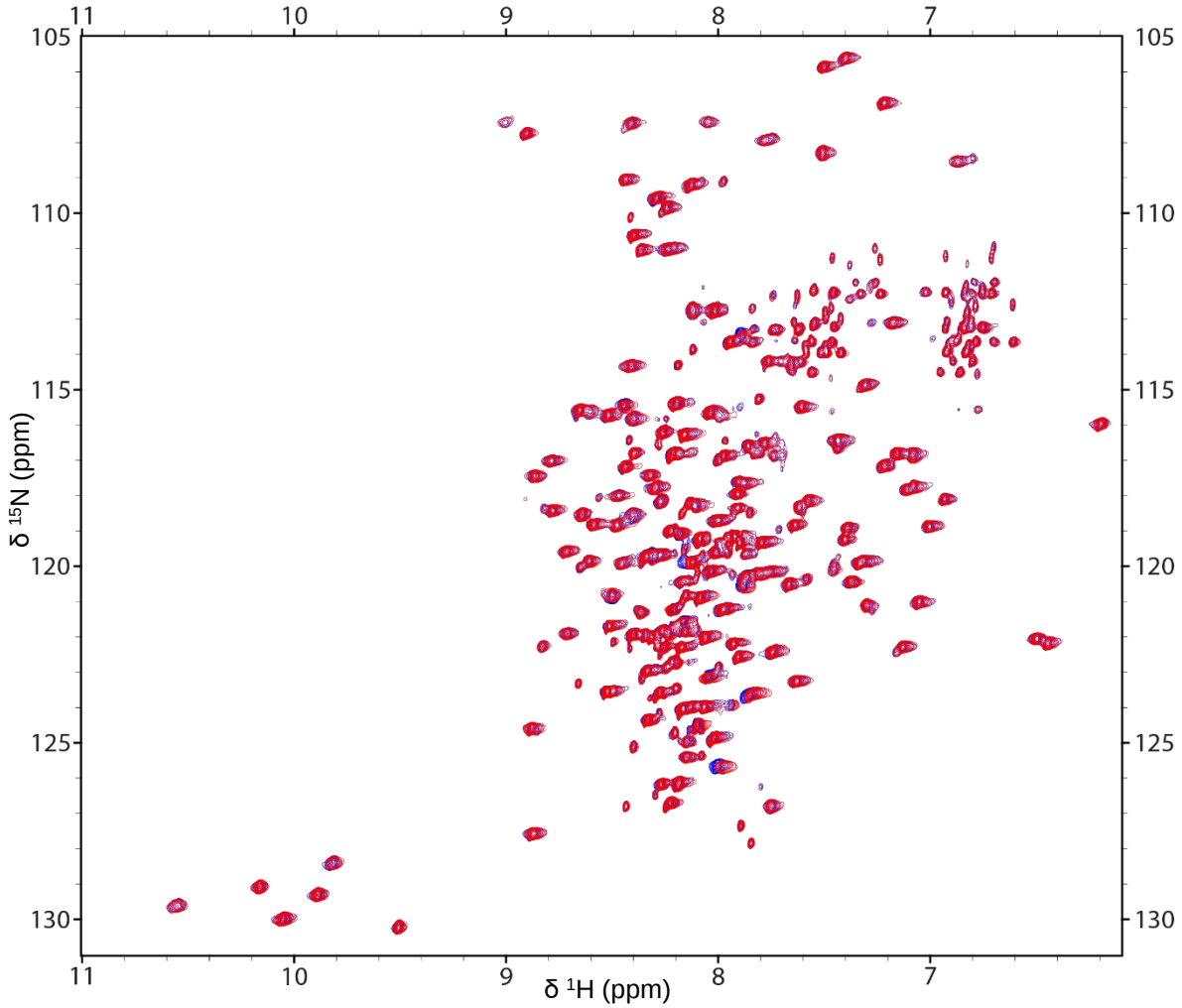

Figure 68: Overlay of 2D-[^{1}H,^{15}N]-TROSY of 200 µM PUMA-BH3 bound ^{2}H,^{15}N-Bcl-xLΔTM with 300 µM 50 % DMPG / 50 % DMPC nanodiscs (blue) and 300 µM Gd^{3+}-containing 50 % DMPG / 50 % DMPC nanodiscs (red). Assignments of Bcl-xLΔTM were the same as in Figure 66.

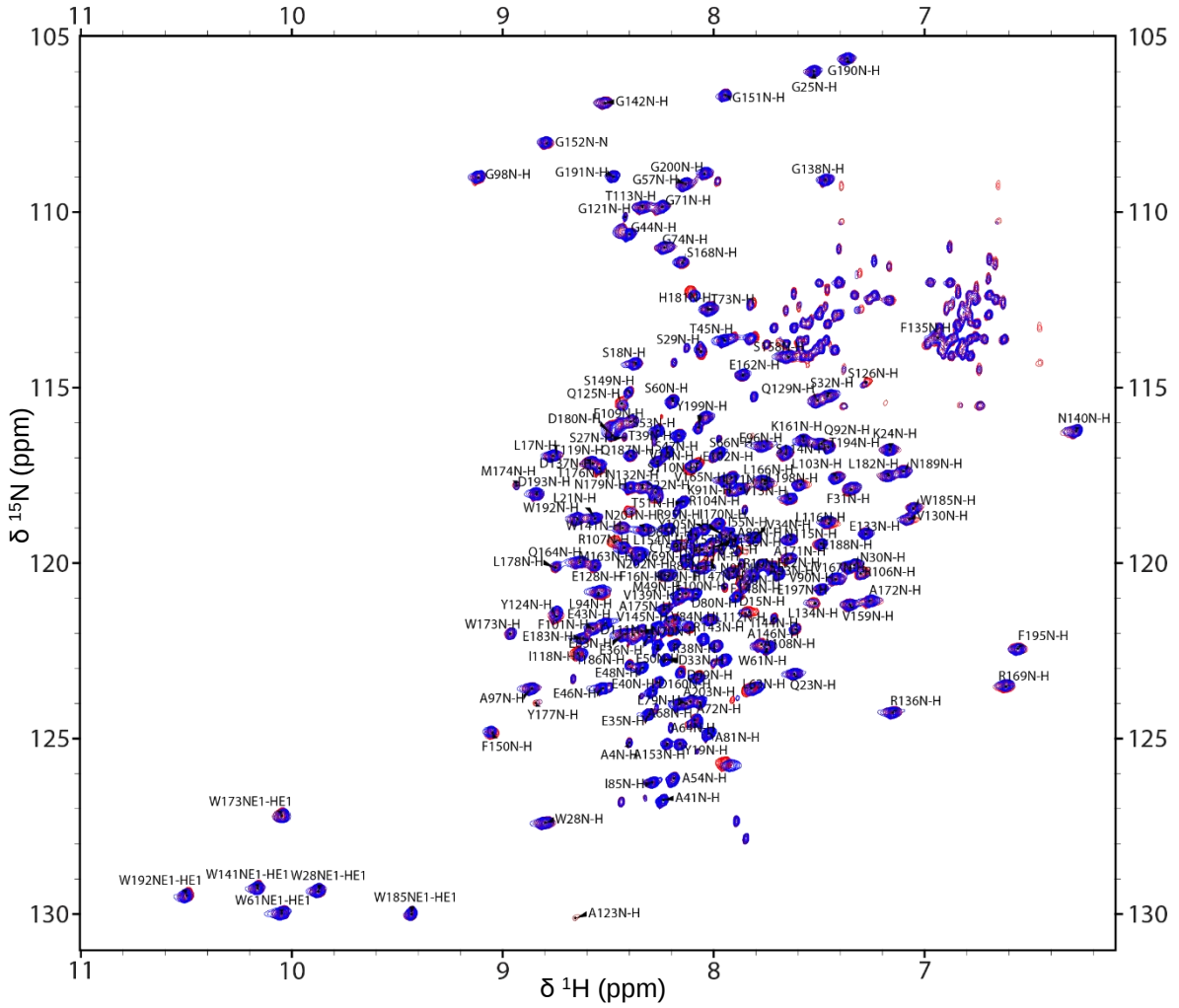

Figure 69: Overlay of 2D-[^{1}H,^{15}N]-TROSY of 200 µM ^{2}H,^{15}N-Bcl-xLΔTM with 300 µM 12.5 % CL / 75 % DMPC nanodiscs (red) and 300 µM Gd^{3+}-containing 12.5 % CL / 75 % DMPC nanodiscs (blue). Assignments of Bcl-xLΔTM are indicated by the one letter amino acid code and the respective sequence position.

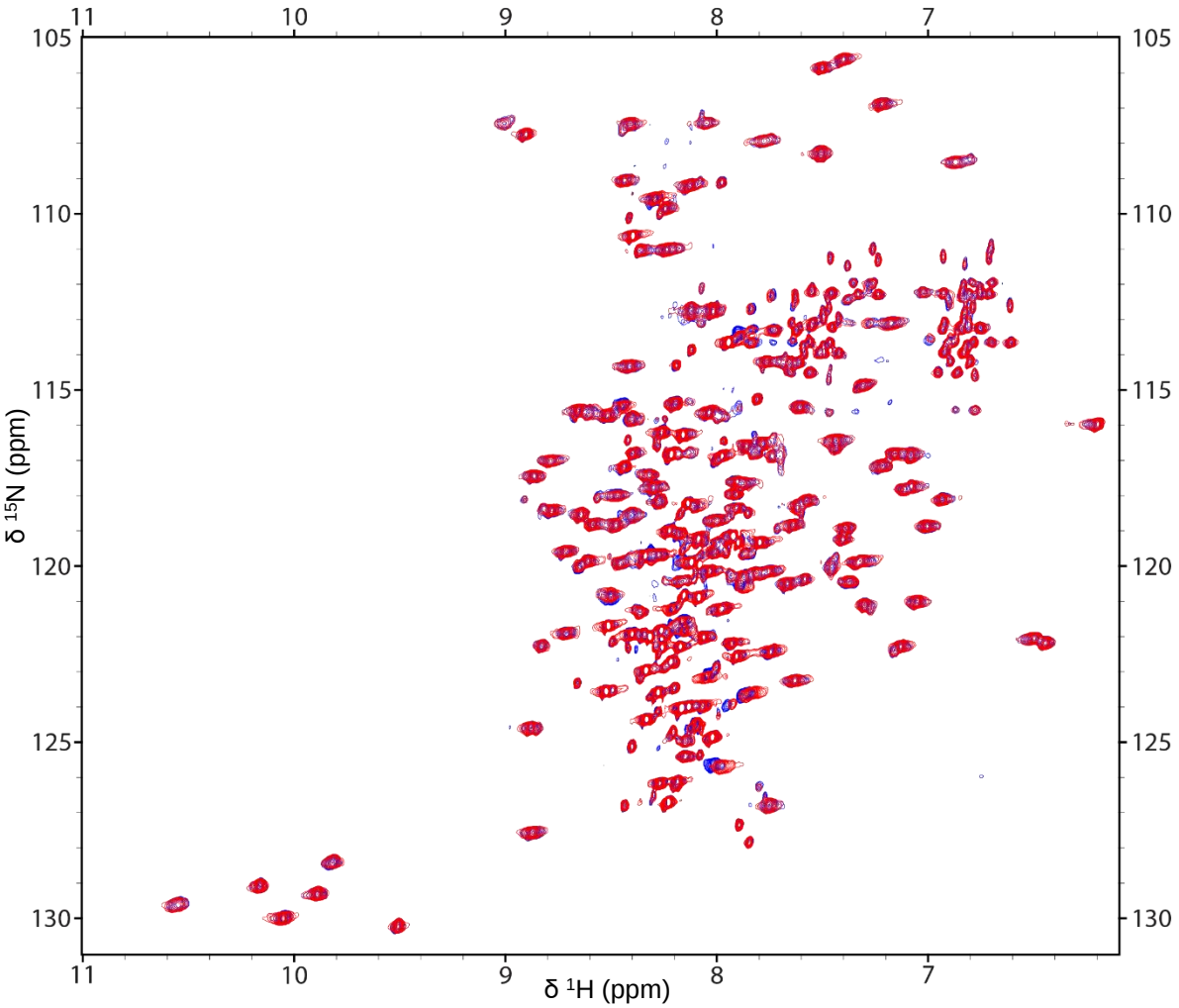

Figure 70: Overlay of 2D-[^{1}H,^{15}N]-TROSY of 200 µM PUMA-BH3 bound ^{2}H,^{15}N-Bcl-xLΔTM with 300 µM 12.5 % CL / 75 % DMPC nanodiscs (blue) and 300 µM Gd^{3+}-containing 12.5 % CL / 75 % DMPC nanodiscs (red). Assignments of Bcl-xLΔTM were the same as for Figure 66.

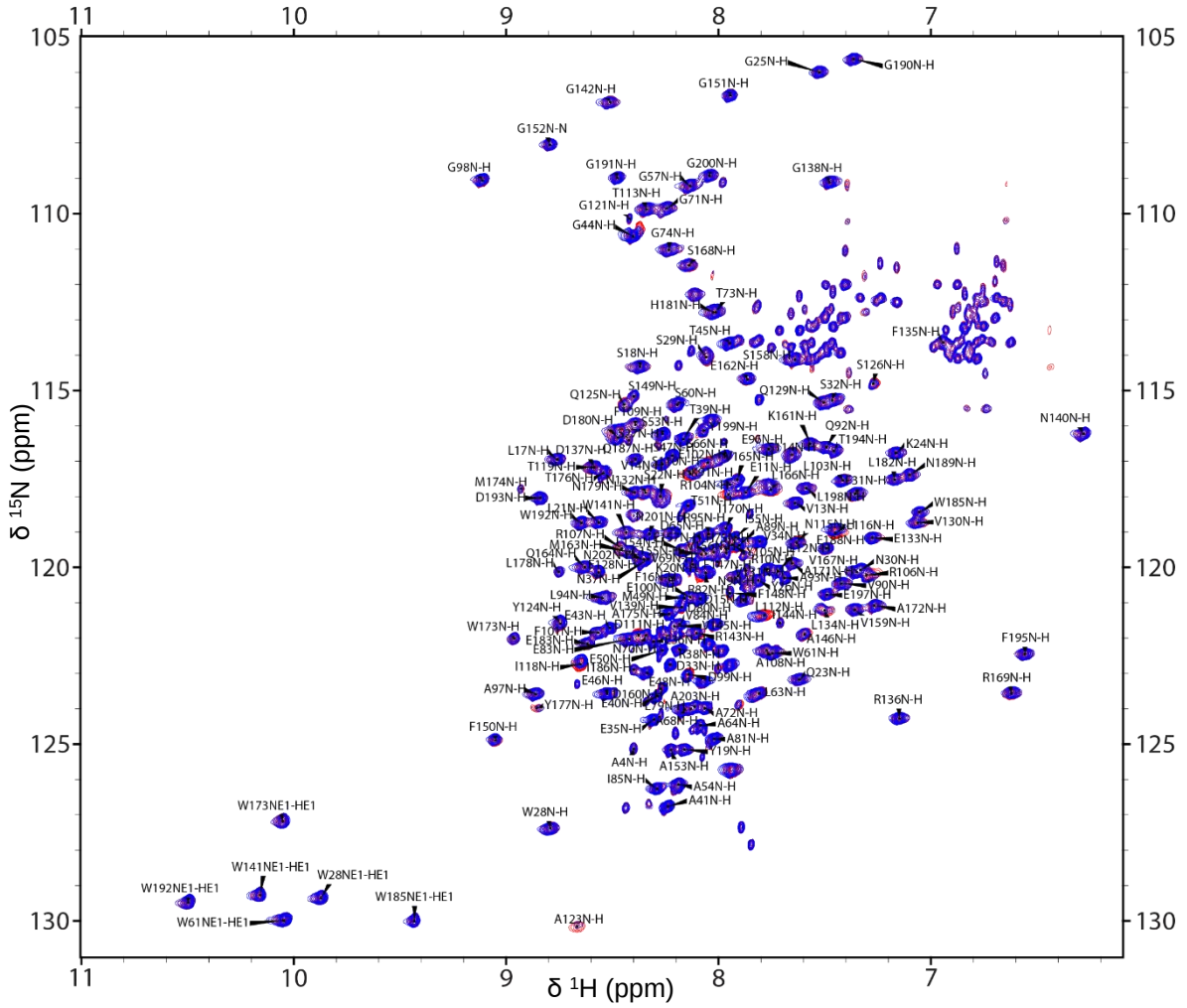

Figure 71: Overlay of 2D-[^{1}H,^{15}N]-TROSY of 200 µM ^{2}H,^{15}N-Bcl-xLΔTM with 300 µM 100 % DMPC nanodiscs (blue) and 300 µM Gd^{3+}-containing 100 % DMPC nanodiscs (red). Assignments of Bcl-xL-ΔTM are indicated by the one letter amino acid code and the respective sequence position.

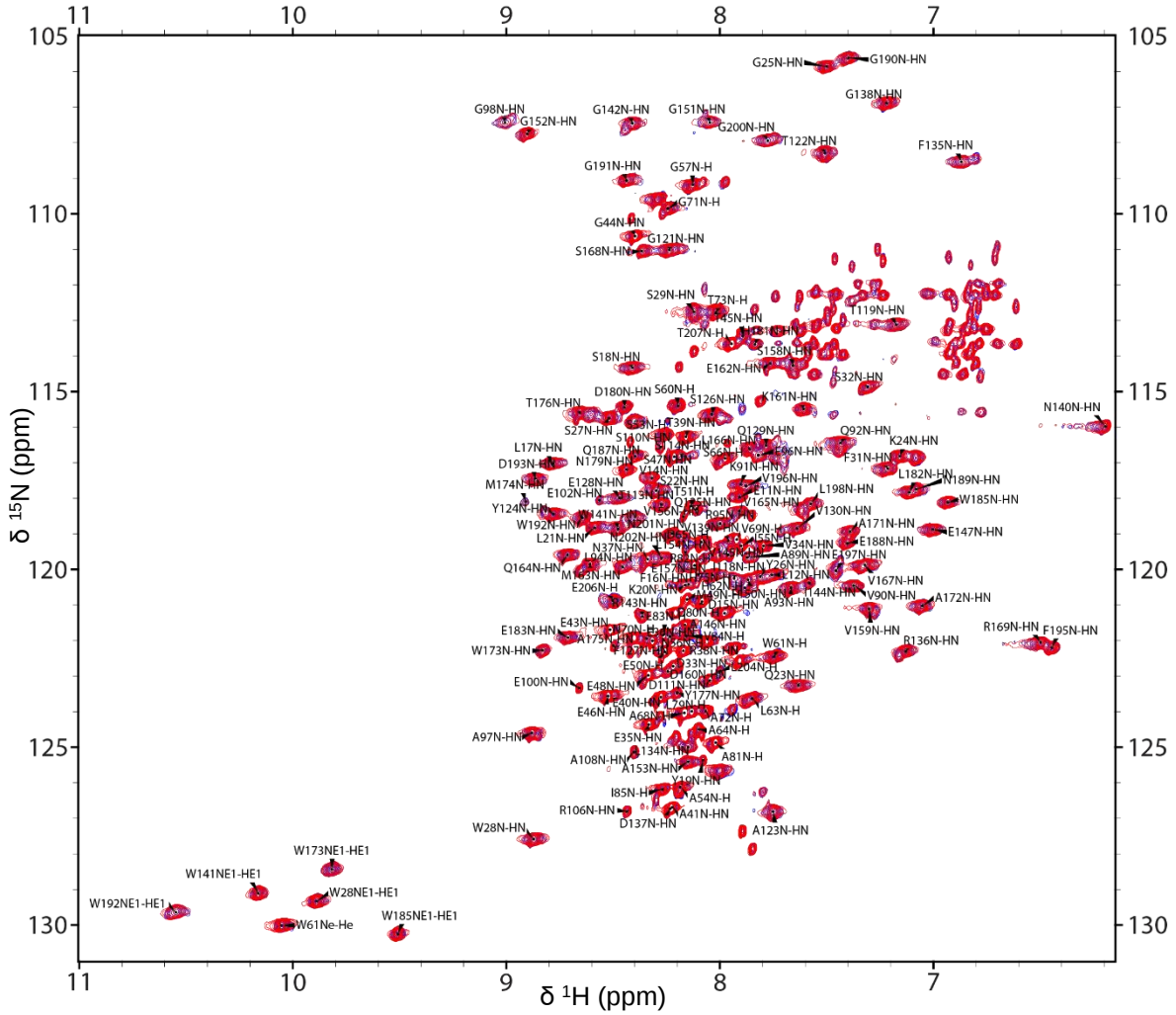

Figure 72: Overlay of 2D-[^{1}H,^{15}N]-TROSY of 200 µM PUMA-BH3 bound ^{2}H,^{15}N-Bcl-xLΔTM with 300 µM 100 % DMPC nanodiscs (blue) and 300 µM Gd^{3+}-containing 100 % DMPC nanodiscs (red). Assignments of Bcl-xLΔTM are indicated by the one letter amino acid code and the respective sequence position.

Bcl-xLTHR-ΔTM – uncut vs isolated cut-fragment (ΔN-Bcl-xL-THRΔTM)

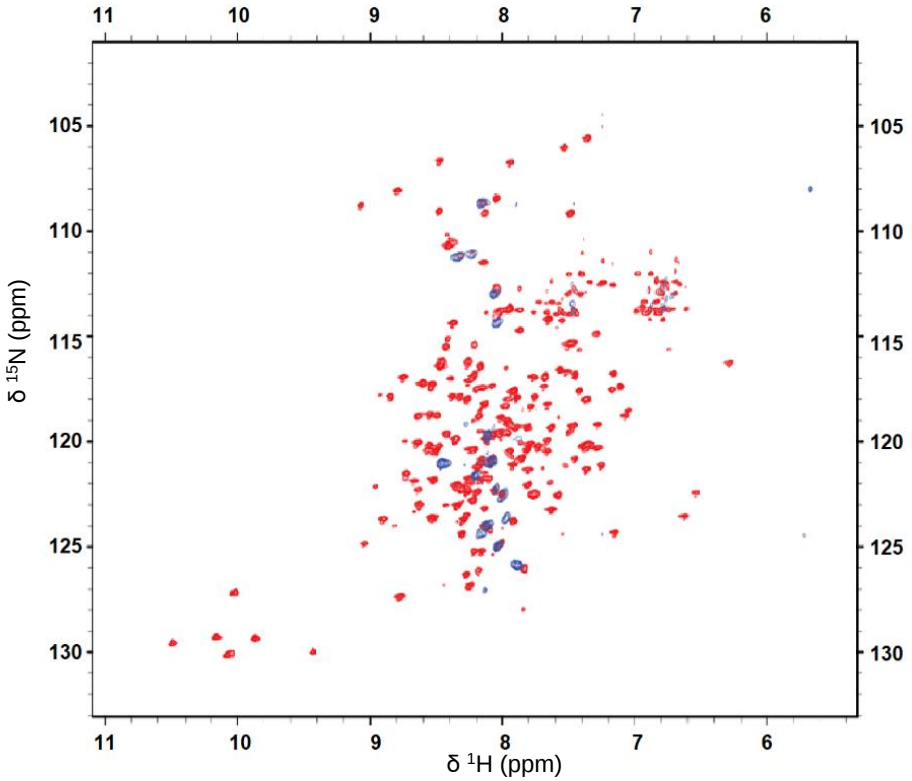

Figure 73: Overlay of 2D-[^{1}H,^{15}N]-TROSY of 200 µM ^{2}H,^{15}N-Bcl-xL-THR (red) and the isolated fragment after cutting the protein and Ni-NTA purification with 7 M urea in blue. The fragment is completely unfolded and did not refold after urea treatment.

Fl-Bcl-xL in 100 % DMPC nanodiscs

Apo – PRE experiments

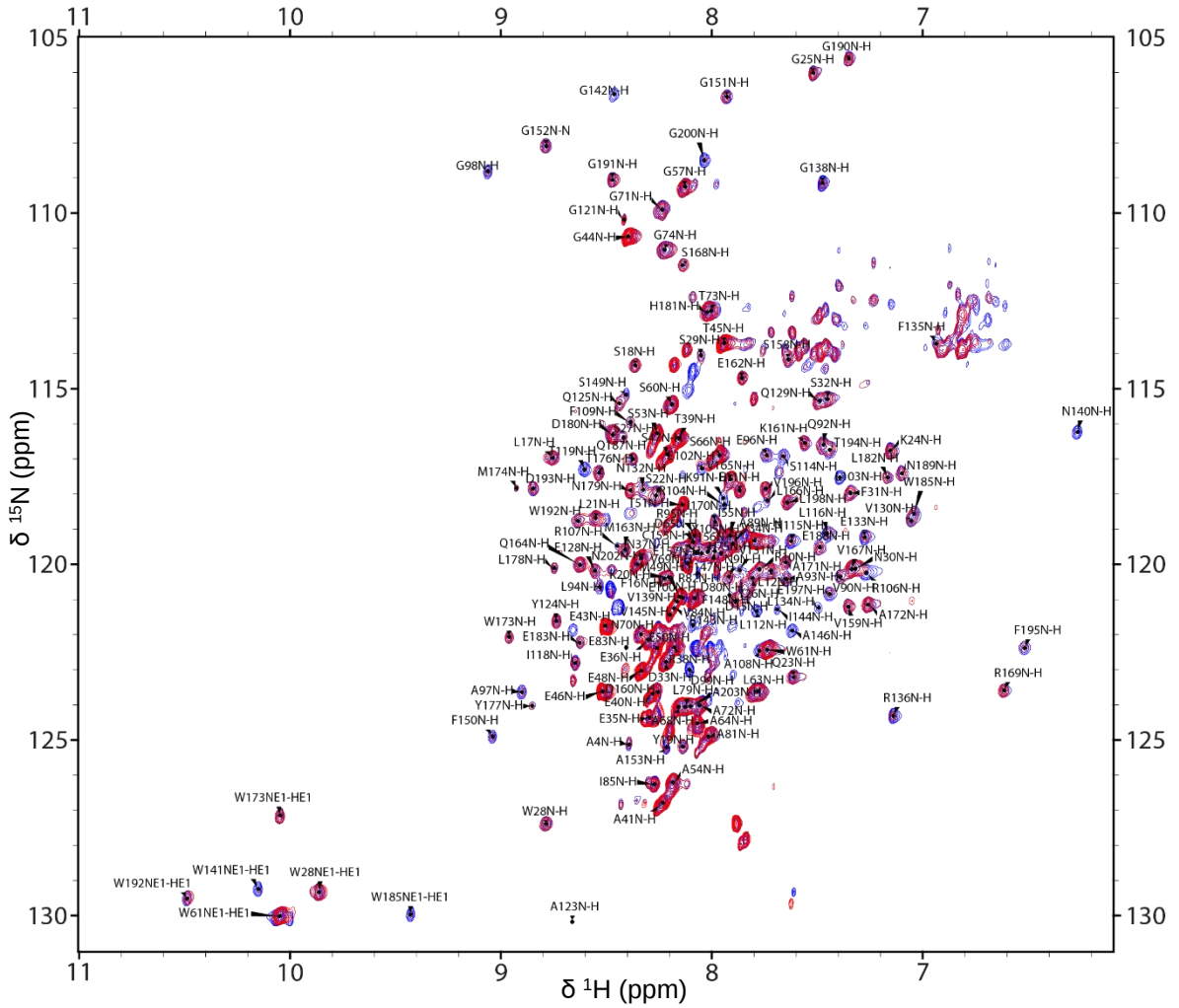

Figure 74: Overlay of 2D-[^{1}H,^{15}N]-TROSY of ^{2}H,^{15}N-Fl-Bcl-xL in 100 % DMPC nanodiscs (blue) and Gd^{3+}-containing 100 % DMPC nanodiscs (red) in apo state. Assignments of Bcl-xL-solu are indicated by the one letter amino acid code and the respective sequence position.

PUMA BH3 bound – PRE experiments

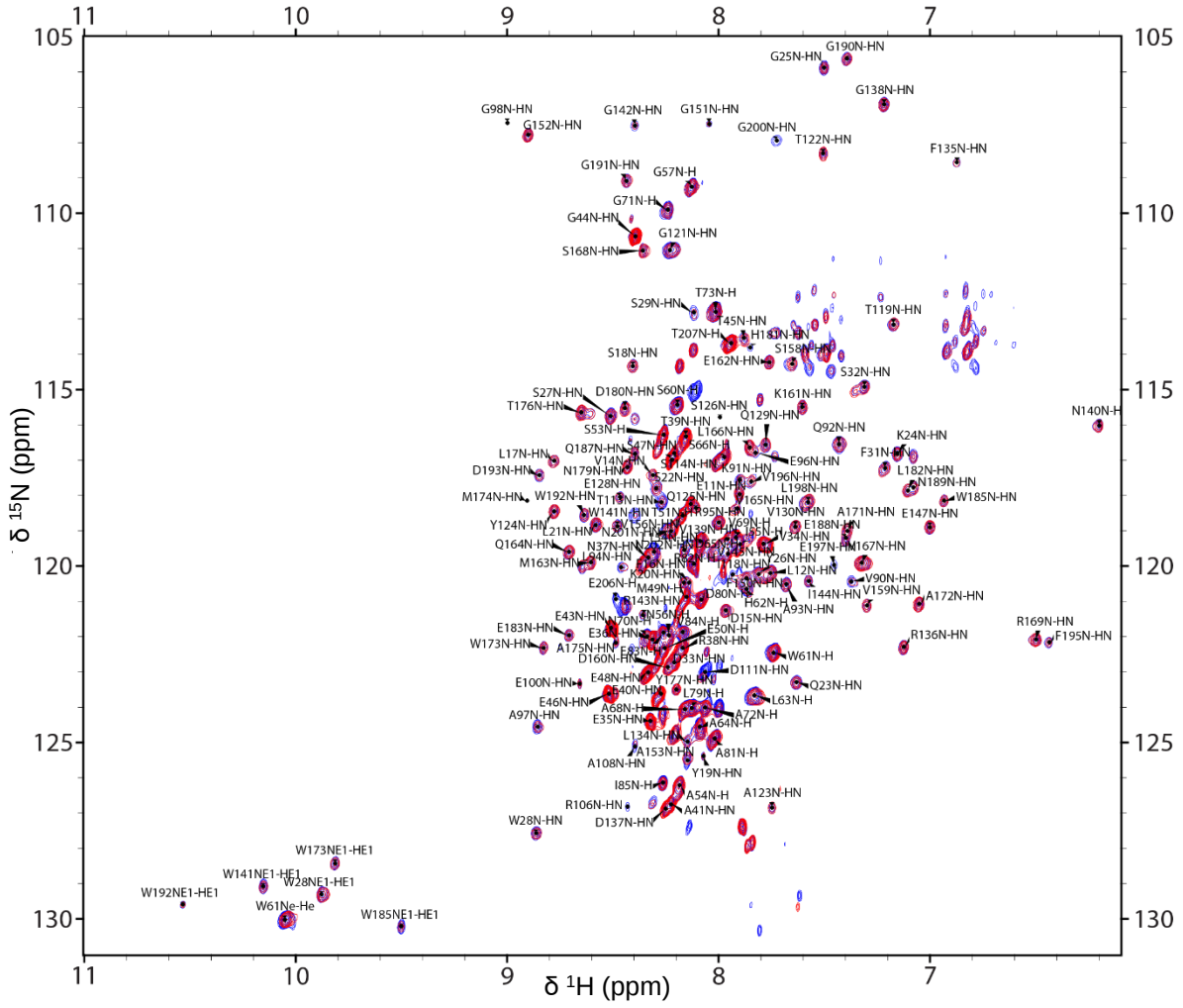

Figure 75: Overlay of 2D-[^{1}H,^{15}N]-TROSY of ^{2}H,^{15}N-Fl-Bcl-xL in 100 % DMPC nanodiscs (blue) and Gd^{3+}-containing 100 % DMPC nanodiscs (red) in PUMA-BH3 bound state (triple excess). Assignments of Bcl-xL-solu are indicated by the one letter amino acid code and the respective sequence position.

Fl-Bcl-xL in 12.5 % cardiolipin and 75 % DMPC nanodiscs

Apo – PRE experiments

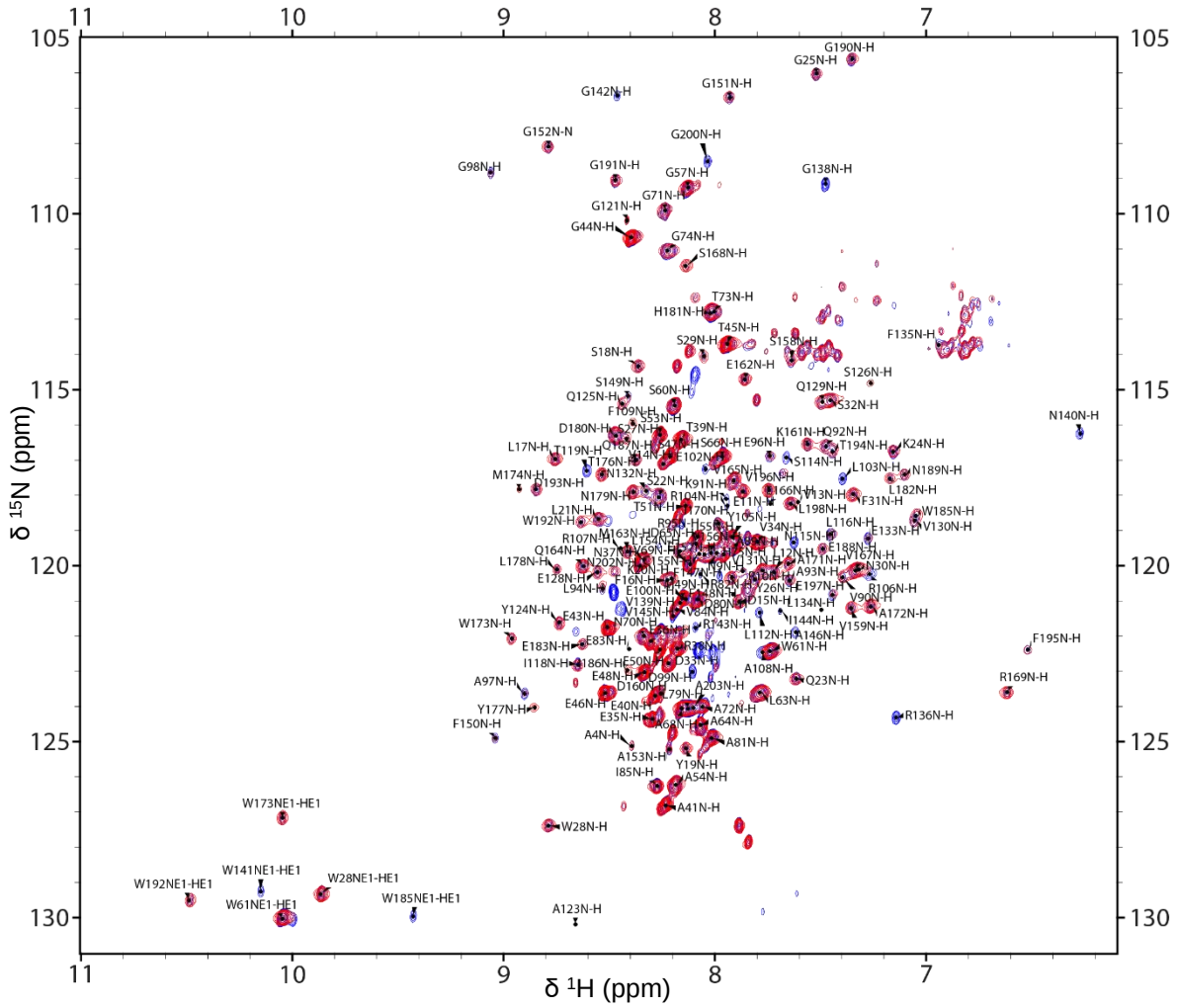

Figure 76: Overlay of 2D-[^{1}H,^{15}N]-TROSY of ^{2}H,^{15}N-Fl-Bcl-xL in 12.5 % CL and 75 % DMPC nanodiscs (blue) and Gd^{3+}-containing 12.5 % CL and 75 % DMPC nanodiscs (red) in apo state. Assignments of Bcl-xL-solu are indicated by the one letter amino acid code and the respective sequence position.

PUMA BH3 bound – PRE experiments

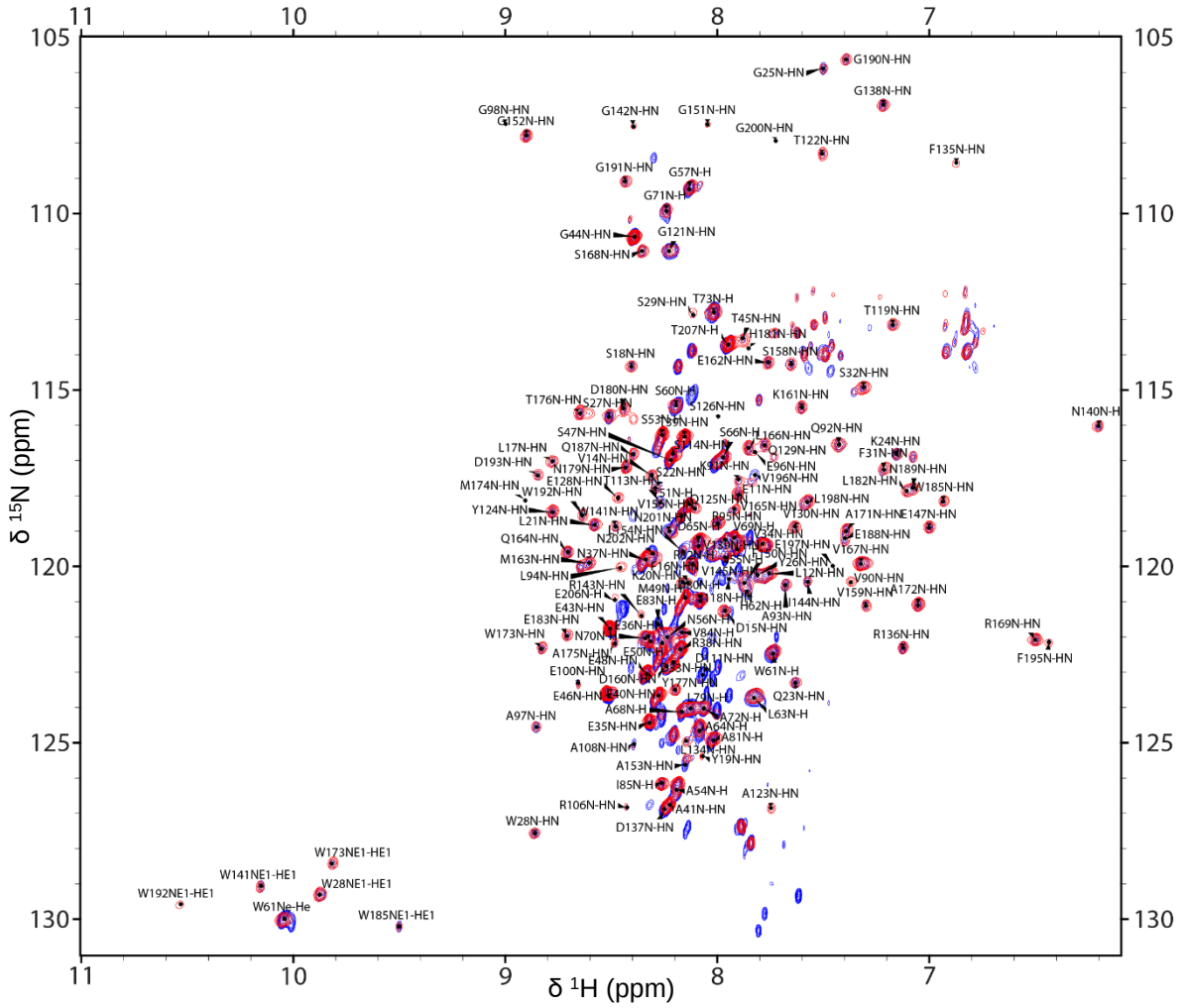

Figure 77: Overlay of 2D-[^{1}H,^{15}N]-TROSY of ^{2}H,^{15}N-Fl-Bcl-xL in 12.5 % CL and 75 % DMPC nanodiscs (blue) and Gd^{3+}-containing in 12.5 % CL and 75 % DMPC nanodiscs (red) in PUMA-BH3 bound state (triple excess). Assignments of Bcl-xL-solu are indicated by the one letter amino acid code and the respective sequence position.

Bcl-xL-THRΔTM cut study with Ni-NTA nanodiscs and Bak BH3 peptide

Apo, effect of cut while bound to the nanodisc

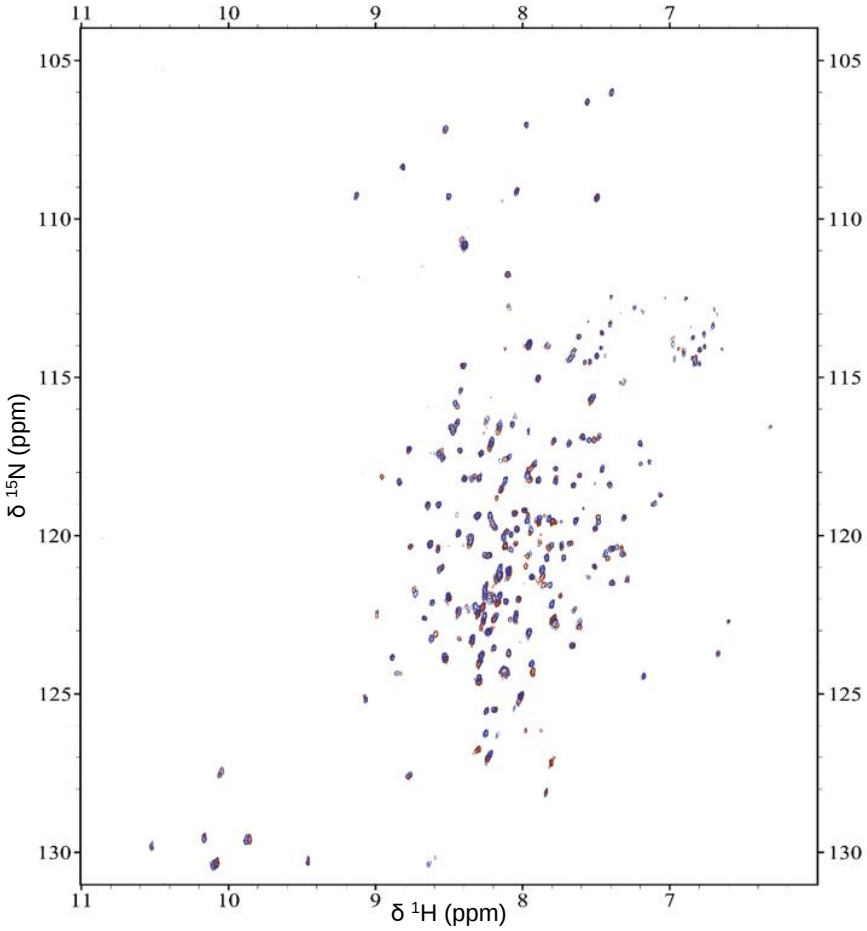

Figure 78: Overlay of 2D-[^{1}H,^{15}N]-TROSY of ^{2}H,^{15}N-Bcl-xL-THRΔTM apo uncut (blue) and cut (red) bound onto Ni^{2+}-containing nanodiscs. Assignments of Bcl-xL-solu are the same as for Bcl-xL-THRΔTM and were not shown for clarity.

BH3-bound vs. BH3-bound and attached to the Ni-NTA nanodisc

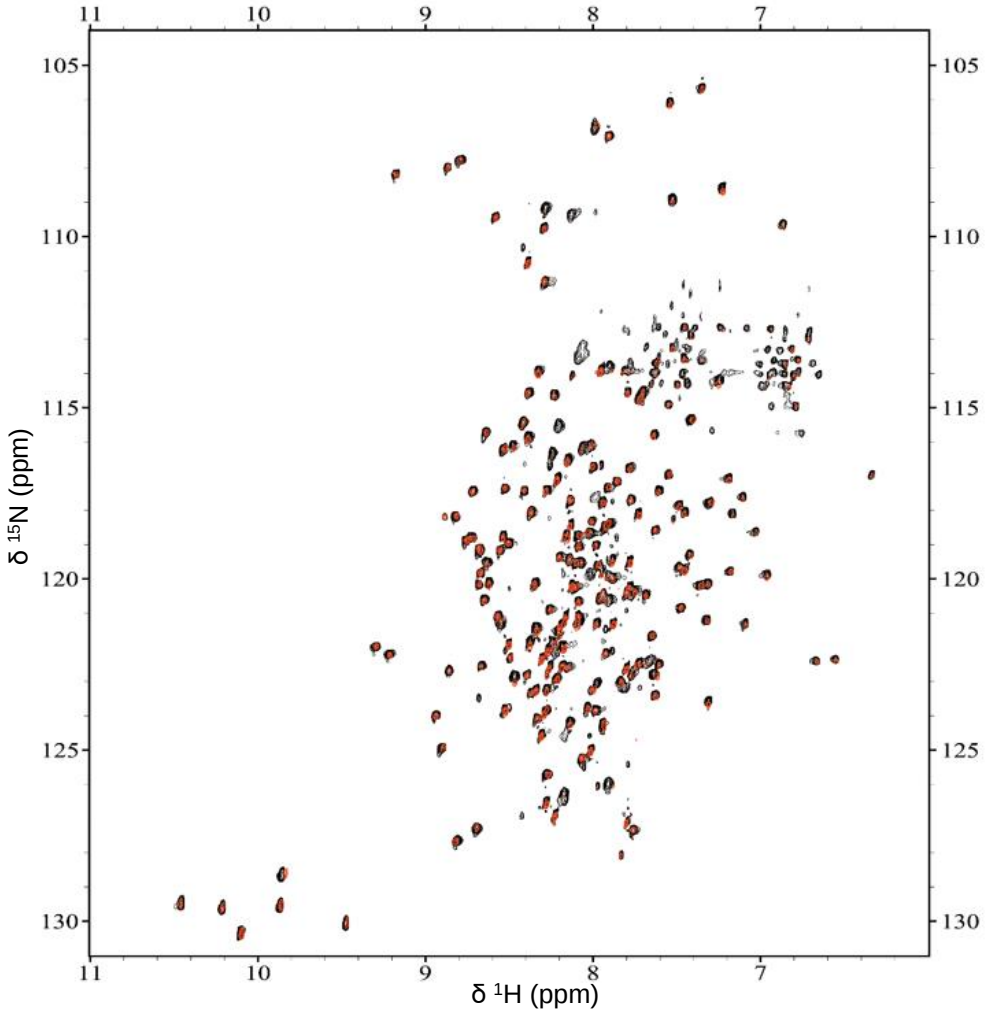

Figure 79: Overlay of 2D-[^{1}H,^{15}N]-TROSY of ^{2}H,^{15}N-Bcl-xL-THRΔTM BH3-bound cut (black) and BH3-bound cut (red) bound onto Ni^{2+}-containing nanodiscs. Several "missing" residues in the nanodisc-bound form are due to the forced membrane attachment. Assignments of Bcl-xL-solu are the same as for Bcl-xL-THRΔTM and were not shown for clarity.